H24/3486

MONASH UNIVERSITY
THESIS ACCEPTED IN SATISFACTION OF THE
REQUIREMENTS FOR THE DEGREE OF
DOCTOR OF PHILOSOPHY
ON..... 4 April 2003 .....
..... [redacted] .....
Sec. Research Graduate School Committee

Under the copyright Act 1968, this thesis must be used only under the normal conditions of scholarly fair dealing for the purposes of research, criticism or review. In particular no results or conclusions should be extracted from it, nor should it be copied or closely paraphrased in whole or in part without the written consent of the author. Proper written acknowledgement should be made for any assistance obtained from this thesis.

WAKE STATES OF A SUBMERGED OSCILLATING CYLINDER AND OF A CYLINDER BENEATH A FREE-SURFACE

A thesis submitted by

JOSIE CARBERRY

in partial fulfilment of the requirements for the degree of Doctor of Philosophy.

Department of Mechanical Engineering

Monash University

(Submitted 5th August, 2002)

TABLE OF CONTENTS

TABLE OF CONTENTS i
NOMENCLATURE v
ABSTRACT vi
STATEMENT OF ORIGINALITY ix
ACKNOWLEDGEMENTS xi

LITERATURE REVIEW AND PRELIMINARY DISCUSSION 1

1.1 INTRODUCTION 1
1.1.1 Vorticity 1
1.2 STATIONARY CYLINDER 2
1.2.1 Wake Regimes: Variation with Reynolds Number 3
1.2.2 Wake Instabilities 8
1.2.3 Spanwise Coherence - Oblique / Parallel Shedding 9
1.3 OSCILLATING CYLINDER: INTRODUCTION 9
1.3.1 Lock-in 10
1.3.2 Forces and Energy Transfer 13
1.3.3 Relating Force and Vorticity 14
1.4 FORCED CYLINDER OSCILLATIONS 19
1.4.1 Characteristic Features of Forces 20
1.4.2 Characteristic Features of Wake Modes 27
1.4.3 Link Between Forces and Wake Modes 30
1.4.4 Non-Transverse Forced Oscillations 31
1.4.5 Non-Circular Bluff Bodies 32
1.5 VORTEX-INDUCED VIBRATIONS OF A CYLINDER 38
1.5.1 Characteristic Amplitude Response 38
1.5.2 Detailed Investigations of Characteristic Wake Modes and Forces 40
1.6 FORCED AND FREELY OSCILLATING CYLINDERS 54
1.6.1 The Nature of Transition 54
1.6.2 Spanwise Correlation and Wake Structure 60
1.6.3 Relating Forced and Free Oscillations 64
1.7 STATIONARY CYLINDER NEAR A SURFACE 67
1.7.1 Boundary Conditions at a Solid or Free-Surface 67
1.7.2 Flow Over a Cylinder Close to a Solid Boundary 69
1.7.3 Forces on a Cylinder Underneath a Free-Surface 72
1.7.4 Wake Structure for a Cylinder Underneath a Free-Surface 73

1.8 SCOPE OF THESIS 80

EXPERIMENTAL METHOD **83**

1.9 FLOW SYSTEM 83
1.10 CYLINDER PROPERTIES 84
1.11 OSCILLATION PROPERTIES 86
1.12 FORCE MEASUREMENT SYSTEM 87
1.13 IMAGE MEASUREMENT SYSTEM 89
1.14 EXPERIMENTAL PROCEDURE 90
1.14.1 Submerged Oscillating Cylinder 91
1.14.2 Stationary Cylinder Underneath a Free-Surface 91
1.15 FORCE POST-PROCESSING 92
1.16 IMAGE POST-PROCESSING 93
1.17 CALCULATION OF FORCE PROPERTIES 95
1.18 COMPUTER PROGRAMS 98

SUBMERGED OSCILLATING CYLINDER **101**

1.19 COMPARISON WITH PREVIOUS WORK 101
1.20 WAKE MODES AND FORCES 104
1.20.1 Stable Wake States 104
1.20.2 Transition Between Wake States 109
1.20.3 Split Forces 113
1.20.4 Idealised Variation of Vortex Force with f_e/f_o 118
1.21 TRANSITION 121
1.21.1 Wake Length 121
1.21.2 State Selection Within the Transition Region 125
1.22 *UNIVERSALITY OF THE LOW- AND HIGH-FREQUENCY STATES: VARIATION WITH A/D AND RE* 129
1.22.1 Variation of Total and Vortex Forces with *A/D* 129
1.22.2 Variation of Total and Vortex Forces with Re 135
1.22.3 Vortex Force: Collapse of Vortex Phase 141
1.22.4 Vorticity Fields 144
1.23 SPECTRAL ENERGY AS A FUNCTION OF FE/FO 149
1.24 INTERMEDIATE WAKE STATE 152
1.24.1 Force Properties 152
1.24.2 Wake Structure and Corresponding Lift Forces 160
1.24.3 Variation of Lift and Drag Phases 171

1.25 RELATE FORCED AND FREELY OSCILLATING CYLINDERS 177
1.25.1 Link Between Forced Wake States and Free Response Branches 177
1.25.2 Wake Structures 183
1.25.3 Prediction of VIV Using Forced Oscillations 190

STATIONARY CYLINDER NEAR A FREE-SURFACE 193

1.26 FORCES ON A CYLINDER NEAR A FREE-SURFACE 193
1.26.1 Variation of Lift and Drag with *h/D* 193
1.27 WAKE MODES NEAR A FREE-SURFACE 196
1.27.1 Mode I Wake: Modified Kármán Wake 197
1.27.2 Mode II Wake: Flow Attached to Free-Surface 200
1.27.3 Mode III Wake: Separated Jet 202
1.27.4 Angle of Lower Shear-Layer 205
1.27.5 Contamination of Free-Surface 206
1.28 SUMMARY 207

CONCLUSIONS 209

1.29 FUTURE WORK / RECOMMENDATIONS 213
1.30 SUPPORTING PAPERS 215

REFERENCES 217

NOMENCLATURE

SYMBOL	DESCRIPTION
ϕ_{drag}	Phase angle of the drag wrt the displacement (drag freq. = $2f_e$, therefore $\phi_{drag} = \phi_{drag} + 180^o$)
ϕ_{lift}	Phase angle of the lift wrt the displacement (lift freq. = f_e)
$\phi_{lift\ vortex}$	Phase angle of the vortex lift wrt the displacement
ω_z	z component of vorticity, $\omega_z = \frac{\partial v}{\partial y} - \frac{\partial u}{\partial x}$
C_D	Drag coefficient – Drag / ½ $\rho U^2_{free} LD$
C_L	Total Lift coefficient – Total Lift / ½ $\rho U^2_{free} LD$
$C_{L\ vortex}$	Vortex Lift coefficient – Vortex Lift / ½ $\rho U^2_{free} LD$
$-C_{PB}$	Base suction coefficient
D	Diameter of cylinder
E	Energy transfer from fluid to cylinder
f	Frequency of free oscillations
f^*	f^*(free) = f/f_{struc}
f_e	Frequency of forced oscillation
f_N	Natural structural frequency (elastically mounted cylinder)
f_{nos}	Natural frequency of oscillating wake
f_o	Natural (Karman) frequency of stationary wake
f_{struc}	Structural frequency
L	Length of the cylinder
L_{cpv}	Streamwise position of the centre of the attached positive vorticity at the top of the oscillation
m_a	Added mass per unit length

m_d	Displaced mass per unit length, for a cylinder $m_d = -\frac{\rho \pi D^2}{4}$
Re	Reynolds number, $\mathrm{Re} = \frac{UD}{\nu}$
St	Strouhal number, $St = \frac{fD}{U}$
U	Free stream velocity
U^*	Reduced Velocity, $U^*(free) = \frac{U}{f_N D}, U^*(forced) = \frac{U}{f_e D}$
	Normalised Reduced velocity $St_o\left(\frac{U^*}{f^*}\right)(free) = \frac{f_o}{f}$
y	Cylinder displacement, $y(t) = A \sin(2\pi f_e t)$

ABSTRACT

The wake states of a circular cylinder undergoing controlled sinusoidal oscillations transverse to a free-stream are examined for a range of flow and oscillation parameters. As the frequency of oscillation passes through the natural Kármán frequency there is a transition between two distinctly different wake states: the low- and high-frequency states. The transition corresponds to a change in the structure of the near wake and is also characterised by a jump in the phase and amplitude of both the total and vortex lift. Examination of the instantaneous force loadings and flow fields within the transition region allow discrimination between the actual wake states and their conventional time-averaged representations. At the largest oscillation amplitudes considered, a third wake state occurs at oscillation frequencies between low- and high-frequency states. This "intermediate wake state" is revealed by instantaneous measurements of the total and vortex lift phases, and the phase-referenced quantitative wake structure. Over the range of flow and oscillation parameters studied the wake states exhibit a number of universal features. The phases of the vortex lift and drag forces have characteristic values for the low- and high-frequency states, which appear to be directly related to the phase of vortex shedding. The transitions between the intermediate state and either the low- or high-frequency states demonstrate a link between changes in the vortex shedding phase and the phase of the vortex lift force. It is also apparent that changes in the phase of the total lift and the phase of vortex shedding are not necessarily linked. The low-frequency, intermediate and high-frequency states show some remarkable similarities to the response branches of elastically mounted cylinders. The equivalence between forced and self-excited oscillations is addressed, and the prediction of flow-induced motion using the results of controlled oscillations is discussed using concepts of energy transfer.

The modification of the Kármán wake of a stationary cylinder by the presence of a free-surface was also considered. The wake displays a number of different modes, depending primarily on the depth of the cylinder and the non-dimensional Froude number. At $Fr = 0.166$ three modes were observed, where in all cases the presence of the free-surface caused the wake to become non-symmetric and there was a net negative lift force on the cylinder. Closer to the surface periodic vortex shedding did not occur and the two wake modes differed significantly from the fully submerged Kármán wake, while for the third mode at deeper submergence depths the response of the wake to the Kármán instability appeared to be amplified.

STATEMENT OF ORIGINALITY

This thesis contains no material which has been accepted for the award of any other degree or diploma in any university, and, to the best of my knowledge and belief, contains no material previously published or written by another person, except where due reference is made in the text.

Josie Carberry

ACKNOWLEDGEMENTS

I would like to express my gratitude to a number of people who have helped me during my candidature: my officemates Michael Eaddy and Katrina Swalwell, as well as the fluids group at Lehigh, in particular Dr Oksan Cetiner, Dr Tom Praisner and Dr Dan Sabatino, for their assistance and generosity.

During my candidature I was fortunate to spend an extended period at Lehigh University. I am very grateful to my associate supervisor Professor Donald Rockwell for giving me the opportunity to use the facilities in the Fluid Mechanics Laboratory and for his ongoing interest, guidance and attention to detail.

My supervisor Professor John Sheridan is, more than any other person, responsible for directing me towards a career in research. I would like to thank him for taking the time to introduce me to fluid mechanics during the final year of my BE, for continually showing me I have a lot to learn, for many opportunities and untold patience.

Financial support for this research program was provided by the US Office of Naval Research and the Australian Research Council. I also acknowledge personal financial support provided by an Australian Postgraduate Award.

I would also like to thank everybody who belayed me on my projects; falling off is a natural part of both sports climbing and doing a Ph.D., but it's always nice when somebody catches you. Finally I would like to thank my family, in particular my sister Emma, and my Mum and Dad; your confidence in me is an integral part of my character and everything I achieve.

1 LITERATURE REVIEW AND PRELIMINARY DISCUSSION

1.1 INTRODUCTION

The periodic shedding of vortex structures from a circular cylinder is one of the most fundamental problems in fluid dynamics. For a wide range of flow conditions vortex structures are shed periodically from the cylinder, forming a characteristic wake pattern known as the Kármán street. The vortex shedding results in a periodic forcing of the body that can, under certain conditions, induce large-scale motion of the cylinder. Vortex-induced vibration is experienced by many natural and engineering structures, the classic example being the Tacoma Narrows bridge. In that case the natural wind over the bridge deck generated forces that resulted in large-scale motion of the bridge, and ultimately its destruction. The interaction between a vibrating body and the structure of the near wake has been extensively studied and remains the subject of ongoing research.

1.1.1 Vorticity

The structure of a wake or flow field is often described in terms of its vorticity field. Vorticity is defined as the curl of the velocity vector:

$$\vec{\omega} = \nabla \times \vec{v} \qquad (1\text{-}1)$$

The characteristic flow over a circular cylinder is most commonly described in terms of the spanwise vorticity:

$$\omega_z = \frac{\partial v}{\partial x} - \frac{\partial u}{\partial y}$$

where, as defined in Chapter 2, the cylinder's axis is aligned in the z direction and the free-stream flow is in the x direction.

The streamwise and transverse components of vorticity are given by:

$$\omega_x = \frac{\partial w}{\partial y} - \frac{\partial v}{\partial z} \text{ and } \omega_y = \frac{\partial u}{\partial z} - \frac{\partial w}{\partial x} \text{ respectively.}$$

Vorticity is defined as the non-symmetric gradient of the velocity fields and can be interpreted as the rate of rotation of a small fluid element about its own axis. Vorticity is Galilean invariant and is therefore not altered by subtracting or adding a mean velocity in any direction. In a homogeneous fluid vorticity is generated only at boundaries by the relative acceleration of flow past the boundary. Vorticity can be generated by flow through a porous boundary, however in this discussion only non-porous boundaries will be considered. Therefore, the generation of vorticity

can be expressed either in terms of the acceleration of fluid past a boundary or a pressure gradient along the boundary, as described by a number of authors including Morton (1983), Reynolds & Carr (1985) and Green (1995). The boundary between water and air is often referred to as a "free surface". As the viscosity of air is small compared to water, when the free surface is not contaminated there is minimal shear stress at the boundary. Therefore the boundary conditions along a flat, clean free surface are zero shear stress and constant pressure: p(surface) = p(atmosphere) ≈ constant. When the free surface is curved, generally due to large pressure gradients under the free surface, there is a relative acceleration of the flow along the surface and a corresponding generation of vorticity. However, when the free surface is contaminated with surfactants a non-zero shear stress at the surface is possible. Thus a contaminated free surface can sustain a pressure gradient underneath the free surface, and vorticity can be generated along a contaminated free surface without surface deformation. When the surface of a free stream flow is contaminated the start of the contamination forms a distinct line known as the Reynolds Ridge, as described by Scott (1982). The Reynolds Ridge is effectively the start of a boundary layer flow underneath a "quasi-free" surface. The boundary layer is often typically thin and therefore difficult to detect.

As discussed by Morton (1983), the generation of vorticity is instantaneous, inviscid and does not require a no-slip boundary condition. The diffusion of vorticity outwards from the boundary into the flow is however a viscous process. In the flow the only mechanism for the decay of vorticity is by cross annihilation during diffusive interaction with vorticity of the opposite sign.

The circulation, Γ, is a scalar measure of the total rotation of the fluid contained within a boundary and can be expressed in terms of either the velocity or vorticity field:

$$\Gamma = \oint_C \vec{u}.d\vec{l} = \int_S \vec{\omega}.\vec{n}\,dS \qquad (1\text{-}2)$$

where S is the surface bound by the closed contour C. The conservation of circulation within a material element, Kelvin's theorem, requires that the net generation of vorticity for unbounded uniform flow past a cylinder is zero. Thus, equal quantities of positive and negative vorticity are generated at the cylinder's surface. However, at a given instant the rate of diffusion of positive and negative vorticity will be different. The vorticity in the wake is a measure of the changes in the flow as it accelerates past the cylinder.

1.2 STATIONARY CYLINDER

The circular cylinder and other similar geometries are common both in nature and in engineering structures and the study of flow over a circular cylinder is of obvious practical significance. The simple nature of the circular geometry means that the physical properties of the cylinder can

generally be non-dimensionalised using only the diameter of the cylinder. Additionally, the flow over a circular cylinder has often been used as a canonical flow, which forms the basis for studies of more complicated geometries.

To some extent, the large body of literature on the circular cylinder can be attributed to the many and varied features of the flow over this simple geometry. The circular geometry provides no sharp edges to promote, or force the separation of the flow; therefore the point at which the flow separates is a function of the flow itself. The symmetrical nature of the circle means that the circular cylinder has no angle of attack and the two-dimensional geometry is independent of the direction of the flow. This point is particularly relevant to an oscillating bluff body, as for a non-circular body the effective angle of attack changes during the oscillations.

Although this study is primarily focused on an oscillating circular cylinder, the properties of the stationary cylinder are relevant. In many cases the wakes observed for an oscillating cylinder are similar to the wakes from a stationary cylinder and in some cases the mode of vortex shedding is the same. In particular, the mechanism or instability that causes vortex shedding in a stationary cylinder are relevant to the wake of an oscillating cylinder.

1.2.1 Wake Regimes: Variation with Reynolds Number

The regimes of the wake of a circular cylinder are typically described in terms of the Reynolds number and have been comprehensively reviewed by a number of authors, including Williamson (1996a) and Zdravkovich (1997). The regimes describe the transition of the wake from laminar flow through to the development of a fully turbulent wake. As Reynolds number increases there is a systematic upstream movement of the point at which the transition to turbulence occurs. Thus the different regimes that develop as Reynolds number increases can be described in terms of the point at which the flow becomes turbulent. The various flow regimes, and in particular the transition between the regimes, are also affected by the level of free-stream turbulence, surface roughness, cylinder aspect ratio, end conditions and blockage. However, in general the regimes of the wakes are adequately described by their dependence on Reynolds number.

Zdravkovich (1997) used the general location of the transition to turbulent flow to describe the wake state or regime. The regimes are split into sub-regime that describe the wake in more detail. The regimes and sub-regimes covering a Reynolds number range from zero through to very large are outlined in table 1-1. Williamson (1996a) used a plot of the base suction coefficient ($-C_{PB}$) versus Reynolds number, as shown in Figure 1-1, to demonstrate the effect of the different Re regimes on the cylinder. A brief summary of the flow regimes for $Re = 10^0 - 10^6$ is provided below:

For very low Reynolds numbers within the laminar regime, the wake remains attached around the entire surface of the cylinder (L1). As Re increases the flow separates from the upper and lower surfaces of the cylinder forming a steady, symmetric and closed near-wake (L2). The wake becomes progressively longer with increasing Re, until at Re = 30-48 the downstream wake becomes unsteady (L3). As Re increases further within the periodic laminar regime, the wake shortens and the onset of periodic vortex shedding occurs at Re = 45-65. The vortex shedding is initiated by the growth of the two-dimensional (transverse) Kármán instability and over a wide range of Reynolds numbers the shedding is strongly periodic. The frequency of vortex shedding is called the Kármán frequency or, in its non-dimensional form, the Strouhal frequency. The vortices are shed alternately from the upper and lower surfaces of the cylinder, resulting in a distinct pattern of oppositely signed vortices, known as the Kármán street. The transverse structure of the Kármán street is very robust and is observed over a wide range of Reynolds numbers.

Table 1-1 Detailed description wake regimes Zdravkovich (1997)

State / Regime	Sub-Regime		Reynolds Number Range
Laminar	L1	No Separation	0 to 4-5
	L2	Closed Wake	4-5 to 30-48
	L3	Periodic Wake	30-48 to 180-200
Transition in Wake	TrW1	Far Wake	180-200 to 220-260
	TrW2	Near Wake	220-260 to 350-400
Transition in Shear Layers	TrSL1	Lower	350-400 to 1k-2k
	TrSL2	Intermediate	1k-2k to 20k-40k
	TrSL3	Upper	20k-40k to 100k-200k
Transition in Boundary Layers	TrBL0	Pre-critical	100k-200k to 300k-340k
	TrBL1	Single Bubble	300k-340k to 380k-400k
	TrBL2	Two Bubble	380k-400k to 500k-1M
	TrBL3	Super-critical	500k-1M to 3.5M-6M
	TrBL4	Post-critical	3.5M-6M to (?)
Fully Turbulent	T1	Invariable	(?) to ∞
	T2	Ultimate	

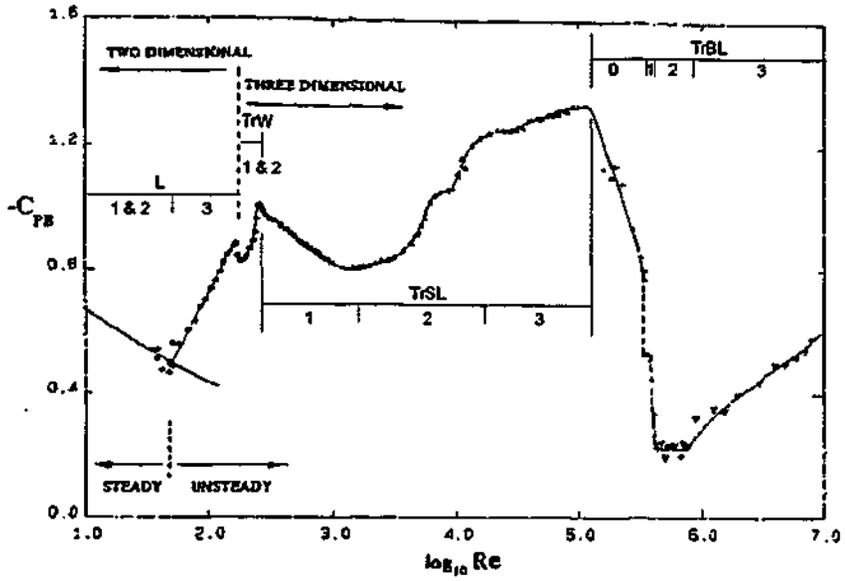

FIGURE 1-1 **Plot of base suction coefficient over a large range of Reynolds numbers from Williamson (1996a), for use in the discussion of vortex shedding regimes. The shedding regimes described by Zdravkovich are also shown.**

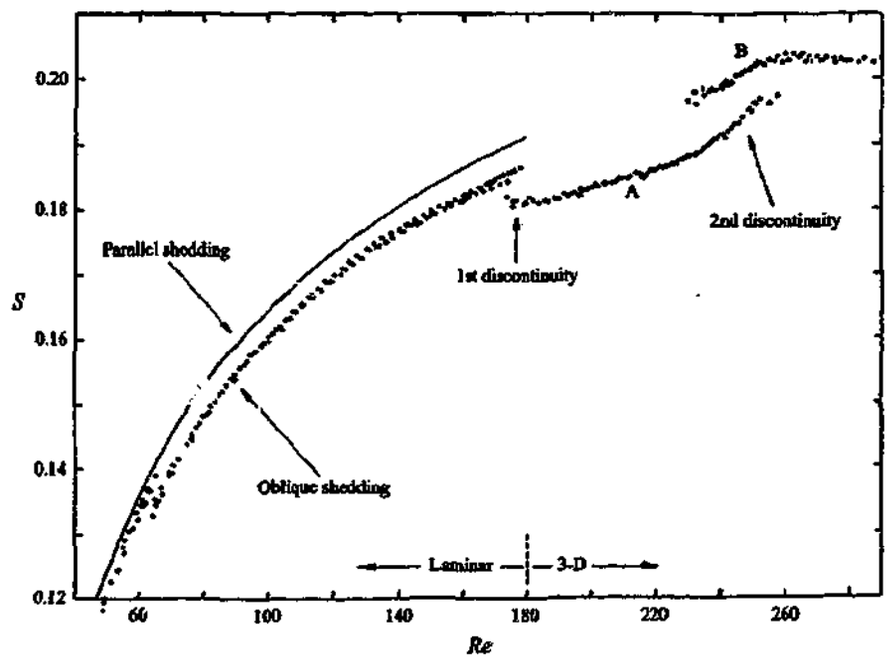

FIGURE 1-2 **Strouhal-Reynolds number relationship over the laminar (L) and wake transition (TrW) regimes. The wake transition is characterised by two distinct discontinuities indicating the onset of the mode A and mode B instabilities. Reproduced from Williamson (1996b)**

The beginning of the wake transition regime at Re= 180-200 corresponds to a sudden drop in both the base suction coefficient and Strouhal number, shown in Figures 1-1 and 1-2 respectively. The changes in $-C_{PB}$ and St are primarily associated with the growth of spanwise instabilities, resulting in a three-dimensional wake structure. This regime consists of two sub-sections that were characterised by Zdravkovich (1997) in terms of the position of the transition to turbulence. For

the first regime (TrW1) the turbulent transition is observed in the near wake but in the TrW2 regime at slightly higher Re the transition has progressed into the near wake. The spanwise structures associated with TrW1 and TrW2 have become widely known as mode A and mode B respectively. The development of the mode A and B wakes from different instabilities and the resulting characteristic wake structures are discussed in detail by Williamson (1996b). The spanwise structures in the mode A and B wakes have distinctly different symmetries and scales. The transition between modes A and B is hysteretic and is characterised by the overlapping discontinuity of the Strouhal number shown in Figure 1-2.

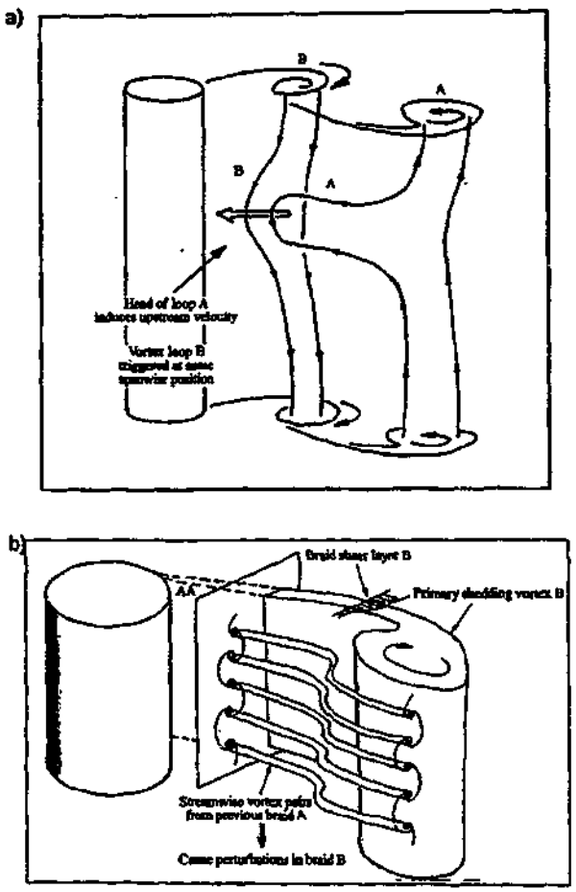

FIGURE 1-3 Physical mechanisms leading to the production of a) out-of-phase mode A vortex loops by deformation of the primary structure by downstream induction, b) in phase mode B loops due to induction from the previous braid. Reproduced from Williamson (1996b)

As discussed by Williamson (1996b) the mode A instability occurs due to the deformation of the primary vortex core. At a given spanwise location, successive primary spanwise vortices of opposite sign are deformed in the same direction by downstream induction as shown in Figure 1-3a. Thus, streamwise vorticies from one braid to the next are of opposite sign and their symmetry is considered to be out-of-phase. The mode B wake is generated by an instability of the braid shear layer region, where the instability is generated by the interaction between the forming shear layer

and the existing streamwise vorticity in the opposite shear layer. As shown in Figure 1-3b the streamwise pattern of the mode B is in phase across successive braids. The spanwise structures of the two modes are distinctly different: the wavelength of the mode A instability scales on the primary vortex core, while the much smaller wavelength of the mode B instability, scales on the thickness of the braid shear layer. The mechanisms described by Williamson (1996b) are consistent with the observations of Zdravkovich (1997) who associated the TrW1 sub-regime (mode A) with the transition of the far wake and the TrW2 sub-regime (mode B) with the transition of the near wake.

As Re increases further the wake moves to the TrSL regime where the transition to turbulence occurs within the shear layer. The beginning of the TrSL regime corresponds to the peak in the base suction at Re = 220-260 and, as discussed by Williamson (1996a), at this point the three-dimensional streamwise vortex structures in the near wake are particularly ordered. As Re increases within TrSL1, the three-dimensionality becomes increasingly disordered and there is an accompanying increase in the length of the wake. The transition between the TrSL1 and TrSL2 regimes, at Re just above 1000, is characterised by a local minima in the base suction as shown in Figure 1-1. The data compiled by Norberg (1998) in Figure 1-4 shows that this point also corresponds to an exceptionally long wake formation length. Additionally, the onset of small-scale vortex structures within the free shear layers also occurs at Reynolds numbers of just above 1000. Prasad & Williamson (1997) showed that the onset of these shear-layer vortices is intermittent. As Re increases further through the TrSL2 and TrSL3 sub-regimes, the transition to turbulence continues to move upstream, until at Re = 1-2 x 10^5 transition occurs in the shear-layer immediately after separation.

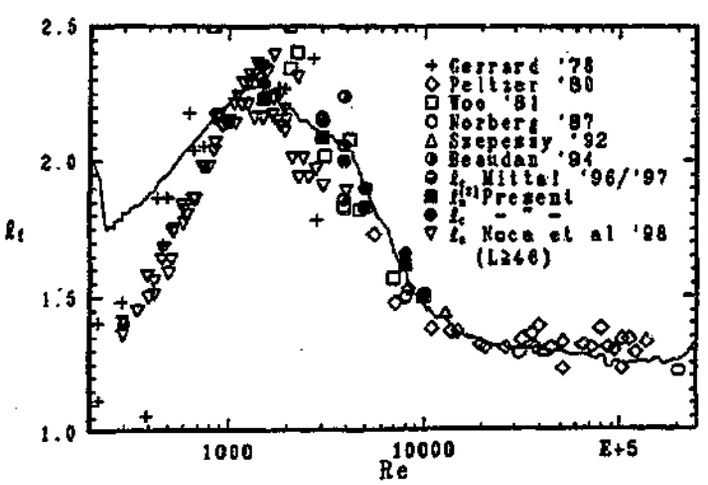

FIGURE 1-4 Variation of vortex formation length with Reynolds number. Reproduced from Norberg (1998).

The transition to turbulence within the boundary layers on the surface of the cylinder, or the TrBL regime, has long been associated with a "crisis" in the drag force. The drag "crisis" refers to a

sudden drop in the value of the mean drag and a corresponding drop in the base suction coefficient shown in Figure 1-1. During the pre-critical (TrBL0) regime, corresponding to the initial decrease in the drag force, the transition to turbulence occurs at the very end of the boundary layer along the spanwise separation line. The abrupt fall in the drag force at the transition between the TrBL0 and the TrBL1 regimes corresponds to the formation of a separation-reattachment bubble on one side fo the cylinder. If the Reynolds number is increased slightly, or if the flow is disturbed slightly, there is a second discontinuous drop in the drag force as a second reattachment bubble forms on the other side of the cylinder (TrBL2). After the reattachment bubbles the flow re-separates at separation angles of much greater than 90° resulting in the formation of a very narrow wake and a corresponding minimum value of the drag force. As Reynolds number increases further, or the flow is perturbed, the separation bubbles begin to break down and the drag begins to "recover" (super-critical regime). The post-critical regime, not shown in Figure 1-1, corresponds to a levelling out of the drag force and base suction coefficient.

1.2.2 Wake Instabilities

A stability analysis seeks to determine if a particular flow will become unstable and the nature of this instability. An impulsive infinitesimal perturbation, generally a delta function, is applied to the base flow of interest and the stability of the flow is determined by the development of a disturbance stream-function. A two-dimensional disturbance stream-function has the general form $\psi(x, y) = \phi(x, y)\exp\{i(kx-\omega t)\}$ and the governing equation is based on the linearised Navier-Stokes equation. The analysis generally seeks to determine the frequency or wavelength of the disturbance (real components of ω and k) at which the maximum temporal or spatial growth rate occurs (imaginary components of ω and k).

The way in which an instability develops is important in predicting the response of the flow to an applied perturbation and the regions of the flow that will be affected. The growth and control of instabilities within wakes has been discussed by a number of authors including, Monkewitz (1988), Huerre & Monkewitz (1990) and Rockwell (1990). These authors describe a number of different types of instabilities in terms of the response of the flow to the instability. Firstly, a flow in which an impulsively generated, small-amplitude disturbance grows can be defined as either absolutely or convectively unstable. The flow is absolutely unstable if the disturbance grows exponentially at the location of its generation. The flow is convectively unstable if the disturbance grows but is convected away from the source, ultimately resulting in the disturbance dying out at its original source. The term local instability indicates that only the "local" velocity profile is unstable with respect to the perturbation. If the whole flow field is contaminated by the response of the local flow field then, as described by Huerre & Monkewitz (1990), the flow field is locally absolutely unstable. A flow is globally unstable when the instability is present throughout the entire flow

field. The existence of a global instability implies the existence of an absolute instability, however the reverse is not true.

An absolutely unstable flow exhibits self-excited oscillations. An example of these self-excited oscillations is the periodic vortex shedding in the wake of a circular cylinder. An absolute instability does not tend to respond to external forcing, although large amplitude forcing may generate mode competition. Conversely, a convective instability is receptive to external forcing and will often lock-on to an applied perturbation.

1.2.3 Spanwise Coherence - Oblique / Parallel Shedding

It is generally assumed that the primary spanwise vortex core is parallel to the axis of the cylinder. However, as discussed in the review of Williamson (1996a), under certain conditions the vortex structures can form an oblique angle to the cylinder's axis. The occurrence of oblique shedding, as opposed to parallel shedding, can have a significant effect on the properties of the wake and the forces on the cylinder. Williamson (1988) found that oblique shedding altered the frequency of large-scale vortex shedding, while Prasad & Williamson (1997) found that oblique shedding caused a delay in the onset of the shear layer instability. Oblique shedding appears to be linked to discontinuities in the flow conditions at the ends of the cylinder. Consequently, in many experiments end plates are fitted to the cylinder to promote parallel shedding.

The wake properties also depend on the aspect ratio (L/D) of the cylinder. Norberg (1994) showed that at low aspect ratios the vortex shedding frequency, the onset of vortex shedding and the base suction coefficient all vary significantly with L/D. Additionally, he found that the effect of aspect ratio varied with Reynolds number and that the flow was particularly sensitive to reduced aspect ratios in the range $Re \approx 4 \times 10^3 - 10^4$, where aspect ratios as large as L/D = 60-70 are needed to approximate an infinite cylinder. However, in general for L/D > 7 when end plates are fitted the effect of aspect ratio becomes relatively small.

1.3 OSCILLATING CYLINDER: INTRODUCTION

Regular shedding of vortex structures from a bluff body results in the body experiencing a periodic force. This periodic forcing can excite the natural structural frequency of the body, resulting in vortex- or flow-induced motion. Vortex-induced vibrations (VIV) typically occur when the natural frequency of the wake approaches the natural structural frequency of the body. When a cylinder is oscillating in response to the flow-induced forcing the total forces on the cylinder differ significantly from those on a stationary cylinder. Examples of vortex-induced vibration are found both in natural and engineering structures and, in many cases, knowledge of the vibration of these structures is a critical design consideration. The vortex-induced motion of deep-sea riser tubes in a current is of significant interest to the off shore petroleum industry. Other cases where VIV is

important include flow over heat exchanges, the motion of bridges, overhead powerlines and chimneys due to wind, as well as marine structures such as tension leg platforms, which are subject to significant currents. VIV of natural structures such as tree branches, with and without leaves, grasses and seaweed is also common.

The force on a stationary cylinder is typically decomposed into the transverse lift force and the in-line drag force. Although the drag force on a stationary cylinder has a large mean component the amplitude of the fluctuating component of the drag force is significantly smaller than the amplitude of the fluctuating lift force on a stationary cylinder. Although the fluctuating component of the drag force on an oscillating cylinder can be significant, the study of vortex-induced motion is often simplified by considering only the transverse motion of the cylinder due to the fluctuating lift force.

The relationship between the vortex-induced motion and the wake of the oscillating body is complicated as these two factors are intrinsically inter-dependent; the flow depends on the motion of the cylinder and the motion of the cylinder depends on the flow. A common approach to simplifying this problem is to control, or force the oscillation of the body and examine the response of the wake to the defined motion. In general the vortex-induced motion of a cylinder is relatively sinusoidal and can be approximated by forcing a cylinder to oscillate with a pure sinusoidal motion at a constant amplitude and frequency. Typically, the effect of changing the frequency of oscillation is studied while the amplitude of oscillation and Reynolds number are held constant.

1.3.1 Lock-in

The terms "lock-in" or "lock-on" are used to describe the wake when the periodic shedding of vortex structures and the resulting fluctuating forces are synchronised with the motion of the body. The frequency of vortex shedding can be quantified by measuring the velocity within the wake or the lift force on the body. The periodic motion of the cylinder is described in terms of its normalised amplitude, A/D and frequency f_e/f_o, where D is the diameter of the cylinder and the excitation frequency f_e is normalised by f_o, the Kármán frequency of the stationary cylinder. The bounds of lock-in are generally defined to include all cases where the most energetic wake frequency coincides with the frequency of oscillation, see for example Stansby (1976), Karniadakis & Triantafyllou (1989) and Hall & Griffin (1993). When the vortex shedding, or wake frequency has a strong spectral peak, lock-in can easily be identified. However, the definition of lock-in is somewhat subjective as it depends on how and where the wake frequency is measured, therefore the exact boundaries of lock-in are not rigorously defined. Lock-in can be demonstrated schematically using a phase plot of the displacement of the body versus lift or wake velocity. In cases where the flow is not locked-on, the most energetic shedding frequency is often close, or equal to the Strouhal frequency of the stationary body.

Vortex-induced motion (VIV) is linked to a strong resonance between the flow and the structure. In general, VIV will not be sustained unless the motion of the body and the fluid forces are synchronised or locked-on. When the body is forced to oscillate, the wake is not necessarily locked-on to the oscillations, however lock-in is most likely to occur when the oscillation frequency is close to the natural Strouhal frequency. Secondary or tertiary lock-in can also occur when the cylinders motion is close to a harmonic of the Strouhal frequency, for example see the work of Stansby (1976). As discussed in the review paper of Griffin & Hall (1991), lock-in can occur in response to a variety of motions including transverse and in-line oscillations of a cylinder or the flow, as well as rotation of a cylinder. This investigation focuses on the interaction between the flow field and a circular cylinder, however many of the features associated with lock-in are observed over a wide range of bluff body geometries.

The range of lock-in for forced oscillations is generally shown as a function oscillation amplitude and frequency. As shown in Figure 1-5 from Karniadakis & Triantafyllou (1989), the range of frequencies over which lock-in is observed increases with the amplitude of oscillation. The general shape of the lock-in boundary shown in Figure 1-5 is consistent with a large body of experimental results, as discussed in the reviews of Pantazopoulos (1994) & Griffin & Hall (1991). Just outside the lock-in boundary there is a region where the flow is still receptive to the oscillation of the body and the frequency of oscillation is still present in the wake spectra.

For a freely oscillating body lock-in is defined as the range of reduced velocity over which the body responds to the flow and VIV occurs, where this range appears to depend on the structural frequency and damping of the body. Although the range of lock-in for both the forced and vortex-induced oscillations also varies with Reynolds number this effect has not been fully investigated.

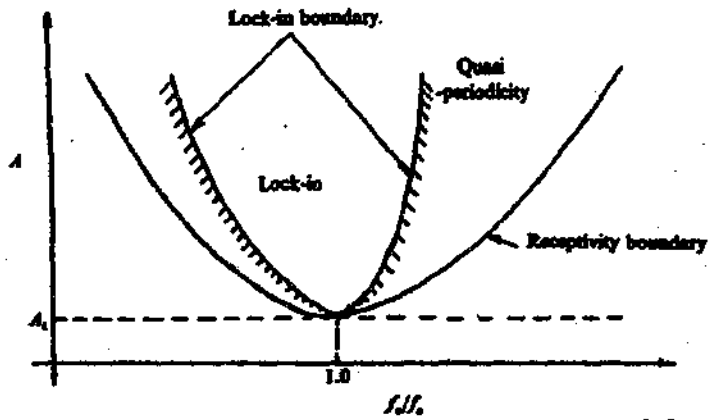

FIGURE 1-5 Schematic demonstrating bounds of lock-in. Reproduced from Karniadakis & Triantafyllou (1989)

When the wake becomes locked-on there is a shift in the frequency of vortex shedding away from the Kármán frequency. There is also significant modification of the wake, and within the receptivity region, the mode of vortex shedding may depart significantly from the Kármán street of

the stationary cylinder. The spanwise correlation of the wake, and therefore also the forces on the cylinder, are significantly affected by the motion of the cylinder. The compilation of results in Figure 1-6, reproduced from Pantazopoulos (1994), shows that for both forced and vortex-induced oscillations the spanwise correlation of shedding increases as the amplitude of oscillation increases. The variation of the spanwise correlation also depends upon the frequency of oscillation. The results of Toebes (1969), Figure 1-7 show significant increase in the spanwise correlation within the lock-in region at f_r' ($= f_e/f_o$) = 1.00, while outside the expected lock-in range at f_r' = 1.25 there is only a very small increase in the correlation length. It seems reasonable to expect that the spanwise correlation of the wake will vary within the lock-in region, and in particular may be a function of the mode of vortex shedding, however the extent of this variation is not known.

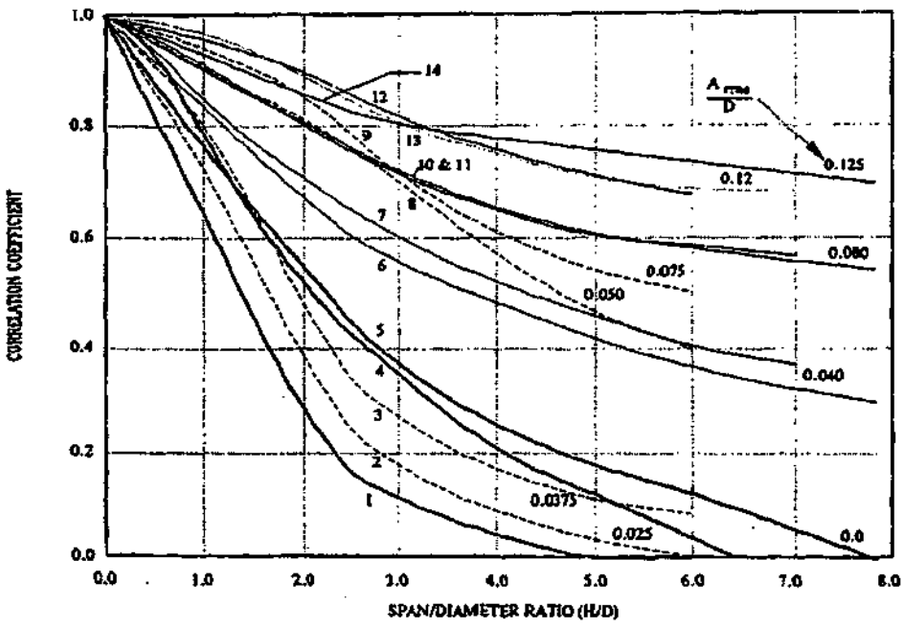

Curve no & Author	Comments
1. Howell-Novak	elastically-mounted, Re = 75,000, A/D = 0.0
2. Howell-Novak	elastically-mounted, Re = 75,000, A/D = 0.025
3. Howell-Novak	elastically-mounted, Re = 75,000, A/D = 0.0375
4. Toebes, (Wootton/Scruton paper)	pressure transducer & hotwire, uniform flow A/D = 0.0
5. Toebes	oscillating cylinder A/D = 0.0
6. Toebes	oscillating cylinder A/D = 0.4
7. Toebes, (Wootton/Scruton paper)	oscillating cylinder A/D = 0.4
8. Howell-Novak	elastically-mounted, Re = 75,000, A/D = 0.05
9. Howell-Novak	elastically-mounted, Re = 75,000, A/D = 0.075
10. Toebes, (Wootton/Scruton paper)	oscillating cylinder A/D = 0.8
11. Toebes	oscillating cylinder A/D = 0.8
12. Howell-Novak	elastically-mounted, Re = 75,000, A/D = 0.125
13. Toebes, (Wootton/Scruton paper)	oscillating cylinder A/D = 0.12
14. Toebes	oscillating cylinder A/D = 0.125

FIGURE 1-6 Correlation along the span of an oscillation cylinder for a range of oscillation amplitudes. Reproduced from Pantazopoulos (1994).

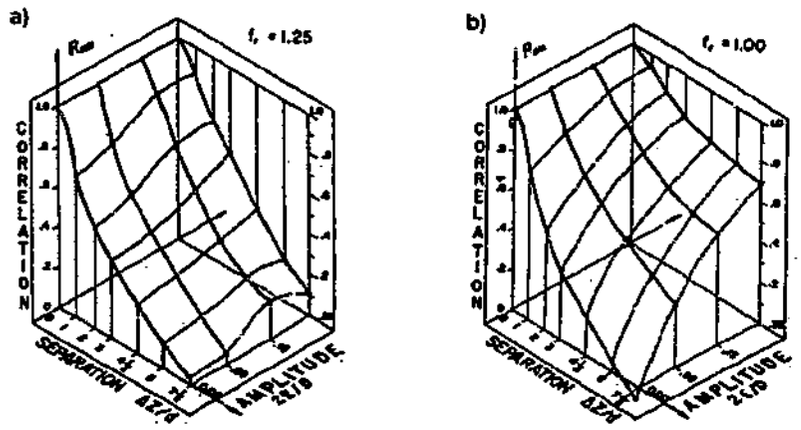

FIGURE 1-7 Variation of the correlation along the span of an oscillating cylinder with the amplitude of oscillation. a) Outside the lock-in range, $f_r = 1.25$ (equivalent to f_e/f_n) and b) at the centre of the lock-in range, $f_r = 1.00$. Reproduced from Toebes (1969)

1.3.2 Forces and Energy Transfer

When the wake is locked-on to the motion of the cylinder the dominant frequency in the lift force is f_e and the lift force is generally sinusoidal in nature. Thus, the lift force can be approximated by a sinusoidal function:

$$Lift(t) \approx (\tfrac{1}{2}\rho U^2 DL)\, C_L \sin(2\pi f_e t + \phi_{lift}) \qquad (1\text{-}3)$$

where C_L is the amplitude of the fluctuating lift coefficient and ϕ_{lift} is the phase of the lift with respect to the displacement of the cylinder $y(t)$. The correlation of the lift force with a sinusoidal signal ($\sin 2\pi f_e t$) is a measure of the accuracy of the approximation in equation 1-3.

When a body moves relative to the fluid there is an exchange of energy between the fluid and the body. The energy transfer is a time dependent variable

$$E(t) = \frac{d\vec{y}}{dt}(t) \cdot \vec{F}(t)$$

where energy transfer from the fluid to the body is defined as positive.

For a cylinder oscillating transverse to the free-stream it is convenient to define the total energy transfer per oscillation:

$$E = \int_{t=0}^{t=T} \vec{C}_L(t) \cdot \vec{V}(t)\, dt$$

where, $\vec{V}(t) = 2\pi f_e A \cos(2\pi f_e t)$, is the velocity of the cylinder and $T = 1/f_e$.

Therefore if we write the lift coefficient as: $C_L(t) \approx C_L \sin(2\pi f_e t + \phi_{lift})$ the normalised Energy transfer, C_E is approximated by

$$C_E \approx \pi C_L (A/D) \sin(\phi_{lift}) \qquad (1\text{-}4)$$

If the lift co-efficient is re-written in terms of the components which are in-phase and out-of-phase with the cylinders displacement, it is clear that the energy transfer is proportional to the out-of-phase component of the lift force:

$$\begin{aligned} C_L(t) &= C_L \sin(2\pi f_e t + \phi_{lift}) \\ &= [C_L \cos(\phi_{lift})] \sin(2\pi f_e t) + [C_L \sin(\phi_{lift})] \cos(2\pi f_e t) \\ &= C_{my} \sin(2\pi f_e t) - C_{dy} \cos(2\pi f_e t) \end{aligned} \qquad (1\text{-}5)$$

where C_{my} is the in-phase component of the lift force and C_{dy} is the out-of-phase component of the lift force. C_{my} is also commonly called the inertia co-efficient while C_{dy} is sometime referred to in the literature as the "drag coefficient". The out-of-phase component, C_{dy} should not be confused with the traditional definition of the drag force, which is the total force on the cylinder in-line with the free-stream. Consequently we will not refer to C_{dy} as the drag coefficient. C_{my} and C_{dy}, or equivalent coefficients, have been used in the literature to describe the lift force, however instead of evaluating C_{dy} we will consider the more physical quantity C_E.

The sign of the energy transfer can also be implied from the value of ϕ_{lift}: the energy transfer from the fluid to the cylinder is positive when $0° < \phi_{lift} < 180°$, otherwise the energy transfer is negative, i.e. from the cylinder to the fluid. The oscillation of an elastically mounted cylinder requires positive energy transfer. However, when the cylinder is forced to oscillate it is not subject to this constraint and all values of ϕ_{lift} are physically possible.

1.3.3 Relating Force and Vorticity

The analyses of Wu (1981), Noca (1997) and Leonard & Roshko (2001) demonstrated that the total fluid force on a body can be expressed as follows. Using the terminology of Leonard & Roshko (2001),

$$\vec{F}_{total} = \rho \frac{d}{dt} \int_{fluid} \vec{\omega} \times \vec{r}\, dV + \rho A_B \frac{d\vec{U}}{dt} \qquad (1\text{-}6)$$

where the volume integral is taken over the entire flow field and A_B is the surface bounding the solid body, in our case the cylinder. Without making the assumptions of potential flow, it is possible to demonstrate, via equation 1-6, that the "apparent mass" force on a circular cylinder is $-\frac{\rho \pi D^2}{4} \frac{dU}{dt}$, as demonstrated by Leonard & Roshko (2001). This expression, which includes the force due to the inertia of the fluid displaced by the cylinder and the force due to the "new" vorticity (sometimes also called the bound vorticity) generated by the acceleration of the cylinder, is valid in the presence of highly separated flow past the cylinder. Govardhan & Williamson

(2000) were the first to describe the consequences of force decomposition, into vortex and apparent mass components, in the interpretation of the phase and amplitude of the lift forces on a freely-vibrating cylinder. Using the present terminology, in essence, their decomposition is,

$$\vec{F}_{total}(t) = \vec{F}_{vortex}(t) + \vec{F}_{am}(t) \qquad (1\text{-}7)$$

in which the apparent mass force is given by:

$$F_{am}(t) = -\frac{\rho \pi D^2}{4}\frac{d^2 y}{dt^2}$$

where $y(t)$ is the displacement of the cylinder.

Therefore by subtracting F_{am}, the apparent mass force from F_{total}, the total fluid force the force due to the movement of vortex structures in the wake F_{vortex}, can be determined. Although F_{vortex} relates the force on a body to the vorticity field it is common to consider only F_{total}. The lift force coefficients can be written in the same fashion as equation 1-7:

$$\vec{C}_L(t) = \vec{C}_{Lvortex}(t) + \vec{C}_{Lam}(t) \qquad (1\text{-}8)$$

where $C_L(t)$ is the total lift force coefficient, $C_{L\,vortex}(t)$ is the component of the lift coefficient due to the vorticity field and $C_{L\,am}(t)$ is the apparent mass lift force coefficient. Govardhan & Williamson (2000) demonstrated that changes in the phase of the total lift force do not necessarily correspond to the changes in the phase of vortex shedding. They calculated the vortex lift force by subtracting the "potential added mass force", which for a circular cylinder is equivalent to $C_{L\,am}(t)$, from the total lift force. For an elastically mounted cylinder, they found that the jump in the phase of the vortex lift force did not occur at the same reduced velocity as the phase jump in the total lift force. The jump in the phase of the vortex lift force corresponded to a change in the phase of vortex shedding. However, the jump in the phase of the total lift force did not necessarily correspond to a significant change in the phase of vortex shedding.

The idea of identifying the force component due to wake was also examined by Lighthill (1986). Lighthill considered two force components: a) a force due to the potential flow, which varies linearly with the velocity field and includes the potential added mass force, and b) a non-linear, vortex force. In essence these two terms are F_{am} and F_{vortex} respectively, which have been evaluated above for the case of a circular cylinder.

For an oscillating cylinder it is common to consider only the properties of total lift force on the cylinder, $C_L(t)$. However, to relate the changes in the structure of the wake to the forces experienced by the cylinder the properties of the vortex lift force, $C_{L\,vortex}(t)$ must also be considered. The vortex lift force is calculated by subtracting the apparent mass force, $C_{L\,am}(t)$ from $C_L(t)$, as described by equation 1-8. The vortex lift is now expressed in the same way as the total lift in equation 1-3:

$$C_{L\,vortex}(t) \approx C_{L\,vortex} \sin(2\pi f_e t + \phi_{lift\,vortex}) \qquad (1\text{-}9)$$

where $C_{L\,vortex}$ is the amplitude of the vortex lift coefficient and $\phi_{lift\,vortex}$ is the phase of the vortex lift force with respect to the cylinders displacement. By definition $C_{L\,om}(t)$ is in-phase with the oscillation of the cylinder. Therefore the out-of-phase components of $C_L(t)$ and $C_{L\,vortex}(t)$ are equal and the energy transfer (equation 1-4) can be written in terms of either the total or vortex lift force:

$$C_E \approx \pi\, C_L\, (A/D) \sin(\phi_{lift}) = \pi\, C_{L\,vortex}\, (A/D) \sin(\phi_{lift\,vortex}) \qquad (1\text{-}10)$$

Thus, the energy transfer is positive when $0° \leq \phi_{lift} < 180°$ and $0° \leq \phi_{lift\,vortex} < 180°$.

Equation 1-6 provides a useful tool for interpreting the flow field. However, using equation 1-6 to calculate the force on the body requires evaluation of the entire vorticity field. As outlined by Noca *et al* (1997, 1999), Noca (1997) and the extensive review of Wu & Wu (1996), methods have recently been developed to evaluate the force on a body using finite and arbitrarily chosen regions of the flow field. The work of Noca et al (1997, 1999) reformulates equation 1-6 into three different forms described as the impulse, momentum and flux equations. Each of these equations allows the force on a body can be calculated using only the velocity field within a finite domain containing that body. These formulations were then applied to the problem of an oscillating cylinder at $Re = 392$, where the velocity field was calculated numerically using a two-dimensional simulation. As shown in Figure 1-8 all three methods were reasonably successful in replicating the lift force on the body, with the relative performance of the methods depending on the resolution of the grid and the velocity field.

FIGURE 1
force on t
calculated
from Noca

FIGURE
field ···
al (1997

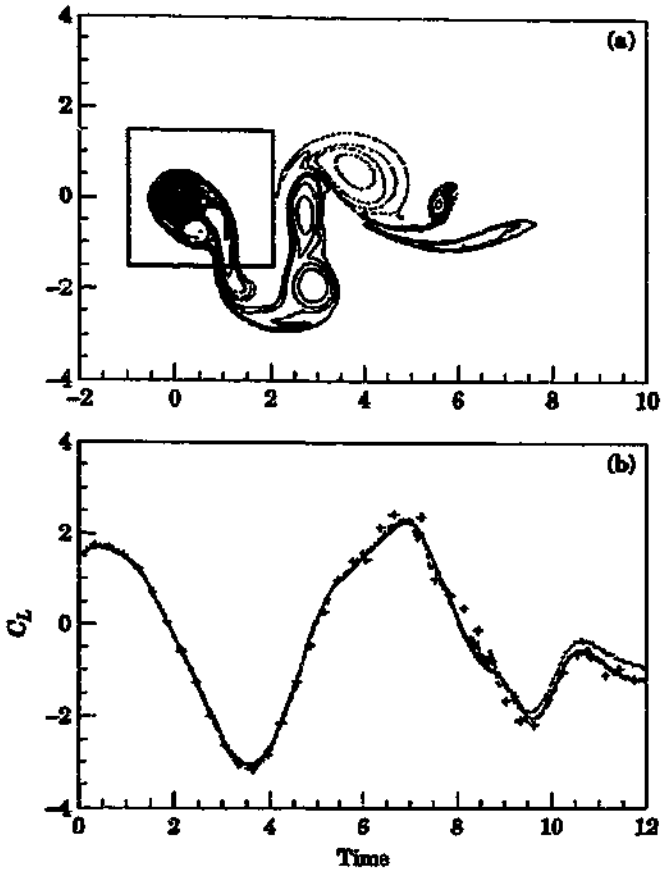

FIGURE 1-8 a) The 2D vorticity fields within the bounding box were used to compute b) the lift force on the cylinder, Re = 392. The three different methods used were compared with the force calculated from the pressure and shear stress on the body: represented by the solid line. Reproduced from Noca et al (1997).

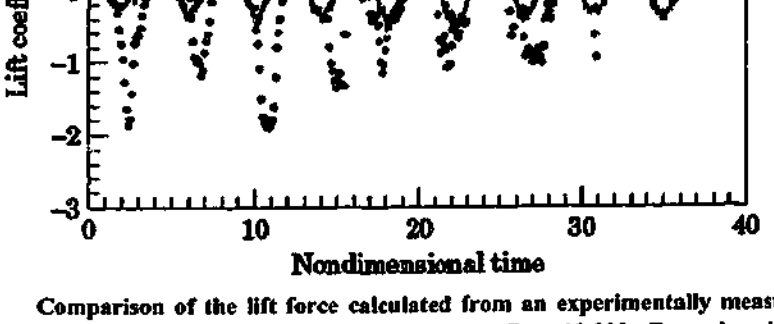

FIGURE 1-9 Comparison of the lift force calculated from an experimentally measured vorticity field ···· with the lift force measured by a force balance ——, Re = 19,000. Reproduced from Noca et al (1997).

However, these methods are less successful when applied to a two-dimensional slice of a fully three-dimensional flow. In Noca *et al* (1997) the "impulse equation" was used to calculate the force on an oscillating cylinder at Re = 19,000, using a two-dimensional slice of the velocity field measured experimentally using DPIV. The forces calculated from the velocity field were then compared with the span-averaged forces on the cylinder measured by a force balance. Although, as shown in Figure 1-9, the calculations were able to capture the average period of the measured lift force, they did replicate the amplitude of the lift force or small variations in phase. The inaccuracy of the calculations was attributed to the three-dimensional nature of the velocity field. Noca *et al* (1999) applied the same method to an oscillating cylinder at a reduced Reynolds number of 100, where the velocity field becomes approximately two-dimensional. The drag force calculated from the velocity fields measured using DPIV was found to compare well with the drag force measured experimentally with a force balance. Presumably measurements and calculations of the lift force for the quasi two-dimensional field would be similarly successful.

These investigations indicate that when the flow conditions are favourable the velocity field can be used to accurately predict the force on a body. In particular, if the lift and drag forces are to be calculated from a two-dimensional slice of a velocity field, this slice must fully represent the entire field, i.e. the velocity field must be two-dimensional. The theoretical equations for calculating the forces can easily be expanded to incorporate a three-dimensional velocity field. However, this path is best pursued numerically, as obtaining the necessary three-dimensional velocity fields experimentally is, at this stage, prohibitively difficult.

1.4 FORCED CYLINDER OSCILLATIONS

When a cylinder is forced to oscillate relative to a free-stream the wake responds to the large-scale motion of the structure. In most cases the cylinder is forced to oscillate relative to the free-stream, however the wake can also be forced by oscillating the free-stream relative to a stationary cylinder. Examples of this type of interaction include: the acoustic perturbation of flow by an external noise source, see Blevins (1985), the feedback generated when the flow structures shed from a body interact with a large downstream body, as discussed by Unal & Rockwell (1987), or marine structures that are subject to periodic wave motion.

The "free-stream" component of the velocity is most commonly generated by continuous flow past a body whose mean position does not vary. Alternatively, the "free-stream" can be generated by towing the body at a constant velocity though a tank of stationary fluid. In terms of relative flow past a body these methods are equivalent, however each method has particular benefits and limitations. The careful use of a towing tank reduces the free-stream turbulence to negligible levels, but the length of the towing tank limits the number of oscillations per experiment. When the flow is generated by external means, such as in a recirculating water channel or wind tunnel, there is effectively no limit on the number of oscillations per experiment, but it is difficult to achieve low turbulence levels.

The oscillation of a body relative to a mean velocity can be achieved in 3 ways:

1. The body oscillates relative to a constant external velocity.
2. The body is held stationary and is subject to an external flow with both mean and oscillatory components.
3. The body moves with variable velocity (consisting of mean and oscillatory components) through a stationary fluid.

As discussed by Lighthill (1954), these three cases can be evaluated in a common reference frame and are equivalent if the flow field is uniform. The displacement of the fluid as the body oscillates relative to the flow causes an inertial force that generates an opposing fluctuating pressure gradient around the body, and corresponding changes in the flow. The fluctuating pressure force is transmitted to the body via pressure waves at the speed of sound. When the wavelength of the acoustic waves is long relative to the length scale of the body, as is generally the case, the transmission of the pressure fluctuations is approximately instantaneous and effectively cancels out the inertia force. Thus, oscillating the body is equivalent to oscillating the flow around the body. A number of studies have considered the case of a stationary cylinder in a fluctuating free-stream. Barbi et al (1985) and Armstrong & Barnes (1986) found that the stationary cylinder wake locks-on to the fluctuations of the free-stream in a similar fashion to the lock-in observed for an oscillating cylinder.

Vortex-induced motion of a body will generally have both transverse and in-line components. However, the flow-induced motion of a cylinder is often simplified by considering only one component of this motion. In these experiments, as in many previous studies, we will consider a cylinder oscillating transverse to the free-stream. As the frequency of forced oscillation, f_e is varied relative to the natural frequency of the stationary cylinder f_o, there are significant changes in both the structure of the near wake and the forces on the cylinder.

1.4.1 Characteristic Features of Forces

A simultaneous jump in the amplitude and phase of the lift force at $f_e/f_o \approx 1$, was first identified by Bishop & Hassan (1963) and has subsequently been observed both experimentally and numerically by a number of investigators, including Moe & Wu (1990), Gopalkrishnan (1993), Staubli (1993a & b), Sarpkaya (1995), Zderi *et al* (1995), Dalheim (1997), Hover et al (1998) Blackburn & Henderson (1999) and Carberry *et al* (2001). The jump in the phase and amplitude of the lift force has been observed over a wide range of flow conditions: Reynolds numbers ranging from 500 to 60,800, amplitudes of oscillation varying from $A/D = 0.11$ to 7.0 and for both experimental results and two-dimensional numerical simulations. A smaller jump in the phase of the lift force was also observed at supercritical Reynolds numbers, $Re = 0.8\text{-}3.0\times10^6$ and $A/D = 0.012$, by Szechenyi & Loiseau (1975). In many cases the results have been plotted in terms of C_{my} and C_{dy}, as defined in equation 1-5, rather than the phase and amplitude of the lift force. However, these two sets of variables are equivalent and C_L and ϕ_{lift} can easily be calculated from C_{my} and C_{dy}.

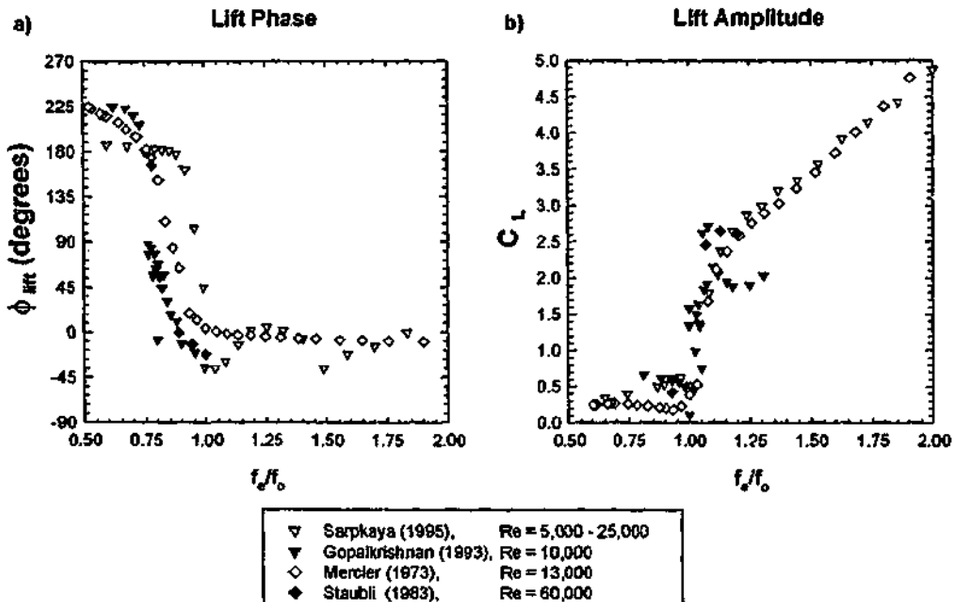

FIGURE 1-10 Compilation of previous data showing the variation of a) the phase of the lift force and b) the amplitude of the lift force with the frequency of oscillation. In all cases the amplitude of oscillation was A/D = 0.5.

A selection of the previous results at $A/D = 0.5$ is shown in Figure 1-10 (a & b), where ϕ_{lift} and C_L respectively are plotted against f_e/f_o for a range of Reynolds numbers between 5000 and 60,000. Each individual set of data shows and abrupt change, or jump in ϕ_{lift} and a corresponding jump in C_L at the same frequency of oscillation. However, between the different data sets there is some variation in the frequency at which the jump occurs. The source of this variation is not well understood, however it may be attributable to changes in the Reynolds number and the level of free-stream turbulence. The simultaneous jump in the both phase and amplitude of the lift force suggests that around $f_e/f_o \approx 1$ there is a significant change in the structure of the wake. Moreover, the large jump in the properties of the lift force suggests that either side of the jump there are at least two distinctly different wake states. One of the aims of this work is to confirm this hypothesis.

The data sets shown in Figure 1-10 show a relatively smooth variation in the phase and amplitude of the lift properties, with a number of data point exhibiting intermediate values between those exhibited either side of the jump. The existence of these intermediate values raises some interesting questions about the nature of the transition between the states observed either side of the jump. For example it is not known if these intermediate values represent a smooth change in the force properties with f_e/f_o or an intermittent transition. The nature of the transition corresponding to the jump in the lift force is an unresolved issue that will be examined further in this work.

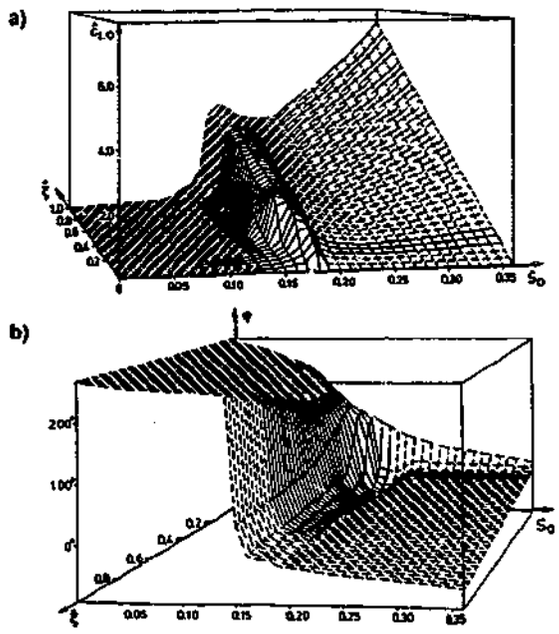

FIGURE 1-11 a) The amplitude of the lift coefficient, C_{LO} and b) the phase of the lift force, φ versus both the oscillation Strouhal frequency, S_o and amplitude of oscillation, ξ (equivalent to A/D). Reproduced from Staubli (1983a).

Similar variations in ϕ_{lift} and C_L as the frequency of oscillation is varied have been reported at both lower and higher amplitudes of oscillation. The carpet plots of Staubli (1983a), shown in Figure 1-11, demonstrate that the jump in ϕ_{lift} and C_L occurs for a wide range of oscillation amplitudes.

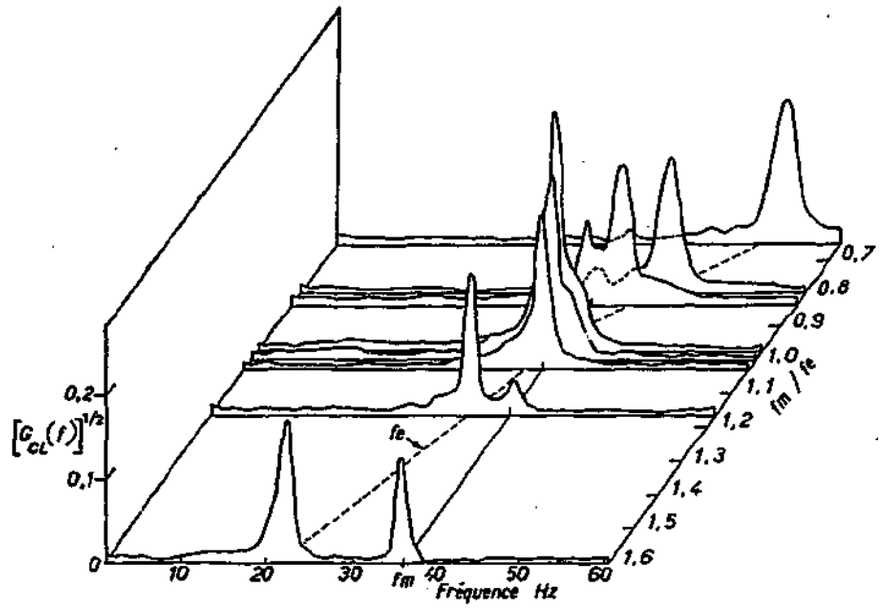

FIGURE 1-12 Variation of the spectral energy of the lift force G_{CL} with the frequency of oscillation f_e for an amplitude of the oscillation of A/D = 0.012 at Re = $2x10^6$. There are two peaks in the spectral energy one at f_e and one close to the Kármán frequency of the stationary cylinder f_m (equivalent to f_{nos}). Reproduced from Szechenyi & Loiseau (1975).

The frequencies present in the wake are generally determined by measuring either the time variations of the velocities within the near wake or the lift force. Examination of equations 1-6 and 1-7 show that the vortex lift force can be expressed in terms of the rate of change of the horizontal vortex moment integrated over the entire vorticity field. Thus, there is a strong correlation between the fluctuations in the wake due to large scale vortex shedding and the variations in the vortex lift force. A local maximum in the vortex lift force represents a peak in the rate of change of the horizontal vortex moment, which is generated by the movement of positive vorticity in the downstream direction (or negative vorticity upstream). Similarly, a local minimum in the vortex lift force corresponds to the maximisation of the rate of change of the negative vortex moment due to the movement of negative vorticity downstream. Although, there is generally a strong correlation between the peaks in the vortex lift force and large-scale vortex shedding these two events do not necessarily occur at the same point in time. Moreover, when the variation of the total lift force on the body is considered there is a second component, the additional mass term described in section 1.3.3 that is in-phase with the acceleration of the body relative to the flow.

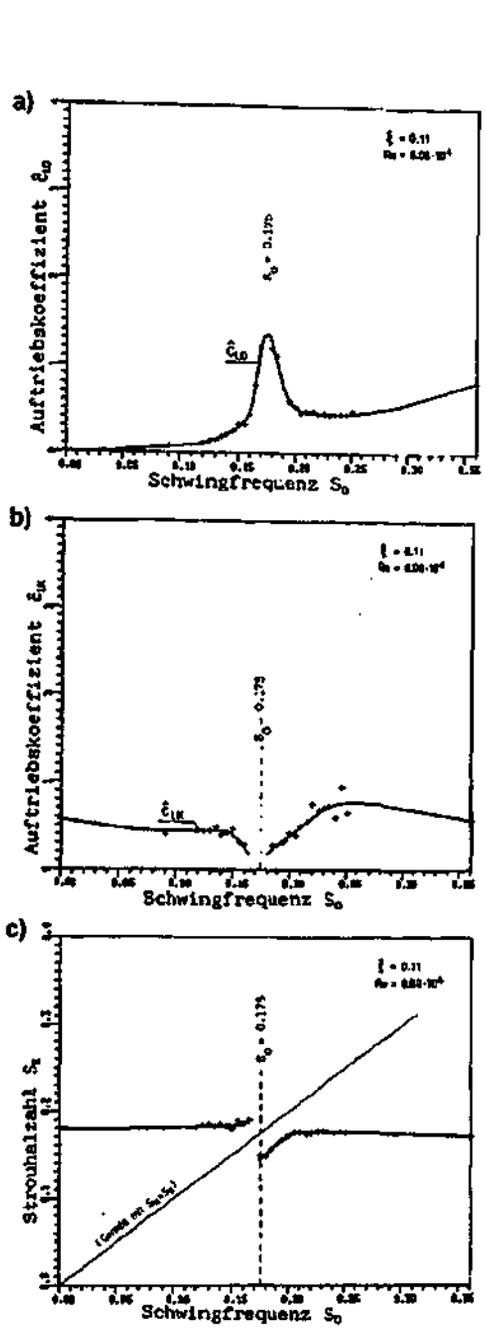

FIGURE 1-13 Variation with the Strouhal frequency of oscillation of a) the component of the lift force at the frequency of oscillation, b) the component of the lift force at S_K (equivalent to the Strouhal number of f_{nos}) and c) the frequency of the spectral peaks at S_K. Reproduced from Staubli (1983a).

When the wake is locked-on to the oscillation of the cylinder the dominant frequency in the wake is the frequency of oscillation f_e. However, in many cases there is an additional frequency, designated f_{nos}, which is present in the wake, where f_{nos} is not a harmonic or sub-harmonic of f_e. The value of f_{nos} is close to, but not necessarily equal to, the natural Kármán frequency of the stationary cylinder wake and it appears that f_{nos} is linked to the natural frequency of the oscillating wake. The spectral peak at f_{nos} has been observed by a number of authors including Staubli (1983a) and Szechenyi & Loiseau (1975). As shown in Figure 1-12, the value of f_{nos} and the relative strengths of the spectral

peaks at f_{nos} and f_e are a function of the oscillation frequency. The frequencies f_{nos} and f_e converge and then diverge as f_e/f_o increases through unity. Additionally, the amplitude of the peak at f_{nos} decreases as f_e approaches f_o and very close to $f_e/f_o = 1$ the f_{nos} peak is not detectable. In Figures 1-13 (a & b) the variation of the amplitude of the peaks at f_e ($\hat{C}_{LO}$) and f_{nos} ($\hat{C}_{LO}$) are plotted as a function of oscillation frequency ($S_o = f_oD/U$). As the frequency of oscillation approaches the Kármán frequency ($S_o = 0.175$) from either above or below, there is a transfer of the energy in the wake from f_{nos}($\hat{C}_{LK}$) to f_e($\hat{C}_{LO}$). This is consistent with the variation of the lift spectra in Figure 1-12. The natural frequency of the oscillating cylinder f_{nos} is close to the Kármán frequency, f_o however, as shown in Figure 1-13c f_{nos} varies with the frequency of oscillation, particularly as f_e approaches f_o.

The amplitude of oscillation strongly influences the susceptibility of the wake to the forced oscillations, and at larger values of A/D the wake is much more likely to become locked-on to the oscillations. Additionally, the results of Staubli (1983a) indicate that when the wake is locked-on the forces on the cylinder vary systematically with the amplitude of oscillation, as shown by the variation of ϕ_{lift} and C_L with A/D (ξ) and f_e/f_o (S_o) in Figure 1-11. As A/D increases there is an increase in the magnitude of the change in both ϕ_{lift} and C_L (i.e. ΔC_L and $\Delta\phi_{lift}$) during the jump. At low A/D the variation of C_L with f_e/f_o in Figure 1-11 takes on the character of a resonance peak around $f_e = f_o$, similar to that observed by Blackburn & Melbourne (1997) at very low amplitudes of oscillation ($A/D = 0.027 - 0.098$). As discussed in section 1.3.3 the lift force is made up of two components: the lift due to the vorticity field, $C_{L\,vortex}$(t) and $C_{L\,am}$(t), apparent mass force due to the relative acceleration of the cylinder. The amplitude of the fluid inertia force, $C_{L\,am}$ varies linearly with the amplitude of oscillation. However, due to variations in the phase and amplitude of the vortex lift force the amplitude of the total lift force does not necessarily increase with increasing A/D.

Figure 1-11 shows that at low oscillation frequencies before the jump ($f_e < f_o$) the values of ϕ_{lift} appear to increase through 180° as A/D increases. Whilst for frequencies above the jump ($f_e > f_o$), as A/D increases there is a decrease in the total lift phase and ϕ_{lift} moves towards, and possibly through, 0°. When the total lift phase moves out of the region $0° < \phi_{lift} < 180°$ the energy transferred to the cylinder changes from positive to negative. Thus, the variation of ϕ_{lift} with A/D, shown in Figure 1-11, indicates that changing the amplitude of oscillation can alter the direction of energy transfer.

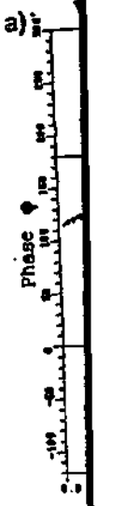

FIGURE 1-
lift force φ
component

The jump i
However, t
indicates th
smaller val
values at m
and C_L and
effect of
extensively
have a sec

The work
$C_{D\,mean}$ dep
systematic
amplitude
occurs at
$C_{D\,mean}$ ar
(1973), G

converge
eak at f_{max}
Figures 1-
otted as a
aches the
rgy in the
Figure 1-
uency, f_o
arly as f_e

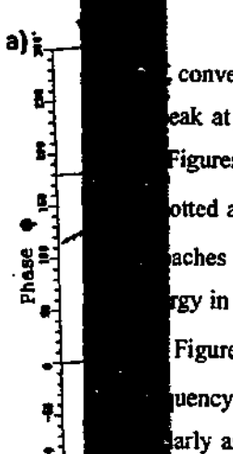

e forced
on to the
ocked-on
n by the
ere is an
ump. At
nce peak
itudes of
o of two
ue to the
linearly
e of the
creasing
s of ϕ_{lift}

FIGURE 1-
lift force φ
component

The jump i
However,
indicates th
smaller val
values at m
and C_L and
effect of
extensively
have a sec

The work
$C_{D\,mean}$ dep
systematic
amplitude
occurs at
$C_{D\,mean}$ ar
(1973), G

$(f_e > f_o)$,
possibly
nsferred
nown in
energy

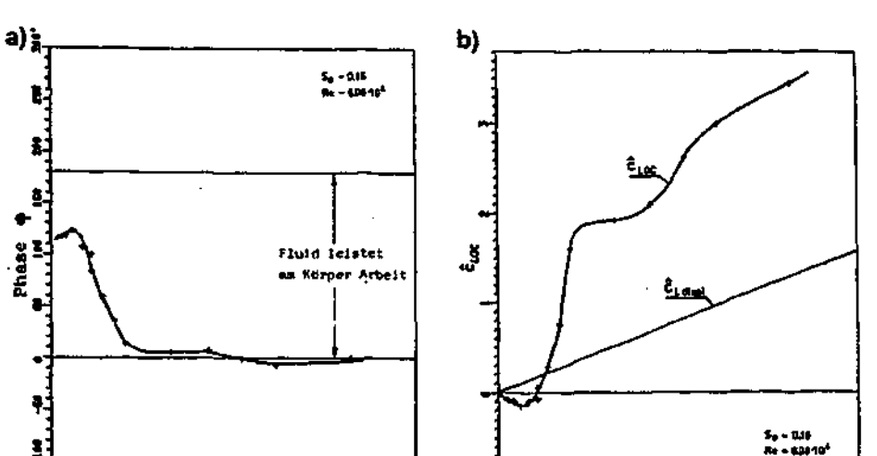

FIGURE 1-14 Variation with the amplitude of oscillation ξ (equivalent to A/D) of a) the phase of the lift force φ (equivalent to ϕ_{lift}) and b) the amplitude of the lift force C_{LOC}. Where C_{LOC} is the component of the lift force at the oscillation frequency. Reproduced from Staubli (1983a).

The jump in the lift force is generally considered as depending upon the frequency of oscillation. However, the variation of ϕ_{lift} and C_L with A/D shown in Figure 1-14 at a constant value of f_e indicates that the point at which the jump in the lift force occurs is also a function of A/D. At smaller values of A/D the amplitude and phase of the lift force in Figure 1-14 are consistent with values at much lower frequencies of oscillation, but as A/D is increased there is a jump in both ϕ_{lift} and C_L and the values are now consistent with those at much higher frequencies of oscillation. The effect of the amplitude of oscillation on the point at which the jump occurs has not been extensively studied and compared with the effect of varying f_e/f_o, the variation of A/D appears to have a second order effect.

The work of Sarpkaya (1978), shown in Figure 1-15, indicates that the mean drag on the cylinder, $C_{D\,mean}$ depends on both f_e/f_o and A/D. As A/D in creases from 0.25 to 0.84 in Figure 1-15 there is a systematic increase in the value of $C_{D\,mean}$ at a given oscillation frequency. While for a constant amplitude of oscillation the value of $C_{D\,mean}$ shows a strong peak around $f_e = f_o$. The peak in $C_{D\,mean}$ occurs at the same point as the jump in the phase and amplitude of the lift force. The peak in $C_{D\,mean}$ around $f_e/f_o \approx 1$ is consistent with the findings of a number of authors including Mercier (1973), Gopalkrishnan (1993), Anagnostopoulos (2000).

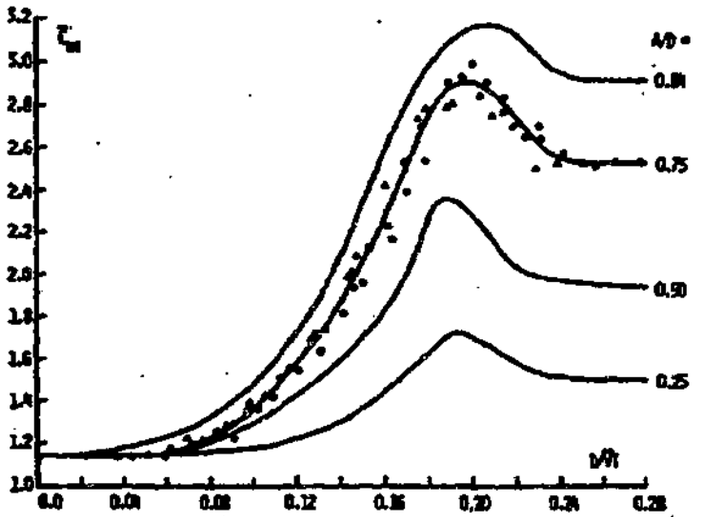

FIGURE 1-15 Variation of the mean drag coefficient C_m (equivalent to $C_{D\ mean}$) with the Strouhal frequency of oscillation, for a range of oscillation amplitudes. Reproduced from Sarpkaya (1978).

1.4.2 Characteristic Features of Wake Modes

The general form of the fluid structures shed into the near wake is often described in terms of the mode of vortex shedding. An oscillating cylinder exhibits a number of different shedding modes as described by the extensive mapping of Williamson & Roshko (1988). The Williamson & Roshko map, shown in Figure 1-16, was obtained over a range of Reynolds numbers, 300<Re<1000, but the shedding regimes are generally expected to persist over a wider range of Reynolds numbers. The map in Figure 1-16 indicates that for our investigation at oscillation amplitudes of 0.6 and below, at frequencies around $f_e = f_o$, we would expect to observe the 2S and 2P shedding modes. The 2S and 2P shedding modes are shown schematically in Figure 1-17. For the 2S mode two single vortices of opposite sign are shed per oscillation, resulting in the formation of the classical Kármán street. The 2P mode corresponds to the shedding of two counter-rotating pairs, or a total of four vortex structures, per oscillation.

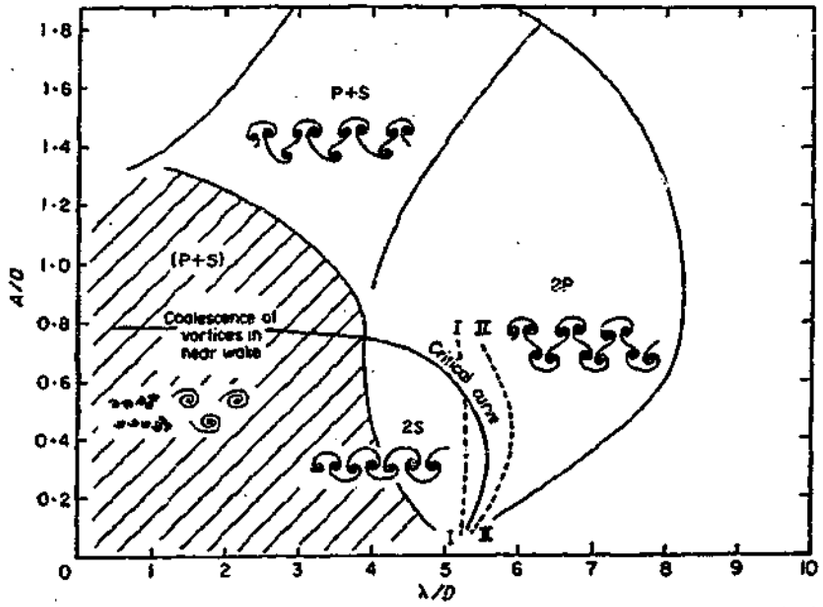

FIGURE 1-16 Map of vortex synchronisation patterns near the fundamental lock-in region. Reproduced from Williamson & Roshko (1988)

FIGURE 1-17 Schematic showing the 2S and 2P modes of vortex shedding. Reproduced from Williamson & Roshko (1988).

As f_e/f_o increased though unity Williamson & Roshko (1988) observed a change in the mode of vortex shedding from 2P to 2S. The investigations of Ongoren & Rockwell (1988a) and Gu *et al.* (1994) also considered the variation of the wake as f_e/f_o increased through unity, focusing on the changes in the phase referenced structure of the near wake. In both these investigations the phase point at which the flow fields were compared corresponded to the maximum displacement of the cylinder. The phase referenced flow fields in Figures 1-18 and 1-19 show that at approximately $f_e/f_o = 1$ there is a "switch" in the sign of the vortex closest to the cylinder, known as the initial vortex. The change in the sign of the initial vortex implies a significant change in the phase of vortex shedding. Whilst the terminology "the switch" was originally applied to a change in the sign of the initial vortex, it is now more widely applied to a large change, or "switch", in the phase of vortex shedding. In Figure 1-18 the switch occurs between $f_e/f_o = 1.00$ and 1.05, while in Figure 1-19, at a slightly different *A/D* and *Re*, the switch occurs between $f_e/f_o = 1.10$ and 1.12. Ongoren & Rockwell (1988a) observed that as the frequency of oscillation increases towards the switch, there is a "substantial decrease in vortex formation length" and that "a necessary condition for the switch to occur is attainment of a minimum of the vortex formation length". This statement implies that there is an increase in the formation length after the switch. However, as will be discussed in section 3.3.1, this point is open to interpretation.

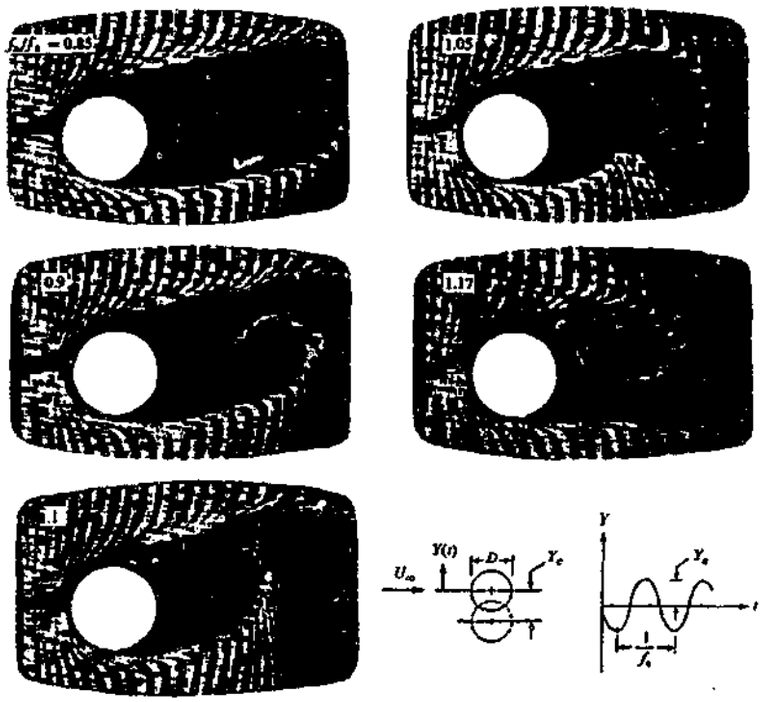

FIGURE 1-18 Effect of forced excitation frequency f_e to natural shedding frequency f_o on the near wake structure, for A/D = 0.13 at Re = 855. All photos taken at maximum negative displacement of the cylinder. Reproduced from Ongoren & Rockwell (1988a).

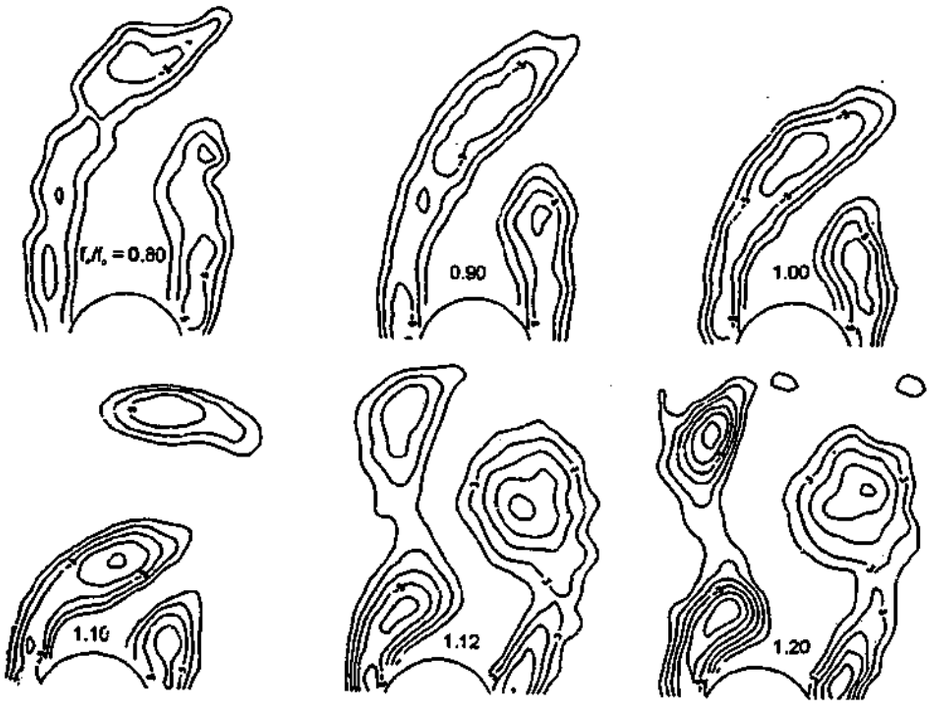

Figure 1-19 Figure 3 Gu *et al.* (1994), A/D = 0.2 and Re = 185

The images from Ongoren & Rockwell (1988a) in Figure 1-18 show that for f_e/f_o below the switch the initial vortex contained within the (black) formation region comes from the upper surface of the cylinder. As f_e/f_o increases the phase referenced position of the initial vortex contracts towards the back of the cylinder. After the switch the phase-referenced initial vortex is formed from the lower surface of the cylinder. The vorticity fields of Gu *et al.* (1994), shown in Figure 1-19, reveal more clearly the nature of the vortex structures. Note: the images in Figure 1-19 were acquired at the extreme left hand side of the oscillation and, compared to the images in Figure 1-18, are at the opposite extreme point of the oscillation cycle. Before the switch the right hand positive vortex is the initial vortex and as f_e/f_o increases there is a decrease of the formation, or wake length, until a "limiting position is reached". After the switch between f_e/f_o = 1.10 and 1.12 the phase-referenced structure of the near wake is clearly different and the initial vortex is now the negative left hand vortex. The switch in the initial vortex indicates that between f_e/f_o = 1.10 and 1.12 there is a significant shift in the phase of vortex shedding, however the magnitude of the phase shift can not be determined from these images as they were acquired at a single phase point.

The evaluation of the wake formation length using flow visualisation also requires careful definitions. The hydrogen bubble visualisation of Ongoren & Rockwell (1988a) does not show the finer structures in the near wake and it appears that the formation length increases after the switch. The more detailed PIV images of Gu *et al.* (1994) suggest there is an increase in the attached wake

length, as the vortices that are about to be shed into the wake remain attached to the cylinder. However, the phase referenced position of the concentration of vorticity immediately behind the cylinder contracts as frequency increases both above and below the switch. The single phase-referenced images in Figures 1-18 and 1-19 are not able to resolve more subtle changes in the phase of vortex shedding. For example, it is not possible to tell whether or not the gradual changes in the wake length are linked to changes in the phase of vortex shedding.

Interestingly, at the relatively low values of A/D and Re investigated by Ongoren & Rockwell (1988a) and Gu *et al.* (1994), the change in the phase of vortex shedding does not correspond to a change in the mode of vortex shedding and the 2P mode of shedding is not evident at lower f_e/f_o. Although the mode of vortex shedding either side of the switch appears to be 2S there are subtle changes in the structure of the near wake. In particular, after the switch, the upper shear layer does not extend across the back of the cylinder and the lower wake tends to angle further away from the centre-line. When the cylinder is forced at frequencies much lower or higher than $f_e/f_o \approx 1$ Ongoren & Rockwell (1988a) found that the vortex shedding can lock-on to a harmonic or sub-harmonic of f_o. In these cases the mode of vortex shedding can depart significantly from the modes observed around $f_e/f_o = 1$.

1.4.3 Link Between Forces and Wake Modes

The investigations considered in sections 1.4.1 and 1.4.2 all suggest that around $f_e/f_o \approx 1$ there are significant changes in the flow over an oscillating cylinder. A number of events have been independently observed at $f_e/f_o \approx 1$: a change in the sign of the initial vortex, or a large change in the phase of vortex shedding, a change in the mode of vortex shedding, a peak in the mean drag force as well as a jump in both the phase and amplitude of the lift force.

The two-dimensional numerical investigation by Blackburn & Henderson (1999) at Re = 500 and $A/D = 0.25$, detected many of the features observed experimentally. At a frequency ratio of just below one they found a simultaneous jump in the phase and amplitude of the lift force. The classical 2S modes of shedding were observed either side of the jump. Although the general mode of vortex shedding for these two cases was 2S, there were subtle differences in the structure of the near wake and in particular the phase of vortex shedding. In addition to the 2S modes, at frequencies just below the jump they observed additional mode branches with unusual asymmetric modes of vortex shedding. Importantly they were able to establish a link between the jump in the lift force and a change in the "phase relationship between vortex formation and cylinder motion". A link between the jump in the phase and amplitude of the lift force and the changes in the mode and phase of vortex shedding, at $f_e/f_o \approx 1$, is yet to be conclusively demonstrated for a fully three-dimensional wake.

1.4.4 Non-Transverse Forced Oscillations

This investigation focuses on a transversely oscillating cylinder, however a number of insightful investigations have considered other displacement profiles. To relate the forced oscillations to a structure that is free to oscillate in 2-dimensions, such as a cable, the most obvious profile involves motion in both the transverse and streamwise directions. However, the relative phase and amplitudes of the streamwise and transverse components of the motion means that there are a large number of motion profiles available to the body. The forced oscillation of a cylinder in both the streamwise and transverse directions has not been extensively investigated. Preliminary investigations of this problem by Jeon & Gharib (2000), found that for a transverse oscillation of $A/D = 0.5$ a Figure-8 motion with an in-line component of $A/D = 0.1$, had a significant effect on the phase of vortex shedding.

A number of investigations have also considered non-transverse, single degree of freedom oscillations, which are in-line with, or angled across the free-stream. Ongoren & Rockwell (1988b) observed that depending on the frequency of oscillation the in-line oscillation of the cylinder produced both symmetric and anti-symmetric modes of vortex shedding. The symmetric shedding involves in-phase shedding of vortices from either side of the cylinder, while the anti-symmetric shedding is characterised by alternate, out-of phase shedding of vortices from either side of the cylinder. An example of anti-symmetric shedding is the classical Kármán mode. In general these modes were unlike those observed for a stationary or transversely oscillating cylinder. Also, at many frequencies of oscillation mode competition and switching between symmetric and ant-symmetric modes of shedding were observed. A number of these modes demonstrated period doubling relative to the classical Kármán mode, thus the frequency of vortex shedding is synchronised with the frequency of the fluctuating in-line drag force. This is consistent with the results of Barbi et al (1986), who found that that for in-line flow oscillations with $f_e/f_o > 1$, the frequency of vortex shedding was locked-on to approximately twice the stationary Kármán frequency.

Ongoren & Rockwell (1988b) also considered oscillations at four different angles to the free-stream flow: 0°(in-line), 45°, 60° and 90°(transverse). As the oscillation angle moved from 90° towards 0° the tendency of the wake to switch from an anti-symmetric mode to a symmetric mode increased. When the wake was oscillating at angle of 45° or 60° the general structure of the wake tended to be parallel with the free-stream. This suggests that when the motion of the cylinder is neither in-line nor transverse it may still be appropriate to define the axes of the lift and drag forces relative to the free-stream direction, rather than the motion of the cylinder. The question of how to define the lift and drag axes is particularly relevant to the problem of a tethered body.

1.4.5 Non-Circular Bluff Bodies

The point at which flow separates from a cylinder is determined by the pressure gradient along the surface. When the geometry of the surface has a sharp edge the flow tends to separate at a fixed location. However, for a cylindrical shape the point at which the flow separates varies not only with free-stream conditions but also during the shedding cycle. The oscillation of the cylinder tends to increases the variation in the flow separation point.

The oscillation of bodies with well-defined separation points has been studied by a number of authors including Ongoren & Rockwell (1988a), Staubli & Rockwell (1989), Lotfy & Rockwell (1993) and Deniz & Staubli (1997, 1998). Ongoren & Rockwell (1988a) found that bodies with triangular, square and circular cross sections all have a threshold value of oscillation frequency at which the "near wake structure breaks into a new mode". For the circular and triangular cross-sections Ongoren & Rockwell observed a switch in the sign of the initial vortex and a corresponding change in the phase of the "vortex arrival" of approximately π at $f_e/f_o \approx 1$. Both the circular and triangular cross-sections had a relatively short "after body" length. However, the square cross-section had a longer after body length and as f_e/f_o increased the flow reattached to the side of the body. In this case there was not a clear switch in the timing of vortex shedding. From this work is not clear if the longer after body length precludes the switch in all cases or if in this particular case the reattachment of the wake interfered with the switch.

A switch in the sign of the initially shed vortex from an oscillating trailing edge, as f_e/f_o passes through unity, has been observed by a number of investigators, including Staubli & Rockwell (1989) and Lotfy & Rockwell (1993). The work of Staubli & Rockwell (1989) showed that the switch in the phase-referenced initially shed vortex from one corner of the trailing edge to the other, corresponded to a jump of order π in the phase of the pressure fluctuations at the trailing edge corner of the plate. Staubli & Rockwell (1989) show that corresponding to the switch there is a jump of approximately 2π in the phase of the pressure fluctuations some diameters upstream of the corner, as depicted in Figure 1-20(b). It is not clear why they define this as a large phase jump rather than an approximately constant phase of close to zero. The pressure fluctuations upstream of the corner are some distance from the vortex shedding. Therefore, it is expected that the relative acceleration of the flow will dominate the pressure fluctuations and the pressure phase will be close to zero either side of the switch. Irrespective of how the upstream pressure phase is defined, the jump in the pressure phase at the corner corresponds to a change in the gradient of the pressure force along the trailing edge.

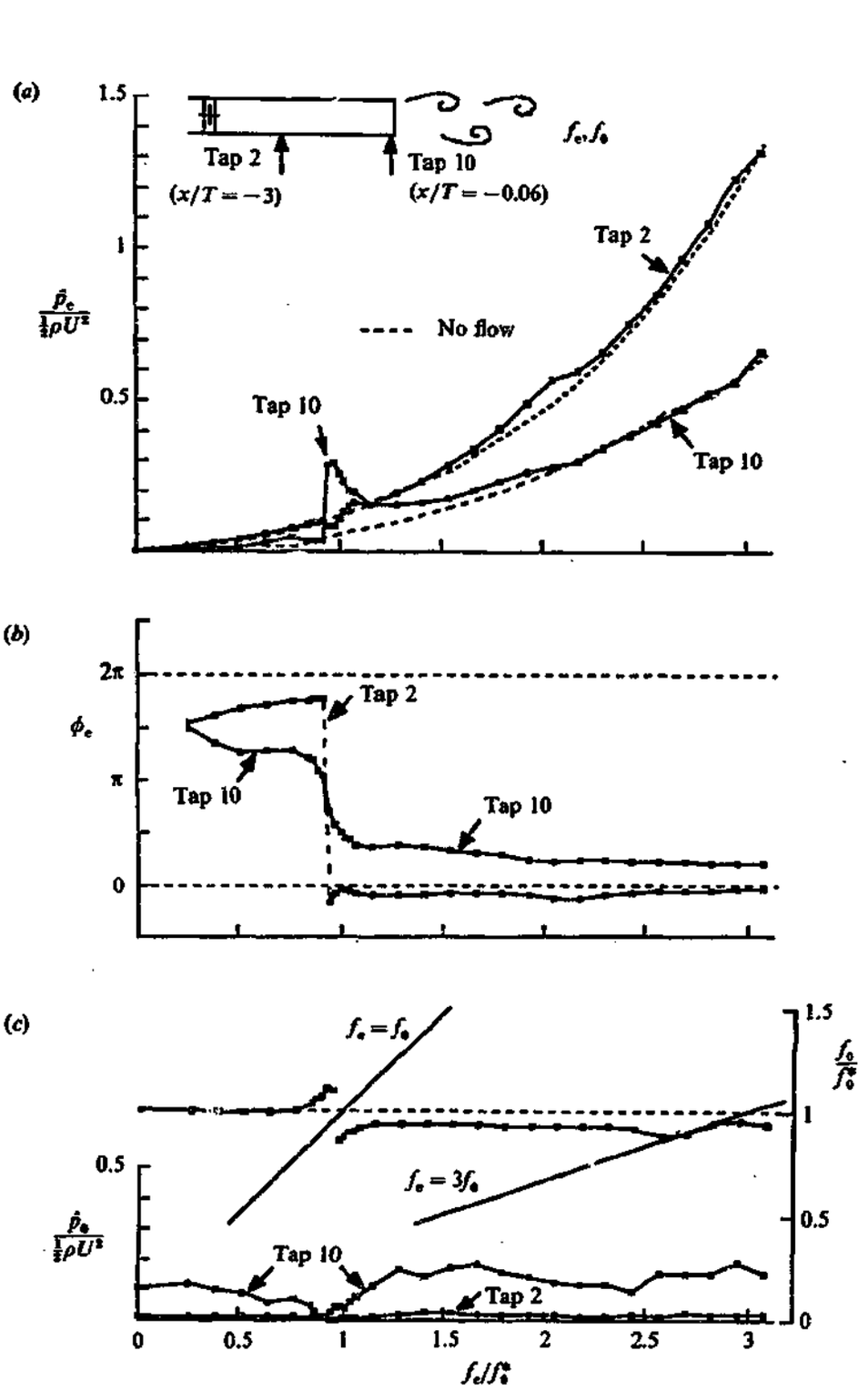

FIGURE 1-20 Typical response characteristics of the pressure fluctuations at amplitude $\eta_e \approx 0.02$ showing: (a) amplitude of pressure fluctuations; (b) phase ample between the pressure fluctuations and the edge displacement; and (c) the amplitude of the self-sustained pressure fluctuations and the associated frequency of the self-sustained vortex shedding. Reproduced from Staubli & Rockwell (1989).

The variation of the amplitude and phase of the pressure fluctuations with f_e/f_o (labelled f_e/f^*_o) is shown in Figure 1-20 (a & b) respectively. The pressures are shown at two locations on the trailing edge: tap 10 at the corner of the plate and tap 2, located three plate thicknesses upstream of the corner. The amplitude of the pressure fluctuations for oscillations in a stationary fluid are plotted along the values obtained with a free-stream flow in Figure 1-20(a).

When a body oscillates in a quiescent fluid, in the absence of large scale vortex shedding, the relative acceleration of the fluid will dominate the pressure forces on the surface of the body. When the trailing edge described above was oscillated with no free-stream flow, the phase of the pressure fluctuations along the trailing edge were close to zero and the amplitude of the pressure fluctuations varied with f_e^2. This indicates that along the trailing edge the apparent mass force, described in section 1.3.3, dominates the pressure force with only a small contribution from the vortex force. However, close to the mid-position of the vertical trailing end there was significant shift in the pressure phase. The authors associated this with the "onset of substantial viscous effects and secondary flows at the midsection", indicating that at this location there was a contribution from F_{vortex}. With the exception of the points around the midsection, the difference between the pressure fluctuations for the free-stream and no free-stream cases is an approximate measure of the contribution of the vortex force. This is illustrated for two tap positions by the dashed (no flow) and solid (free-stream flow) lines in Figure 1-20(a). The pressure at a given location is a function of the relative phases and amplitudes of the vortex and apparent mass components. Therefore, when the trailing edge is oscillating in the presence of a free-stream and the contribution from the vortex force is out-of-phase with the motion of the body, the amplitude of the pressure fluctuations will actually be less than the value when there is no flow.

At the corner of the trailing edge (tap 10 in Figure 1-20a) there is a sharp jump in the amplitude of the pressure co-efficient at $f_e/f_o \approx 1$, and both the phase and amplitude of the pressure fluctuations depart significantly from those generated by the oscillation of the body in stationary fluid. However, the amplitude and phase of the pressure fluctuations at tap 2, upstream of the trailing edge, are similar to the stationary flow values. This suggests that close to $f_e/f_o \approx 1$ the pressure force at the corner of the trailing edge there is a significant contribution from the vortex force, where as further upstream the pressure on the plate is dominated by the apparent mass force. Interestingly, the jump in the amplitude and phase of the pressure fluctuations at the corner of the plate when $f_e/f_o \approx 1$ are very similar to the behaviour of the lift force on an oscillating cylinder.

The variation of the pressure along the surface of an oscillating cylinder is not well understood. However, it is reasonable to expect that many of the features observed by Staubli & Rockwell (1989) for an oscillating trailing edge will also be observed for a cylinder. In particular, the jump in the lift force on the cylinder at $f_e/f_o \approx 1$ is expected to correspond to a jump in the phase of the

fluctuating pressures near the separation points, similar to that observed by Staubli & Rockwell for the trailing edge. Also, near the front stagnation point the pressures on the cylinder should be dominated by the additional mass force and therefore the corresponding pressure phase would be very close to 0° for all oscillation frequencies.

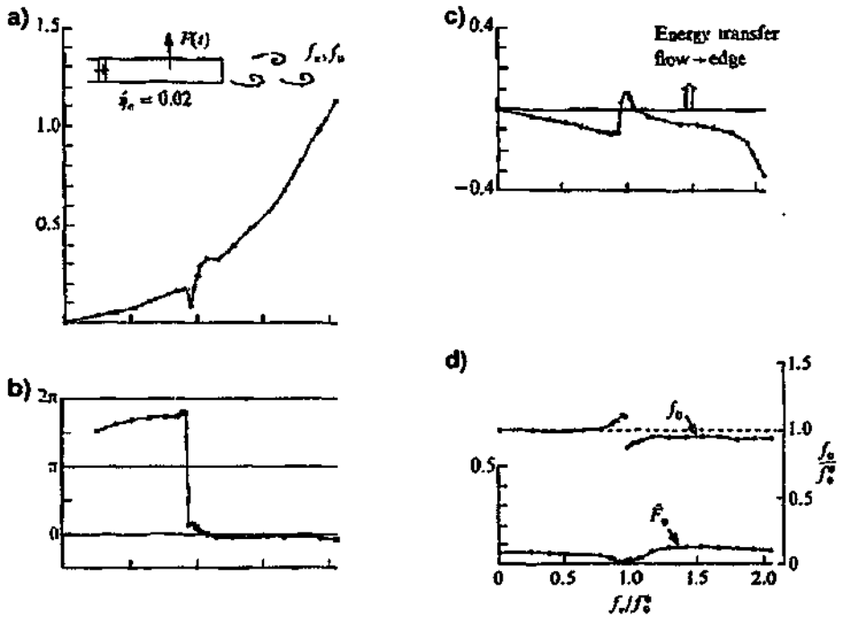

FIGURE 1-21 Response characteristics of the resultant loading upon an oscillating trailing edge at amplitude $\eta_e = 0.02$ showing: (a) the amplitude of the force component F_e at the excitation frequency f_e; (b) phase angle of F_e relative to the displacement; (c) energy transfer between the fluid and the body; (d) amplitude of the force component at the self-excited frequency f_o (equivalent to f_{nos}). Reproduced from Staubli & Rockwell (1989).

When variation of the total loading on the trailing edge with f_e/f_o, shown in Figure 1-21 (a & b), is very similar to the variation of the lift force on an oscillating cylinder. The energy transfer was calculated from the amplitude and phase of the force and is shown Figure 1-21c. For all but a small region around $f_e/f_o = 1$ the energy transfer is negative, indicating that these forced oscillations could not occur due to flow-induced forces. The "self-excited" force component on the trailing edge is equivalent to the lift force at the natural frequency of the oscillating body, f_{nos} described in section 1.4.1. The variations of both the amplitude and frequency of the "self-excited" force on the oscillating trailing edge, shown in Figure 1-21d, are almost identical to those observed for the forced oscillation of a cylinder in Figure 1-13 (b & c). Staubli & Rockwell (1989) also found that the jump in the phase and amplitude of the lift force on the oscillating trailing edge at $f_e/f_o \approx 1$ corresponded to substantial changes in the phase of vortex shedding. Despite the physical differences in the trailing edge and cylindrical geometries, when the bodies are forced to oscillate there are a number of surprisingly similar features as f_e/f_o passes through unity.

The forces and wake modes for oscillating rectangular and octagonal profiles were investigated by Deniz & Staubli (1997) at $Re = 10^5$ and a range of oscillation amplitudes: $A/D = 0.05 - 0.30$. For a rectangular cylinder with a streamwise length to diameter ratio of $L/D = 2$ a jump in the phase of the lift force, as shown in Figure 1-22, was observed for a range of oscillation amplitudes. However, this jump occurred not at $f_e/f_o \approx 1$ but when the forcing frequency coincided with f^*, the frequency of the impinging vortices shed from the leading edge. At $f_e \approx f^*$ there was not a corresponding jump in the amplitude of the lift force, however as shown in Figure 1-22 at $f_e/f_o \approx 1$ there was a local maxima in the amplitude of the lift force. For this geometry, the interaction between the leading edge instability (ILEV) and the Kármán or tailing edge vortex shedding appears to result in a scenario that is more complicated than for the trailing edge and circular cylinder geometries discussed above.

When the angle of the rectangle was rotated such that the centre-line of the rectangle forms an angle of $\alpha = 10°$ with the free-stream the wake of the stationary rectangle moved to an alternate-edge vortex shedding mode: one vortex separated at the leading edge and on the opposite surface a second vortex separated at the trailing-edge resulting in a Kármán type mode. The vortex separating at the leading edge does not appear to impinge on the trailing edge. When the rectangle was oscillated transversely across it's centre-line a jump in both the phase and amplitude of the lift force occurred close to $f_e = f_o$.

Flow visualisation of the oscillating rectangular body at $\alpha = 0°$ showed that the mode of vortex shedding varies strongly with the excitation frequency, as can be seen in Figure 1-22. The variation in the vortex shedding corresponding to the amplification of the lift amplitude as f_e passes though f_o is shown by comparing images ③ and ④. As the wake goes from ③ to ④ the motion of the rectangle becomes increasingly synchronised with the formation of trailing edge vorticity, resulting in a contraction of the wake and a change in the distribution of the flow structures throughout the wake. However, there does not appear to be a large change in the phase of vortex shedding. As the excitation frequency passes though f^* images ⑤ and ⑥ show a clear change in the phase of vortex shedding, where these changes correspond to a jump in the phase of the lift force. Interestingly, immediately before the jump in the phase of vortex shedding the vortex shedding in ⑤ results in the formation of counter rotating pairs, which initially appear similar to the 2P mode observed for an oscillating cylinder. However, the mechanisms resulting in the counter rotating pairs in ⑤ appear to be quite different. Each large vortex structure contains vortex structures formed at both the leading and trailing edges, which have coalesced behind the trailing edge. The relative timing of the leading and trailing edge vorticity results in the large vortex structures, of opposite sense, forming in close proximity in the near wake, resulting in the formation of a counter rotating pair. As the excitation frequency increases to $f_e \approx f^*$. shown in ⑥,

the vortex structures formed at the leading-edge are enhanced and there is a change in the timing of the large wake vortices, resulting in a change in both the mode and phase of vortex shedding.

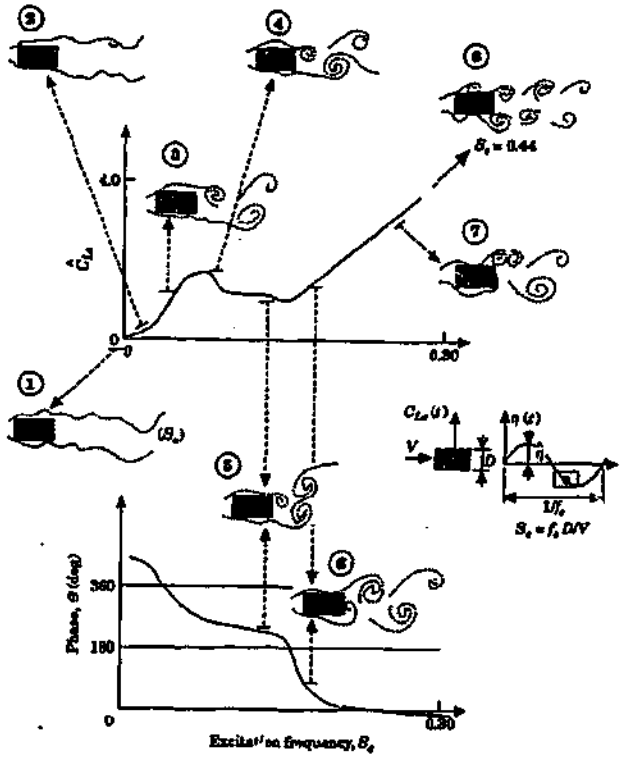

FIGURE 1-22 Overview of typical flow structures observed around the rectangular profile in relation to amplitude and phase of the measured lift forces; $\alpha = 0°$; A/D = 0.10; $Re_{visual} \approx 10^4$, $Re_{forces} \approx 10^5$, reproduced from Deniz & Staubli (1997).

Deniz & Staubli (1997) also tested an octagonal slightly "tapered" profile, with a slightly longer L/D = 3.33. At both $\alpha = 0°$ and 10°, there was no jump in the lift phase, which increased slowly from -90° towards 0°.

For the rectangular profile the jump in the lift phase was observed at either the frequency of the impinging vortices or the frequency of the Kármán vortices, depending on the orientation of the rectangle. This underlines the robustness of the jump in the phase of the lift force, which has been observed in oscillating circular cylinders, triangles, rectangles and trailing edges. However, the mechanisms which dictate the oscillation frequency at which this jump occurs for a given body shape are not yet well understood. Additionally, it is not known why the jump in the lift phase occurs for some long bodies, such as the oscillating trailing edge of Staubli & Rockwell (1989) and not in others, such as the octagonal cylinder of Deniz & Staubli (1997).

1.5 VORTEX-INDUCED VIBRATIONS OF A CYLINDER

Regular vortex shedding from a body induces periodic force on the body. When a periodic force is applied to a body that has elasticity, either in its mounting or in the body itself, then it is free to vibrate. The response of the body to the flow-induced forces depends on the magnitude and frequency of the forces and the properties, particularly the natural frequency, of the body. Depending on these properties the motion of the body can become extreme, resulting in catastrophic structural failure or excessive noise.

When flow-induced vibrations occur the structure is responding to forcing that is generated by the instability of the wake, however when the oscillations are forced a locked-on wake is responding to the forced motion of the structure. This is the fundamental difference between a forced and freely oscillating system. If however, the forced motion is identical to the flow-induced motion then the wakes, including the flow instabilities within the wakes, will be the same. Typically the flow-induced motions are studied by varying the relationship between the natural frequency of the wake for a stationary body and the natural structural frequency of the body. Varying the velocity of the flow past the body has the effect of changing the natural wake frequency, known as the Kármán frequency, but it also changes the Reynolds number. However, for the Reynolds number regimes most commonly considered ($Re < 2\text{-}3x10^5$) the flow regimes are very robust and typically do not vary significantly with Reynolds number.

The transverse oscillation of a one-degree-of-freedom (1-dof) elastically mounted rigid cylinder relates directly to our work on the forced transverse oscillation of a cylinder. However, there are a number of closely related structures which are also of interest, these include cables, cantilevered or leaf beams, tethered cylinder and a 2-dof elastically mounted rigid cylinder.

1.5.1 Characteristic Amplitude Response

The work of Feng (1968) is the classical experiment on vortex-induced vibration of an elastically mounted cylinder. The amplitude response of the cylinder as the flow velocity is changed is shown in Figure 1-23b. Brika & Laneville (1993) observed a similar amplitude response for a long slender cable, as shown in Figure 1-23a. The structural damping values, ζ for these two experiments differ by an order of magnitude, however the mass damping parameters, $m^*\zeta = 0.41$ for the cable and 0.36 for the elastically mounted cylinder, are similar.

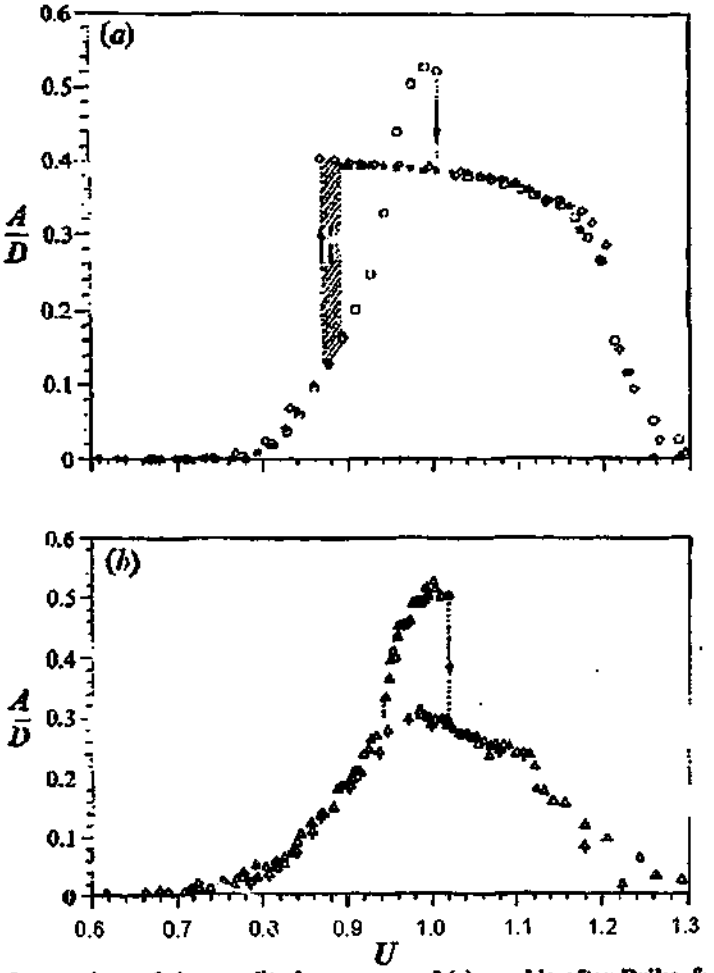

FIGURE 1-23 Comparison of the amplitude response of (a) a cable after Brika & Laneville (1993) and (b) an elastically mounted cylinder after Feng (1968). Reproduced from Brika & Laneville (1993)

The amplitude responses for both the elastically mounted cylinder and the long cable in Figure 1-23 demonstrate at least 2 different branches. As the free-stream velocity is increased from zero the onset of synchronisation is defined as the point at which the cylinder begins to oscillate in response to the forces generated by periodic vortex shedding. At the edges of the response region the motion of the cylinder is quasi-periodic, however within the core of the response region the oscillations are synchronised with, or locked-on to, the vortex shedding. The amplitude of the oscillation increases with increasing reduced (non-dimensionalised) velocity, U^*, until at a certain point there is a transition to another response branch indicated by the sharp jump in the amplitude of oscillation. Brika and Laneville (1968) also measured the phase of vortex shedding with respect to the motion of the cylinder using a hot-wire located in the wake. They found that the abrupt change in the amplitude of oscillation as the wake moved between the different response branches corresponded to a jump in the phase of vortex shedding, as shown in Figure 1-24. They also used low-resolution flow visualisation to show, for the first time, a direct link between the transition between the

different response branches and a change in the mode of vortex shedding. For the response branch at lower U^* the wake exhibited the 2S mode of shedding, while for the higher U^* response branch the mode of shedding was 2P.

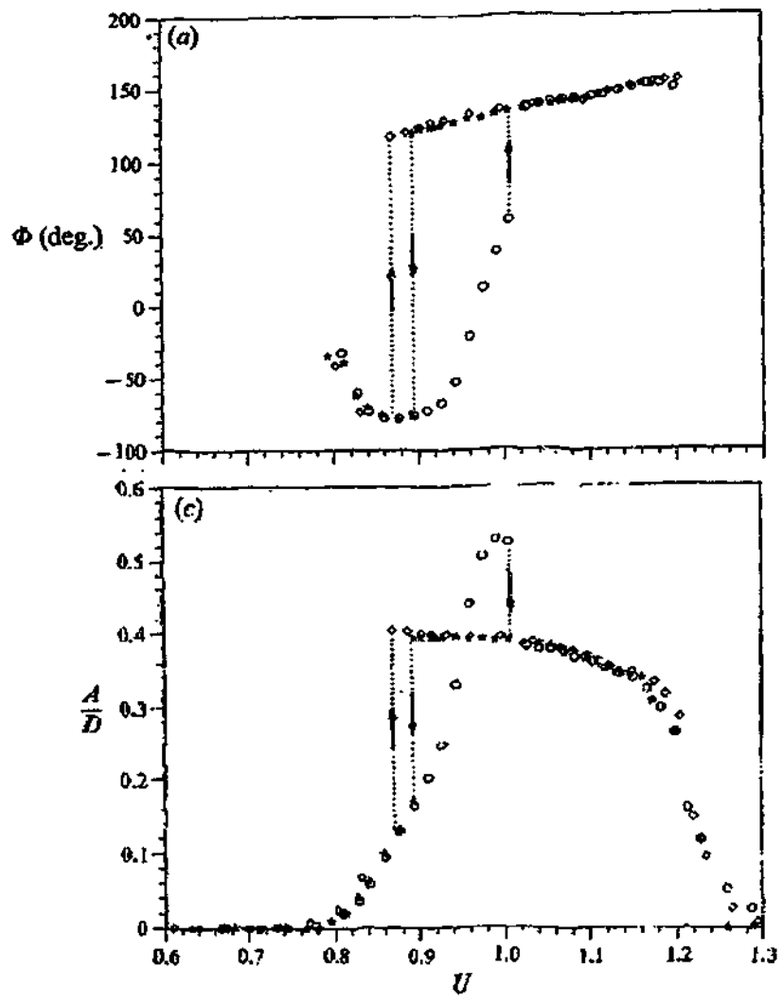

FIGURE 1-24 (a) The phase of vortex shedding (measured using a hot-wire in the wake) and (b) the relative vibration amplitude versus the relative flow velocity. The velocity is changed progressively: O increasing velocity, ★ decreasing velocity, ◇ increasing velocity with large steps. Reproduced from Brika & Laneville (1993)

1.5.2 Detailed Investigations of Characteristic Wake Modes and Forces

Detailed investigations of the wake modes and forces on elastically mounted cylinders have been undertaken by a number of investigators, notably Khalak & Williamson (1996, 1997 and 1999), Gharib (1999) and Govardhan & Williamson (2000). As the free-stream velocity varies the cylinder exhibits two or three different response branches. The number of branches depends upon

the non-dimensionalised mass-damping parameter, $m^*\zeta$, of the cylinder and its supporting structure. Historically there has been some inconsistency in the naming of the different branches but the definitions of Khalak & Williamson (1999) are now becoming well accepted. The response branches are most commonly defined in terms of the amplitude response, as shown in Figure 1-25, for both low and high values of $m^*\zeta$. At relatively high values of m*ζ, such as in the Feng (1963) experiments, the wake response generates two branches: the initial excitation branch at low U^* and the lower branch at higher U^*. At lower values of $m^*\zeta$ there is an additional response branch between the initial and lower branch. The additional branch has a high amplitude response and is appropriately called the upper branch. The transition between the initial and lower branches at high values of $m^*\zeta$ is hysteretic. At low $m^*\zeta$ the transition between the initial and upper branches is hysteretic and the transition between the upper and lower branches is intermittent.

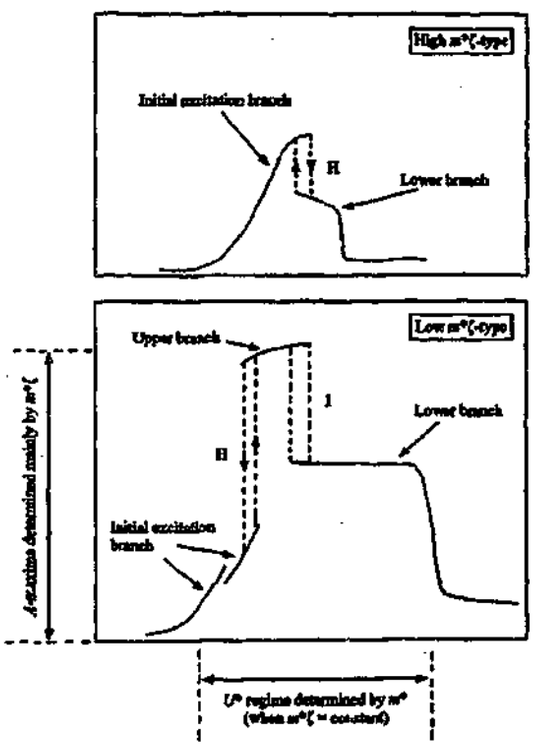

FIGURE 1-25 The two distinct types of amplitude response are shown schematically, (a) the high (m*ζ) response exhibits two branches (initial and lower) while (b) the low (m*ζ) response exhibits three branches (initial, upper and lower). The transition between modes are either hysteretic (H) or intermittent (I). Reproduced from Khalak & Williamson (1999).

The link between the different response branches and the change in the mode of vortex shedding was made by Brika & Laneville (1993) and Williamson & Roshko (1988). Subsequently, the nature of the transition, the forces on the cylinder and the mode of vortex shedding have been studied in much greater detail by a number of investigators, including Khalak & Williamson (1996, 1997, 1999) and Govardhan & Williamson (2000). Each of the response branches displays a

characteristic near wake structure that can be broadly described in terms of the modes of vortex shedding defined by Williamson & Roshko (1988). The vortex formation modes of the response branches have been studied in detail by Govardhan & Williamson (2000) using DPIV and are shown in Figure 1-26 for low values of $m^*\zeta$ where all three branches exist. At higher values of mass damping only the initial and lower branches are observed, and typically the amplitude of oscillation for these branches is diminished. However, at higher $m^*\zeta$ the general structure of the near wake for these two branches is essentially the same as for the low $m^*\zeta$ cases shown in Figure 1-26.

As indicated by Brika & Laneville (1993) the mode of vortex shedding for the initial branch, shown in Figure 1-26a, is 2S and two single vortex structures of opposite sign are shed into the wake per oscillation. For both the upper and lower branches two counter rotating vortex pairs are shed per oscillation and the mode of vortex shedding is 2P. However, for the initial branch, shown in Figure 1-26b, the second vortex structure within each pairing is considerably weaker than the first and the shedding mode is described as weakly 2P. The lower branch 2P mode, shown in Figure 1-26c, has vortex pairs of more equal strength and the counter rotating pairs persist further downstream.

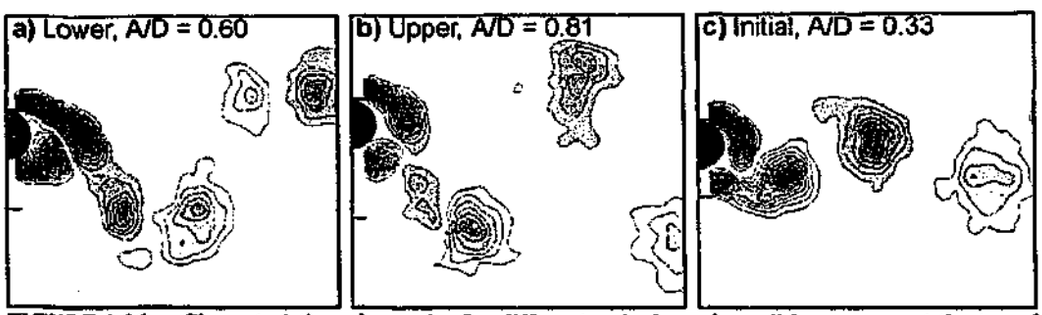

FIGURE 1-26 Characteristic wake modes for different wake branches, all images are at the top of the cylinders oscillation. The modes of vortex shedding are for (a) the initial branch the 2S-mode, (b) the upper branch the 2P-mode with uneven pair strength and (c) the lower branch 2P-mode with pairs of comparable strength. Reproduced from Govardhan & Williamson (2000).

As indicated by Figure 1-27a, the range of U^* over which the elastically mounted cylinder oscillates is a function of mass ratio. As m^* decreases there is a significant increase in the range of U^* over which the synchronisation region extends. In particular, there is a large increase in response range of the upper and lower branches. For low values of $m^*\zeta$ Khalak & Williamson (1999) demonstrated that when the response branches are plotted against $(U^*/f^*)St_o$, instead of U^*, there is a good collapse of the synchronisation range, as well as the amplitude response of the initial and lower branches. The collapse of the amplitude response for the initial and lower branches is shown in Figure 1-27(b) for two different values of m^*. The amplitude of the upper branch does not collapse and the amplitude of oscillation for the upper branch tends to increase with decreasing m^*. At higher $m^*\zeta$ the amplitude of the lower branches decreases with increasing

$m^*\zeta$ and, as shown in Figure 1-28, the amplitude response does not collapse when plotted against $(U^*/f^*)St_o$.

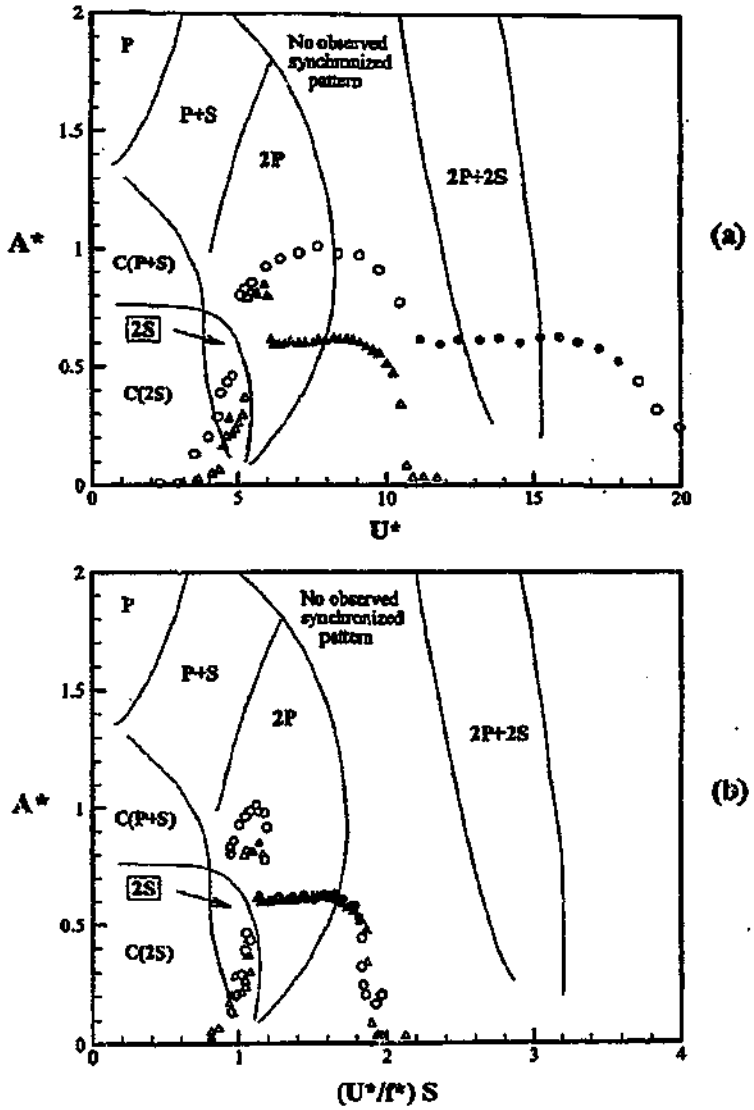

FIGURE 1-27 (a) amplitude response for two different mass ratios at low $m^*\zeta$ from Govardhan & Williamson (2000): O $(m^* + C_A)\zeta = 0.0110$, $\triangle$ $(m^* + C_A)\zeta = 0.0145$. In (b) the initial and lower branch regimes shown in (a) collapse when plotted against $(U^*/f^*).St_o$. Reproduced from Govardhan & Williamson (2000)

The "Griffin plot" Figure 1-29 shows that for low values of $m^*\zeta$ (i.e. low values $(m^*+C_A)\zeta$), the maximum oscillation amplitude for the lower branch has an approximately constant value of A^*_{max} = 0.6, where A^*_{max} is the maximum amplitude for the specified response branch. The fact that A^*_{max} is approximately constant indicates that a collapse of the amplitude response data is possible, although it may not necessarily occur. Of particular interest is the fact that, as shown in Figure 1-27, the lower branch maintains the maximum amplitude of oscillation over a wide range of reduced velocities, essentially to the edge of the synchronisation region.

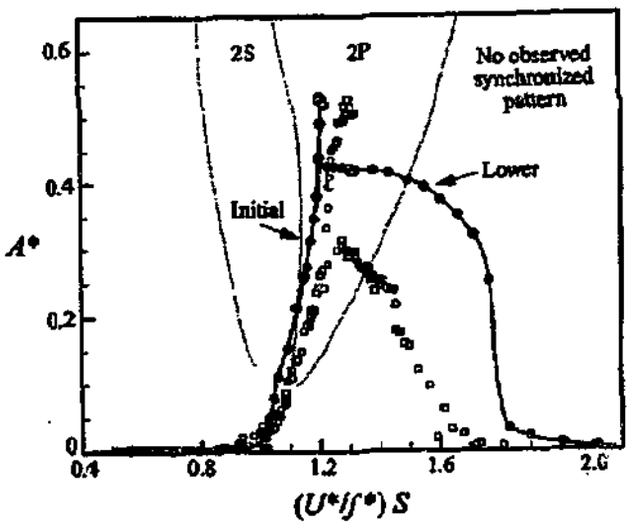

FIGURE 1-28 The amplitude response for the initial and lower branches at higher $m^*\zeta$. □ Feng (1968), $(m^* + C_A)\zeta = 0.251$, ● Govardhan & Williamson (2000). Reproduced from Govardhan & Williamson (2000).

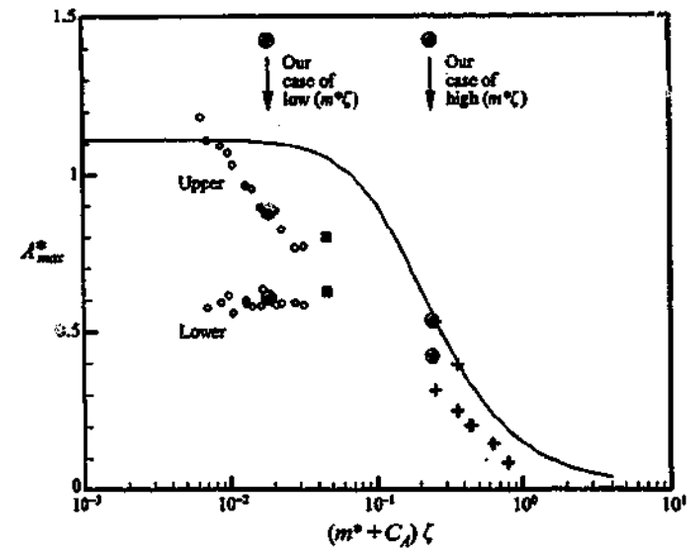

FIGURE 1-29 Modified "Griffin" plot showing the peak amplitude A^*_{max} for the different response branches. + Feng (1968); ⊡ Hover et al (1988); O Khalak & Williamson (1999); —— Skop & Balasubramanian (1997). Reproduced from Govardhan & Williamson (2000).

The maximum amplitude for the upper branch in Figure 1-29 varies with the mass-damping parameter $(m^* + C_A)\zeta$. This indicates that the response amplitude for the upper branch will not collapse unless it is plotted against a parameter that includes a mass-damping term and explains why there was not a full collapse of all the response branches in Figure 1-27(b). At higher values of mass-damping the maximum response amplitude varies strongly with $(m^* + C_A)\zeta$ and, as expected, at large values of mass-damping the amplitude response of the cylinder tends to zero. The variation of the peak response amplitude at high $m^*\zeta$ again indicates that when the amplitude

response is plotted against a parameter that does not include a mass-damping term a collapse of all the data is not possible.

The collapse of the initial and lower branch response curves onto the $(U^*/f^*)St_o$ curve, indicates that for lower values of $m^*\zeta$, the parameter $(U^*/f^*)St_o$ is the dominant parameter governing the amplitude response of these branches. The amplitude response of the upper branch varies with both $m^*\zeta$ and $(U^*/f^*)St_o$, however Govardhan & Williamson (2000) found that the point at which the wake transitions from the upper branch to the lower branch occurred at an approximately constant value of $U^*/f^* \approx 5.75$, as indicated by the dashed line in Figure 1-30. Additionally, after the transition, the frequency of oscillation in the lower branch f^*_{LOWER} is not a function of U^*, but increases with decreasing m^* according to the relationship:

$$f^*_{LOWER} = \sqrt{\frac{m^* + C_A}{m^* - 0.54}} \qquad (1\text{-}11)$$

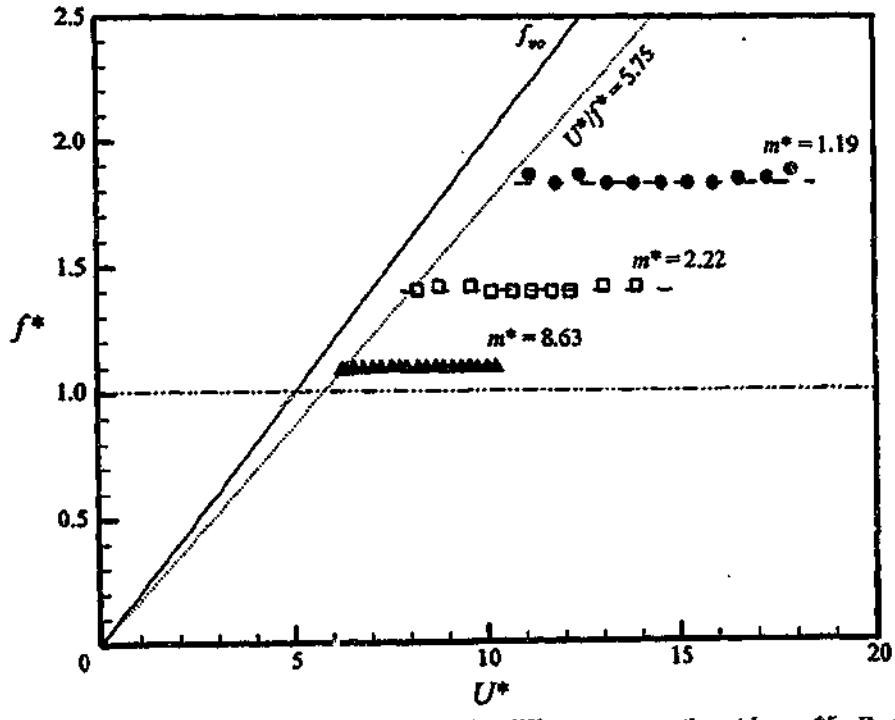

FIGURE 1-30 Lower branch frequency response for different mass ratios at low $m^*\zeta$. Reproduced from Govardhan & Williamson (2000).

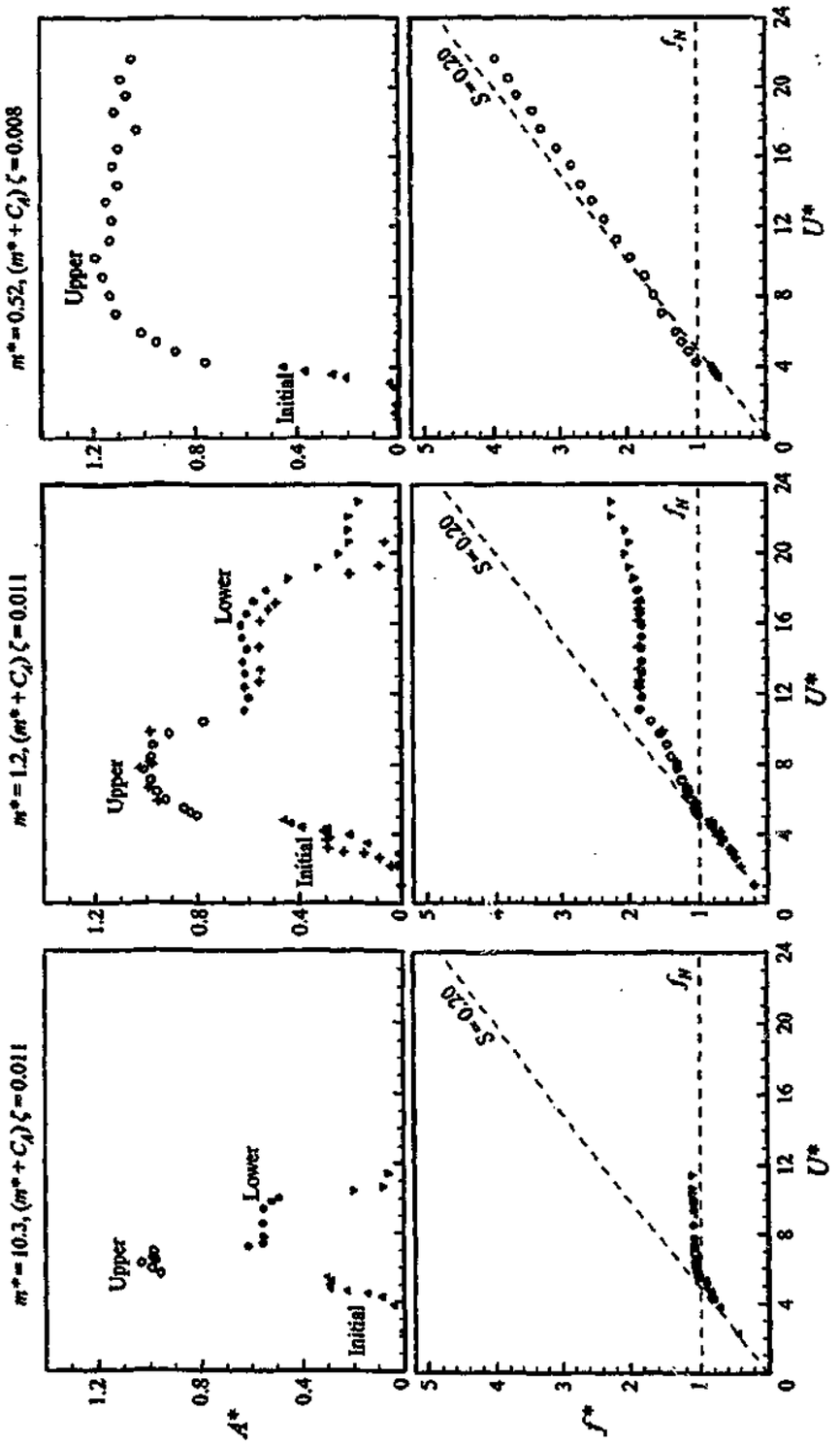

FIGURE 1-31 Amplitude and frequency response of an oscillating cylinder as m* is reduced below $m^*_{CRIT} = 0.54$. Reproduced from Govardhan & Williamson (2000).

After the transition to the lower branch the frequency of oscillation does not vary significantly, therefore f^*_{LOWER} is approximately constant and is equal to the value of f^* at which the transition from the upper to lower branches occurs. Govardhan & Williamson used this fact to predict a critical mass ratio, $m^*_{CRIT} = 0.54$ below which the transition from the upper to the lower branch no longer occurs. Their results suggest the when $m^* \leq m^*_{CRIT}$, the wake does not transition to the lower branch and the upper branch response can, in theory, persist as U^* increases to infinity. This remarkable finding relies on the physical result that at low m^* values the cylinder can oscillate at frequencies well above the natural structural frequency. The amplitude and frequency response of the cylinder at low values of m*, including $m^* < m^*_{CRIT}$, are shown in Figure 1-31. For $m^* > m^*_{CRIT}$ the range of U^* over which the upper branch extends increases with decreasing m^*, but remains finite. However, for m^* below m^*_{CRIT} the upper branch persists up to the maximum values of U^* possible in the experimental facility and would theoretically extend to $U^* = \infty$. In practise, it is unlikely that the upper branch will extend to $U^* = \infty$, as the flow will move into different Reynolds number and Mach number regimes.

Govardhan & Williamson (2000) considered both the total lift force on the cylinder, $C_L(t)$, and the vortex component of the total lift force, $C_{L\ vortex}(t)$, see section 1.3.3 for a discussion of these parameters. The variations of the phase and amplitude of the total lift force with U^* are shown in Figures 1-32(a) and (b) respectively. The phase of the potential added mass force (which is equal to the apparent mass force) is constant, but its amplitude varies with $(A f^{*2})/U^{*2}$. When the wake moves between the different response branches the amplitude of the potential added mass, $C_{L\ am}$, varies with the amplitude and frequency of the response. At the transition points there are also generally changes in the phase and amplitude of the total lift force and thus the transitions correspond to a significant change in the relationship, both phase and amplitude, between the total and potential mass forces. The vortex force is calculated by vectorially subtracting $C_{L\ am}(t)$ from $C_L(t)$. As the wake moves between the different branches the change in the relationship between $C_{L\ am}(t)$ and $C_L(t)$ causes a corresponding change in the relationship between the total and vortex lift forces. Thus, the nature of the variation of C_L with U^*, shown in Figure 1-32(a), is very different in shape from that of $C_{L\ vortex}$, shown in Figure 1-32(c). More significantly, when $C_{L\ am}(t)$ is subtracted from the total lift force the phase of the upper branch switches from just above 0° to just below 180°. Therefore for values of $m^*\zeta$ where the wake response has three branches, the jump in $\phi_{lift\ vortex}$ occurs at a different value of U^* to the jump in ϕ_{lift}. The jump in $\phi_{lift\ vortex}$ corresponds to a large change in both the phase and mode of vortex shedding. The jump in ϕ_{lift} between the upper and lower branches does not correspond to a significant change in the phase of vortex shedding and, although there are changes in the distribution of vorticity, the general mode of shedding remains 2P. When the lift forces and motion of the cylinder are sinusoidal equation 1-10,

reproduced below, describes a simple relationship between the phase and amplitude of the total lift force, shown in Figure 1-32(a & b) and the vortex lift force, shown in Figure 1-32 (c & d).

$$C_E \approx \pi\, C_L\, (A/D)\, \sin(\phi_{lift}) = \pi\, C_{L\,vortex}\, (A/D)\, \sin(\phi_{lift\,vortex}) \qquad \text{(1-10, reproduced)}$$

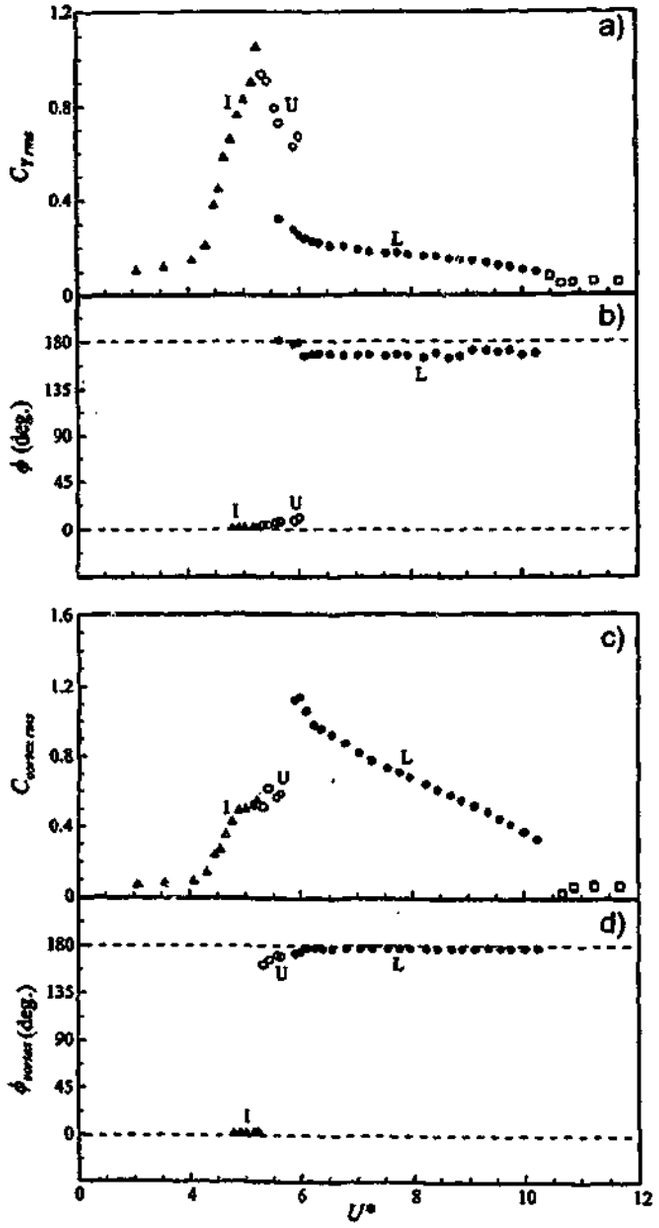

FIGURE 1-32 Variation of the phase and amplitude of a) the total and b) vortex lift force for low $m^*\zeta$. The jump in the phase of the total lift force ϕ_{lift}, occurs between the upper and lower branches while the jump in the phase of the vortex lift force $\phi_{lift\ vortex}$ occurs between the initial and upper branches. Reproduced from Govardhan & Williamson (2000).

Govardhan and Williamson (2000) found that the transition from the initial to the upper branch, and the corresponding jump in $\phi_{lift\,vortex}$, occurs when the frequency of oscillation passes through the

natural frequency of the structure in the fluid, i.e. f passes through $f_{N\,water}$, ($f^* = 1$). They also showed that when the lift force and motion of the cylinder are accurately represented by sinusoidal functions, as the frequency of oscillation passes through $f^* = 1$ the equations of motion predict a jump in ϕ_{lift}. The development of the equations below follows essentially the same logic as Govardhan & Williamson but the manipulation of the terms is slightly different.

In equation 1-12, the equation of motion of an elastically mounted cylinder is written in terms of the vortex force, where the apparent mass force term is contained on the left hand side as $(m_a\ \ddot{y})$ where the added mass per unit length, $m_a = -(\rho\pi D^2)/4 = -m_d$.

$$(m + m_a)\ddot{y} + c\dot{y} + ky = \bar{F}_{vortex}(t) \qquad (1\text{-}12)$$

By assuming that the motion and the vortex lift force can be represented by a pure sinusoidal signal:

$$\bar{F}_{vortex}(t) \approx C_{L\,vortex}\sin(\omega t + \phi_{lift\,vortex}), \qquad y(t) \approx A\sin(\omega t)$$

and solving for the frequency of oscillation, it follows that:

$$\frac{f}{f_{N\,water}} = f^* = \sqrt{1 - \frac{1}{kA}C_{L\,vortex}\cos(\phi_{lift\,vortex})} \qquad (1\text{-}13)$$

Careful examination of equation 1-13, shows that as $\phi_{lift\,vortex}$ goes from the first quadrant ($0° < \phi_{lift\,vortex} < 90°$) to the second quadrant ($90° < \phi_{lift\,vortex} < 180°$) during the transition from the initial to the upper branch, the second term under the square root passes through zero. Therefore, equation 1-13 shows that at the transition between the initial branch and upper branch the frequency of oscillation must pass through $f^* = 1$. Although the frequency of oscillation in equation 1-13 is written in terms of the in-phase component of the lift force, $F_{lift\,vortex}\cos(\phi_{lift\,vortex})$, it can also be written in terms of the out-of-phase component of the lift force. Therefore, unlike the energy transfer, the frequency of oscillation varies with both the in-phase and out-of-phase components of the lift force.

Re-writing the equation of motion in terms of the total lift force allows us to examine the effect of the jump in ϕ_{lift} at the transition between the upper and lower branches:

$$m\ddot{y} + c\dot{y} + ky = \bar{F}_{total}(t), \qquad (1\text{-}14)$$

where F_{total} is the total lift force. For a sinusoidal lift force and cylinder motion the frequency of oscillation expressed in terms of the total lift force is:

$$\frac{f}{f_{N\,vacuum}} = \sqrt{1 - \frac{1}{kA}C_L\cos(\phi_{lift})} \qquad (1\text{-}15)$$

Following the same argument as presented above for the jump in the vortex lift phase, Equation 1-15 shows that f passes through $f_{N\,vacuum}$ as $\cos(\phi_{lift})$ passes through zero during the transition from the upper branch to the lower branch.

For all the values of m^* and $m^*\zeta$ considered by Govardhan & Williamson (2000) the transition between the initial and upper branches occurred at approximately $f^* = 1$. These results are consistent with the argument associated with equation 1-13 presented above. This transition corresponds to the jump in $\phi_{lift\,vortex}$ and a change in both the mode and phase of vortex shedding. A characterisation of both this transition and the transition between the upper and lower branches is shown schematically in Figure 1-33. Figure 1-33 indicates that the transition between the upper and lower branches occurs at $f = f_{N\,vacuum}$, as predicted by equation 1-15. This is consistent with the experimental results of Govardhan & Williamson (2000) for m^* substantially greater than m^*_{CRIT}, e.g. $m^* = 8.63$. However, as m^* approaches m^*_{CRIT} the transition between the upper and lower branches appears to occur well above the natural frequency of the structure in a vacuum. An example of this is shown in Figure 1-31: at $m^* = 1.2$ the transition between the upper and lower branches occurs at $f^* \approx 1.9$, however $f^*_{N\,vacuum} (= f_{N\,vacuum}/f_N)$ is equal to 1.35. This result suggests that the transition frequency predicted by the idealised approximation of the lift force and motion of the cylinder in equation 1-15 does not hold at lower values of m^*. This implies that at very low values of m^* the lift force and cylinder motion are not accurately represented by sinusoidal functions.

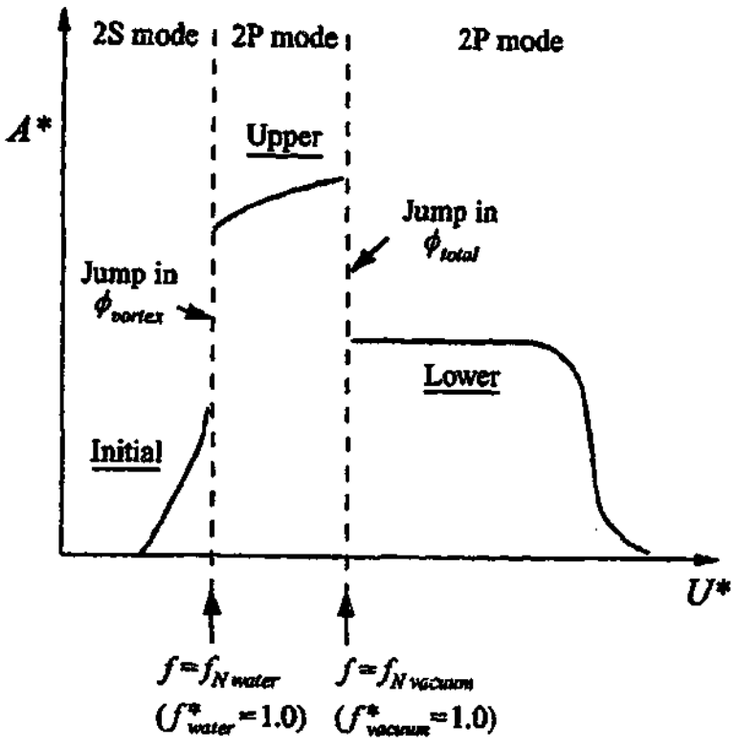

FIGURE 1-33 Schematic diagram of the low m*ζ type of response showing the three principal branches and the two jump phenomena. Reproduced from Govardhan & Williamson (2000).

Further evidence that equation 1-15 does not describe the frequency of oscillation at the transition between the upper and lower branches at lower branches of m^* can be found in the experimental results of Govardhan & Williamson (2000). They found that the frequency of oscillation for the lower branch, f_{LOWER}, is given by equation 1-11. As shown in Figure 1-31 the frequency of oscillation is constant after the transition from the upper to the lower branch. Therefore, the frequency at which the transition between the upper and lower branches occurs is approximately equal to f_{LOWER}. Re-stating the pertinent equations from Govardhan & Williamson (2000) and their derivations we have:

Transition frequency, $f^*_{UPPER \rightarrow LOWER}$

$$f^*_{LOWER} = \sqrt{\frac{m^*+C_A}{m^*-0.54}} = \sqrt{\frac{m^*+C_A}{m^*-m^*_{CRIT}}}$$

Experimental result:
Govardhan & Williamson (2000)

$$f^*_{N\,vacuum} = \frac{f_{N\,vacuum}}{f_{N\,water}} = \sqrt{\frac{m^*+C_A}{m^*}}$$

Theoretical results derived by assuming

$\vec{F}_{lift\,vortex}(t) \approx F_{lift\,vortex} \sin(\omega t + \phi_{lift\,vortex})$
and $y(t) \approx A \sin(\omega t)$

Comparing the two equations for , $f^*_{UPPER \rightarrow LOWER}$ we see that at larger values of m^*, where $m^* >> m^*_{CRIT}$, f^*_{LOWER} is very close to the theoretical value $f^*_{N\,vacuum}$.

Further examination of $f_{N\,vacuum}$ for mass ratios approaching and below m^*_{CRIT} also indicates that equation 1-15 does not correctly predict the frequency of oscillation at the transition between the upper branches. The experimental results of Govardhan & Williamson (2000) indicate that for $m^* \leq m^*_{CRIT}$ the transition from the upper branch to the lower branch does not occur and f^* increases linearly with U^*. This implies that the frequency of oscillation can increase towards $f^* = \infty$ without a transition from the upper branch to the lower branch. If, as predicted by equation 1-15, the transition between the upper and lower branches were to occur at $f = f_{N\,vacuum}$ then for $m^* >> m^*_{CRIT}$ the natural frequency of the structure in a vacuum would need to be equal to infinity. However, this is not physically reasonable as while the mass of the cylinder remains finite $f_{N\,vacuum}$ $(\approx (k/m)^{1/2})$ also remains finite.

As shown in Figure 1-31, the variation of f^* with U^* is different for each of the different response branches. For the initial branch the frequency of oscillation increases linearly with U^* until at $f^* \approx 1$, the wake moves to the upper branch. Within the upper branch f^* continues to increase linearly with U^*, however the gradient is slightly reduced. Following the transition to the lower branch f^* is approximately constant indicating that a limiting value has been reached. As discussed above, at low values of m^* the frequency of oscillation for the upper branch can increase above $f_{N\,vacuum}$ and the value of f^* at which the transition from the upper to lower branch occurs is best described by equation 1-11. For low values of m^*, close to and below m^*_{CRIT}, the cylinder oscillates at frequencies well above the natural structural frequency at high U*. The experimental results for $m^* = 0.52$in Figure 1-31 show the somewhat surprising result that the structure can undergo vortex-induced vibrations at frequencies that are at least four times $f_{N\,water}$.

A simple manipulation of equation 1-11 shows at higher values of m^* the frequency at which the transition from the upper to lower branches occurs, $f^*_{UPPER \rightarrow LOWER}$ ($\approx f^*_{LOWER}$), tends towards $f_{N\,vacuum}$:

$$f^*_{LOWER} = \sqrt{\frac{m^* + C_A}{m^* - m^*_{CRIT}}}$$

$$\frac{1}{f^{*2}_{LOWER}} = \frac{m^*}{m^* + C_A} - \frac{m^*_{CRIT}}{m^* + C_A}$$

$$\frac{1}{f^{*2}_{LOWER}} = \left(\frac{f_{N\,water}}{f_{N\,vacuum}}\right)^2 - \left(\frac{f_{N\,water}}{f_{N\,CRIT}}\right)^2,$$

defining $f_{N\,CRIT} = \sqrt{\frac{k}{m_{CRIT}}}$ and $f^*_{N\,CRIT} = \frac{f_{N\,CRIT}}{f_{N\,water}}$

$$f^*_{N\,LOWER} = \sqrt{\frac{1}{\left(\frac{1}{f^*_{N\,vacuum}}\right)^2 - \left(\frac{1}{f^*_{N\,CRIT}}\right)^2}}$$

Thus, when m^* is significantly greater than m^*_{CRIT}, $\frac{1}{f^*_{N\,vacuum}}$ is much greater than $\frac{1}{f^*_{N\,CRIT}}$ and f^*_{LOWER} tends to $f^*_{N\,vacuum}$.

1.6 FORCED AND FREELY OSCILLATING CYLINDERS

1.6.1 The Nature of Transition

Previous results indicate that the jump in the lift force on a cylinder undergoing forced oscillations corresponds to a transition between two different wake states. A number of aspects of this transition are similar to those for the elastically mounted cylinder at the transitions between the initial wake branch and either the upper or lower branches. For both the forced and free oscillations, the transitions are characterised by a number of events including a change in the phase of vortex shedding, a change in the mode of vortex shedding or an abrupt changes in the phase and amplitude of the lift force. For an elastically mounted cylinder Govardhan & Williamson (2000) showed that the transition between the initial branch and either the upper or lower branches corresponds to a change in both the mode of vortex shedding and a jump in the vortex lift phase. Previous investigations on the forced oscillation of a cylinder indicate that similar changes may also occur simultaneously around $f_e/f_o = 1$, moreover these changes would correspond to a transition between two different wake states. However, the changes in the structure of the near wake and the forces on the cylinder around $f_e/f_o = 1$ have not been conclusively linked. Additionally, the mechanisms that cause the transitions observed for both the forced and free oscillations of a cylinder are not well understood.

Many different physical systems exhibit a number of different states. The nature and properties of a transition between different states have been studied in numerous fields of science. A transition is said to be hysteretic if the position in parameter space at which the transition occurs depends upon whether the independent variable is being decreased or increased. When a transition is hysteretic the established state tends to persist slightly longer before the system makes the transition to the other state. Hysteresis indicates that the flow has a "memory" and that the previous flow conditions influence the point at which transition occurs. For an oscillating cylinder transition is characterised by a sharp change in the lift force as the frequency of oscillation passes through $f_e/f_o \approx 1$. Typically hysteresis is observed when a controlling variable, such as the flow velocity or the frequency of oscillation, is varied continuously or in small discrete steps. The controlling variable can be "reset" between each different experimental value if the experiment is restarted from a third reference state. An example of this is an experiment where the flow velocity is varied but between each value the flow is brought to rest and the disturbances allowed to die out before testing at a different flow velocity. In this case, depending on the rate at which the flow velocity is ramped up, hysteresis is much less likely to be evident.

The relative stability of different states and hysteretic transition between states has been investigated in many areas of science. As discussed by Visintin (1991) a system will always seek

to attain the most stable state, or in other words the state where the energy potential is minimised. An example of a system occupying a stable state is a simple harmonic oscillator, where the potential energy of the system, plotted against the position of the mass, is a deep symmetric well and the potential energy of the mass is minimised at the bottom of the well. The positions available to the mass vary with its kinetic energy and, as the kinetic energy is dissipated by friction, a mass with limited kinetic energy will be found towards the bottom of the well. Thus, the mean position of the mass is the bottom of the well and it will oscillate about that position with a displacement distribution that depends on the kinetic energy of the mass. The same concept can be applied to more complicated systems and the potential energy of the system can be plotted in phase space in a similar fashion.

Consider a system that can be characterised by two variables $q(t)$ and $p(t)$, where q is the independent variable (analogous to f_e/f_o) and p is the dependent variable (analogous to ϕ_{lift} or C_L). Over the range of q to be considered, there is a transition between two distinctly different states. The potential energy of this system, for a fixed value of the independent variable q, can be plotted as a function of p as shown in Figure 1-34a. The shape of the potential energy $\varphi(p)$ curve will change smoothly with the independent variable q. The system tends to minimise, either globally or locally, the potential φ and the stable states available to the system in Figure 1-34a are labelled "State I" and "State II". The most stable state is where the potential is absolutely minimised, state II in Figure 1-34a. The local minima of state I is also stable and is described as a metastable state. The system will persist in the metastable state until the fluctuations within the system allow it to overcome the potential barrier $\Delta\varphi$. The time taken for the system to obtain the most stable equilibrium state depends on the energy of the fluctuations. If the potential barrier $\Delta\varphi$ is very large, the system can maintain a meta-stable state for periods of time that are much longer than the time scale of an experiment and the most stable state is not observed. A schematic of a hysteretic transition is shown in Figure 1-34b, where the change in states corresponds to a sharp jump in the value of the dependent variable p. Hysteresis occurs when the independent variable, q, is varied smoothly through a transition region, $q_{LT}<q<q_{UT}$. When $q<q_{LT}$ state I is the only stable state available to the system, as q increases through q_{LT} state II becomes a metastable state. As q increases further towards q_{UT}, state II becomes more stable than state I. However, as the system is already in state I, it will not transition to state II until it is able to overcome the potential barrier and, as discussed above, the meta-stable state may persist for some time. In a noisy system transition will occur well before $q = q_{UT}$. When q is decreased from values of $q>q_{UT}$ the same process occurs resulting in a hysteretic overlap of states.

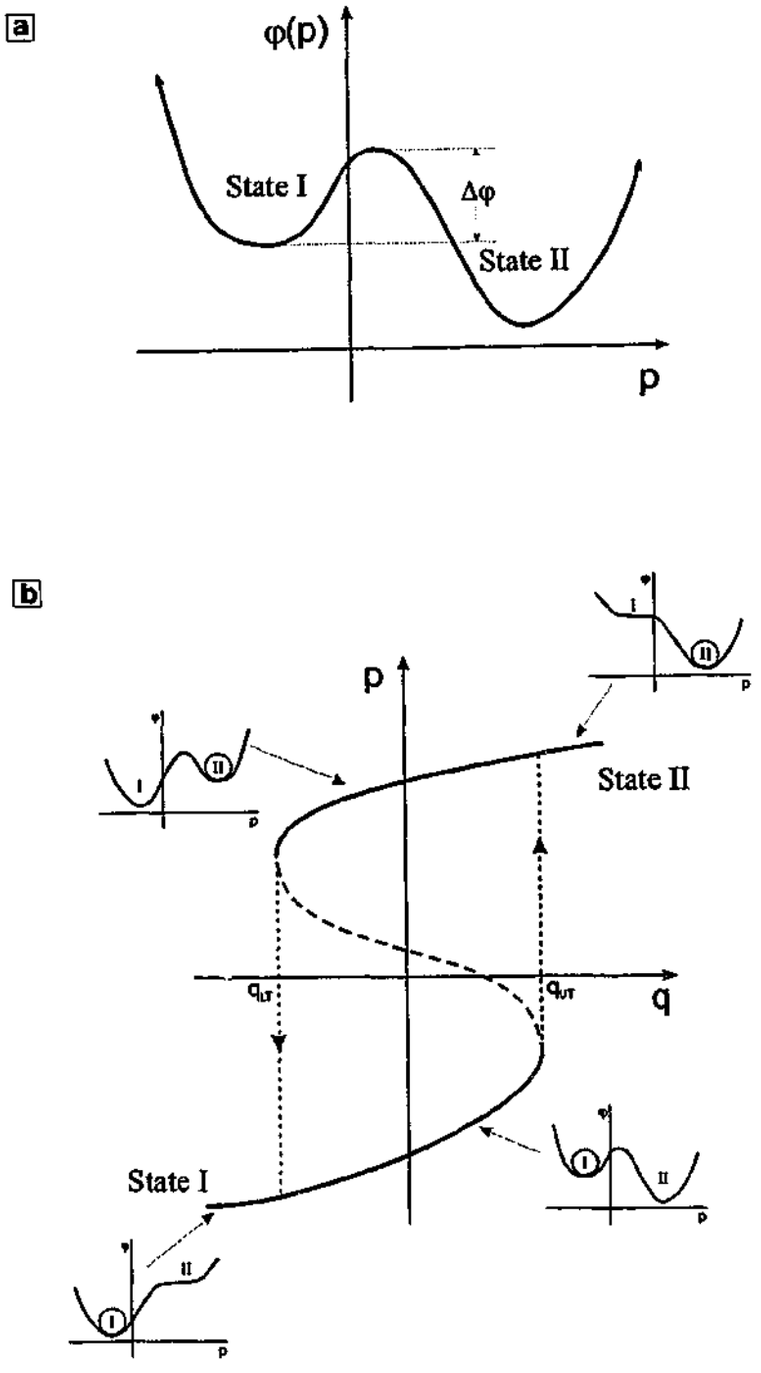

FIGURE 1-34 a) The double well potential of a system with two stable states, where w is the dependent variable and φ is the potential energy for a fixed value of u, the independent variable. b) Schematic showing a hysteretic transition from state I to state II where the inserts show the variation of the potential energy at points throughout the transition.

Bishop & Hassan (1963) investigated the phase and amplitude of the lift force on a cylinder over a range of oscillation frequencies by varying f_e/f_o in a continuous fashion, with out allowing the

cylinder to come to rest in between data runs. When the frequency was increased the value of f_e/f_o at which the transition occurred was higher than when the frequency was decreased, hence the transition is described as hysteretic. Gopalkrishnan (1983) conducted similar experiments in a towing tank, where between experimental runs at different values of f_e/f_o the oscillations cease and the flow is allowed to settle. Bringing the flow to rest between experimental runs has the effect of removing the "memory" of the flow and in this case hysteresis was not observed.

Ingenious experiments by Brika & Laneville (1993) examined a freely oscillating long cable using different methods to vary the reduced velocity. (Note: to avoid confusion, when we are discussing the results of Brika & Laneville the terminology of Khalak & Williamson (1999) will be used to describe the different response branches.) As well as incrementally increasing and decreasing the reduced velocity, they also considered the effect of changing the size of the increments. When the velocity was increased or decreased with small steps ($\Delta U^* \approx 0.02$), indicated in Figure 1-24 by the symbols ∘ and ★ respectively, there was a clear hysteresis. However, when the velocity was increased with large steps ($\Delta U^* \approx 0.04$), represented in Figure 1-24 by the symbol ◇, the transition from the initial the lower branch occurred at a much lower velocity. Irrespective of the size of the velocity increments, the response either side of transition was consistent with either the initial or lower branches.

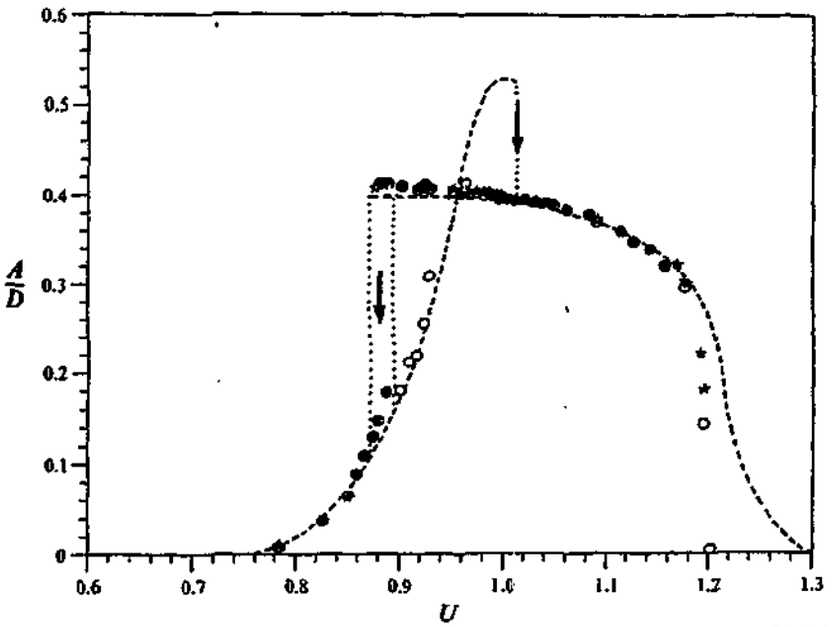

FIGURE 1-35 The amplitude responses of the impulsive regimes as a function of U^* (labelled U in figure) compared to the results of the progressive regimes: ☆initial state from rest, O initial state from a pre-excited amplitude: — progressive regimes. Reproduced from Brika & Laneville (1993)

Brika & Laneville described the method of changing the flow velocity in an incremental fashion as a "progressive" regime. They also considered a second method, described as an "impulse regime", where for each different flow velocity the cable was in a constant initial state before the cable was

released and allowed to move to a final state. Two different initial conditions were considered; a stationary cable or a cable undergoing forced large amplitude oscillations. The amplitude responses from the controlled initial states or "impulsive" regimes were then compared with those of the "progressive" regimes. For the "progressive" regimes the velocity is changed incrementally and therefore the initial state depends on the state for the previous velocity. As shown in Figure 1-35, the initial state of the system affects the velocity at which transition occurs. The amplitude response of the cable released from rest falls on either the initial ($U^* \leq 0.87$) or the lower ($U^* \geq 0.88$) response branches. However, within the small region, $0.87 \leq U^* \leq 0.88$ the amplitude response of the cable released from rest tends first towards a state which is consistent with the lower branch but after a period of time there is a transition or "break" of the amplitude response to a lower level. The "break" in the amplitude of oscillation is accompanied by an abrupt change in the phase of vortex shedding, as shown Figure 1-36, and the final state is fully consistent with the initial branch. Thus, within this transition region both the initial and lower branches are observed. Interestingly, the transition region lies at the lower end of the hysteretic transition region defined by the progressive regimes and the system tends to remain in the initial branch down to relatively low values of U^*.

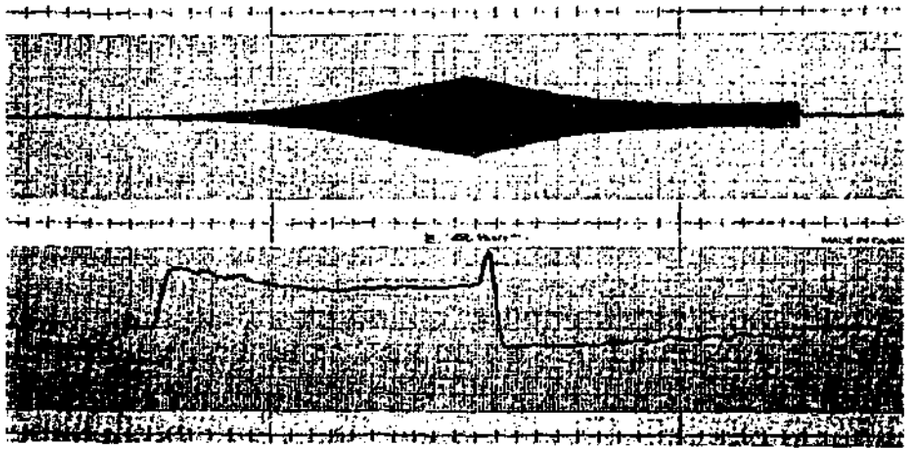

FIGURE 1-36 The amplitude response (upper plot) and vortex phase (lower plot) for a cable starting from rest at $U^* = 0.87$. Each *major* division on the time axis represents approximately 90 oscillations at the natural frequency of the cable. Reproduced from Brika & Laneville (1993)

The response of the cable released after initial forced large oscillations is also shown in Figure 1-35. In this case the transition also begins at the lower end of the hysteretic transition region, but there were a relatively wide range of velocities, $0.88 \leq U^* \leq 0.95$, where the response of the system was not unique and both the initial and lower branch responses were observed. Additionally, as shown in Figure 1-37, at $U^* = 0.92$ a self-excited transition from the lower branch to the initial branch was observed. This transition occurred approximately 60 seconds, or over 1000 oscillation cycles, after the system first became established in the lower branch.

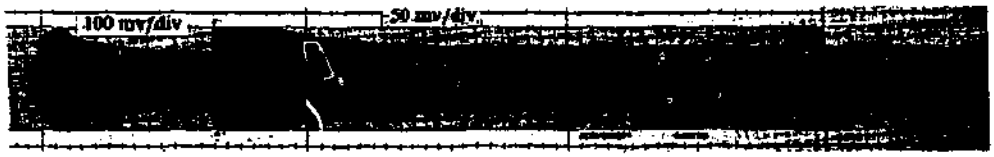

FIGURE 1-37 Response trace showing a self-excited transition from the lower branch to the upper branch at $U^* = 0.92$, for a initial state with large amplitude oscillations, (note the change in scale). Reproduced from Brika & Laneville (1993).

In summary, the experiments by Brika & Laneville (1993) show that the selection of a particular state within a transition region, where a system is able to exhibit more than one state, is effected by the initial state of the system and the nature or size of changes in the governing parameters. However, outside the transition region the final wake state depends only on the values of the governing parameters. There are other factors not discussed by Brika & Laneville that may also influence the state section for an oscillating cylinder, these include the level of free-stream turbulence and Reynolds number.

The numerical investigation of Blackburn & Henderson (1999) considered the forced oscillation of a cylinder using a two-dimensional approach at low Reynolds numbers. They found that there was a band of oscillation frequencies, centred on the value of f_e/f_o where the jump in the lift force was observed, where no single periodic mode of vortex shedding was observed. They attributed this result to an "almost-periodic switching between wake states". This result contrasts with the hysteretic transition observed by Bishop & Hassan (1963). It is not known if the contrasting nature of the transition observed by Blackburn & Henderson (1999) is due to the low value of Reynolds number, the zero level of free-stream turbulence, or if transition was altered by the two-dimensional nature of the wake.

For an elastically mounted cylinder with higher values of $m^*\zeta$, Khalak & Williamson (1997) found a hysteretic transition between the initial branch and the lower branch. This result is consistent with the transition observed by Brika & Laneville (1993) for an oscillating cable. However at low values of $m^*\zeta$, where there are three response branches, Khalak & Williamson (1997) found that the transition between the initial branch and the upper branch was hysteretic, but the transition between the upper branch and lower branch was intermittent. For velocities within the intermittent transition region, the phase and amplitude of the cylinders response switched in a non-periodic fashion between values that were consistent with either the upper or lower branches. As the velocity increased within the transition region, the system tended to spend a greater proportion of its time in the lower branch.

The hysteretic transition between the initial and upper branches indicates that the system has a tendency to remain in the established state and the system does not switch repeatedly between states. This suggests that a significant perturbation is required to move between the initial and upper branches. In contrast, during the intermittent transition the system repeatedly switches

between the upper and lower branches, suggesting that only a small perturbation is required for this transition to occur. Intuitively, this is consistent with the magnitude of the changes corresponding to the two different transitions. The transition between the initial and upper branches corresponds to a change in both the mode and phase of shedding, but the upper to lower branch transition corresponds to a change only in the distribution of vorticity, while the phase and general mode of vortex shedding remain the same.

Within a transition region there are two or more stable states in which a system can exist, but typically there will be a state that is the most stable state. The state that the system selects depends upon the initial state of the system and the relative level of perturbation within the system and depending on these factors a system may not necessarily be in the most stable state for the prevailing flow conditions. It is difficult to determine an initial state that guarantees the system will select the most stable wake state. Therefore, when the behaviour of a system within a transition region is investigated the initial state of the system must also be considered. In theory, a transition is typically associated with the point where there is a change in the most stable state. However, in practise, it is not possible to define a transition point without also rigorously defining the initial conditions and for different experimental techniques and conditions some variation in the point at which transition occurs should be expected.

1.6.2 Spanwise Correlation and Wake Structure

The investigation of Hover *et al.* (1998) considered the spanwise correlation of the lift force along a cylinder undergoing free and forced oscillations. The forces were measured using force balances located at either end of the cylinder and a correlation coefficient was calculated from these two force signals. For the forced oscillations, over a range of oscillation amplitudes, $A/D = 0.2$-0.9, and reduced velocities, $U^* = 4.5$ - 6.75, the spanwise correlation co-efficient was always greater than 0.84. For the free oscillations the cylinder was not elastically mounted but the free oscillations were instead generated using a novel real-time force-feedback control system. The average value of the instantaneous forces measured at each end of the cylinder were used to drive a numerical simulation of a mass-dashpot-spring system and the cylinder was then forced to move with the appropriate motion using a servomotor. The response of the cylinder produced using this method, shown in Figure 1-38a, agrees well with the results from the elastically mounted cylinder of Khalak & Williamson (1999). Within the response region the lift forces measured at either end of the cylinder were very well correlated with the exception of the region between $U^* = 5.0 - 6.25$ corresponding to the distinct dip in the correlation co-efficient in region III of Figure 1-38b. Figure 1-38c shows that the dip in spanwise correlation corresponds to a jump of approximately 180° in the phase of the lift force which, when combined with the change in the amplitude response, is consistent with the transition between the initial and lower response branches. In region III of

Figure 1-38 the lift phase exhibits a number of intermediate values which are not consistent with either the initial or lower response branches and which were not observed by either Khalak & Williamson (1999) or Govardhan & Williamson (2000). One possible explanation for the intermediate values of ϕ_{lift} (or ϕ) is that during the time over which each data point was acquired the system occupied both response branches.

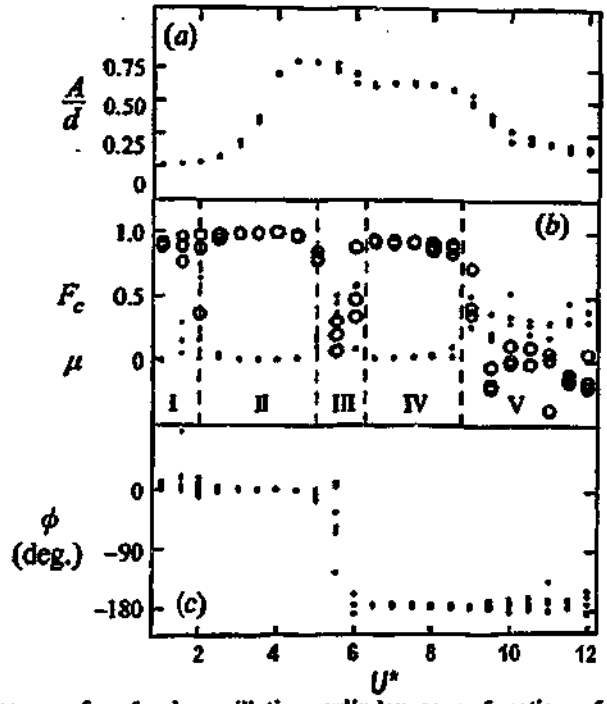

FIGURE 1-38 Response of a freely oscillating cylinder as a function of reduced velocity: a) amplitude of response: b) correlation coefficient F_C and standard deviation μ between the forces measured at the ends: c) phase angle ϕ between the force and displacement. In a) and c) points form both ends of the cylinder are plotted. Reproduced from Hover *et al* (1998).

The dip in the spanwise correlation appears to be linked to the transition between the initial and lower branches. However, it is not clear if the low spanwise correlation is a result of changes in the phase of vortex shedding along the cylinder or if there are changes in the spanwise structure of the wake close to transition. It is generally assumed that transition occurs uniformly along the span of the cylinder, however the spanwise nature of transition, and indeed the spanwise structure of the wakes for the different response branches, are not well understood.

For the forced oscillation of a tapered cylinder, Techet (1998) and Techet *et al.* (1998) showed the wake can exhibit "hybrid" modes, where the wake forms one mode along part of the cylinders span and another mode along the rest of the span. A schematic of a "hybrid" mode with a spanwise transition between the 2S and 2P wake modes is shown in Figure 1-39. The tapered cylinder encourages transition between wake modes along the span of the cylinder because the effective values of Re and A/D vary with spanwise location. In separate experiments, Techet (1998) showed that at reduced velocities close to where the hybrid modes start to occur, there is a sharp decrease in

the spanwise correlation of the force along the tapered cylinder. However, neither Hover *et al* (1998) nor Techet (1998) directly linked the variation in the spanwise correlation to changes in the vortex structures along the span of the cylinder.

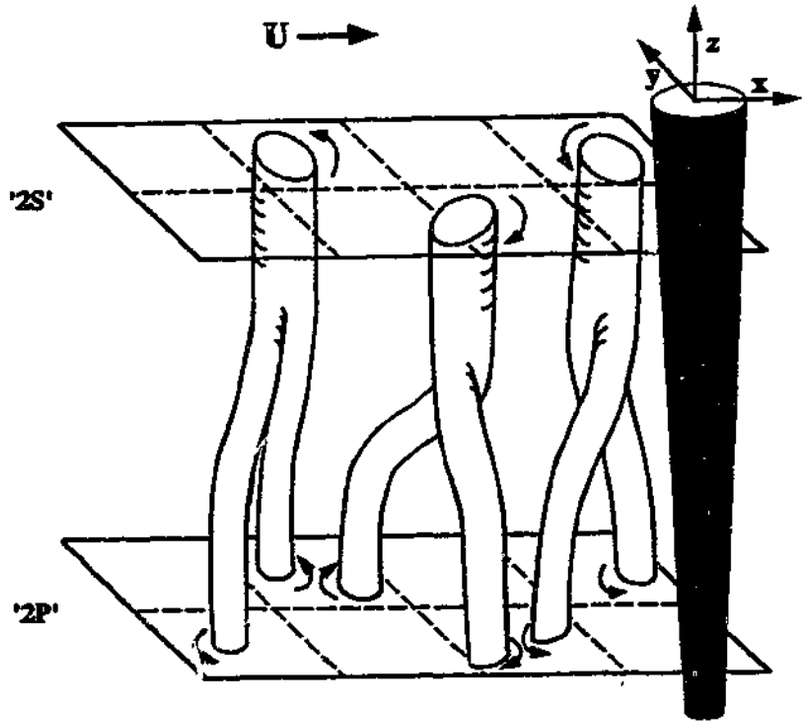

FIGURE 1-39 Suggested topology of the vortex reconnection between the 2P and 2S modes along a tapered cylinder. Reproduced from Techet (1998)

The spanwise structure of a stationary cylinder has been extensively studied, however little is known about the three-dimensional structure of an oscillating cylinder. Cetiner (1998) measured the streamwise vorticity along the span of an oscillating cylinder for a variety of forced oscillation profiles. She found that for transverse cylinder oscillations the level of streamwise vorticity (ω_x) could be as high as 1/3 of the spanwise vorticity (ω_z). The instantaneous spanwise and streamwise vorticity fields in Figure 1-40(a & b) respectively show the structure of the near wake for transverse oscillations at a given amplitude and frequency. The spanwise vorticity structures proved to be highly repeatable and the structure of the wake in Figure 1-40c, phase-averaged over 32 images, is very similar to the instantaneous wake structure. In contrast, despite the relatively high level of streamwise vorticity the location of these structures was not repeatable and the phase-averaged streamwise vorticity field in Figure 1-40d tends to zero. The levels of streamwise vorticity are obviously significant but their influence on the forces experienced by the cylinder and the transition between different wake states is not well understood. Interestingly the two-dimensional simulations of the forced cylinder oscillations by Blackburn & Henderson (1999),

which model only the spanwise vorticity, were able to capture the jump in the phase and amplitude of the lift force.

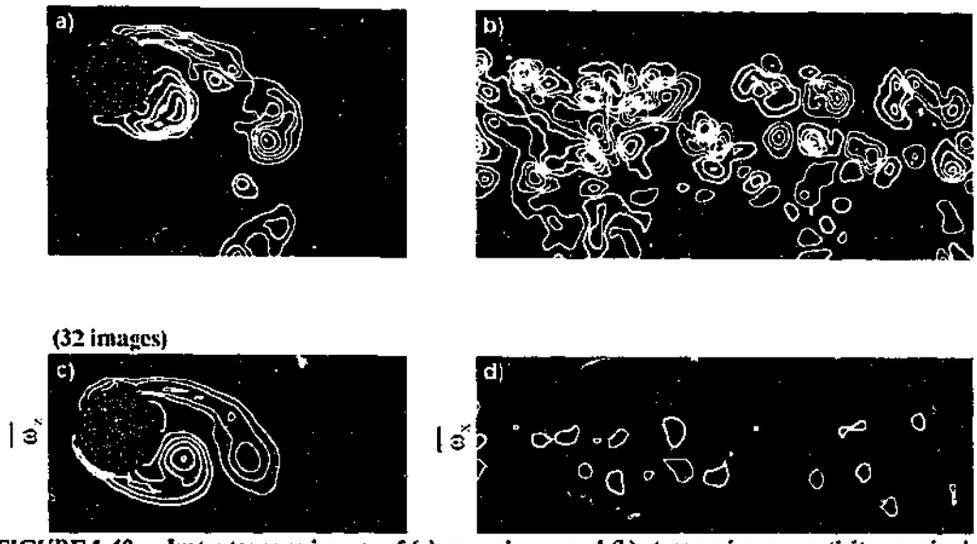

FIGURE 1-40 Instantaneous images of (a) spanwise ω_z and (b) streamwise, ω_x vorticity acquired at the maximum vertical displacement of the cylinder, f_e/f_o = 1.0, A/D = 0.95. The spanwise and streamwise positions of images (a) and (b) respectively are indicated by the vertical lines in the other image. The corresponding phase-averaged images are shown in (c) and (d). Reproduced from Cetiner (1998).

A complementary numerical and experimental study on the vortex-induced vibration of a cylinder, Blackburn et al (2001), found that "three-dimensional simulations are required to reproduce the response envelope observed experimentally". They also found that for the 2P mode of shedding there are significant spanwise structures in the wake as shown in Figure 1-41.

FIGURE 1-41 Instantaneous isosurfaces of pressure (predominantly spanwise) and streamwise vorticity from three-dimensional simulations of the vortex-induced vibrations of a cylinder at St U* = 1.33 (2P mode of shedding). Reproduced from Blackburn *et al* (2001)

1.6.3 Relating Forced and Free Oscillations

As discussed in section 1.3, the structure of the near wake and the forces on a structure oscillating due to vortex-induced forces have often been studied using forced sinusoidal oscillations. The reviews of the forced and freely oscillating cylinders in sections 1.4 and 1.5, demonstrate that these two cases do in fact have much in common; both the forced and freely oscillating cylinders appear to display two or more distinctly different states as the frequency of oscillation varies relative to the Kármán frequency. These states are typically characterised by the mode of vortex shedding and the phase of the lift force and the values of f_e/f_o or $(U^*/f^*)St_o$ at which they occur are very similar.

At this point it is important to consider the parameters that are used to describe the forced and freely oscillating cases. When the cylinder is forced to oscillate the properties of the system are generally considered as a function of f_e/f_o where as discussed previously f_e is the frequency of oscillation which is physically varied during the experiment and f_o is the Kármán frequency of the stationary cylinder. Using the fact that Strouhal number is essentially constant over the Re range considered, f_e/f_o can also be expressed in terms of a reduced velocity $U^* = U/f_eD$. In some experiments the flow velocity U is varied instead of f_e. Except for small variations in the Reynolds number these cases are equivalent. For the freely oscillating cylinder the frequency of oscillation is not an independent variable and the properties of the system are always considered as a function of the flow velocity. Additionally, the frequency of oscillation is generally normalised using the natural frequency of the structure f_N instead of the Kármán frequency, therefore $U^* = U/f_ND$. This choice of a different definition of U^* is quite fundamental and illustrates the difference between the forced and freely oscillating cases.

Interestingly Khalak & Williamson (1999) found that when the response of the elastically mounted cylinder was plotted against $(U^*/f^*)St_o$, rather than U^* much of the data collapsed onto a single curve as described in section 1.5.2. Evaluating the components of $(U^*/f^*)St_o$:

$$\frac{U^*}{f^*}St_o = \frac{U}{f_ND}\frac{f_N}{f}\frac{f_oD}{U}$$
$$= \frac{f_o}{f}$$

Therefore, plotting the data in terms of $(U^*/f^*)\ St_o$ is effectively plotting the response of the system as the frequency of oscillation varies relative to the Kármán frequency, which is to very similar to the way the results of the forced oscillations are plotted. Comparing the parameters, f/f_o for a freely oscillating cylinder and f_e/f_o for the forced oscillations, it is apparent that in both cases the frequency being normalised by f_o is the frequency at which the cylinder is oscillating. However, f is the frequency at which the freely oscillating system responds to the natural instability of the

wake, whereas for the forced oscillations f_e is the frequency at which the natural instability is forced.

The apparent similarities in the modes of vortex shedding and variation of ϕ_{lift} for the forced and freely oscillating cylinders indicates that the forced oscillations are modelling many of the important aspects of the vortex-induced motion. However, the crucial question remains: can we use the forced oscillation of a body to predict the vortex-induced motion of an elastically mounted body? It has generally been assumed that the results of forced oscillations can be used to understand the freely oscillating cylinder, however very few efforts have been made to predict the vortex-induced motion using the forced oscillation results. In part this is due to the extensive force mapping required to undertake such an exercise, as the force on the cylinder must be known as a function of both the frequency and amplitude of oscillation.

Staubli (1983) attempted to predict the vortex-induced motion of a cylinder using the force data shown in Figure 1-11 and the equation of motion for an elastically mounted body. Inherent in this calculation was the assumption that the motion of the freely oscillating cylinder is either sinusoidal or can be predicted using a sinusoidal motion. Staubli (1983b) also pointed out that as a freely oscillating cylinder requires positive energy transfer from the fluid to the cylinder, the forced oscillations must result in positive energy transfer, i.e. $0° < \phi_{lift} < 180°$, before they can be used to predict flow-induced motion. The majority of Staubli's data in Figure 1-11 shows values of ϕ_{lift} that indicate negative energy transfer. However, Staubli (1983b) interpreted the relative small band of oscillation frequencies (S_o = 0.14-0.17) where $0° < \phi_{lift} < 180°$ as the "range of fluid-excited vibrations of the freely oscillating cylinder". It should be noted that much of this data corresponds to the region where the lift phase is changing rapidly, taking on "intermediate" values that are not consistent with the values of ϕ_{lift} either side of the jump. As shown in Figure 1-42, his calculations were relatively successful in predicting the initial response branch of the freely oscillating cylinder for small positive values of ϕ_{lift} close to 0°. However, for $\phi_{lift} \approx 100°$ the calculations did not predict the response of the cylinder. Examination of Figure 1-11 reveals that the values of ϕ_{lift} close to 100° are in fact intermediate values that are not consistent with the values of ϕ_{lift} either side of the jump. It is not known if these intermediate values of ϕ_{lift} correspond to a third wake state or if the intermediate values are the result of averaging data containing two different wake states. Interestingly, the data of Khalak and Williamson (1999) and Govardhan & Williamson (2000) for an elastically mounted cylinder does not show these intermediate values of ϕ_{lift}.

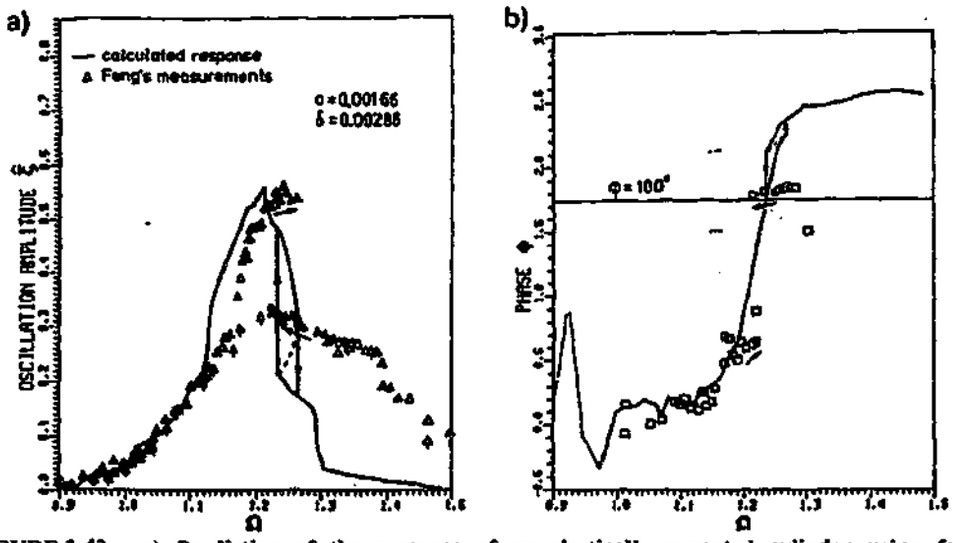

FIGURE 1-42 a) Prediction of the response of an elastically mounted cylinder using forced oscillation and comparison with experimental results of Feng: b) phase angle of the lift force, ϕ_{lift} within the lock-in range. Reproduced from Staubli (1983b).

Many of the previous investigations of forced cylinder oscillations obtained values of ϕ_{lift} that correspond to negative energy transfer and therefore predict that vortex-induced motion will not occur. The extent of these regions of negative energy transfer and the ramifications for the relationship between the forced and freely oscillating cylinder, will be considered further in this work.

1.7 STATIONARY CYLINDER NEAR A SURFACE

1.7.1 Boundary Conditions at a Solid or Free-Surface

Unbounded flow past a stationary cylinder results in periodic shedding of vortex structures from the cylinder and the formation of the characteristic Kármán street. When the flow is bounded by a surface the structure of the wake and the forces on the cylinder can be significantly altered as shown by Bearman & Zdravkovich (1978) and Miyata *et al.* (1990). The surface interface between a liquid and a gas, for example water and air, is typically described as a free-surface and, as discussed by Rood (1995) and Gharib & Weigand (1996), the boundary conditions at a free-surface are significantly different from those at a solid boundary. The tangential pressure gradient along a solid surface results in the generation of vorticity and at a no-slip boundary all the vorticity is parallel to the surface. A clean free-surface is not a no-slip boundary, but instead has a zero-shear-stress boundary condition. Along a flat clean free-surface orientated along the x-y plane $\tau_{yx} = \tau_{yz} = 0$, $\partial v/\partial z = \partial v/\partial x = \partial w/\partial y = \partial u/\partial y = 0$ and both surface-parallel vorticity and surface-parallel vorticity flux are zero. Thus, as described by Batchelor (1967) in contrast to a solid boundary the zero-shear condition along a clean flat free-surface permits only surface-normal vorticity, forcing vortex lines to terminate normal to the free-surface.

When a free-surface is deformed the viscous flow beneath the curved surface generates a shear on the boundary which, in order to preserve the zero-shear boundary condition, must be counteracted by the generation of vorticity. If the flow is inviscid then by definition the shear is zero and the zero shear stress boundary condition is trivial. The surface-parallel vorticity at the curved viscous free-surface can be described using curvilinear co-ordinates along the curved surface and writing the vorticity in terms of the surface shear stress. The surface-tangent vorticity ω_z is given by:

$$\omega_z = \frac{1}{r}\frac{\partial}{\partial r}(ru_\theta) - \frac{1}{r}\frac{\partial u_r}{\partial \theta} \qquad (1\text{-}16)$$

and the shear stress due to the fluid beneath the free-surface is:

$$\tau_{r\theta} = \mu\left(r\frac{\partial}{\partial r}\left(\frac{u_\theta}{r}\right) - \frac{1}{r}\frac{\partial u_r}{\partial \theta}\right) \qquad (1\text{-}17)$$

therefore

$$\omega_z = \frac{\tau_{r\theta}}{\mu} + \frac{2u_\theta}{R_s} - \frac{2}{R_s}\frac{\partial u_r}{\partial \theta} \qquad (1\text{-}18)$$

where R_s is the local radius of curvature of the surface. Equation 1-18 is the boundary condition for a free-surface, where the three terms on the right hand side represent the sources of vorticity due to:

(i) The shear stress at the interface with the adjoining fluid which is negligible for a clean water-air interface, but becomes significant when the water surface is contaminated by surfactants;

(ii) Flow under a curved surface or the generation of vorticity due to deformation of the surface;

(iii) Changes in the velocity along the surface. This is effectively an unsteady term representing generation of vorticity due to movement of the surface.

When the free-surface is flat the second and third terms on the right hand side of equation 1-18 tend to zero and vorticity is only generated when the free-surface is contaminated. Gharib & Weigand (1996) showed that the flux of surface-parallel vorticity at a deformed contaminated surface is given by:

$$-\nu\frac{\partial\omega_s}{\partial r}=\frac{\partial u_s}{\partial t}+\frac{1}{2}\frac{\partial(u_s^2+u_r^2)}{\partial s}+\frac{1}{\rho}\frac{\partial p}{\partial s}+g\cos\alpha-u_r\omega_s \qquad (1\text{-}19)$$

where s is a local surface co-ordinate parallel to θ and α is the local angle of the free-surface to the gravitational vector.

The Froude number, $Fr = U/(g\,L)^{1/2}$ is the non-dimensional parameter used to describe the behaviour of free-surface flows, where U is the free-stream velocity and L is a characteristic length scale. In many cases the flows depend both on Fr and Re. In open channel flows the Froude number describes the ratio of the wave speed of the free-surface disturbances, which vary with $(g\,L)^{1/2}$, to the free-stream velocity, U. When used in this way Fr describes the ability of a disturbance to travel upstream and is analogous to the dimensionless Mach number for compressible flows.

For a body close to a free-surface in deep flow the Froude number is applied differently. In this case Fr represents the ratio of the fluid inertia force to the gravitational force, where Fr is actually the square root of this ratio. In these cases the Froude number describes the propensity of a free-surface to deform and generate free-surface waves in response to forcing from the flow structures beneath the surface. Typically the Froude number used for flow over a cylinder is $Fr = U/(g\,D)^{1/2}$ where the length scale for both the inertial and gravitational forces is the diameter of the cylinder. Sheridan *et al.* (1997) considered using the depth of the cylinder below the free-surface as the length scale for both the inertial and gravitational forces, *i.e.* $Fr = U/(g\,h)^{1/2}$. However, neither $U/(g\,D)^{1/2}$ or $U/(g\,h)^{1/2}$ identified a critical Froude number at which the wake transitioned between different states. Irrespective of whether D, the diameter of the cylinder or h, the depth of the cylinder, was used as the characteristic length scale in Fr, Sheridan *et al.* (1997) found that

increasing *Fr* caused similar systematic changes in the wake. Unless specifically stated the Froude number used in this text will be based on the diameter of the cylinder.

1.7.2 Flow Over a Cylinder Close to a Solid Boundary

The boundary conditions at a solid wall are different from those at a free-surface. However, in both cases the flow is constrained by the boundary and these two different flows exhibit a number of similar features. Bearman & Zdravkovich (1978) measured the mean pressure distribution on a cylinder close to a solid wall, as well as the mean pressure distribution along the wall. The mean pressure distribution on a cylinder in unbounded flow is symmetric about the centre-line of the cylinder, however as the gap between the cylinder and the wall decreases the pressure distribution on the cylinder becomes non-symmetric. As shown in Figure 1-43, for gap ratios of $G/D = 0.4$ and 0.1, the asymmetry of the pressure distributions increases as the cylinder approaches the wall, where G is the distance between the wall and the cylinder. As G/D decreases the front stagnation point rotates towards the surface as does the separation point furthest from the wall, but there is only a relatively small change in the position of the separation point adjacent to the wall. Additionally, as G/D decreases there are also changes in the pressure distribution along the wall. As the flow approaches the gap between the wall and the cylinder there is an initial increase in the pressure on the wall, but further downstream there pressure decreases rapidly as the flow accelerates between the cylinder and the wall. The peak negative pressure occurs just downstream of the cylinder's centre and the magnitude of peak wall pressure increases as G/D decreases. The non-symmetric pressure distribution on the cylinder results in a net force that pushes the cylinder away from the solid surface and, unlike a cylinder in unbounded flow, the net lift force on the cylinder is not zero.

Despite the obviously asymmetric pressure distribution in Figure 1-43 at $G/D = 0.4$, measurements of the velocity fluctuations behind the cylinder indicated that for this gap ratio periodic vortex shedding is still occurring. Moreover, the Strouhal frequency of this vortex shedding is only slightly higher than for unbounded flow. Bearman & Zdravkovich measured the velocity fluctuations in both shear layers; finding in both cases a strong spectral peak at the shedding frequency. However, the peak obtained in the shear layer closest to the wall was less energetic than the peak for the shear layer further away from the wall. As the gap ratio decreased the relative difference in the energy of these two peaks increased. The velocity spectra in the near wake indicate that periodic vortex shedding persisted for gap ratios down to $G/D = 0.3$. For $G/D \leq 0.2$ relatively weak high frequency fluctuations occurred in the shear layer furthest from the wall and periodic fluctuations were not observed in the shear layer closest to the wall, indicating that regular Kármán shedding is suppressed. The asymmetry of the pressure distributions at $G/D = 0.1$ in Figure 1-43(b), where regular vortex shedding is suppressed, is much more accentuated than for the

case shown in Figure 1-43(a), at G/D = 0.4, where periodic shedding occurs. In both cases the front stagnation point and the separation point closest to the wall have rotated towards the wall and there is a sharp peak in the negative pressure on the wall as the fluid passes through the gap. The most notable difference between the two cases is that at G/D = 0.1 the pressure distribution on the portion of the cylinder adjacent to the wall has rotated in the same direction as the front stagnation point, so that the peak negative pressure occurs further downstream than at G/D = 0.4. Additionally, at G/D = 0.1 the mean pressure distribution on the surface of the cylinder next to the wall does not exhibit a significant adverse pressure gradient suggesting that there may have been a change in the nature of flow separation.

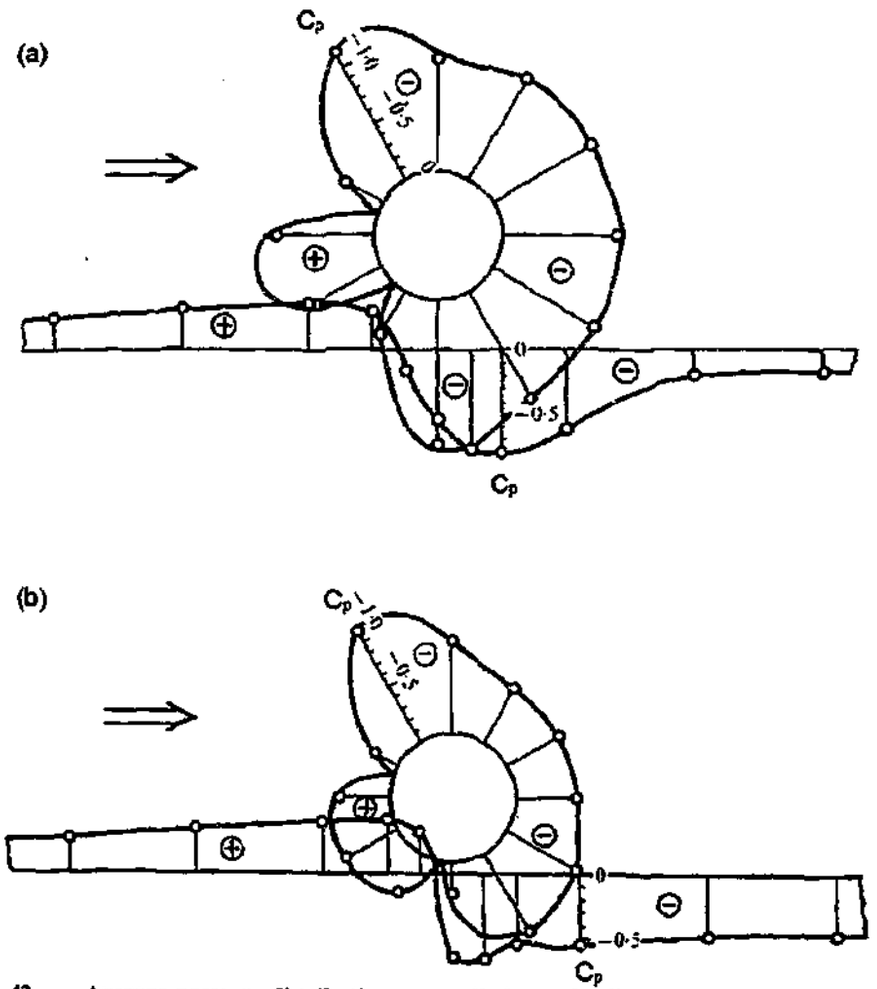

Figure 1-43 Average pressure distribution on a cylinder and solid wall for flow over a cylinder near a wall, for a) a cylinder to wall gap of G/D = 0.4 and b) G/D = 0.1. Reproduced from Bearman & Zdravkovich (1978).

Flow visualisation, PIV and hot film measurements by Price *et al.* (2000) found that the apparent suppression of vortex shedding at small G/D corresponded to the formation of long attached shear

layers that did not interact with each other in an organised periodic fashion. For small gaps they found that the wall boundary layer separated upstream of the cylinder, where the size of the separation bubble decreased and the separation point moved downstream as *G/D* increased. They predicted that the formation and position of the separation bubble would vary both with the *G/D* and a Reynolds number based on the distance of the cylinder from the leading edge of the plate.

For gap ratios at which periodic shedding is observed a number of investigations, including Bearman & Zdravkovich (1978), Angrilli *et al.* (1982) and Price *et al.* (2000), have observed an increase in the shedding frequency as the gap between the cylinder and the wall decreases. The frequency of vortex shedding increases smoothly with a peak value occurring just prior to the suppression of vortex shedding. However, there is some disagreement in the magnitude of the increase in shedding frequency. For relatively high Reynolds numbers of $2.5\text{-}4.5\text{x}10^4$ Bearman and Zdravkovich (1978) observed only a very small increase in Strouhal frequency of between 2-3%. However, for Re = 2860-7640 Angrilli *et al.* (1982) observed an increase of up to 10% and at Re = 1200-1900 Price *et al.* (2000) observed a much larger increase in the shedding frequency of up to 40%. None of the investigators reported significant variation of the shedding frequency within the Reynolds numbers ranges of their investigations.

1.7.3 Forces on a Cylinder Underneath a Free-Surface

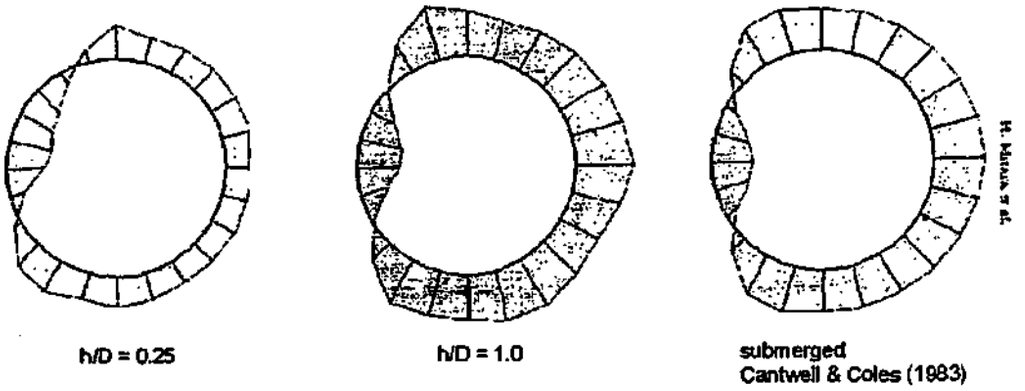

Figure 1-44 Plot of time-averaged pressure distributions on a cylinder underneath a free-surface for a) h/D = 0.25, b) h/D = 1.0 and c) a fully submerged cylinder. Reproduced from Miyata *et al.* (1990).

Miyata *et al.* (1990) conducted experiments on a cylinder beneath a free-surface at $Re = 4.96 \times 10^4$ and $Fr = 0.34$. In Figure 1-44 the pressure distribution around a cylinder beneath a free-surface, measured by Miyata *et al.* (1980), are compared with the symmetric pressure distribution measured by Cantwell & Coles for a fully submerged cylinder, where h is the depth of the top of the cylinder below the surface. As the cylinder moves towards the free-surface there is a clockwise rotation of the front stagnation and separation points and, as shown in Figure 1-44(a & b), the front stagnation point moves closer to the free-surface. The pressure distribution on a cylinder beneath a free-surface exhibit many of the characteristics described by Bearman & Zdravkovich (1978) for a cylinder close to a solid surface. (Note; the configuration of the cylinder near the solid surface in Figure 1-43 has the cylinder above the surface, therefore when a cylinder is underneath a free-surface the geometry of the system is flipped.)

Miyata *et al.* (1990) found that for $0.35 < h/D \leq 1.75$ the fluctuating lift force on the cylinder was strongly periodic, with an approximately constant Strouhal number of 0.19. These results are similar to those observed for a fully submerged cylinder and indicate that periodic vortex shedding is occurring. As h/D decreased below 0.35 there was a sudden drop in the spectral energy of the lift force at $St \approx 0.19$, indicating that the close proximity of the free-surface was causing a partial suppression of vortex shedding. At the smallest cylinder depths, $h/D \leq 0.335$, the peak at $St \approx 0.19$ was no longer present and there was a small peak at $St \approx 0.3$ in both the lift spectra and the pressure spectra close to the upper and lower separation points. Miyata *et al.* (1990) found that for these very small h/D the pressure fluctuations were strongest in the upper shear layer adjacent to the free-surface. These results are in contrast to the findings of Bearman & Zdravkovich (1978) for flow over a cylinder near a wall. Miyata *et al.* (1990) attributed the relative strength of the pressure

fluctuations in the upper shear layer to an interaction between the vortex shedding and the free-surface.

Figure 1-45 shows the variation of the mean lift and drag forces, measured by Miyata *et al.* (1990), as the cylinder approaches the free-surface. For $h/D > 0.35$ the mean drag is approximately constant, however as h/D decreases below 0.35 the suppression of strongly periodic vortex shedding corresponds to a sharp drop in the mean drag. The mean negative lift force on the cylinder increases steadily as the cylinder approaches the surface. Interestingly, for $0.35 < h/D \leq 1.75$ the frequency of vortex shedding remained approximately constant despite the changes in the mean lift force on the cylinder and the asymmetry in the pressure distribution.

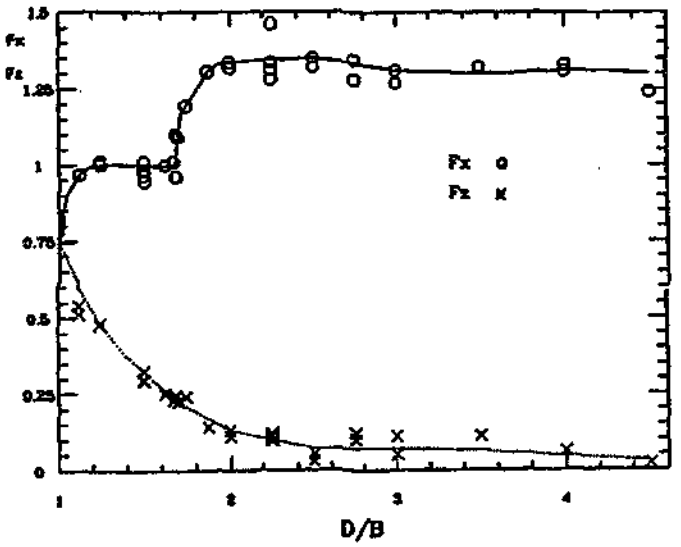

Figure 1-45 Variation of mean drag (F_x) and negative mean lift (F_z) with cylinder depth D_c/B, where $D_c/B = 2h/D + 1$. Reproduced from Miyata *et al.* (1990).

Miyata *et al.* (1990) also presented the time varying pressure distributions at cylinder depths of h/D = 0.25 and 1.0, which are either side of the sharp drop in the spectral energy at the Strouhal shedding frequency. At the smaller cylinder depth of $h/D = 0.25$ the wake is only weakly periodic and the variations in the time dependent pressure distribution are relatively small. However, further away from the free-surface at $h/D = 1.0$ there is a significant level of variation in the time dependent pressure distributions which is consistent with periodic vortex shedding.

1.7.4 Wake Structure for a Cylinder Underneath a Free-Surface

The potential flow solution for bounded flow over a body clearly shows that the structure of the flow is altered by the presence of the boundary and depends also upon the nature and proximity of the boundary. The experimental results of Miyata *et al.* (1990) and Sheridan *et al.* (1997) for a viscous, turbulent, three-dimensional flow over a cylinder beneath a nominally clean water-air interface show that the wake structure depends not only on h/D but also on Re and Fr. Additionally, it is also expected that a number of secondary factors, including the level of free-stream turbulence and the aspect ratio of the cylinder, can also effect the structure of the wake.

Flow visualisation of relatively large diameter polystyrene beads by Miyata *et al.* (1990) indicated that the structure of the near wake varies significantly with h/D. At $h/D = 1.0$ the flow visualisation in Figure 1-46(a) shows the formation of a strong vortex structure very close to the back of the cylinder, and it was reported that the time varying wake structure resembled Kármán shedding from a fully submerged cylinder. However, the length of the attached wake in Figure 1-46(a) appears to be significantly shorter than for a fully submerged cylinder at similar values of Re. When the depth of the cylinder is reduced to $h/D = 0.25$ there is a distinct change in the wake structure, as shown in Figure 1-46(b). The wake is clearly angled downwards and the length of the wake is much longer than both the wake at $h/D = 1.0$ and also the wake of a fully submerged cylinder. A large vortex structure forms in the lower wake while the upper wake is relatively disorganised and does not have a clear structure. Additionally, the flow visualisation suggests that the free-surface is not flat, with the appearance of free-surface waves downstream of the cylinder. At the smallest cylinder depth of $h/D = 0.063$ the wake is similar to the wake at $h/D = 0.25$: the lower shear layer has a distinct downward angle, there is a large vortex structure in the lower wake and free-surface deformation is apparent immediately behind the cylinder. As h/D decreases from 1.0 to 0.063 the flow visualisation shows a rotation of the front stagnation point towards the free-surface that is consistent with the changes in the pressure distribution discussed above.

The flow visualisation in Figure 1-46 shows that the structure of the wake varies with h/D but the different wake modes are not clearly defined. Additionally, the relatively large polystyrene beads, which were 1mm in diameter or 0.6 % of the cylinder diameter, may have altered the flow, particularly at small values of h/D.

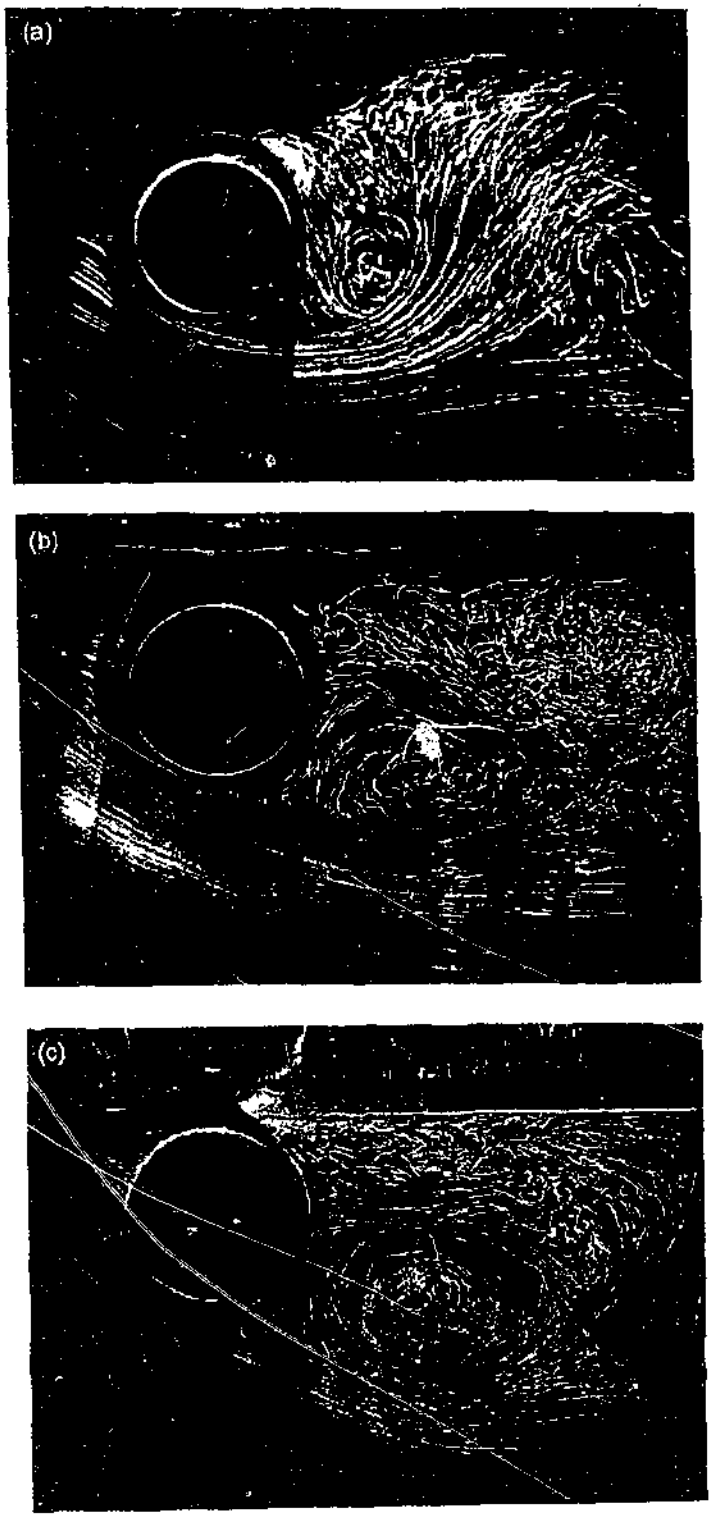

Figure 1-46 **Flow visualisation of flow around a cylinder underneath a free-surface at a) h/D = 1.0, b) 0.25, c) 0.063 for $Re = 4.96 \times 10^4$ and $Fr = 0.34$. Reproduced from Miyata *et al.* (1990).**

Qualitative PIV measurements by Sheridan *et al.* (1995, 1997) at $0.22 \leq Fr \leq 0.97$ showed that the wake of a cylinder underneath a free-surface exhibits a number of different states. The wake states depend both on Fr and h/D and, as discussed in section 1.7.1, the variation of the wake with h/D can also be expressed in terms an alternative Froude number, $U/(g\,h)^{1/2}$. As the cylinder approaches the free-surface Sheridan *et al.* (1997) observed a number of wake states that were distinctly different from the Kármán wake of a fully submerged cylinder. These states were divided into two basic classes depending upon the behaviour of the jet of high velocity fluid moving over the top of the cylinder. For cylinder positions further from the free-surface and at lower Froude numbers the jet tended to remain attached to the free-surface, but at smaller submergence depths and higher Fr the jet separated from the free-surface.

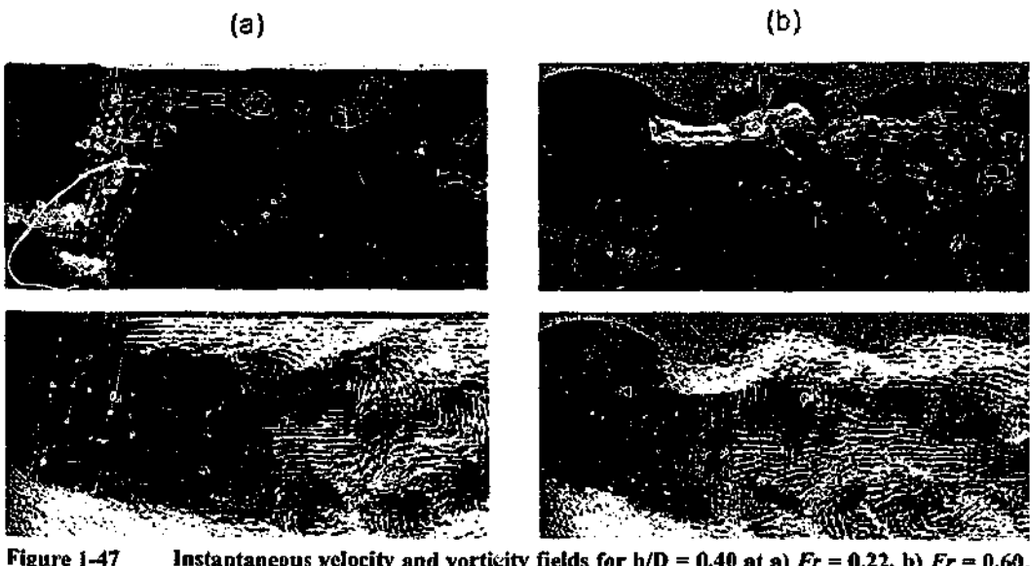

Figure 1-47 Instantaneous velocity and vorticity fields for h/D = 0.40 at a) Fr = 0.22, b) Fr = 0.60. Reproduced from Sheridan *et al.* (1997).

The velocity and vorticity fields for two cases where the flow over the top of the cylinder remains attached to the free-surface are shown in Figure 1-46, for a cylinder depth of h/D = 0.4 and two different Froude numbers, Fr = 0.22 and 0.60. In both cases the wake length is much longer than for a fully submerged cylinder and the lower shear layer has a downward angle. At the lower Froude number of 0.22 the free-surface behind the cylinder is relatively flat and vorticity is not generated due to free-surface curvature. At the higher Froude number of 0.60, the flow over the cylinder causes significant deformation of the free-surface resulting in the formation of free-surface waves and the generation of vorticity at the free-surface. The velocity fields in Figure 1-47 clearly show that in both cases the high-speed fluid remains attached to the free-surface, although the free-surface waves at Fr = 0.60 cause local separation and subsequent re-attachment of the flow.

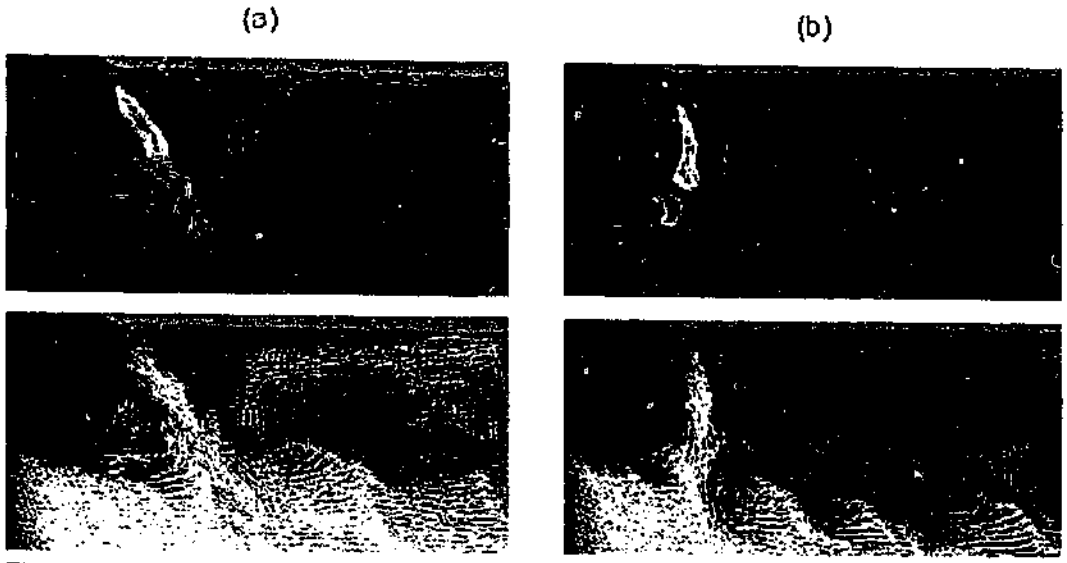

Figure 1-48 Instantaneous velocity and vorticity fields at two different times illustrating the variability in the wake state at Fr = 0.6 an h/D = 0.31. The high velocity fluid above the cylinder forms a) a free-jet and b) a jet which is attached to the back of the cylinder. Reproduced from Sheridan *et al.* (1997).

Sheridan *et al.* (1997) found that the transition from a wake with high-speed flow attached to the free-surface to a flow that separates from the free-surface is associated with either an increase in *Fr* or a decrease in *h/D*. In Figure 1-48(a) the high-speed fluid separates from both the free-surface and the cylinder immediately after passing through the relative narrow gap above the cylinder. The separated free-jet forms a downward angle across the rear of the cylinder. As shown in Figure 1-48(b), for the same flow conditions the jet can also separate from the free-surface but remain attached to the rear surface of the cylinder. The two wake states shown in Figure 1-48, at $Fr = 0.6$ and $h/D = 0.31$ indicate that for these flow conditions the wake was metastable alternating between the formation of a free-jet and a jet which is attached to the rear of the cylinder. Sheridan *et al.* (1997) also observed a similar metastable wake at Fr = 0.6 and h/D = 0.45. These wake modes were also visualised by Hoyt & Sellin (2000) using a tracer liquid. Typically, the formation of the free-jet occurs at lower values of *Fr* or cylinder positions that are further away from the surface. The attachment of flow to the rear of the cylinder occurs when the modification of the wake by the free-surface is greatest, *i.e.* at the smallest values of *h/D* and large *Fr*. It is not immediately apparent from the flow visualisations of Miyata *et al.* (1990) close to the free-surface if the upper shear layer separates from, or is attached to, the free-surface. However, Figure 1-46(b & c) does show that, as for the wake states observed by Sheridan *et al.* (1997), the attached wake is relatively long and the lower shear layer is angled downwards.

The wake states depend on the influence of the free-surface, which increased either by moving the cylinder closer to the free-surface or by increasing *Fr*. Thus, the value of *Fr* affects the range of *h/D* over which a wake state occurs. However, neither the Froude number based on the cylinder's

diameter, or an alternative Froude number based on the cylinder's depth, allowed the identification of a critical value at which the wake transitioned between the two states. At a given *Fr* in a deep flow the full extent of the free-surface region can be traversed by varying *h/D*. However, for a cylinder which is immediately adjacent to the free-surface the wake cannot tend towards the fully submerged case without reducing the free-stream velocity to zero. Therefore, within a given Reynolds number regime, it is most logical to classify the wake states in terms of their dependence on *h/D* at a given Froude number.

Furthest away from the influence of the free-surface the flow visualisation and pressure distributions of Miyata *et al.* (1990) indicate that the wake exhibits periodic vortex shedding and is similar to the wake of a fully submerged cylinder, however the properties of this wake state are not well known. As the cylinder moves closer to the free-surface there is a large increase in the wake length, as shown in Figure 1-47, and the high-speed flow over the top of the cylinder is attached to the free-surface. As h/D is decreased further the jet of high-speed flow separates from the free-surface forming a separated free-jet, as shown Figure 1-48(a). Finally, as shown Figure 1-48(b), when the cylinder is closest to the free-surface the jet of fluid remains attached to the cylinder. In all cases the close proximity of the free-surface causes the lower shear layer to have a distinct downward angle.

1.7.5 Effect of Free-Surface Contamination

A free-surface is an interface between two different fluids, typically air and water. The large difference in the relative densities of water and air results in a free-surface stress that is effectively zero for a clean free-surface. However, as discussed by Scott (1982), if a surface-active contaminant, or surfactant accumulates on the surface the shear stress and surface tension at the boundary change accordingly. In general, surfactants act to reduce the surface tension, producing a non-zero shear stress boundary condition. If we consider the first term on the right hand side of equation 1-18 it is evident that a non-zero shear at the boundary can result in the generation of free-surface vorticity, as discussed by Warncke *et al.* (1996).

The presence of an obstruction or blockage at or immediately underneath the surface of a free-stream promotes the accumulation of surfactant, generating local boundary conditions that are quite different from the regions where the surface is relatively uncontaminated. Such situations are found commonly in nature, for example a semi-submerged tree branch in a natural stream or the diversion of flow around a rock. A similar effect is generated in a water channel when the flow is obstructed by the presence of an experimental model near the free-surface, or the diversion of the flow at the end of the working section. Thus, unless extreme care is taken to maintain a clean surface a build up of surfactant may occur. The surfactant that accumulates behind an obstruction moves at a reduced velocity relative to the free-stream flow, resulting in the formation of a

boundary layer underneath the non-zero shear boundary. The accumulation of surfactant at the surface of a free-stream flow also results in the formation of a phenomenon known as the Reynolds Ridge at the leading edge of the surface contamination. A schematic detailing the general features of the flow near a Reynolds ridge is shown in Figure 1-49. As discussed by Scott (1982) the elevated ridge of fluid immediately upstream of the surfactant is attributed to the retardation of flow approaching the non-zero shear stress boundary and the corresponding surface tension gradient. The curvature of the free-surface at the ridge results in additional generation of free-surface vorticity. Detailed measurements of the Reynolds ridge by Scott (1982) and Warncke *et al.* (1996) have shown that the curvature of the free-surface increases with the free-stream velocity. The presence of a Reynolds ridge is a clear indication of surface contamination and, as shown by Scott (1982), the Reynolds ridge can occur at relatively low levels of surface contamination.

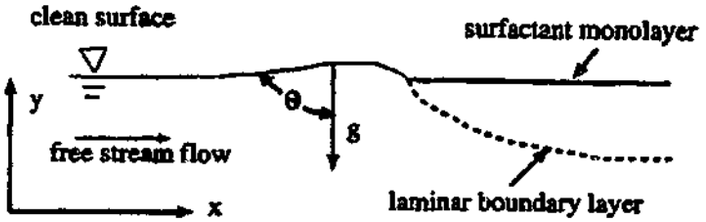

Figure 1-49 Schematic of flow near a Reynolds ridge. Reproduced from Warncke *et al.* (1996)

When the shear stress is zero at the surface vortex filaments must connect normally to the free-surface, however the non-zero shear generated by free-surface contamination alters the way in which vorticity interacts with the free-surface. In their study of the interaction between spatially modulated vortex pairs and a free-surface Willert & Gharib (1994, 1997) found that the for both the contaminated and clean free-surface the surface normal vorticity of the vortex tube formed local regions of connection with the free-surface. However, the shear forces caused by a relatively small amount of surface contamination appeared to inhibit the connection process and resulted in an increase in the formation of secondary vorticity. The study of flow around a surface-piercing cylinder by Warncke-Lang & Gharib (1998) also found that the structure of the flow immediately under the free-surface was significantly altered by the presence of free-surface contamination. The main factor contributing to these changes was an increase in the redirection of surface-normal vorticity to surface-parallel vorticity due to a non-zero surface tension gradient.

1.8 SCOPE OF THESIS

The literature reviewed in the previous sections raises a number of important questions related to the current investigation of the wake states of an oscillating cylinder. However, some of the questions raised by the literature are difficult issues that extended well beyond the case of an oscillating cylinder. One of the aspects considered in the current investigation is the nature of the transition between different wake states of an oscillating cylinder. The question that underlies this work, and the large number of studies preceding it, is; why does a transition between two different wake states occur at a particular point in time and parameter space. An analogous and similarly difficult question is; for given flow conditions, what determines the stability of a particular wake state. A transition between two different states is not unique to the case of an oscillating cylinder and in fact transitions are observed in many different fields of science. For example, a particle may undergo a transition between different energy levels, or the flow along a wall may undergo a transition from laminar to turbulent flow. This investigation does not seek to answer the ultimate question as to why a transition between different wake states occurs, rather it seeks to determine the nature of the transitions and the properties of the wake states either side of the transition. In the remainder of this section the specific questions arising from the literature review that form the basis for this research program will be discussed.

As the forcing frequency of the oscillating cylinder passes through $f_e/f_o \approx 1$ a number of investigations have independently observed changes in the lift force on the cylinder or changes in the phase-referenced structure of the near wake, as discussed in section 1.4. A link between the wake mode and forces on the cylinder was established numerically by Blackburn & Henderson (1999). However, there were some differences in the modes of vortex shedding observed by Blackburn & Henderson and the shedding modes observed experimentally. These differences may be attributably to their simulation being 2-dimensional, and also at low Reynolds number and oscillation amplitude. Using simultaneous force and flow field measurements the present investigation aims to establish a conclusive experimental link between the jump in the lift force and the changes in the phase-reference structure of the near wake. The establishment of this link will allow the identification of at least two wake states, where changes in the lift force and wake structure correspond to a transition between different wake states. A major component of this investigation is to determine the properties of these wake states, for example the values of the phase and amplitude of the vortex lift and drag forces and their variation with f_e/f_o is currently unknown. An interesting aspect of the vortex forces, discussed in section 1.3.3, is their direct relationship with the structure of the wake, in particular the rate of change of the vorticity field. This investigation will seek to qualitatively link the changes in the vortex lift and drag forces to changes in the mode and phase of vortex shedding.

As discussed in section 1.4.1 the jump in the lift forces is observed over a wide range of flow conditions, notably a range of *Re* and *A/D*. However, the occurrence and nature of systematic changes in the total and vortex lift and drag forces as *Re* and *A/D* are varied are not known. Additionally, it is not known how changes in *Re* and *A/D* affect the structure of the near wake. Intuitively, it is expected that increasing the oscillation amplitude will increase the length of the attached wake, but it is not known if this causes changes in the mode of vortex shedding. Specifically, it is not clear if changes in *A/D* and *Re* result in the 2P mode of shedding being observed in some cases but not in others.

An important aspect of this investigation is the relationship between the forced and freely oscillating cylinders discussed in section 1.6. The methodology of forced oscillation experiments is typically to use forced oscillations to simply the study of flow-induced motion. However, a link between the forced oscillation wake states and the free response branches is yet to be established. Moreover, it is not known how well the forced oscillations model the motion of the freely oscillating cylinder or if the results of the forced oscillations can be used to predict flow-induced motion. The properties of the forced wake states, determined in the current investigation, will be compared with the experimental results for an elastically mounted cylinder, in particular those of Govardhan & Williamson (2000).

The relationship between the forces on the cylinder and the structure of the near wake will also be considered for a stationary cylinder beneath a free-surface. As discussed in section 1.7 a number of previous investigations have observed a suppression of vortex shedding as the cylinder position approaches the free-surface. Sheridan *et al.* (1997) found that the wake exhibits a number of different modes, depending primarily on *Fr* and *h/D* and Miyata *et al.* (1990) measured changes in the forces on the cylinder as *h/D* decreased. However, the nature of the relationship between the structure of the near wake and the forces on the cylinder has not been established. The current investigation will seek to determine this relationship using simultaneous force and flow field measurements. There are a number of additional issues that will also be considered in this work. The investigation by Sheridan *et al.* (1997) was performed at high Froude numbers where significant surface deformation occurred. It is not known if the same or similar wake states exist at lower *Fr* where free-surface deformation is effectively eliminated. Additionally, very little is known about the structure of the wake for cylinder positions where periodic vortex shedding occurs but the forces on the cylinder are modified by presence of the surface.

2 EXPERIMENTAL METHOD

In this section the experimental facilities and techniques used to obtain the results will be described. Additionally the post processing techniques and calculations that were used to evaluate the data will also be outlined.

2.1 FLOW SYSTEM

The experiments were performed in a free surface recirculating water channel at the Lehigh University fluid mechanics laboratories. The plexiglass working section had a width of 914 mm, depth 609 mm and was 4928 mm long. Upstream of the working section the flow passed through a 2:1 contraction followed by a Nomex® honeycomb and a fine wire screen, in combination these components act to straighten the flow and reduce the free-stream turbulence level to less than 1%. An axial flow pump, with an electronic controller was used to obtain flow velocities in the working section of between 0.056 and 0.180 m/s.

The free-stream velocity, U_{free} was evaluated using two different methods: the average velocity of a mutually buoyant body through the working section and measurements of the Strouhal shedding frequency from a circular cylinder. The first method, employing the mutually buoyant body had previously been used in this water channel to measure U_{free} at lower flow velocities. However, for the flow velocities used in these experiments this method proved unreliable and for the majority of experiments U_{free} was determined by measuring the fluctuating lift force on the cylinder and calculating the Strouhal frequency. The free-stream velocity was then evaluated by utilising the relationship between the Strouhal number and the Reynolds number which is supported by a large body of experimental data, in particular the careful experiments of Norberg (1994). Over the range of Reynolds numbers studied, the Strouhal number has been found to vary only slightly with Re, between St = 0.200 to 0.211, and U_{free} was calculated after only a small number of iterations of Re and U_{free}. The aspect ratio of the cylinder and the dimensions of the end plates were also considered in this calculation. The uncertainty in the values of U_{free} is of particular interest as it systematically affects the force and energy coefficients as U_{free}^2 was used in the normalisation of these properties. The frequency resolution of the lift spectra causes an uncertainty in U_{free} of less than 1%, however there was an additional uncertainty due to the nature of the Strouhal peak. At Reynolds numbers of around 2000 the long formation length of the wake resulted in a Strouhal peak that was relatively broad banded, increasing the uncertainty in U_{free} to 3%. However, at higher Reynolds numbers above 4000, the Strouhal peak was well defined and the uncertainty in U_{free} was around 1%.

2.2 CYLINDER PROPERTIES

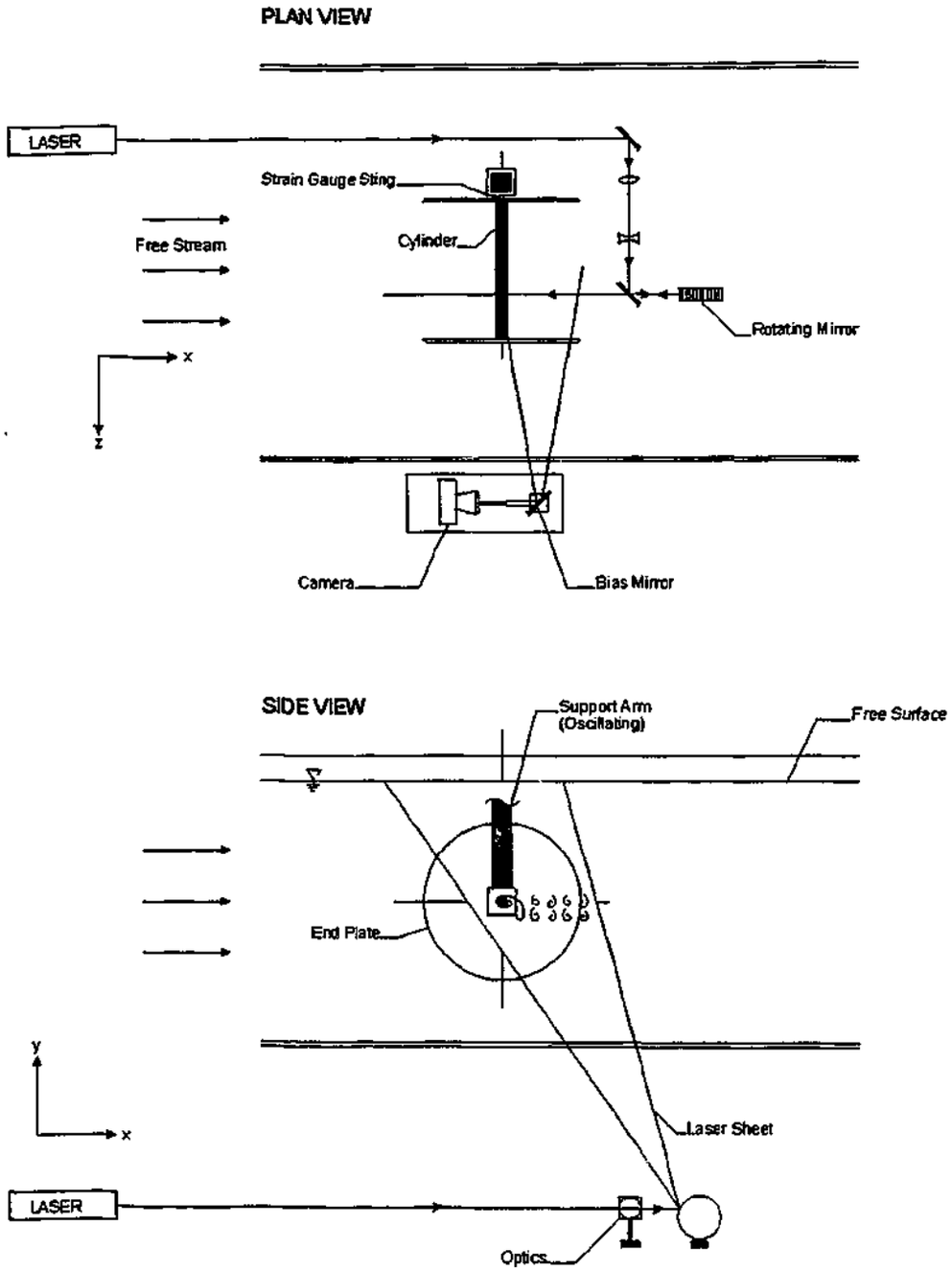

Figure 2-1 **Schematic showing cylinder and oscillation system in working section.**

The cylinder is mounted horizontally such that its spanwise axis is parallel to the free-surface and perpendicular to the free-stream as shown in the schematic of the experimental set-up in Figure 2-1. Two different cylinders, 25.4 mm and 50.8 mm in diameter were used to obtain a Reynolds number

range of 2300 - 9100. The smaller 25.4 mm cylinder was used at Re = 2100-2400, while the 50.8 mm cylinder was used primarily for experiments at Re = 4400 and 9100. The 50.8 mm cylinder was also used for a set of "overlap" experiments at Re = 2850, giving results which were very similar to those obtained at Re = 2100-2400 with the 25.4 mm cylinder. The 25.4 mm cylinder, shown in Figure 2-2(a), was 317.5 mm long, giving an aspect ratio of 12.5. A transparent laser window was incorporated into the cylinder to allow the laser sheet to illuminated the flow bind the cylinder, while the remainder of the cylinder was filled with air and the outer surface was matt black. To minimise the deflection of the laser sheet at the cylinder, the laser window was filled with distilled water and the clear plexiglass wall were very thin. After passing through the laser window the laser widow the intensity of the laser sheet was reduced and while the PIV particles were still illuminated, the percentage of bad vectors increased.

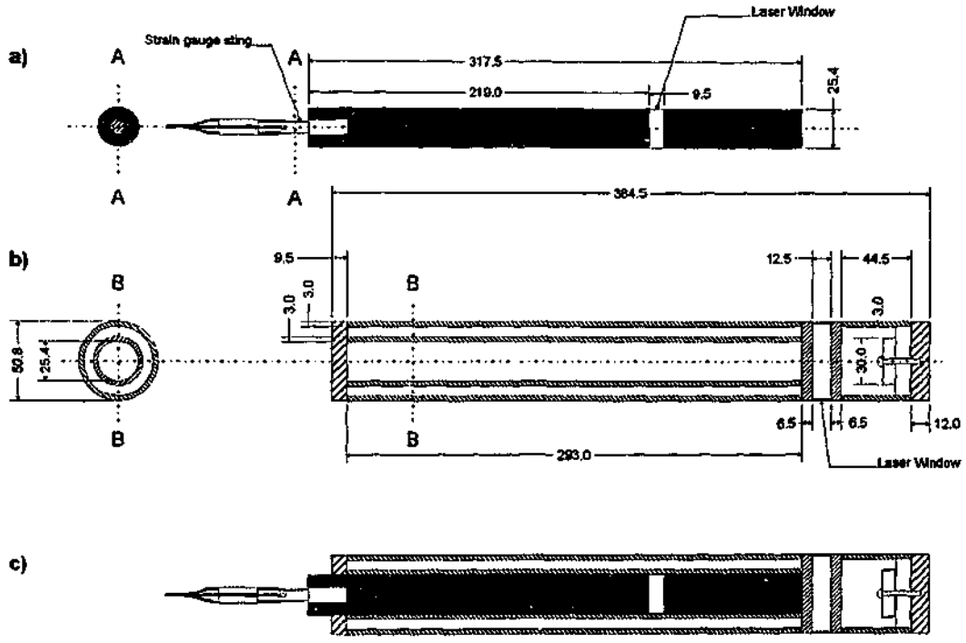

Figure 2-2 Detailed schematic of a) the 25.4 mm cylinder, b) the 50.8 mm cylinder shell which was designed to fit over the 25.4 mm cylinder and c) the assembled 50.8 mm cylinder.

The larger 50.8 mm cylinder, shown in Figure 2-2(b), was designed to fit over the smaller 25.4 mm cylinder, shown in Figure 2-2(a), allowing easy installation without the need to re-instrument the strain gauge system. The assembled 50.8 mm cylinder, shown in Figure 2-2(c) had a length of 384.5mm, an aspect ratio of 7.6 and was also fitted with a water-filled laser window. To reduce end effects, both cylinders were fitted with end plates that oscillated with the cylinder. The end plates were 368 mm in diameter and 6.4 mm thick with a 30° outward bevel. There was a small

gap of 1-2 mm between the free end of the cylinder its end plate, while adjacent to the strain gauges the cylinder fits through the end plate.

The natural structural resonance frequencies of both cylinders was significantly higher then the maximum frequency of forced oscillation. The 25.4 mm cylinder had a mass of 90.2 g and a resonance frequency of 20.0 Hz, which was well above the maximum frequency of forced oscillation of 1.2 Hz. The 50.8 mm cylinder was much heavier, weighing 581.9 g, resulting in a structural resonance frequency of 6.3 Hz that is almost six times the maximum forcing frequency of 1.1 Hz. However, when the 50.8 mm cylinder was forced at frequencies close to 1.1 Hz, corresponding to the flow conditions at Re = 9100, small levels of additional vibrations at the frequency of oscillation were observed. At the lower Reynolds number of 4500 the frequency of oscillation was lower and the motion of the cylinder appeared to be purely sinusoidal.

2.3 OSCILLATION PROPERTIES

The cylinder was oscillated transverse to the free stream such that its vertical motion was given by

$$y(t) = A \sin(2\pi f_e t) \qquad (2\text{-}1)$$

where A and f_e are the amplitude and frequency of oscillation respectively. To minimise the initial impulsive forces on the system, the oscillations were always started from the lowest point in the cylinder's displacement cycle where the instantaneous velocity is zero. The standard experimental procedure was to vary the frequency of oscillation about $f_e/f_o \approx 1$ (within the range $0.5 \leq f_e/f_o \leq 1.90$) while maintaining a constant oscillation amplitude and free-stream velocity. A detailed investigation of the frequency dependence of the wake was undertaken at $A/D = 0.5$ and a Reynolds number of approximately 2300. The investigation was then expanded to consider the frequency dependence of the wake at a range of amplitudes (A/D = 0.25 - 0.6) and Reynolds numbers (Re = 2100 - 9100).

The motion of the cylinder was driven by a high resolution stepper motor, Parker AX57-102 controlled by a Parker PC-23 indexer. The motion profiles were generated by a Lehigh program, SFG, Magness (1990) which defines the motor displacement at discrete time intervals. These profiles were edited to incorporate TTL triggering signals to the camera and bias mirror. In this way the PIV images were captured at prescribed points in the oscillation cycle. The motion profiles was executed by another Lehigh program ALT, Magness & Troiano (1991). The number of signals in the profile, including the TTL commands was limited to 475 by the ALT program and the minium time interval between stepper motor commands was 0.006 seconds. These two restrictions are the limiting factors determining the resolution of the cylinders motion.

2.4 FORCE MEASUREMENT SYSTEM

The forces on the cylinder were measured using a strain gauge system, Tomlinson (1996). The strain gauges were mounted on a ¼" sting, shown in Figure 2-3, was machined out of a brass rod with strain gauges located on the surfaces of the square mid-section. One end of the strain gauge sting was inserted into the cylinder with an interference fit, while the other end was clamped into the external support system Figure 2-4.

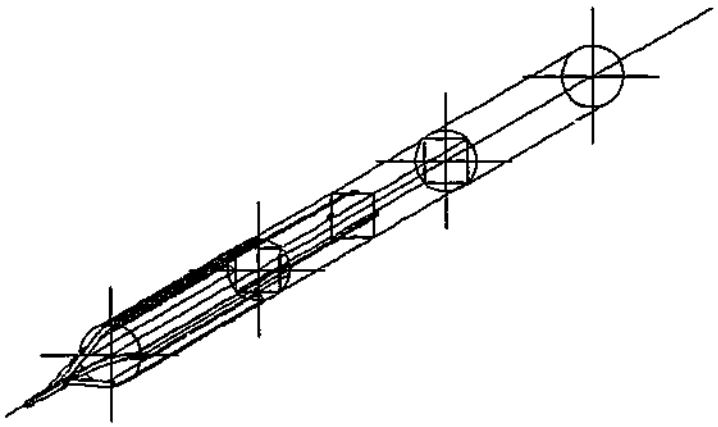

Figure 2-3 **Isometric drawing of the strain gauge sting.**

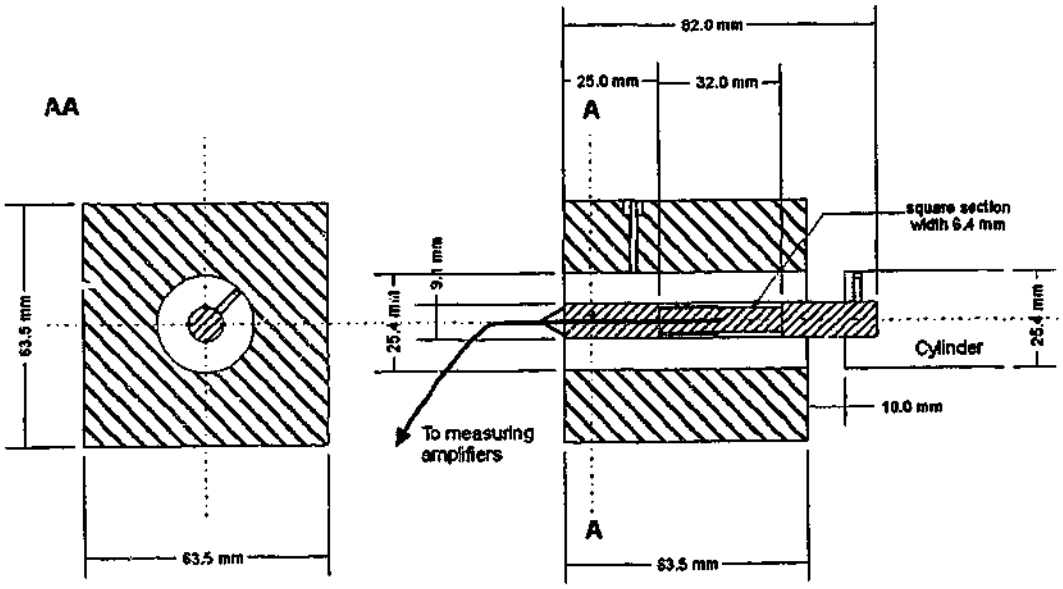

Figure 2-4 **Drawing of the strain gauge sting, the sting holder and the attachment of the sting to the cylinder.**

The strain gauges were configured into two full Wheatstone bridges, i.e. two strain gauges on each of the four faces, and underwent an extensive water proofing procedure prior to installation. The

average strain on the horizontal and vertical faces is directly related to the total moment generated by the lift and drag forces respectively and the strain gauges measure the span averaged forces on the cylinder. The signals from the strain gauges were amplified (Hottinger Baldwin Messtechnik GMBH; CLIP Electronic AE-301-S6) and filtered (Kronhn-Hite 3750) using a low-pass filter at a cut off frequency of 8 Hz and a gain of 20 dB. The signals were acquired using an A/D board and recorded using the ALT program, Magness & Troiano (1991). The majority of the force data presented was calculated using 4096 data points (from a total of 5000) acquired at a sampling period of 0.08 seconds, giving a Nyquist frequency of 6.25 Hz.

The experimental set-up had two different time based systems: the computer controlling the stepper motor, which sends signals at discrete time intervals to the stepper motor and the image acquisition system and the A-D board which acquires force measurements at discrete time intervals. Our interest in the phase of the lift and drag forces with respect to the cylinders displacement requires that these two times systems remains synchronised to a tiny percentage of an oscillation period, over at least 400 oscillations. However, for an A-D board sampling period of 0.08 seconds there was an error in the sampling rate of ± 0.00002 seconds. While his is appears to be a very small error, over 5000 acquisitions the error accumulates to a unacceptable percentage of an oscillation cycle (up to 10%) and results in a phase difference between the motion of the cylinder controlled by the stepper motor computer and the corresponding forces on the cylinder acquired through the A-D board. This error does not affect the phase accuracy of the image acquisition, however it means that we are unable to use the input to the stepper motor to relate the lift and drag forces to the displacement of the cylinder. This problem was overcome by directly measuring the displacement of the cylinder using a linear transducer. The displacement signal was conditioned and acquired through the A-D board in exactly the same way as the lift and drag force signals, thus eliminating any relative phase shift imparted by the filters.

The output of the strain gauges was calibrated in air by hanging static weights on the cylinder to generate a known moment at the centre of the strain gauges. The voltage produced by the moment of the point force is then related to the moment generated by a evenly distributed vertical force acting along the length of the cylinder producing a relationship between the voltage outputs of the lift strain gauges and a span averaged lift fluid force. The horizontal drag axis was calibrated by rotating the cylinder 90° anti-clockwise. As expected the relationship between the span-averaged forces on the cylinder and the output voltages were highly linear. The calibration also allowed us to align the axis to within ±5°. The non-zero vertical buoyancy force on the cylinder was eliminated by off setting or zeroing the vertical force. As a part of the experimental procedure both the lift and drag forces on the cylinder under zero flow conditions were offset to zero at the beginning of, and at regular intervals during, each set of experiments. The regular offsetting of the strain gauge voltages was required as the mean output of the gauges were subject to significant

drift, possibly due to temperature effects. The amplitude of fluctuating forces on a cylinder oscillating in stationary fluid were always consistent with the results of Bearman *et al.* (1985) and were not effected by the drift in the mean values.

2.5 IMAGE MEASUREMENT SYSTEM

A two-dimensional cross-section of the velocity field around the cylinder was measured using a laser-scanning version of high-image density PIV, Rockwell *et al* (1993). Extensive reviews of the PIV techniques used in these experiments are given by Adrian (1986, 1991), Rockwell *et al* (1992, 1993) and Rockwell & Lin (1993). The flow field was illuminated using a continuous Argon-ion laser (Coherent Innova Series) with a maximum power output 30 W. However, the camera settings were optimised for a power output of 6-10 W, which was the maximum laser power that could be maintained throughout the duration of an experiment. As shown in Figure 2-1, the laser beam was directed along the length of the channel into a flat surface steering mirror, passing through a collimating lens pair before turning 90° onto a rotating mirror. The rotating mirror (Lincoln Laser Co.) had 48 facets and was driven by a variable frequency motor (Lincoln Laser Co. VFC-2) where the motors frequency was measured using a high-resolution frequency counter (Philips PM6672). The rotating mirror produced a scanning laser beam that sweeps across the flow field at a scanning frequency that is equal to the number of facets multiplied by the rotational frequency of the mirror. The collimating optics generated a laser sheet thickness of between 1-2 mm and for PIV measurements laser scanning frequencies of between 290 and 620 Hz were used. The high frequency of the laser sheet means that the structure of the near wake and the mode of vortex shedding can be observed in real time during the experiment. The PIV images were recorded on high resolution Kodak TMAX 400 35 mm film using a Canon EOS-1 N RS camera fitted with a 100 mm Canon macro lens. The flow was seeded with 14μm silver-coated particles (Conduct-O-Fil particles, Potters Industries Inc.) which have a specific gravity of slightly less than 1 and for the free-stream velocities used, the particle "drop out rate" was low enough to obtain over an hour of high quality PIV data.

Prior to each set of experiments the image-based parameters were determined by running a set of test experiments to determine the extreme flow conditions. Based on these experiments the laser scanning frequency, camera shutter speed, camera aperture and bias velocity were selected to optimise the PIV images over the range of expected flow conditions.

The scanning laser illuminates the flow field a number of times during each film exposure, resulting in multiply exposed images. In order to measure the flow velocity the separation of the particle in each exposure must be large enough to be resolved, however if the separation is too large the motion of the particle during the exposure can not be accurately represented by a single velocity vector. The optimum particle spacing depends upon the resolution of the film and

resolution at which the image is digitised and was found to be approximately 0.2 mm of film. The laser scanning frequency was set so that where possible the optimum particle spacing was obtained in the flow regions of greatest interest, while maintaining a maximum particle spacing of less then 1-1.2 mm of film. Once the scanning frequency was optimised the shutter speed of the camera was selected to allow 4-6 particle exposures per image. For a given shutter speed the intensity of each image was a function of the laser power, the camera aperture and the seeding density of the particles in the flow. Shutter speeds of between 1/30 and 1/100, with lens apertures of between f= 4.0 and 7.1 were used to acquire the PIV data.

To resolve the ambiguity of the flow direction in the recirculation regions the images were shot through a rotating bias mirror. The bias mirror imparts an additional constant velocity to the flow field that is then subtracted from the velocity fields during post-processing. The bias mirror rotates at a constant velocity during the exposure and the center of the image exposure coincides with point at which the surface of the mirror is at 45° to the camera. As discussed by Raffel and Kompenhans (1995) the rotation of the mirror during the exposure generates distortion-induced errors, however as the movement of the mirror was less then 1° these errors were considered negligible and were not corrected for. The motion of the bias mirror was driven by a galvanometric scanner (General Scanning Inc. CX-660) and the bias velocity was generated using a triangular ramp displacement function of known period. The bias velocity was constant for each set of experiments and was evaluated using biased images of stationary fluid. The bias velocity was selected to be greater then the highest reverse flow velocity and for the flow conditions studied. bias velocities of between 0.085 and 0.155 m/s were required.

The number of flow field images per oscillation was limited by the framing rate of the camera. In general, it was possible to obtain 8 images per oscillation although in some cases the image acquisition was limited to 6 images per oscillation. Additionally in some situations only one image was taken per cycle to maximise the time span of the data set which was limited by the number of shots per roll of film. In all cases, the timing of image acquisition was based on the cylinder position within the displacement cycle.

2.6 *EXPERIMENTAL PROCEDURE*

Two different types of experiments were undertaken. The majority of the experiments were on a fully submerged cylinder oscillating transverse to the flow however an investigation of the flow over a stationary cylinder immediately under a free-surface was also undertaken.

2.6.1 Submerged Oscillating Cylinder

Each set of experiments on an oscillating cylinder involved the oscillation of the cylinder over a range of frequencies at fixed values of A/D and Re, although in some cases a number of values of

A/D were considered. At the start of each set of experiments the flow was "seeded" with particles and the channel was run at high velocity to promote the distribution of the particles. When the particles were evenly distributed the channel flow was turned off. Following a settling period the output voltages of the strain gauges were offset to zero and the bias velocity was measured using the stationary flow conditions. Unbiased images of a ruler next to the cylinder were also taken to confirm the spatial calibration of the PIV images. The length of time that the flow was stationary was minimised to reduce the "drop out" of the PIV seeding particles. When the channel flow was restarted the pump frequency was adjusted to obtain a free-stream velocity within the Reynolds number regime of interest and the velocity remained constant for the duration of the experiment. The frequency of the pump was not used to calibrate the free-stream velocity as the volume of water in the channel, and therefore the volume flow rate varied due to evaporation and other factors. Prior to the start of the experiments force data from a fully submerged stationary cylinder was acquired to determine the Strouhal shedding frequency that was subsequently used in conjunction with the data of Norberg (1994) to accurately determine the free-stream velocity. The lift and drag on a submerged stationary cylinder were also measured during and at the conclusion of the experiments. As well as increasing the accuracy of the Strouhal frequency calculations, these additional measurements were also used to determine if there was significant drift in the mean values of the lift and drag forces.

For each value of f_e/f_o the cylinder started oscillating from rest at $t = 0$, corresponding to the start of the force measurements. Initial transients were recorded in the force data and for most frequencies a steady state was reached after only 3-4 oscillations. Once the cylinder was set oscillating at a certain frequency and amplitude, these parameters were fixed. Following each experiment the cylinder remained stationary in the free stream for a time equivalent to more then 500 Kármán cycles. This procedure is in contrast with a number of other experiments, where the frequency was varied in a continuous fashion while the cylinder continued to oscillate.

2.6.2 Stationary Cylinder Underneath a Free-Surface

The set-up and calibration procedures for the experiments on the stationary cylinder in close proximity to a free-surface were similar to those described in section 2.6.1 for the fully submerged oscillating cylinder experiments. During the set-up procedures the cylinder is a long way below the free-surface and is effectively fully submerged. At the beginning of the experiments the cylinder is raised to the free-surface such that for low free-stream velocities, and therefore low Froude numbers, the top of the cylinder just intersects with the free-surface. This vertical position of the cylinder is then set as a cylinder depth, $h = 0$. The cylinder depth was then varied systematically to determine the effect of varying h/D on the structure of the near wake and the forces on the cylinder. After the cylinder was moved to a new position there was a delay of approximately 5 minutes

before measurements were taken to allow the disturbance to die out and for the new wake mode to become established. As the cylinder was stationary it was not possible to acquire the PIV images at predetermined phase referenced positions and the images were acquired at a constant framing rate.

2.7 FORCE POST-PROCESSING

After the force and displacement data were acquired they required extensive processing. The procedures used are described below.

The oscillation of the cylinder results in an additional force which is due to the inertia of the cylinders mass and which must be subtracted before the forces on the cylinder can be compared with the results of previous experiments. The moment generated at the strain gauges by the oscillation of the cylinder's mass depends upon the distribution of mass along the cylinder and is given by:

$$M_{inertia}(t) = a(t).\int_0^L m_l(z).z.dz \qquad (2\text{-}2)$$

$$M_{inertia}(t) = A\omega^2 \sin(\omega t + \phi_{cyl}) \int_0^L m_l(z).z.dz \qquad (2\text{-}3)$$

where L is the spanwise distance from the strain gauges to the end of the cylinder and $m_l(z)$ is the mass per unit length as a function of spanwise position.

The mass inertia force acts in-line and in-phase with the acceleration of the cylinder and therefore for transverse cylinder oscillations acts purely in the lift direction making no contribution to the drag force. The voltages from the strain gauges were converted first to a total moment using the calibration factor obtain from a point load. The moment due to the inertia of the cylinder's mass was then subtracted from the lift moment and the span averaged lift and drag forces were then calculated from the remaining total moments.

The lift and drag forces contained significant levels of high frequency noise and were bandpass filtered in the frequency domain. The lower limit of the band filter was centred at 0.05 Hz to eliminate a very low frequency wave that contaminated the signal. The upper limit for the band filter was typically 2-3 times the frequencies of interest and the bandwidth of the smoothing function was 0.01 Hz wide. The linear transducer that was used to measure the displacement of the cylinder was not designed for accurate high repetition displacement measurements and the quality of the signal was such that it could not be used directly in correlation calculations. The displacement function of the cylinder was already known from the input to the stepper motor, and as discussed in section 2.4 the reason the displacement was measured directly is the discrepancy in the sampling period of the A-D board. Therefore the primary reason for measuring the

displacement signal directly was to determine an accurate value for the frequency of oscillation, which is consistent with the sampling period of the A-D board, in order to relate the lift and drag forces to the cylinders motion. Despite the fact that the displacement signal was relatively noisy, the frequency of oscillation was calculated to within 0.0001% by performing an iterative correlation of the displacement signal with a sinusoidal signal of variable period. Once the frequency of oscillation was known the displacement of the cylinder as a function of time was calculated using equation 2-1 and the position of the cylinder at $t = 0$.

As the cylinder is installed into the rig the strain gauges axes were aligned to within ±5°. However, a misalignment of up to 5° results in significant leakage of the larger amplitude lift force into the drag force and the drag becomes clearly non-symmetric. By checking that the PIV flow fields were highly symmetric we were able to confirm that the non-symmetry of the drag was due to the misalignment of the axes. The misalignment of the axes was calculated by maximising the correlation coefficients for lift correlated with $\sin(2\pi f_e t)$ and drag correlated with $\sin(4\pi f_e t)$. The misalignment of the 25.4 mm cylinder was –4.2°, while the 50.8 mm cylinder was misaligned by 2.2°. The lift and drag forces were subsequently corrected for the misalignment of the cylinder resulting in a significant improvement in the symmetry of the smaller amplitude drag force.

2.8 IMAGE POST-PROCESSING

The primary output from PIV measurements is the velocity field. The majority of our flow fields are presented in terms of vorticity: $\omega_z = \frac{\partial v}{\partial x} - \frac{\partial u}{\partial y}$, which was calculated directly from the discrete velocity field using a 9 point weighted average. The flow diagram in Figure 2-5 gives an overview of the steps required to generate a final vorticity field from a film based PIV image of the flow field. A number of the steps shown in Figure 2-5 are discussed in more detail below.

The TMAX film negatives containing the flow field images were developed using standard black and white film processing techniques. The resolution of the TMAX film is very high, 300 lines/mm, however the image was digitised prior to processing and the final resolution of the image was limited by the film-scanning device. The images were digitised using two different Nikon scanners: at Lehigh a Nikon LS-3510 with a resolution of 125 pixels/mm was used, while at Monash the films were scanned at 106 pixels/mm using a Nikon CoolScan II.

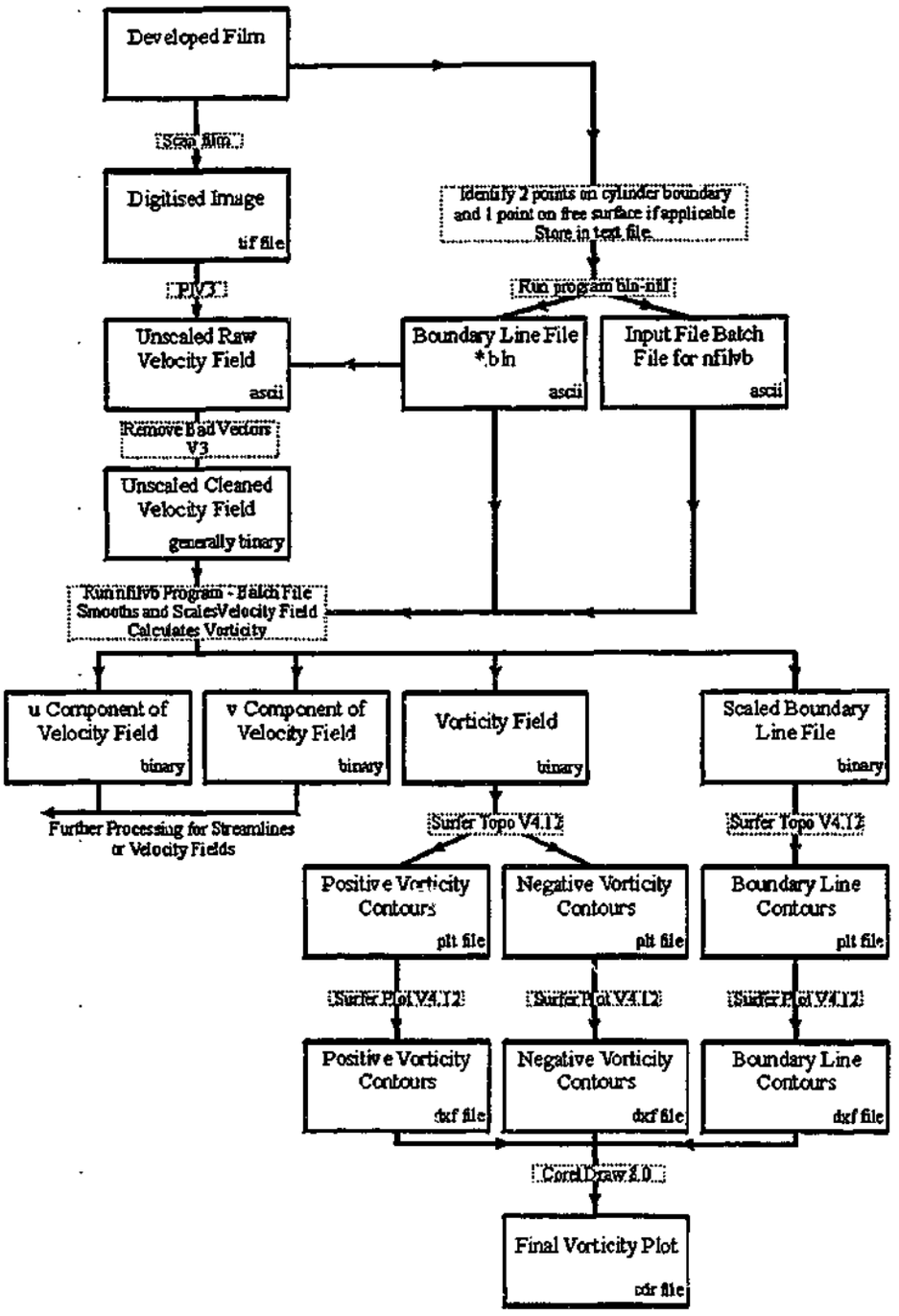

Figure 2-5 Flow diagram showing the standard processing procedure to produce a vorticity field from a PIV film image.

The velocity fields were calculated using a Lehigh program, PIV3, Seke (1993), which employed a single-frame cross correlation technique. In all cases an initial interrogation window of 90x90 pixels was used which was then converted within PIV3 to an FFT window size of 128 (*i.e.* 2^7). A cross-correction was performed between this window and another window displaced 10 pixels in

the free-stream, or x direction. In order to satisfy the Nyquist sampling criterion an overlap ratio of 0.5 was used. Additionally, a centroid method of peak detection was employed with a peak validation factor of 0.3. The resulting velocity fields contained 3500-5220 vectors and generally there were only a small number of bad vectors (< 20) in the regions of flow away from the reflections generated by cylinder's body or the free-surface. The spatial resolution was between $\Delta x = \Delta y = 1.065$ - 2.318 mm for the 25.4 mm cylinder, while for the 50.4 mm cylinder the resolution was $\Delta x = \Delta y = 3.090$ mm.

The phase averaged velocity and vorticity fields were calculated to examine the repeatable features of the flow field. When the cylinder was fully submerged the phase reference wake was symmetric about the horizontal axis, i.e. the wake at the top of the oscillation is the mirror image of the wake at the bottom of the oscillation. Therefore, by inverting the images 180° from the phase point of interest we obtained two images per oscillation for phase averaging. The non-phase-averaged or mean velocity and vorticity fields were also calculated for both the oscillating and stationary cylinders. The mean fields for the oscillating cylinder were calculated in the same way as for the stationary cylinder, with the instantaneous position of the cylinder changing relative to the fixed reference frame of the mean field. As the PIV data was recorded on film, care must be taken to align the velocity fields before averaging which was done using the centre of the cylinder as the reference point. The displacement of the oscillating cylinder from the centre-line of the wake was also needed to align each image. In all cases where the wake was periodic the average fields were calculated using images representing one or more complete cycles.

2.9 CALCULATION OF FORCE PROPERTIES

The mean and fluctuating lift and drag forces were calculated from the filtered time signals. In general these properties were calculated from 4096 data points or 160-320 cylinder oscillations. When the lift and drag signals are relatively sinusoidal the average peak amplitude of the fluctuating forces was calculated by multiplying the standard deviation by $\sqrt{2}$, and unless stated the amplitude of the fluctuating forces are the average peak value, not the standard deviation.

When the cylinder was forced to oscillate transverse to the flow, for all cases studied the wake was "locked on" to the cylinder's motion and the most energetic frequency in the lift force was f_e and the correlation of the lift signal with a sinusoid was greater then 0.6. Thus, the lift force can be approximated by a sinusoidal function of the form,

$$\text{Lift}(t) \approx (\tfrac{1}{2}\rho U^2 DL)\, C_L \sin(2\pi f_e t + \phi_{lift}) \qquad (2\text{-}4)$$

where C_L is the amplitude of the fluctuating lift coefficient and ϕ_{lift} is the phase with respect to the cylinder's displacement $y(t)$. Both C_L and ϕ_{lift} were calculated in the time domain using data points from over 400 cylinder oscillations. The lift phase, ϕ_{lift}, was calculated using the cross correlation

of the cylinder's lift and displacement, where ϕ_{lift} is represented by the location of the first maxima in the correlation function. The cross correlation function of the lift and displacement signals is essentially sinusoidal, and the resolution of ϕ_{lift} was increased by fitting the correlation function in the vicinity of the first maxima with a sinusoidal function. The phase lag of the sinusoid fitted to the correlation function was iterated to within 0.001 seconds, which for 0.7 Hz lift signal is equivalent to an uncertainty in ϕ_{lift} of ±0.5°.

The dominant frequency of the drag force is $2f_e$, therefore to relate the phase of the drag to the displacement of the cylinder we approximate the general form of the drag force as:

$$\text{Drag}(t) \approx (\tfrac{1}{2}\rho U^2 DL)\, C_D \sin[2(2\pi f_e t + \phi_{drag})] + C_{D\,mean} \qquad (2\text{-}5)$$

where C_D is the amplitude of the fluctuating drag coefficient, $C_{D\,mean}$ is the mean value of the drag coefficient and ϕ_{drag} is the phase of the drag with respect to the cylinder's displacement $y(t)$. The drag phase was determined by first calculating the cross correlation of the drag signal with the square of the displacement signal. The phase of the drag force with respect to the cylinder's displacement was calculated by finding the time lag of the first maxima in the correlation function and relating this to the displacement period ($1/f_e$ not $1/2f_e$). Using this definition ϕ_{drag} only has physical significance over a range of 180°. The drag force tends to be less sinusoidal than the lift force, however in all cases the values of ϕ_{drag} presented were calculated from drag traces whose correlation coefficient with a sinusoidal signal is greater then 0.6. This approach allowed us to calculate values of ϕ_{drag} for all cases except $A/D = 0.25$ at $Re = 4400$.

The cylinders vertical motion results in the transfer of energy between the cylinder and the fluid. The energy transferred between the fluid and the cylinder per cycle is defined as:

$$E = \int_0^T \dot{y}\, Lift(t)\, dt \qquad (2\text{-}6)$$

where $\dot{y} = 2\pi f_e A \cos(2\pi f_e t)$

and the lift force can be represented by equation 2-4: $\text{Lift}(t) \approx (\tfrac{1}{2}\rho U^2 DL)\, C_L \sin(2\pi f_e t + \phi_{lift})$

Therefore when the lift force is sinusoidal the normalised Energy transfer, C_E is approximated by

$$C_E \approx \pi C_L \frac{A}{D} \sin(\phi_{lift}) \qquad (2\text{-}7)$$

The energy transfer from the fluid to the cylinder is positive when $0° < \phi_{lift} < 180°$, otherwise the energy transfer is negative, i.e. from the cylinder to the fluid. The oscillation of an elastically mounted cylinder requires positive energy transfer. However, a cylinder forced to oscillate is not subject to this constraint and all values of ϕ_{lift} are physically possible.

If the lift co-efficient is re-written in terms of its in-phase and out-of-phase components, we see that the energy transfer, equation 2-7 is proportional to the out-of-phase component of the lift force:

$$C_L(t) = C_L \sin(2\pi f_e t + \phi_{lift})$$

$$= [C_L \cos(\phi_{lift})]\ \sin(2\pi f_e t) + [C_L \sin(\phi_{lift})]\ \cos(2\pi f_e t)$$

As discussed in section 1.3.3 the total lift force, $C_L(t)$ can be expressed in terms of $C_{L\,vortex}(t)$, the lift force due to the vorticity field and $C_{L\,am}(t)$, the contribution to the lift force from the apparent mass. For convenience we reproduce equation 1-8:

$$\tilde{C}_L(t) = \tilde{C}_{Lvortex}(t) + \tilde{C}_{am}(t)$$

In a significant proportion of the previous literature the vortex lift force has not been considered and the total lift force is referred to simply as the "lift force". In this document the term "total lift force" rather than "lift force" will be used in cases where the vortex lift force has been evaluated and discussed. When the cylinder oscillates transverse to the flow $C_{L\,am}$ is in-phase with the oscillation of the cylinder and is given by:

$$C_{L\,am}(t) = \frac{F_{am}(t)}{\frac{1}{2}\rho U^2 LD}$$

$$= 2\pi^3 St_o^2 \left(\frac{f_e}{f_o}\right)^2 \frac{A}{D}\sin(\omega t) \qquad (2\text{-}8)$$

where St_o is the Strouhal number of the stationary cylinder. The normalized vortex lift force $C_{L\,vortex}(t)$, was calculated by subtracting $C_{L\,am}(t)$ from $C_L(t)$, the total lift force co-efficient and as discussed in section 1.3.3, the vortex lift force can be expressed in the same way as the total lift force in (2-4):

$$C_{L\,vortex}(t) \approx C_{L\,vortex} \sin(2\pi f_e t + \phi_{lift\,vortex}) \qquad (2\text{-}9)$$

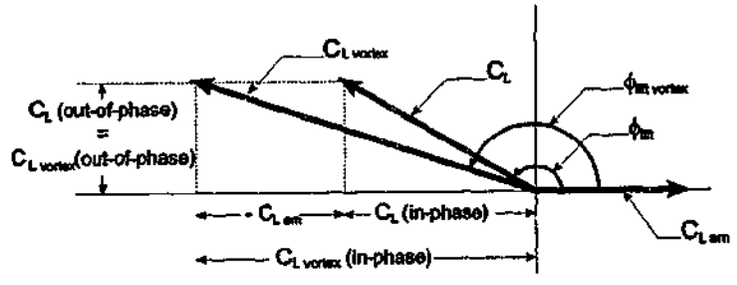

Figure 2-6 **Vector diagram showing the relationship between $C_L(t)$ and $C_{L\,vortex}(t)$**

The vectorial relationship between the total lift force and the vortex lift force is shown in Figure 2-6.

When the forces and the cylinder's displacement were plotted on the same axis it was obvious that for some frequencies of oscillation there were significant variations in the phase and amplitude of the forces on the cylinder. These changes were quantified by calculating the instantaneous phase and amplitude of both the lift and drag forces as a function of time. The instantaneous phase of the lift force was calculated by correlating a small segment of the lift trace with the sinusoidal displacement function. Similarly to find the instantaneous phase of the drag force a small segment of the drag force was correlated with the square of the displacement function. Typically the length of the force segments corresponded to three cylinder oscillations and the resulting instantaneous phase was taken at the centre of the segment. The instantaneous amplitude of the fluctuating forces was calculated using the peak values over a small segment of the force traces, where the segment length used was generally shorter than two oscillation cycles.

2.10 COMPUTER PROGRAMS

A number of programs were written to supplement commercial packages and existing Lehigh software. A brief summary of the programs is outlined below.

Table 2-1 Summary of computer programs

PROGRAM	FUNCTION
Experimental and initial Processing	
ModPro.pas	*Given*: number of images, delay times and stepper motor displacement profile Calculates and inserts bias mirror and camera TTL commands in the stepper motor displacement profile.
Bln-nfil.pas	*Given*: access to a coordinate file containing 2 points on the cylinder, the cylinders radius, magnification, velocity scale, bias velocity and smoothing factor. Calculates boundary line file and writes the input file for the Lehigh program nfilvb.
Bln-sur.pas	Similar program to Bln-nfil but is for free surface flows. Requires a point on the free surface in the coordinate file.
Force Processing	
ForceDat.cpp	*Given*: raw lift, drag and displacement files. Given: calibration factors for lift, drag and cylinder mass distribution.

	Given: A, U_{free}, cylinder dimensions, axis angle, approximate oscillation periods, filter specifications. This is the main force-processing file; it performs the following procedures on multiple sets of data. Results are output for each data set as well as a summary file. • Corrects for axis angle. • Calculates accurate axis angle • Calibrates lift and drag • Subtracts in-phase force components (generally inertia) from lift • Normalises forces → C_L, C_D • Calculates lift and drag spectra • Filters lift and drag • Calculates lift and drag phase • Calculates C_{my} and C_{dy} • Calculates correlated / non-correlated lift • Calculates displacement
SplitDat.cpp	*Given*: force files output from ForceDat and 2 time segments Calculates the force properties for the 2 individual time segments.
AxisAngle.cpp	*Given*: force files output from ForceDat Calculates the relative angle of the strain gauge axis to the global axis. Iterate program with ForceDat to calculate axis angle.
SegPhaseAmp.cpp	*Given*: force files output from ForceDat Calculates instantaneous lift phase and amplitude for each oscillation using a correlation of segments of the force traces. The length of the segments for both the phase and amplitude calculations can be specified.
Flow Field Processing	
YFlip.cpp	*Given*: velocity field (ASCII) and cylinder boundary file (ASCII) Flips a velocity field in the y direction (change position of vectors and

Abbotsford Notch A Send Doubleday Melbourne 95236025

	sign of v component). For a symmetric wake this double the number of images available for phase averaging
AveFieldsAny.cpp	*Given*: multiple velocity fields (ASCII) and their associated cylinder boundary files (ASCII), for either fully submerged or free-surface cases • Changes the origin of the coordinate system to the cylinder center • Calculates vorticity for each case – boundary condition ignores all co-ordinates within cylinder. • Calculates average velocity and vorticity over multiple cases
WakeLength.cpp	*Given*: velocity field (ASCII) and cylinder boundary file (ASCII) Measure of wake length using attached positive vorticity • Changes the origin of the coordinate system to the cylinder center • Calculates vorticity for each case • Calculates vertical location of maximum positive vorticity for each streamwise location i.e. locus of positive maximum vorticity • Calculates total attached positive vorticity (attached vorticity: upstream of cut off point below minium vorticity threshold) • Calculates vorticity moment due to attached vorticity • Calculates effective center of maximum positive vorticity

3 SUBMERGED OSCILLATING CYLINDER

In this chapter the frequency dependence of the wake of a cylinder undergoing forced oscillations transverse to the free-stream is investigated for a range of oscillation amplitudes and Reynolds numbers. As discussed in sections 1.4 and 1.5, both the wake structure and the forces on a cylinder, are known to exhibit abrupt changes as the frequency of oscillation passes through the natural Kármán frequency of the stationary cylinder wake. As f_e/f_o passes through unity the lift force shows a sharp increase in amplitude and a phase "jump" of close to 180°. Separate studies have shown that around $f_e/f_o = 1$ there also are significant changes in the timing and structure of the near wake. The questions raised by these two sets of observations provide the primary motivation for this research. In the initial sections of this chapter we show conclusive evidence that the changes in the lift force and wake structure are intrinsically linked to a transition between different wake states. The remaining sections consider the nature of the transition between wake states, the universality of the wake states and the relationship between the wake states for a cylinder that is forced to oscillate and the response branches of a freely oscillating cylinder. The initial detailed investigation of the wake states focuses on a single set of flow conditions: $Re = 2300$ and $A/D = 0.5$. The range of parameters are subsequently expanded to consider a range of Reynolds numbers, $Re = 2300$ to 9100, and oscillation amplitudes, $A/D = 0.25$ to 0.6.

For all but the lowest oscillation frequencies at $A/D = 0.25$ the wake was "locked on" to the cylinder oscillation and the dominant frequency in the lift forces was f_e and the correlation of the synchronised lift signal with a sinusoid was greater than 0.6. Thus, as discussed in section 2-9 the lift force can be approximated by a sinusoidal function:

$$\text{Lift}(t) \approx (\tfrac{1}{2}\rho U^2 DL)\, C_L \sin(2\pi f_e t + \phi_{lift}) \qquad \text{(2-4 reproduced)}$$

where C_L is the amplitude of the fluctuating lift coefficient and ϕ_{lift} is the phase with respect to the cylinder's displacement $y(t)$.

3.1 COMPARISON WITH PREVIOUS WORK

In Figure 3-1(a & b) results from the current investigation showing the variation of ϕ_{lift} and C_L, respectively with f_e/f_o are compared with results from a number of previous studies. The data in Figure 3-1 were obtained over a Reynolds number range of 2 300 to 60,800 and in all cases the amplitude of oscillation was $A/D = 0.5$. These plots demonstrate generic features that are evident both in the previous work of Sarpkaya (1995), Gopalkrishnan (1993) and Staubli (1983b) and in the present study. At low values of f_e/f_o below the jump, the lift force has a small amplitude and is approximately out-of-phase with the cylinder displacement, $y(t)$. As f_e/f_o increases the lift properties do not vary significantly until, at a particular value of f_e/f_o, there is simultaneously an

abrupt increase in C_L and a shift in ϕ_{lift} of the order of 180°. As f_e/f_o increases further the lift properties change gradually: C_L increases and ϕ_{lift} decreases. Thus, at higher values of f_e/f_o the lift force is large in amplitude and is approximately in phase with the oscillation of the cylinder.

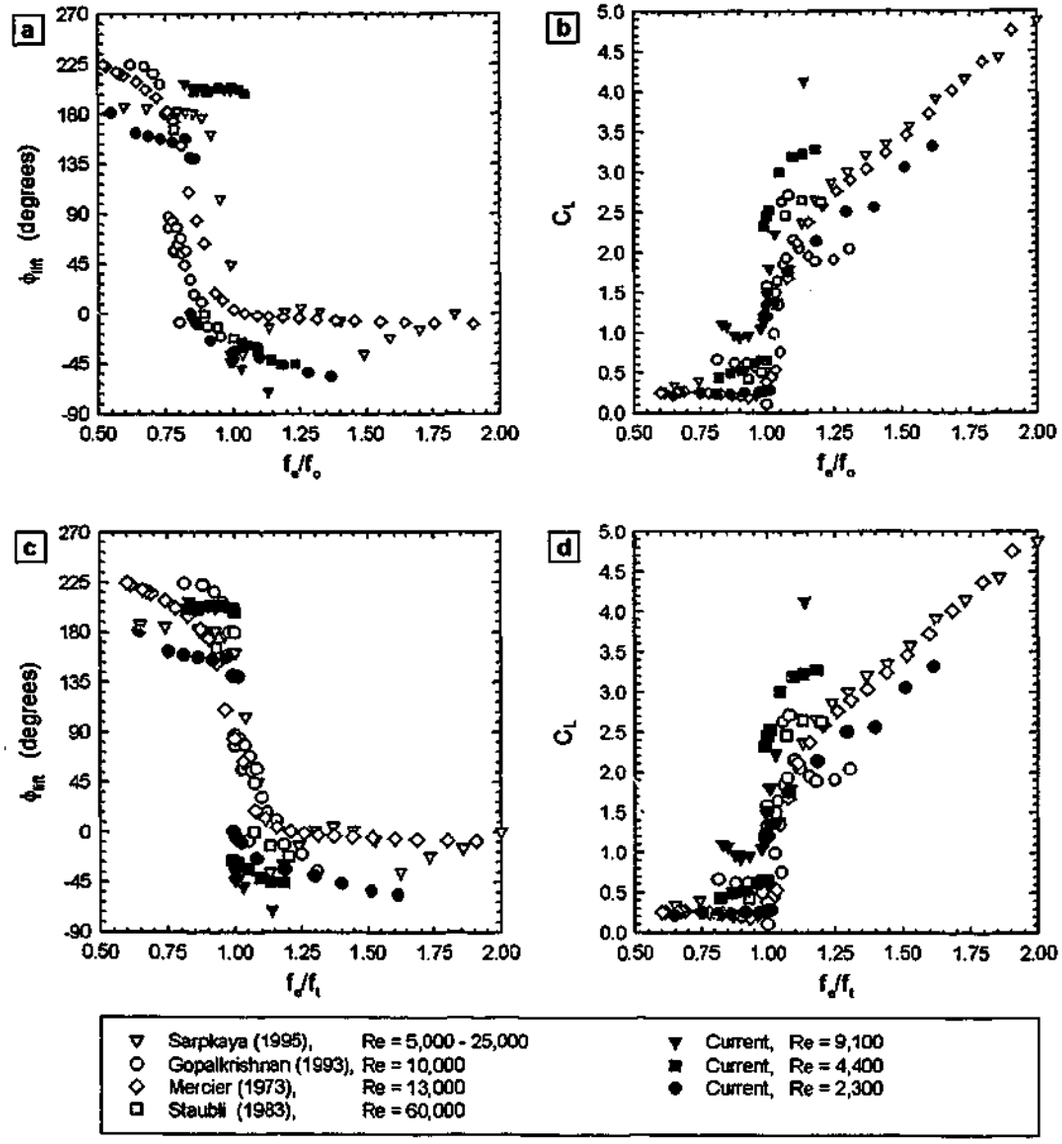

Figure 3-1 Data from previous experiments: ϕlift and CL as a function of fe/fo, A/D = 0.5.

The sharp changes in the phase and amplitude of the lift force represent a transition from a low-frequency lift force to a high-frequency lift force. The properties of the lift force are associated with either low oscillation frequencies before transition, or high frequencies after transition. Before transition C_L is small and ϕ_{lift} is large, while after transition C_L is large and ϕ_{lift} is small, and generally negative. The frequency at which this change occurs is defined as the transition frequency f_t. For the different data sets in Figure 3-1(a & b) there is some variation in the transition

frequency. While the reason for this variation is not well understood, Staubli (1983b) observed similar variations over a Reynolds number range of 25,300 – 271,000. When the oscillation frequency is normalised by the transition frequency, as shown in the plots of C_L and ϕ_{lift} versus f_e/f_t in Figure 3-1(c & d), the universal nature of the jump in the phase and amplitude of the lift force are clearly evident.

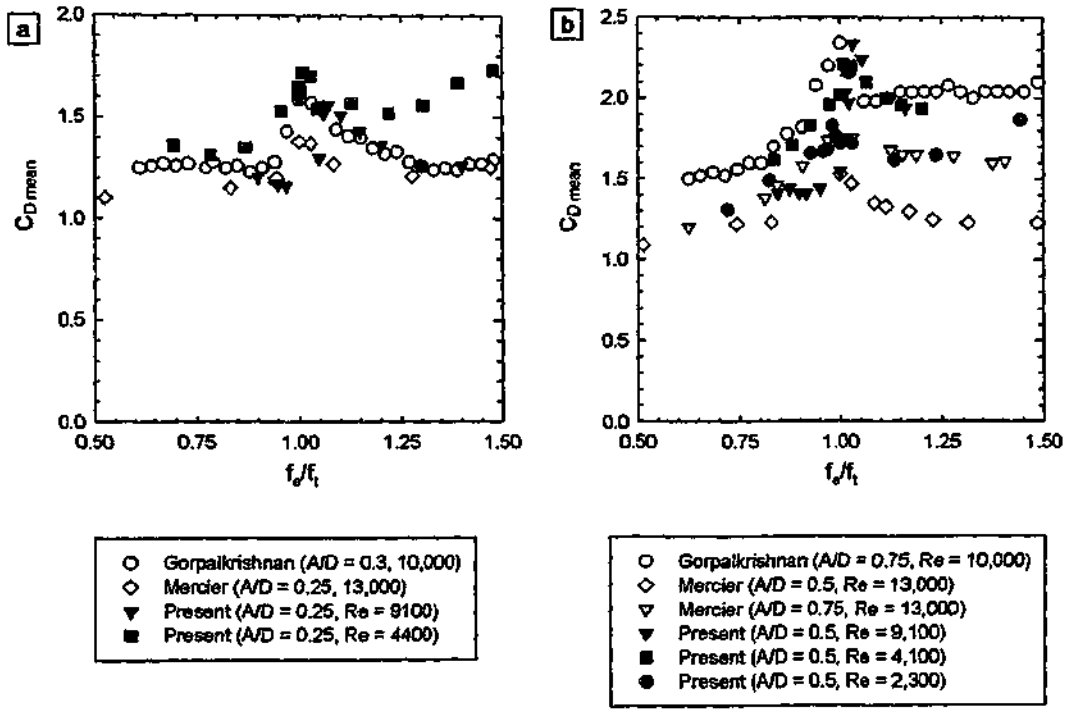

Figure 3-2 Data from previous experiments: $C_{D\,mean}$ as a function of f_e/f_o.

A compilation of results demonstrating the variation of the mean drag with f_e/f_t is shown in Figure 3-2. The results are for a range of A/D and Re values and include data from the current experiments. There is a broad peak in $C_{D\,mean}$ at the point corresponding to the transition in the lift force, but otherwise $C_{D\,mean}$ does not vary strongly with f_e/f_o. Thus, despite the jump in the phase and amplitude of the lift force at transition, the values of $C_{D\,mean}$ either side of this transition are very similar. The general shape of $C_{D\,mean}$ vs. f_e/f_t does not show a show dependence on either Re or A/D, however as A/D increases there is an upward shift in the value of $C_{D\,mean}$.

3.2 WAKE MODES AND FORCES

3.2.1 Stable Wake States

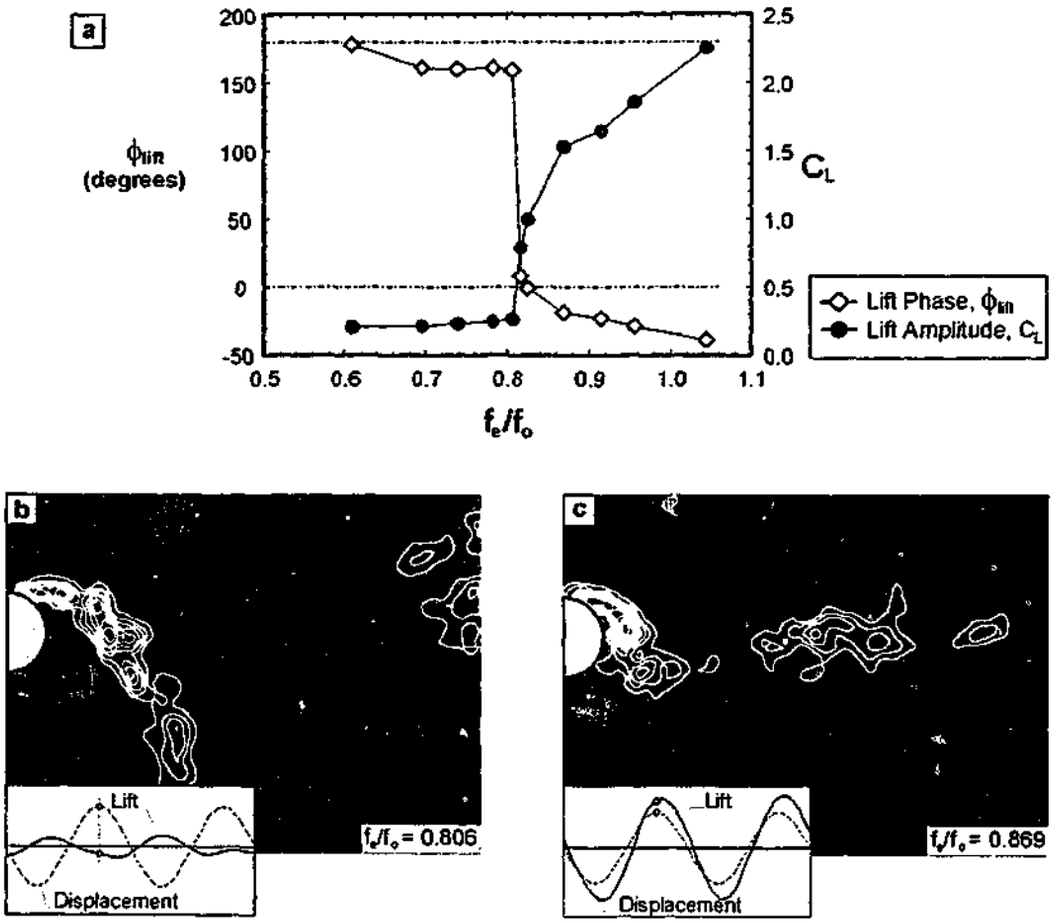

Figure 3-3 a) Lift phase ϕ_{lift}, and amplitude of the lift coefficient C_L as a function of frequency ratio f_e/f_o at A/D = 0.5, Re = 2300. Instantaneous vorticity fields are shown in b) and c). The time trace inserts show the instantaneous lift and displacement, where the timing of the image acquisition is indicated by a small circle.

The variation of the phase and amplitude of the lift coefficient with f_e/f_o at A/D = 0.5 and Re = 2300 is shown in Figure 3-3(a). At lower values of f_e/f_o, below f_e/f_o = 0.81 the lift properties are consistent with those found by previous investigations at f_e/f_o below the sharp jump in the lift force. Similarly, the lift properties for f_e/f_o > 0.81 are consistent with those found by previous investigations at f_e/f_o above the jump. The instantaneous vorticity fields in Figure 3-3(b & c) show the wake structure for values of f_e/f_o either side of the transition. The images, both acquired at the top of the cylinder's oscillation cycle, show two distinctly different wakes. Figure 3-3(b) is representative of the wake structure at lower f_e/f_o before transition, while Figure 3-3(c) is representative of the structure of the wake after the transition. Comparison of the two cases shows

that the phase-referenced vortex structure about to be shed into the near wake are of opposite sign. In Figure 3-3(b), at $f_e/f_o = 0.806$, a negative vortex structure is about to be shed from the attached shear layer while a positive initial vortex forms close to the cylinder. After the transition, at $f_e/f_o = 0.869$, the structure that is shed into the wake at the same phase point in the oscillation is positive and the initial vortex is negative. The change in sign of the phase referenced vortex structures is consistent with the shift of approximately 180° in the lift phase. Over the range of f_e/f_o studied ($f_e/f_o = 0.5 - 2.0$), for frequencies of oscillation below the transition the basic characteristics of the low-frequency wakes were always consistent with the wake in Figure 3-3(b), while for f_e/f_o above the transition, the high-frequency wakes were consistent with the wake in Figure 3-3(c). In this section the general features of these two wakes and the forces on the cylinder are discussed for a specific set of flow parameters ($A/D = 0.5$ and $Re = 2300$). Subsequently, it will be shown that many of these features are very robust and can be used to describe the wakes for a wide range of A/D and Re.

The wake modes either side of the transition are now considered in more detail. The time evolution of the near wake vortex structures for the low- and high-frequency wakes are shown by the phase averaged vorticity fields in Figure 3-4 and Figure 3-5 respectively, where each phase averaged image corresponds to 9 instantaneous images. The phase averaged images at the top of the oscillation, Figure 3-4(a) and Figure 3-5(a), have the same general form as the corresponding instantaneous images in Figure 3-3. This indicates that the repeatability of large scale features in the ω_z field is very high. At the top of the oscillation, the low-frequency wake in Figure 3-4(a) has a long negative vortex structure extending across the base of the cylinder and into the lower half of the wake. However, at the same phase of the oscillation cycle the attached negative vorticity in the high-frequency wake, shown in Figure 3-5(a), takes the form of a small concentrated structure at the base of the cylinder. As the cylinder moves downwards, the negative vorticity in the low-frequency wake is shed as two separate structures, as shown in Figure 3-4(b - d). The negative vorticity from the end of the attached shear layer is shed into the lower half of the wake and forms a counter-rotating pair with previously shed positive vorticity. The negative vorticity closer to the cylinder is shed into the upper wake, and eventually forms a second counter-rotating pair with a portion of the positive vorticity shed as the cylinder moves upwards in Figure 3-5(f - h). Thus, the vorticity forms two counter rotating pairs per cycle and, following the terminology of Williamson & Roshko (1988), the shedding mode is described as 2P. The mode of vortex shedding for the high-frequency wake is clearly different. As the cylinder begins to move downwards in Figure 3-5(a & b) a single positive vortex is shed into the near wake and the lower shear layer tends to have a distinct angle away from the centre-line of the wake. A second shedding event occurs half a cycle later, when a single negative vortex is shed just after the bottom of the displacement cycle, resulting in the classical Kármán, or 2S, mode of shedding. The evolution of the low- and high-

frequency wake modes is similar to the modes observed by Govardhan & Williamson (2000) for an elastically mounted cylinder. The relationship between the wakes of the forced and freely oscillating cylinders will be discussed in more detail in section 3.7.

In Figure 3-4 the low-frequency wake there are very low levels of vorticity and velocity in the region immediate behind the base of the cylinder. The streamwise extent of this region is a measure of wake length and is analogous to the formation length of a stationary cylinder. The variation of the size of this region will be discussed further in section 3.3.1. In contrast to the low-frequency mode, the high-frequency wake has virtually no region of low vorticity immediately behind the cylinder, and the vortex structures form very close to the cylinder. The vorticity fields in Figure 3-4 and Figure 3-5 indicate that the transition from the low- to the high-frequency wake corresponds to a change in the timing of the vortex shedding and also a change in the mode of vortex shedding. The two modes of vortex shedding generate significantly different distributions of vorticity downstream of the cylinder. In the high-frequency wake, negative vorticity is found predominantly in the upper half of the wake, while the lower wake is dominated by positive vorticity. However, for the low-frequency wake, vorticity of both signs is found throughout the vertical extent of the wake.

The low- and high-frequency wake states, described above, have characteristic lift properties and phase reference distributions of vorticity. The low-frequency wake in Figure 3-4 corresponds to small values of C_L and large values of ϕ_{drag}, the phase referenced initial vortex at the top of the oscillation cycle is positive and the mode of vortex shedding is 2P. The properties of the high-frequency state, shown in Figure 3-5, are distinctly different; C_L is large, ϕ_{lift} is small and the 2S wake has a positive initial vortex at the top of the oscillation cycle.

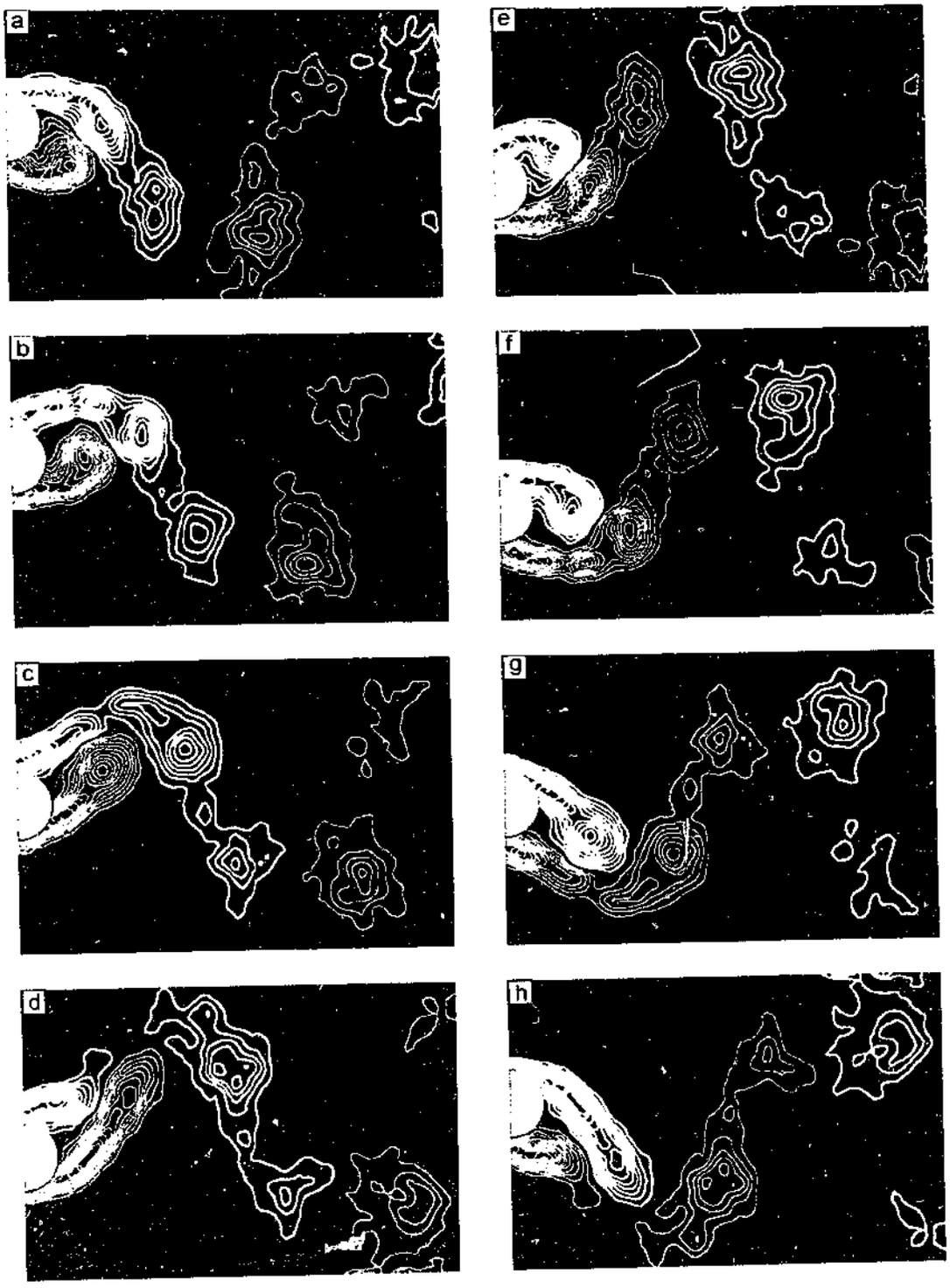

Figure 3-4 Phase averaged images showing the evolution of the vortex structures during the cylinder's oscillation cycle for the low-frequency wake mode: $f_c/f_n = 0.806$, $A/D = 0.5$, $Re = 2300$. The images were acquired at evenly space intervals such that a) and e) are at the extreme maximum and minimum points of the displacement cycle respectively and c) and g) are at the mid-points.

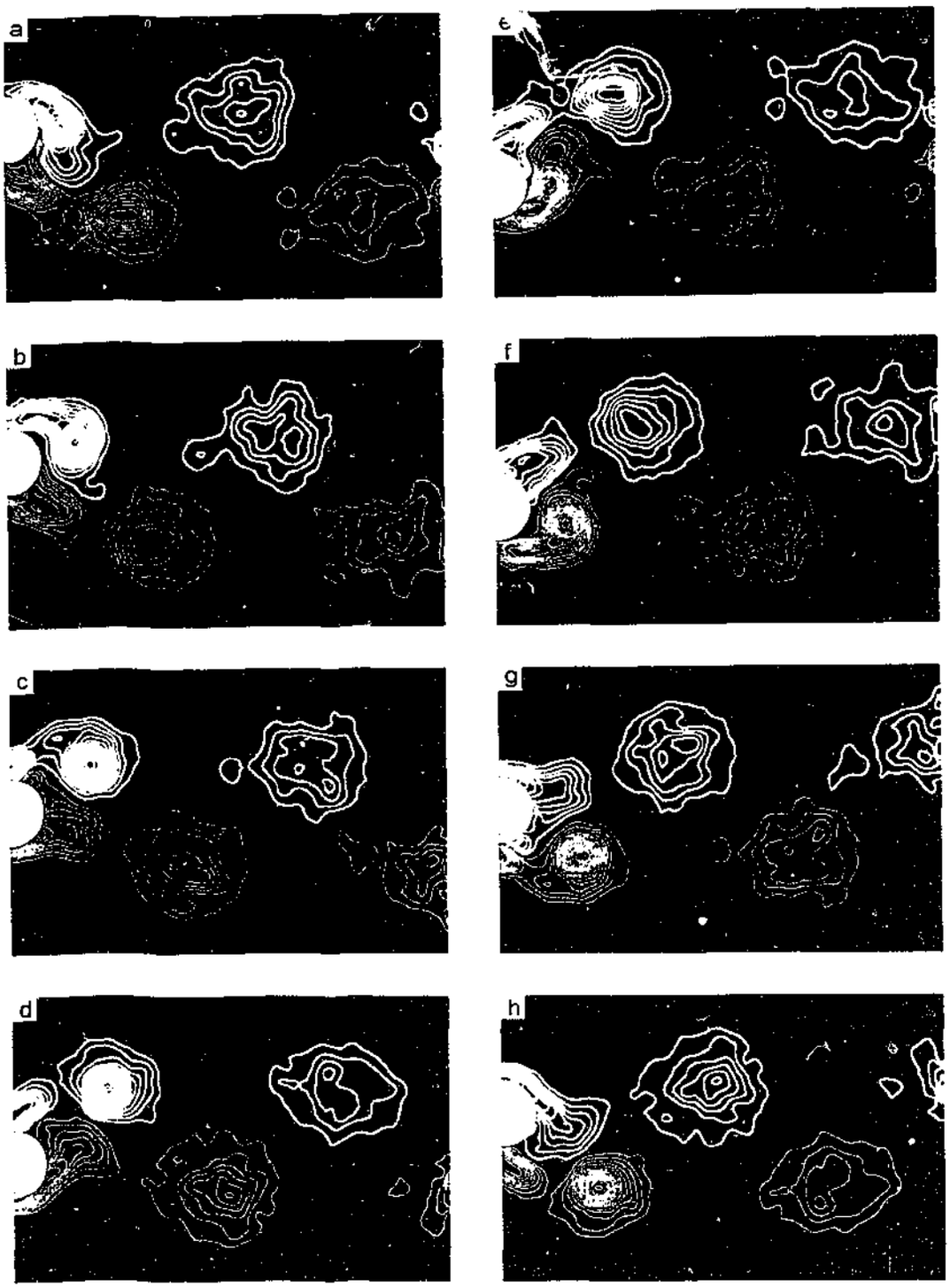

Figure 3-5 **Phase averaged images showing the evolution of the vortex structures during the cylinder's oscillation cycle for the high-frequency wake mode: $f_c/f_n = 0.869$, $A/D = 0.5$, $Re = 2300$. The displacement phase of the images is as for Figure 3-4.**

3.2.2 Transition Between Wake States

The wake and force properties for oscillation frequencies immediately surrounding the transition between wake states were examined in detail in order to understand the nature of the transition between wake states. At each value of f_e/f_o, the wake state at $t = 0$ is that of a stationary cylinder in a free stream. For $t > 0$ the cylinder oscillates at a constant frequency and the oscillating wake appears to be fully established less than 10 oscillations after $t = 0$. For a narrow band of frequencies close to transition, after a number of oscillations self-excited changes were observed in the lift properties. The band of frequencies over which self-excited transitions are observed is called the transition region. It will be shown, by comparing the force and wake properties on either side of these self-excited changes that these changes correspond to a transition from the low-frequency state to the high-frequency state.

A typical example of these self-excited changes is shown in Figure 3-6, where the changes begin after more than 150 oscillation cycles. The lift trace and corresponding instantaneous values of C_L and ϕ_{lift} are shown in Figure 3-6(a & b) respectively. For time less than 97 seconds the lift forces are consistent with the low-frequency state described previously: the lift coefficient is small in amplitude and is approximately out-of-phase with the cylinder's displacement. Conversely, for times after 128 s the lift force is consistent with the high-frequency wake state. In between these two states ($97 < t < 128$) there is a region where the lift force is not consistent with either the low- or high-frequency states. The expanded time trace in Figure 3-6(c) shows the changing relationship between the lift and displacement as the wake moves from the low- to high-frequency wake state. The wake patterns in Figure 3-6(d) and Figure 3-6(e) were acquired at the top of the oscillation cycle, at the times indicated on the lift trace. These images are representative of the wake structures either side of the self-excited transition. The evolution of the vorticity fields before and after the self-excited transition is represented by the phase averaged images in Figure 3-7 and Figure 3-8 respectively. The phase averaged images were calculated using 9 instantaneous images and the general structure of the phase averaged wakes at the top of the oscillation, in Figure 3-7(a) and Figure 3-8(a), correlate well with the instantaneous images in Figure 3-6(d & e) respectively. Despite the fact that the oscillation frequency is constant, the wake states either side of the self-excited transition are clearly different. Before the transition the values of C_L and ϕ_{lift} are consistent with the low-frequency state. Moreover, the wake is shedding in the 2P mode and is clearly consistent with the steady-state low frequency state, described in conjunction with Figure 3-4. After the self-excited transition the wake structure is consistent with the high-frequency wake in Figure 3-5 and the force properties are also consistent with the high-frequency state. Thus, the wake states either side of the self-excited transition are consistent with the wake states at much lower and higher frequencies.

Accurate Batch & Seal Bookbinders Melbourne 95236044

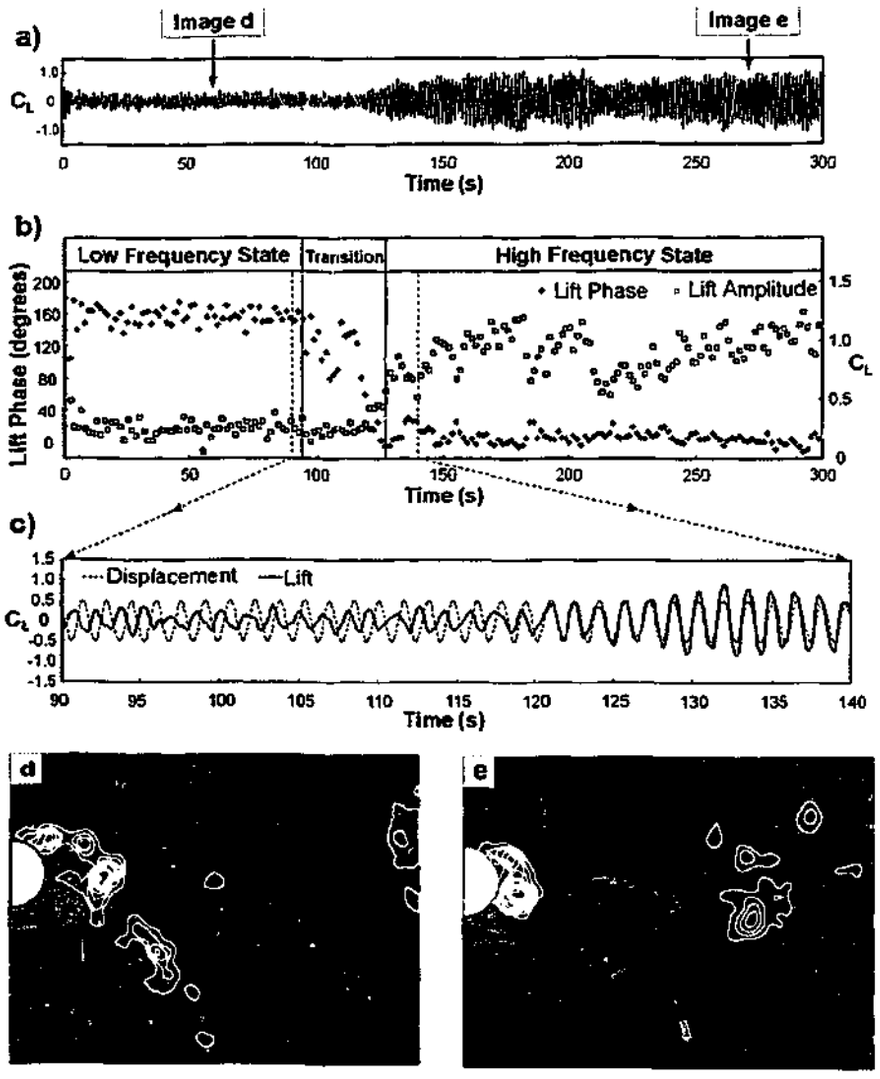

Figure 3-6 The lift time trace a) shows a self-excited transition occurring after more than 150 oscillation cycles at a constant excitation frequency of $f/f_o = 0.815$. The corresponding variation in the instantaneous values of the phase and amplitude of the lift coefficient are shown in b). The lift and displacement traces during the transition are shown in more detail in c). The wake modes either side of the self-excited transition are shown at time = 60 s, corresponding to image d) and time = 270 s representing image e), where both images were acquired at the top of the oscillation cycle.

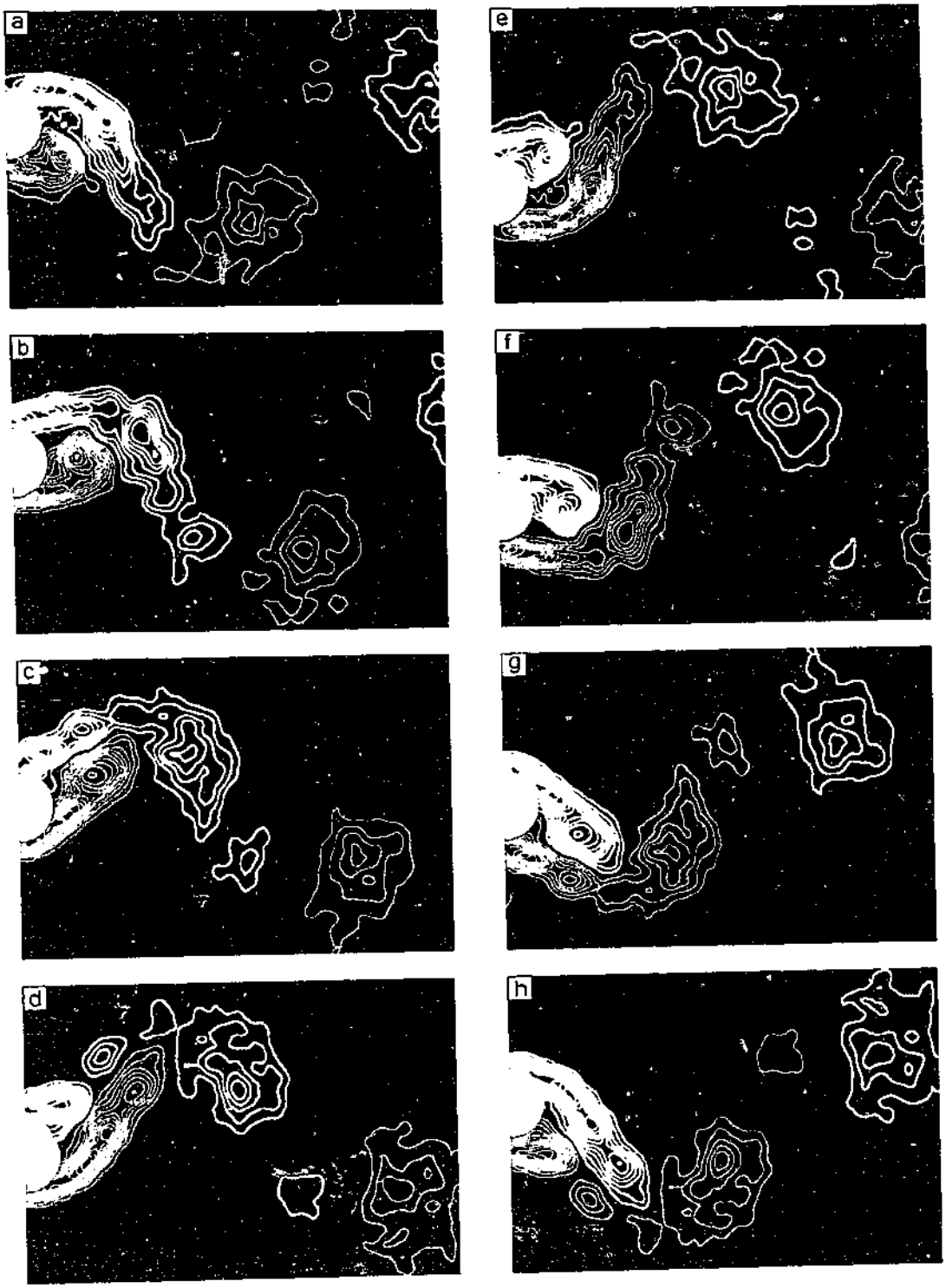

Figure 3-7 Phase averaged images showing the evolution of the vortex structures before a self-excited transition at $f_s/f_n = 0.815$, $A/D = 0.5$ and $Re = 2300$, where the wake structure is consistent with the low-frequency wake state. The phase of the images is as for Figure 3-4

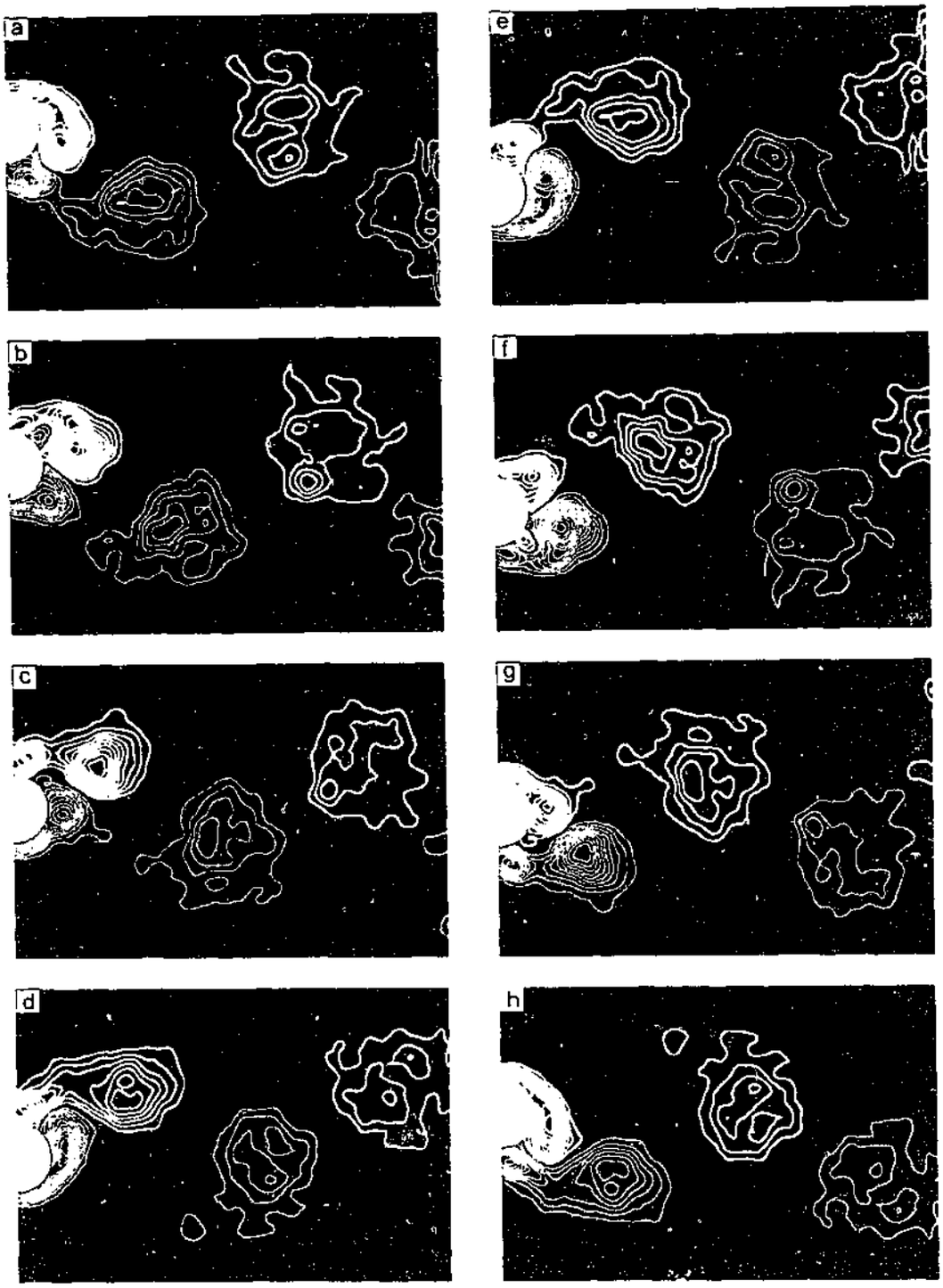

Figure 3-8 Phase averaged images showing the evolution of the vortex structures after a self-excited transition at f_s/f_o = 0.815, A/D = 0.5 and Re = 2300, where the wake structure is consistent with the high-frequency state. The phase of the images is as for Figure 3–4

For A/D = 0.5 and Re = 2300, the self-excited transition always followed the sequence described above and, once the high-frequency wake state was established, a return to the low-frequency state was never observed. After the transition to the high-frequency state there is some variation in C_L and ϕ_{lift}, which was not observed at higher values of f_e/f_o. During this variation, there appears to be an inverse relationship between the instantaneous values of C_L and ϕ_{lift}. The nature of this variation and the behaviour of the wake within the transition region will be discussed in more detail in section 3.6.

3.2.3 Split Forces

At a given time the values of C_L and ϕ_{lift} can be used to differentiate between the low- and high-frequency wake states. For example, either side of the self-excited transition in Figure 3-6(b) the instantaneous values of C_L and ϕ_{lift} were used to identify the segments during which the wake was in either the low- or high-frequency state, as indicated by the boxes above the graph. When segments, each containing only a single wake state, are analysed separately the difference in the force properties for the two states is evident. In Figure 3-9 the properties within the transition region have three separate data points for each oscillation frequency: the light coloured triangular points were calculated from data containing the low-frequency state only, while the darker triangular points represent the high-frequency state data. When the data was not split into segments containing a single wake state the value, represented by the open circular points, is a weighted average of the two wake states.

In Figure 3-9 the properties of the lift force, drag force and energy transfer are presented as functions of f_e/f_o, for A/D = 0.5 and Re = 2300. Within the transition region the time traces have been split into segments containing either the low- or high-frequency wake state. The variation of the force properties over the full range of f_e/f_o is shown in Figure 3-9(a), while in Figure 3-9(b) the transition region has been enlarged to show clearly the variation of selected properties. The split forces from the low-frequency wake state continue the trends shown by the single state data at lower frequencies. Similarly, the split forces from the high-frequency wake state are consistent with the data at higher oscillation frequencies. Presenting the data so that each data point contains data corresponding to a single wake state illustrates that the change in the wake state corresponds to the discontinuous change in the phase and amplitude of the lift force.

Lift Force

The variation of the phase and amplitude of the lift force in Figure 3-9(a)(*i* & *ii*) respectively is consistent with the results of previous experiments, as shown in Figure 3-1. Within the transition region the averaged values of ϕ_{lift} are weighted strongly towards the high-frequency state, not only because this state occurred for longer, but also because of the relatively high amplitude and

coherence of high-frequency state lift force. It is possible that in this transition region results of previous studies have calculated data points using force traces containing a mixture of low- and high-frequency states. This could explain why intermediate values of ϕ_{lift} have been reported in previous investigations, but in our data the intermediate values occur only for data points representing more than one wake state. Additionally, as the intermediate values of ϕ_{lift} appear to be linked to the averaging of data from two different wake states this may explain the change in the direction in which ϕ_{lift} rotated during the transition reported by Gopalkrishnan (1993) for increasing oscillation amplitudes.

Energy Transfer

As discussed in section 1.3.2 the energy transfer from the fluid to the cylinder per oscillation is simply the time integral of the product of the lift force and the cylinder's velocity. Thus, for an approximately sinusoidal lift force the energy transfer can be represented by:

$$C_E \approx \pi\, C_L\, (A/D)\, \sin(\phi_{lift}) \qquad \text{(1-4 reproduced)}$$

The variation of the energy transfer between the fluid and the cylinder is shown in Figure 3-9(a)(*iii*). For the low-frequency state the energy transfer is small, positive and relatively constant. The direction of the energy transfer can always be gauged from ϕ_{lift} and the positive values of C_E for the low-frequency state correspond to values of ϕ_{lift} that are just below 180°. At the transition from the low- to high-frequency state there is a large increase in C_L, but ϕ_{lift} jumps downward towards 0° and $\sin(\phi_{lift})$ is very small, resulting in small values of C_E. The first split high-frequency state value of C_E at $f_e/f_o = 0.840$ is positive, corresponding to a value of ϕ_{lift} which is just above 0°. However, at $f_e/f_o = 0.846$ ϕ_{lift} is below 0° and C_E is small and negative. As f_e/f_o increases further, C_E becomes increasingly negative.

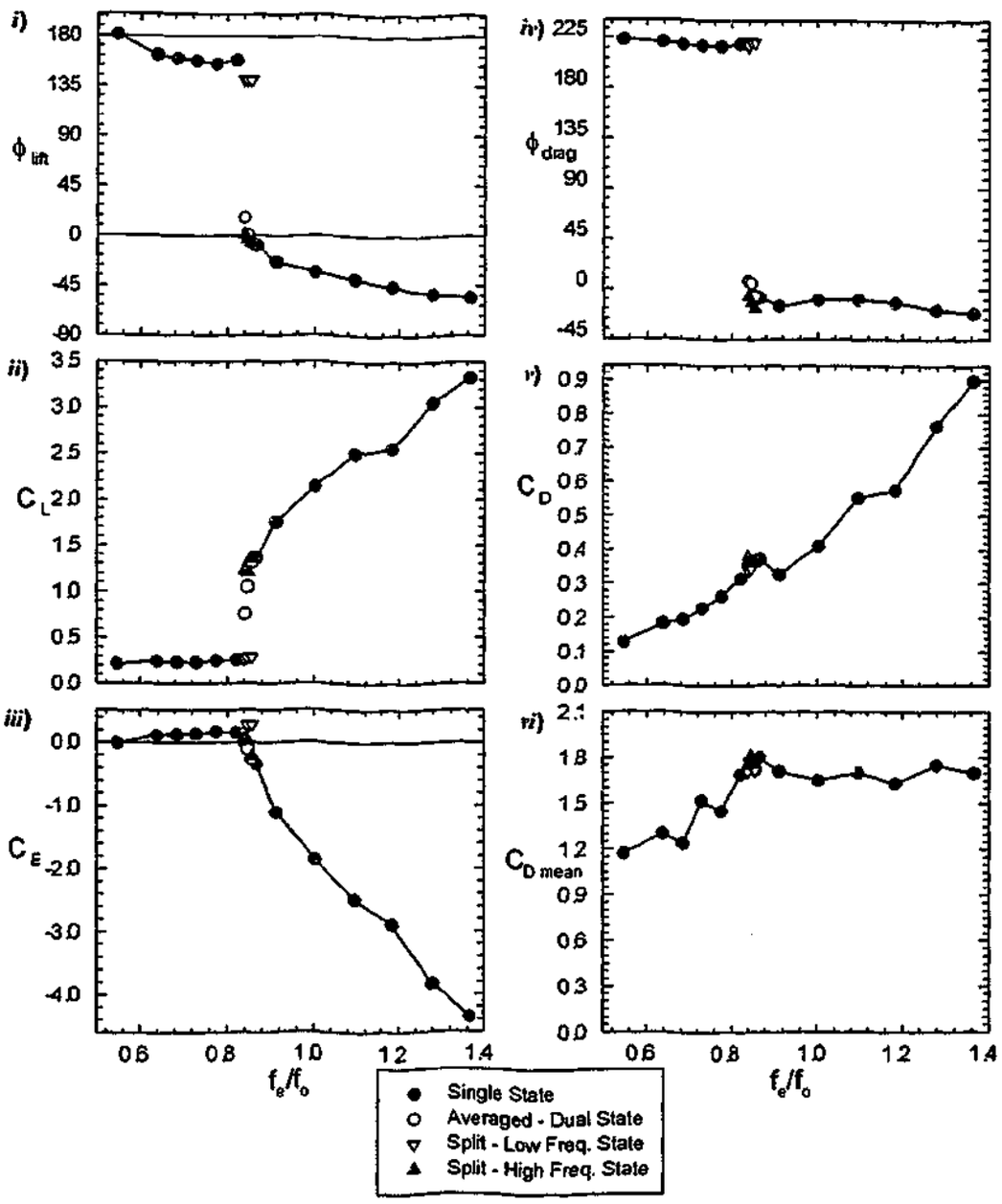

Figure 3-9a) Variation of the lift, drag and energy transfer with f_e/f_o: i) ϕ_{lift}, ii) C_L, iii) C_E, iv) ϕ_{drag}, v) C_D, vi) $C_{D\,mean}$. The circular data points are the values calculated using the entire data trace: ● representing a single wake state outside the transition region, ○ representing a weighted average of more than one wake state inside transition region. The triangular data points within the transition region represent data segments containing a single wake state only: ▲ low-frequency wake state segment, ▽ high-frequency wake state segment.

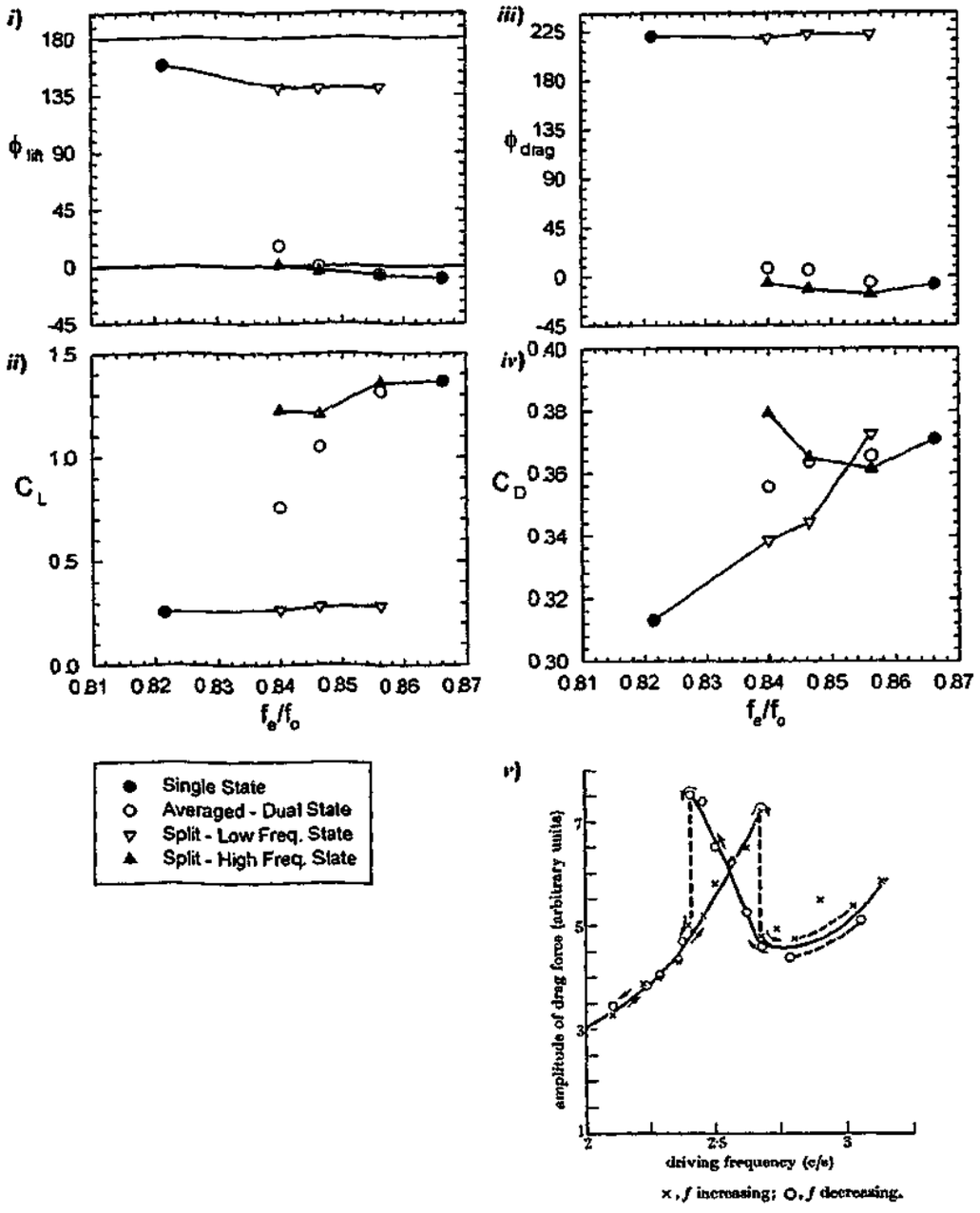

Figure 3-9b) Enlarged plots showing in detail the transition region for selected plots in part a) : *i)* ϕ_{lift}, *ii)* C_L, *iii)* C_E, *iv)* ϕ_{drag}, *v)* C_D, *vi)* $C_{D\,mean}$. For comparison in *v)* the results of Bishop & Hassan (1963) are reproduced showing a hysteretic variation of C_D through transition as f_e/f_o is varied in a continuous fashion.

Drag Force

The magnitudes of the fluctuating and mean drag force are of obvious physical importance, but until now the phase of the drag force has received little attention. The dominant frequency of the drag force is two times the frequency of oscillation ($2f_e$), therefore to relate the phase of the drag to the displacement of the cylinder the general form of the drag force was approximated as:

$$\text{Drag}(t) \approx (\tfrac{1}{2}\rho U^2 DL)\, C_D \sin[2(2\pi f_e t + \phi_{drag})] + C_{D\,mean} \qquad (3\text{-}1)$$

where C_D is the amplitude of the fluctuating drag coefficient, $C_{D\,mean}$ is the mean value of the drag coefficient and ϕ_{drag} is the phase of the drag with respect to the cylinder's displacement $y(t)$. Using this definition ϕ_{drag} only has physical significance over a range of 180°, i.e. $\phi_{drag} = \phi_{drag} \pm 180°$, as ϕ_{drag} is the phase of the drag signal with respect to a signal whose period is twice that of the drag. Therefore, shifting ϕ_{drag} by 180° does not change the relationship between the drag and the displacement and is in fact analogous to shifting the lift phase by 360°. The drag force tends to be less sinusoidal than the lift force, however in all cases the values of ϕ_{drag} presented were calculated from drag traces whose correlation coefficient with a sinusoidal signal is greater than 0.6. This approach allowed us to calculate ϕ_{drag} over the full range of f_e/f_o for all cases except $A/D = 0.25$ at $Re = 4400$.

In Figure 3-9(a)(*iv*) ϕ_{drag} is plotted as a function of f_e/f_o. At the transition from the low- to high-frequency state, Figure 3-9(a)(*iv*) shows that there is a jump in the drag phase of approximately 240° as ϕ_{drag} drops from 225° to -15°. The vortex lift force (not shown in Figure 3-9) and the drag force represent the forces on the cylinder due to changes in the vorticity fields. Thus the drag phase is plotted such that the jump in ϕ_{drag} at transition is in the same direction and of a similar magnitude to the jump in $\phi_{lift\,vortex}$. The vortex forces on the cylinder will be discussed further in section 3.4.3. According to the definition of the drag phase in equation 3-1 any value of ϕ_{drag} is equivalent to $\phi_{drag} \pm 180°$, therefore the jump in ϕ_{drag} can also be correctly described as a downward jump of approximately 60° from 45° to -15°. The established convention is to present ϕ_{lift} such that the transition from the low-to high-frequency state corresponds to a downward jump in ϕ_{lift}, but the lift and drag phases can also be presented such that at the transition there upwards jump in the phase. Although it may appear unnecessary to present a large downward phase shift of say 270°, rather than a smaller 90° phase shift in the opposite direction, this consideration does not have enough merit to break with the established convention.

The overall trend of the drag amplitude in Figure 3-9(b)(*iv*) is to increase with increasing f_e/f_o, with a small peak around transition. This result is broadly consistent with the observations of Bishop & Hassan (1963), however the results of Bishop and Hassan (1963) were presented in arbitrary units precluding direct comparison of the two data sets. As shown in Figure 3-9(b)(*v*), by varying f_e/f_o in

Australasian Medical & Scientific Booksellers Melbourne 95236035

a continuous fashion Bishop and Hassan (1963) obtained a pronounced cross-over in the values of C_D over a wide hysteretic transition region. The higher values of C_D appear to occur at the highest attainable frequencies for the low-frequency state and the lowest attainable frequencies for the high-frequency state. In our case, f_e/f_o was varied in a stepwise fashion with the wake returning to the stationary cylinder state between each value of f_e/f_o. Interestingly, closer examination of the transition region in Figure 3-9(b)(*iv*) shows that the values of C_D for the low- and high-frequency states "cross-over" between the 2nd and 3rd transition point. The crossover region in Figure 3-9(b)(*iv*) is confined to values of f_e/f_o where a self-excited transition occurs but the general nature of the crossover is similar to that observed by Bishop & Hassan (1963) in the hysteretic transition region.

The mean drag in Figure 3-9(a)(*vi*) increases only slightly with increasing f_e/f_o with a very small peak around the transition between the low- and high-frequency states. These results are generally consistent with the results of previous experiments shown in Figure 3-2. However, it appears that the magnitude of the peak in $C_{D\,mean}$ near transition may vary with flow parameters such as *Re* and *A/D*.

While there is an abrupt change in ϕ_{drag} as the wake moves from the low to high-frequency state, the changes in C_D and $C_{D\,mean}$ are relatively minor. As f_e/f_o increases or decreases towards the transition the values of both C_D and $C_{D\,mean}$ increase and the transition between wake states is associated with a small peak in C_D and $C_{D\,mean}$ rather than an abrupt jump. Thus, despite the distinct change in the structure of the near wake at transition, the changes in the overall vertical movement of vorticity results in relatively small changes in C_D and $C_{D\,mean}$. The increase in C_D and $C_{D\,mean}$ as the wake approaches transition indicates that there are some systematic changes in the vertical distribution of vorticity as the wake approaches transition. At other values of *A/D* and *Re* the peaks in C_D and $C_{D\,mean}$ are more exaggerated and in some cases there is a small jump in C_D at transition.

3.2.4 Idealised Variation of Vortex Force with f_e/f_o

A thought experiment will now be outlined which relates the lift and drag forces on the cylinder to the vorticity field and attempts to predict the general dependence of the vortex forces on f_e/f_o for a given idealised mode of vortex shedding.

The vortex force on a body can be written according to equation 1-6 as

$$\bar{F}_{vortex}(t) = -\rho \frac{d}{dt} \int_{Vc} \bar{r} \times \bar{\omega}\, dV \qquad (3\text{-}2a)$$

Considering only the contribution from the spanwise vorticity component ω_z, the drag force (which is equal to the vortex drag force) on the cylinder varies with

$$-\frac{d}{dt}\int_{V_c}\bar{y}\times\bar{\omega}_z\,dV \qquad (3\text{-}2b)$$

Therefore a positive drag force occurs when positive vorticity (ω_z), typically generated on the lower surface of the cylinder moves downwards and when negative vorticity, from the upper surface of the cylinder, moves upwards. Similarly the vortex lift force varies with

$$-\frac{d}{dt}\int_{V_c}\bar{x}\times\bar{\omega}_z\,dV \qquad (3\text{-}2c)$$

Thus a positive vortex lift force is generated by the downstream movement of positive vorticity and by the upstream movement of negative vorticity. The time derivative in equations 3-2 indicates that force is generated by the change in the position of the vorticity, rather than the fact that the vorticity has a position that is a certain distance from the cylinder. Examination of equation 1-6, which relates the vorticity field to the force on the cylinder, allows interpretation of the vortex lift and drag forces in terms of the time dependent spanwise vorticity field.

A simplified view of vortex shedding is that it involves the movement of vorticity in both the vertical and streamwise directions. In a symmetric wake the shedding of both positive and negative vorticity results in a net downstream movement of both signs of vorticity and, on average, the positive and negative vorticity are displaced by an equal and opposite amount in the vertical direction. The drag force does not differentiate between the vertical downward movement of positive vorticity and the movement of negative vorticity upwards, as both instances result in a positive contribution to the drag force. The vortex lift force however does differentiate between the streamwise movement of vorticity of the opposite sign, with the downstream movement of positive vorticity resulting in a positive contribution to the lift force and the movement of negative vorticity downstream causing a negative contribution to the lift force. When the wake is symmetric and phase locked the peaks in the lift force occur once per oscillation and the structure of the wake corresponding to consecutive peaks will be essentially the same. However, there are two peaks in the drag force per oscillation and at consecutive peaks the wake will be a mirror image of itself. Although consecutive peaks in the drag force correspond to two different wake structures the drag force cannot be used to differentiate between the two wakes. This is the physical reason underlying the statement in section 3.2.3 that $\phi_{drag} = \phi_{drag} \pm 180°$.

The variation of the forces on the cylinder as f_e/f_o increases will now be considered for the case of an idealised mode of shedding where the phase-referenced vorticity distribution does not vary with f_e/f_o. During the oscillation cycle the drag force on the cylinder varies with time according to the rate of change in the vertical distribution of vorticity. The magnitude of the mean drag force $C_{D\,mean}$ depends on the net movement of vorticity during the oscillation cycle. Typically, during an oscillation cycle there is a net displacement of positive vorticity downwards, and an equivalent net

displacement of negative vorticity upwards, resulting in a positive mean drag force. Thus, it can be argued that $C_{D\,mean}$ is associated with the mean vertical width of the wake. During the oscillation the fluctuating component of the drag force, and also the lift force, depends the mode of vortex shedding. Assuming that the vortex shedding mode, or in other words the distribution of the vorticity during the oscillation cycle, does not vary with f_e/f_o then, for this idealised case, the mean drag force will not vary with f_e/f_o. As f_e/f_o increases the period of the oscillation cycle becomes shorter and to generate the same distribution of vorticity throughout the cycle the rate of change of $\int_{Vc} \bar{y} \times \bar{\omega}_z \, dV$ must increase. Therefore, for the idealised case the amplitude of the fluctuating drag force C_D will increase linearly with f_e/f_o.

The same argument can be applied to the vortex lift force. For a fully submerged cylinder, equal amount of positive and negative vorticity are convected downstream during an oscillation cycle resulting in a zero mean vortex lift force. The fluctuating vortex lift force is generated by the variation of the streamwise vorticity distribution during the oscillation cycle. Therefore, as for the drag force, for an idealised constant mode of vortex shedding the amplitude of the vortex lift force increases linearly with f_e/f_o.

The total lift force on the transversely oscillating cylinder has two components: the vortex lift force and the apparent mass force. The mean apparent mass force over an oscillation cycle is zero however the amplitude of the apparent mass force increases with f_e/f_o squared. The argument above indicates that for a constant mode of vortex shedding the amplitude of the vortex lift force increases linearly with f_e/f_o. However, as the vortex and apparent mass components of the lift force are generally not in-phase with each other the variation of the total lift force with f_e/f_o is complicated.

The experimental results in Figure 3-2 and Figure 3-9 show that away from the transition region $C_{D\,mean}$ increases only slightly with increasing f_e/f_o and in some cases outside the transition region $C_{D\,mean}$ is essentially constant. Additionally, the experimental results in Figure 3-9 show that outside the transition region C_D increases almost linearly with increasing f_e/f_o. The peaks in both $C_{D\,mean}$ and C_D as f_e/f_o approaches the transition region indicate that the vertical distribution of vorticity is modified prior to the transition occurring. The experimental results, showing the variation of the vortex lift force with f_e/f_o, will be discussed in section 3.4.

3.3 TRANSITION

The transition between the low- and high-frequency states results in significant changes in both forces on the cylinder and the structure of the near wake. Therefore, it is important to have an understanding of how and why this transition occurs. A transition between two states occurs in a large number of flows, for example the transition between a laminar flow and a turbulent flow. However, determining the exact origin of a transition between two different states is a very difficult problem. Using stability theory it is often possible to determine how the stability of a system changes leading up to and during a transition, but such analyses do not necessarily explain why the system is changing. Generally speaking, transitions occur when the controlling parameter, in our case f_e/f_o, reaches a critical value. Further changes in the controlling parameter cause the original state to become unstable and the system moves to a new state. The variation of the forces on the cylinder as f_e/f_o approaches transition, in particular the almost constant values of ϕ_{lift} and ϕ_{drag} shown in Figure 3-9(a)(*i* & *iv*) give very little indication that transition is about to occur. In this section we examine the systematic changes in the structure of the near wake as f_e/f_o increases toward transition, as well as the changes in the nature of the self-excited transition as f_e/f_o increases within the transition region.

3.3.1 Wake Length

The vorticity fields in Figure 3-10 show the changes in the structure of the near wake as f_e/f_o increases from 0.695 to 0.869. The vorticity fields were calculated by phase averaging 9 consecutive images at the extreme displacement of the cylinder, with the exception of the image at $f_e/f_o = 0.781$, where only 7 images were available. These images represent a "short term" average wake structure and demonstrate subtle changes in the two wake modes with changing oscillation frequency. The decrease in the peak vorticity due to the averaging of instantaneous vorticity fields did not vary with either f_e/f_o or wake state.

Figure 3-10(a) shows the low-frequency wakes as f_e/f_o increases from 0.695 to 0.815. As f_e/f_o increases the general mode of shedding is unchanged but there is a decrease in the streamwise length of the attached vortex structures. Over this range of frequencies ϕ_{lift} and ϕ_{drag} are approximately constant (in section 3.4 it will be shown that $\phi_{lift\ vortex}$ is also essentially constant). Therefore, the changes in the position of the vortex structures in Figure 3-10(a) are not phase related but are due to a contraction of the wake. These observations are consistent with those of Ongoren and Rockwell (1988), and Gu *et al* (1994).

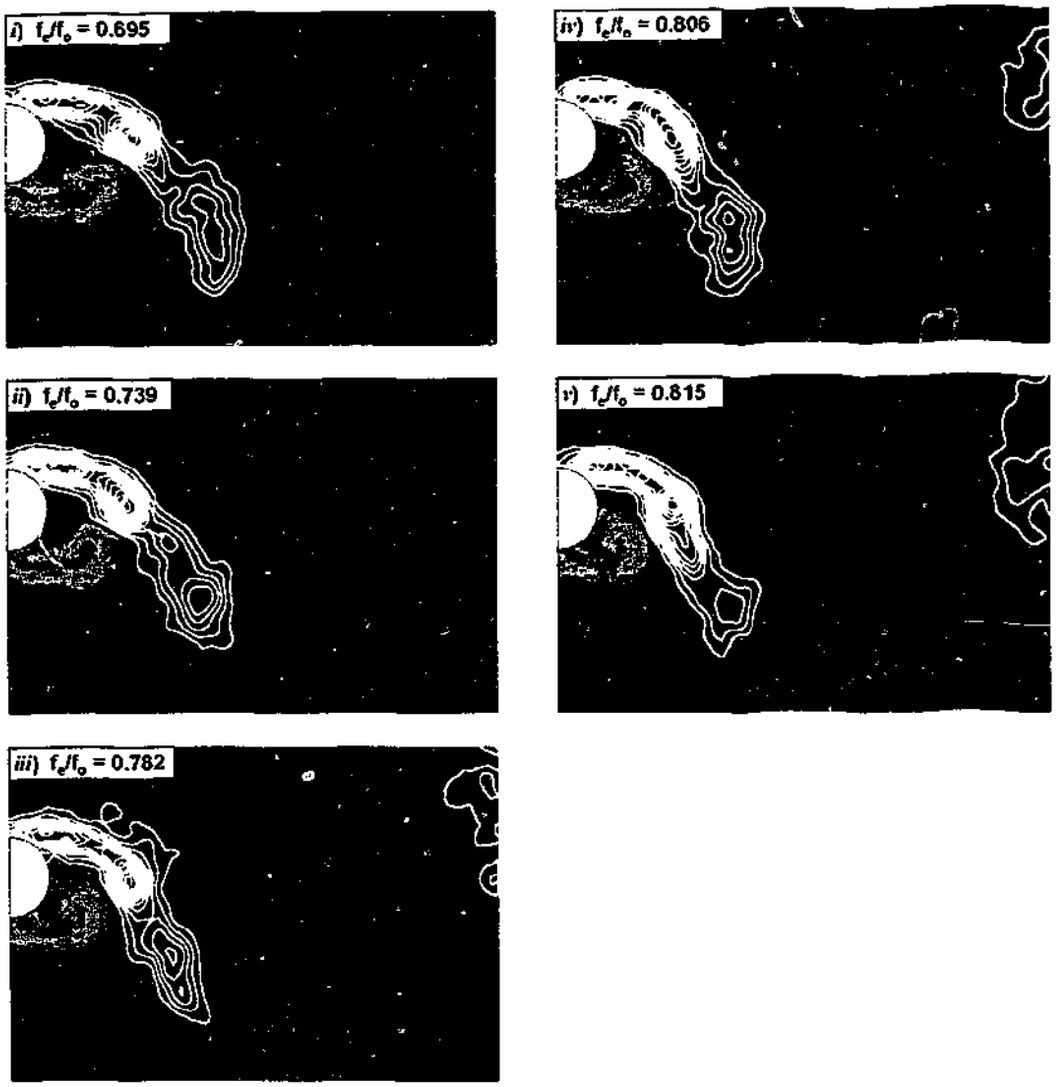

Figure 3-10(a) Phase averaged vorticity fields showing the variation of wake length with f_e/f_o for the low-frequency state. All images are at the top of the cylinder's oscillation.

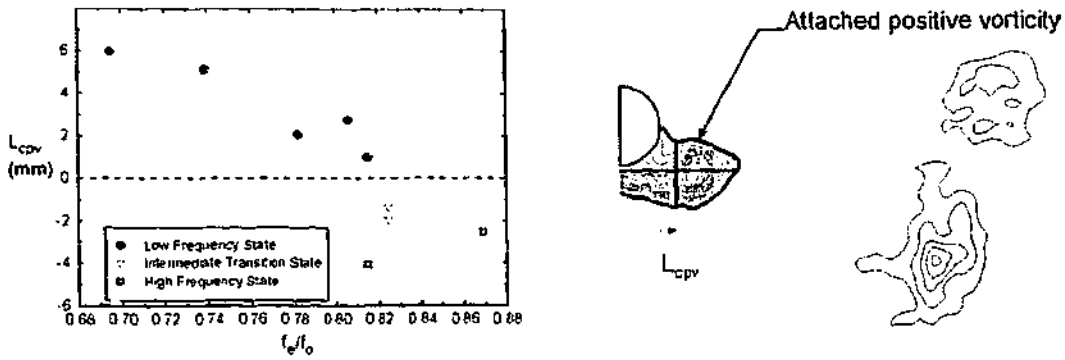

Figure 3-10(b) Variation of the phase related streamwise position of the centre of attached positive vorticity, L_{cpv} with f_e/f_o and wake state. The schematic on the right hand side demonstrates the definition of L_{cpv} at the top of the cylinder's oscillation.

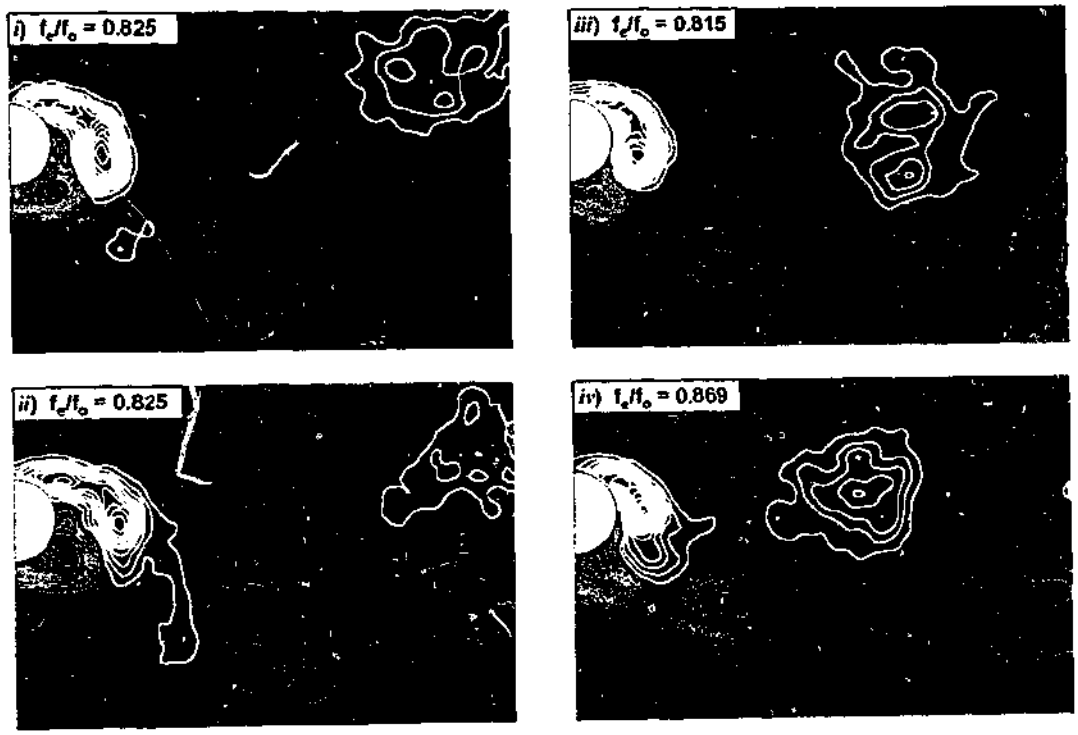

Figure 3-10(c) Phase averaged vorticity fields at higher values of f_e/f_o. In images *i)* and *ii)* the wake appears to be in an intermediate state, while in *iii)* and *iv)* the wake is in the high-frequency state.

At f_e/f_o = 0.815 and 0.825 a self-excited transition from the low- to the high-frequency state was observed. For f_e/f_o = 0.815 the low- and high-frequency modes are shown in Figure 3-10(a)(*v*) and Figure 3-10(c)(*iii*) respectively where for the high-frequency mode the vorticity is wrapped tightly around the cylinder and the wake length is clearly shorter. The vorticity fields in Figure 3-10(c)(*i* & *ii*) at f_e/f_o = 0.825 were acquired at two separate time periods when the wake appeared to be in between the low- and high-frequency wake states. During these periods the values of C_L and ϕ_{lift} were not fully consistent with either the low- or high-frequency states and the

corresponding structure of the near wake is also not fully consistent with either the low-frequency wake in Figure 3-10(a) or the high-frequency wakes shown in Figure 3-10(c)(*iii & iv*). This wake can be described as an intermediate wake, where properties of the intermediate wake state will be discussed further in section 3.6.

Although visual inspection of Figure 3-10 reveals a contraction of the wake as f_e/f_o increases, there is no single universally accepted method to calculate the length of the wake. Historically, the wake formation length has been defined in a number of ways, generally using a series of point measurements with high temporal resolution. Our PIV data has limited temporal resolution but high spatial resolution and a different method to represent the wake length is chosen. Given the nature of the problem we are investigating it is logical to calculate the wake length either at a fixed phase point, or over a very large number of phase points. The variation of the wake length at the top of the cylinder's oscillation can be quantified by calculating L_{cpv}, the streamwise distance from the base of the cylinder to the centroid of the attached positive vorticity. The region of attached vorticity was defined by applying a threshold minimum vorticity level to determine the boundary. Due to the experimental difficulties in resolving the boundary layer around the front of the cylinder, L_{cpv} was calculated by taking moments of the attached positive vorticity downstream of the centre of the cylinder. A schematic demonstrating the definition of L_{cpv} is shown in Figure 3-10(b). L_{cpv} is not a direct measure of wake length, but is a property that appears to vary directly with the wake length and is also easily quantified at a particular phase point. Moreover, for the case of an oscillating cylinder the phase referenced length of the attached positive vorticity appears to be related to the transition between the low- and high-frequency wake states.

Figure 3-10(b) shows that as f_e/f_o increases from 0.695 towards transition the wake remains in the low frequency state but L_{cpv} decreases. However, as f_e/f_o increases further the low-frequency state is no longer stable and there is a transition from the low- to the high-frequency state. The variation of L_{cpv} with f_e/f_o shows that the transition to the high-frequency wake corresponds to a contraction of the wake below a certain critical length. For frequencies within the transition region, after startup the wake moves first to the low-frequency wake state and the wake length is very close to the critical value. From cycle to cycle there is some variation in the wake length but after the transition to the high-frequency state the wake length is significantly shorter. Interestingly, at transition L_{cpv} becomes negative *i.e.* the centre of the positive vorticity moves back behind the rear of the cylinder. However, the fact that there is a of change in sign of L_{cpv} at transition is not necessarily physically significant as the calculation of L_{cpv} does not include all attached positive vorticity, and is related to a particular phase point in the cylinder's oscillation.

In light of the changes in the length of the near wake preceding transition, observed in both this and the previous work of Ongoren & Rockwell (1988a) and Gu *et al.* (1994), it is reasonable to suggest that the wake length plays a role the low- to high-frequency state transition. The most robust feature of the transition is the large shift in the phase of vortex shedding. Vortex shedding depends on interaction between the two shear layers and as the wake contracts this interaction is altered. The contraction of the wake as f_e/f_o increases towards transition does not result in significant changes in the mode or phase of vortex shedding. However, the contraction of the wake below a critical length coincides with the transition and a change in the way the shear layers interact. If the interaction, which originally resulted in vortex shedding at a particular phase point, is significantly altered by the contraction of the wake below a critical length then this contraction may be the reason for the transition to the different stable wake state. For the case of the oscillating cylinder, after the transition to the new wake state the vortex shedding occurs at a very different phase point and at $A/D = 0.5$ there is a change in the mode of vortex shedding from 2P to 2S.

As f_e/f_o increases towards transition there is an increased disparity in the relative strength of the vortices in the "2P pairing". This is demonstrated in Figure 3-10(a), where for increasing f_e/f_o there is a decrease in the strength of the positive vortex structure that has been shed into the upper wake. Although this field of view does not show the pairing of the positive and negative vorticity the symmetry of vortex shedding means that the relative strength of the upper and lower positive vortex structures are indicative of the relative strength of the vortices within the counter rotating pairs: *i.e.* the weaker positive vortex in the upper wake forms a counter rotating pair with a stronger negative vortex. The formation of the 2P mode depends on each of the shear layers shedding two separate structures. In Figure 3-10(a - e) the long negative vortex structure deforms into two structures as it interacts with the positive vorticity in the lower shear layer. As f_e/f_o increases, the wake contracts causing the long negative vortex structure to be located further around the base of the cylinder. Additionally as f_e/f_o increases the vortex structure that is about to be shed from the end of the shear layer becomes progressively weaker, resulting in vortex pairs of unequal strength. Interestingly, despite the changes in the length of the attached wake and the relative strength within the vortex pairing, prior to the transition both the lift and drag phase remain relatively constant.

3.3.2 State Selection Within the Transition Region

Within the transition region at $A/D = 0.5$ the system tends to be in one of two stable states: the low- or high-frequency states. At $A/D = 0.5$ and $Re = 2300$, the self-excited transition was irreversible and transition always occurred from the low-frequency state to the high-frequency state. Therefore, for frequencies of oscillation within the transition region when the cylinder starts oscillating the wake state changes first from the stationary cylinder state to the low-frequency state, then, after a period of time, the wake undergoes a self-excited transition to the high-frequency state.

The range of frequencies over which the self-excited transition was observed is quite narrow and at $A/D = 0.5$ and $Re = 2300$ the self-excited transition was observed for $0.806 \leq f_e/f_o \leq 0.821$. In Figure 3-11(a) the average time from startup to transition is plotted as a function of f_e/f_o, where each value was calculated from 4-6 separate experiments and the vertical bars represent one standard deviation. As f_e/f_o increases within the transition region both the average time to transition and the variation in the time to transition decrease.

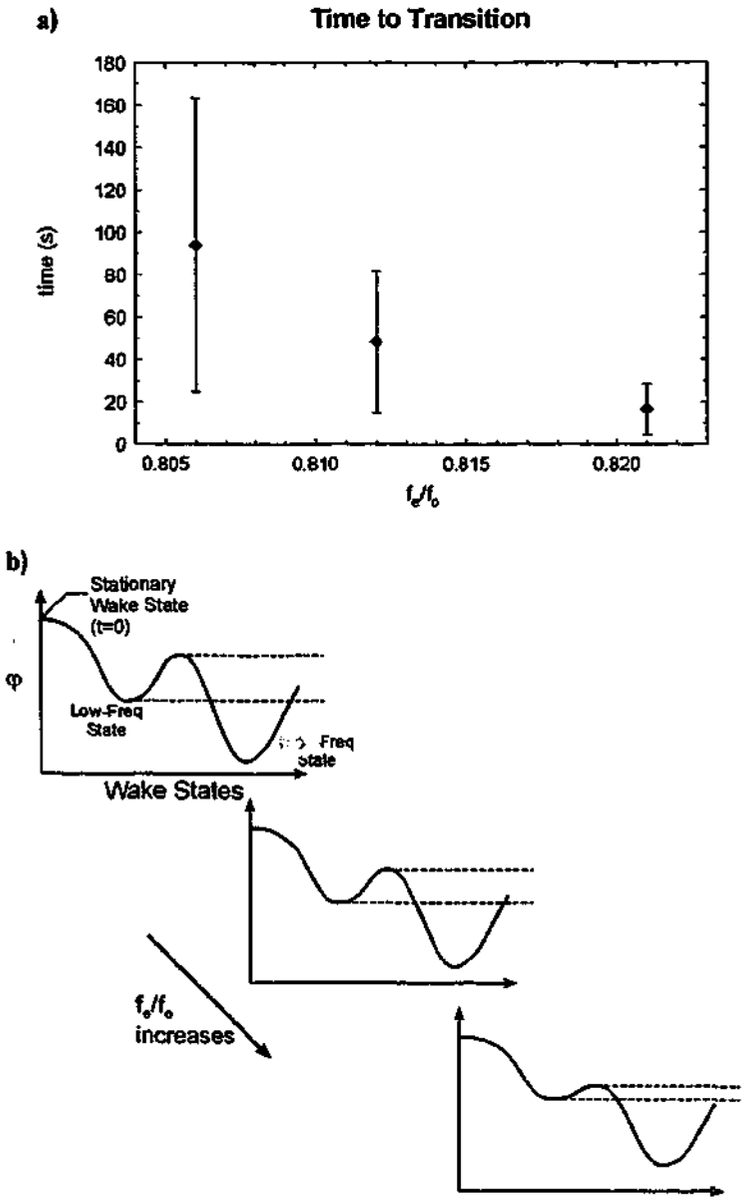

Figure 3-11 a) The variation of the time from startup to the self-excited transition to the high-frequency state, at $A/D = 0.5$ and $Re = 2300$. b) Schematic showing an idealised variation of the stability of the meta-stable system, represented by an idealised system potential energy φ, as f_e/f_o increases through the transition region.

Within the transition region at $A/D = 0.5$ and $Re = 2300$, the wake moves to the low-frequency state immediately after start up but after the self-excited transition the wake remains in the high-frequency state and the high-frequency state appears to be the most stable state. Thus, within the transition region the low-frequency state can be interpreted as a metastable state; which may persist for a period of time but eventually the wake will move to the more stable high-frequency state. For the wake to transition from the metastable low-frequency state a certain level of perturbation is required. As the low-frequency state becomes less stable the level of perturbation required for the transition will decrease and at any given instant the probability that transition will occur is increased. Therefore, the average time from start-up to the self-excited transition is a measure of the stability of the low-frequency state. The decrease in the average time to transition, shown in Figure 3-11(a), indicates that as f_e/f_o increases the metastable low-frequency state becomes less stable.

Figure 3-11(b) is a graphical representation of the variation of the relative stability of the low- and high-frequency states as f_e/f_o increases within the transition region. The potential energy of the system φ is not a quantity that we are able to measure and is used somewhat loosely to represent a variable that is minimised by a stable system. As described in section 1.6.1, a metastable state occurs when the potential is locally minimised but there is another more stable state where the potential is absolutely minimised. Within the transition region at $A/D = 0.5$ and $Re = 2300$ the low-frequency state is a metastable state. As f_e/f_o increases the stability of the low-frequency state, represented by the depth of the well in Figure 3-11(b), decreases until the low-frequency state is unstable and the wake is exclusively in the high-frequency state.

During the experiments it was observed that transition could be "forced" by disturbing the flow upstream of the cylinder. These large and unquantified perturbations were generated using an oscillating rod located several meters upstream of the cylinder. For values of f_e/f_o just below the transition region the perturbations caused a transition to the high-frequency state, but after a number of oscillations the wake returned to the low-frequency state. This suggests that for these values of f_e/f_o the high-frequency state can exist as a metastable state but that the low-frequency state is more stable.

When the cylinder starts oscillating at $t = 0$ the initial stationary cylinder becomes unstable and the wake must move to a state which is stable or metastable. For oscillation frequencies within the transition region at $A/D = 0.5$ and $Re = 2300$ the wake always moved from the stationary cylinder state to a metastable low-frequency state. The fact that the wake has an initial preference for the low-frequency state is represented schematically in Figure 3-11(b) by placing the metastable low-frequency state between the unstable stationary cylinder state and the stable high-frequency state. The relationship between the initial unstable stationary cylinder state and the low- and high-frequency states is expected to depend on the flow and oscillation parameters. If, for an amplitude

of $A/D = 0.5$, the Reynolds number is increased from 2300 to 9100 a change in the nature of the self-excited transition is observed. Within the transition region at $Re = 9100$ the wake moves first to the high-frequency state and after a period of time there is a self-excited transition to the low-frequency state. The self-excited transition, from the high- to low-frequency state is shown in Figure 3-12 in terms of the total lift phase. Immediately after startup ϕ_{lift} is close to -45° and therefore consistent with the high-frequency state, however after $t \approx 200$ s there is a self-excited transition and ϕ_{lift} moves to a value of just over 180°, which is consistent with the low-frequency state. The reversed direction of the self-excited transition at $Re = 9100$ compared to $Re = 2300$ indicates that in this case the wake prefers to move from the stationary cylinder state to a meta-stable high-frequency state. At other values of A/D or Re a self-excited transition was not always observed, indicating that the transition region is either very narrow or does not exist. Changing the relationship between the initial stationary cylinder state, at $t = 0$, and the low- and high-frequency states by changing A/D or Re may alter the value, or values, of f_e/f_o at which the transition between the two states occurs. Additionally, the change in the relative stability of the initial stationary cylinder state and the low and high-frequency states may also affect the nature of the self-excited transition and the width of the transition region.

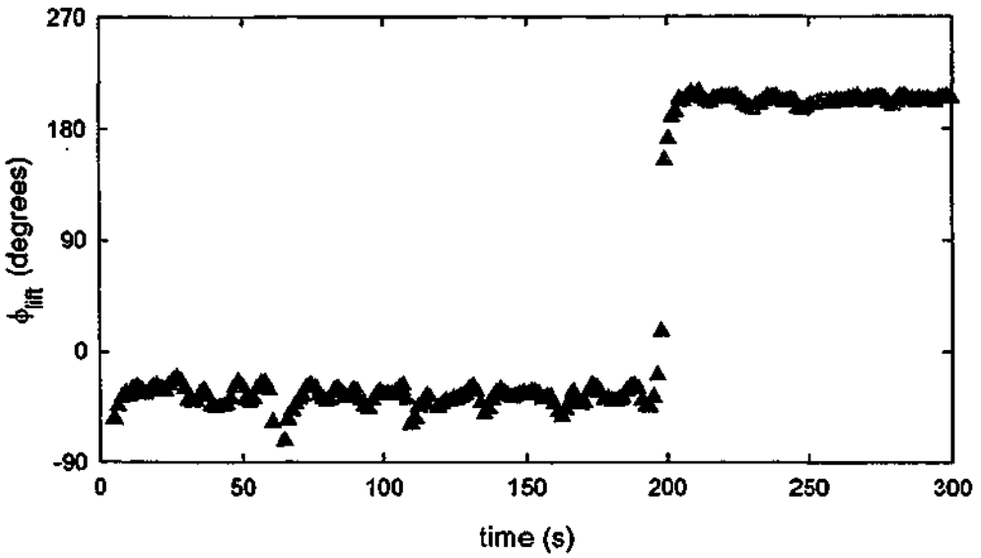

Figure 3-12 Variation of ϕ_{lift} during a "reverse" self-excited transition from the high-frequency state to the low-frequency state at $A/D = 0.5$, $Re = 9100$ and $f_e/f_o = 0.992$.

3.4 UNIVERSALITY OF THE LOW- AND HIGH-FREQUENCY STATES: VARIATION WITH A/D AND Re

Until now the focus has been on the frequency dependence of the wake for constant values of Reynolds number and oscillation amplitude. The investigation is now extended to look at three Reynolds numbers, Re = 2300, 4400 and 9100, and a range of oscillation amplitudes, A/D = 0.25, 0.4, 0.5 and 0.6. Rather than consider the forces on the cylinder as a function of A/D and Re for a fixed frequency of oscillation, the frequency dependence of the forces at different values of A/D and Re is examined. The compiled data from previous experiments, presented in Figure 3-1, shows that the simultaneous jump in ϕ_{lift} and C_L, occurs for a wide range of Reynolds numbers (Re = 2300 to 60,000). Additionally, Staubli's (1983a & b) data shows a similar jump in ϕ_{lift} and C_L for a wide range of oscillation amplitudes ($A/D \approx 0.02 - 1.0$). Therefore, the transition at $f_e/f_o \approx 1$ appears to be a universal feature of these flows for a wide range of A/D and Re.

In the following section the frequency dependence of the phase and amplitude of the lift force is considered for a range of oscillation amplitudes. As discussed in section 1.3.3, the total force consists of two components: a vortex component due to the vorticity in the cylinder's wake and an apparent mass component that is directly related to the cylinder's acceleration. Traditionally the total lift force has been referred to as the "lift force" and up to this point this convention has been followed. However, in this section the vortex force component of the lift force is also examined and the results will be discussed in terms of the "total lift" and "vortex lift" to clearly differentiate between the two. For consistency we will continue to use ϕ_{lift} and C_L, rather than $\phi_{lift\ total}$ and $C_{L\ total}$ to represent the phase and amplitude of the total lift force. The variation of the vortex forces with f_e/f_o and A/D are then considered in terms of $\phi_{lift\ vortex}$, C_L, C_E, ϕ_{drag}, C_D and $C_{D\ mean}$. Finally the universality of the forces on the cylinder and the mode and phase of vortex shedding are considered for a range of oscillation amplitudes and Reynolds numbers.

3.4.1 Variation of Total and Vortex Forces with A/D

In Figure 3-13 the phase and amplitude of the total lift force on the cylinder are plotted as a function of f_e/f_o for A/D = 0.4, 0.5 and 0.6, at Re = 2300. These experiments focused on a narrow range of f_e/f_o close to transition, but the frequency range incorporates both the low- and high-frequency wake states. As A/D increases form 0.4 to 0.6 Figure 3-13(a) shows that there is a significant increase in the value of ϕ_{lift} associated with the low-frequency state: at A/D = 0.4, the average values of ϕ_{lift} before transition is approximately 102°, whereas at A/D equal to 0.5 and 0.6 the average values of ϕ_{lift} before transition are 154° and 193° respectively. The fact that the value of ϕ_{lift} for the low-frequency state passes through 180° as A/D increases from 0.5 to 0.6 is significant because it means there is a change in the direction of the energy transfer between the fluid and the

cylinder. For A/D = 0.4 and 0.5 ϕ_{lift} is less than 180°, thus positive energy is delivered to the cylinder from fluid, indicating that vortex-induced vibrations would occur. However, at higher A/D the energy transfer is negative. Intuitively this makes sense, as the oscillations of an elastically mounted cylinder do not oscillation amplitudes above a certain value, *i.e.* above a certain amplitude the net energy transfer to the cylinder is no longer positive. The value of ϕ_{lift} for the high-frequency state does not vary significantly with A/D. Therefore as A/D increases from 0.4 to 0.6 there is a significant increase in the downward jump in ϕ_{lift} at transition. At higher Reynolds numbers Staubli (1983b) also found that $\Delta\phi_{lift}$ at transition increases with A/D. For frequencies of oscillation close to transition Figure 3-13(b) shows that for both wake states there was only a small change in the values of C_L as A/D increased from 0.4 to 0.6. However, our data at higher Re and Staubli's previous results suggest that C_L increases with A/D and that this effect is most obvious at higher frequencies well above transition.

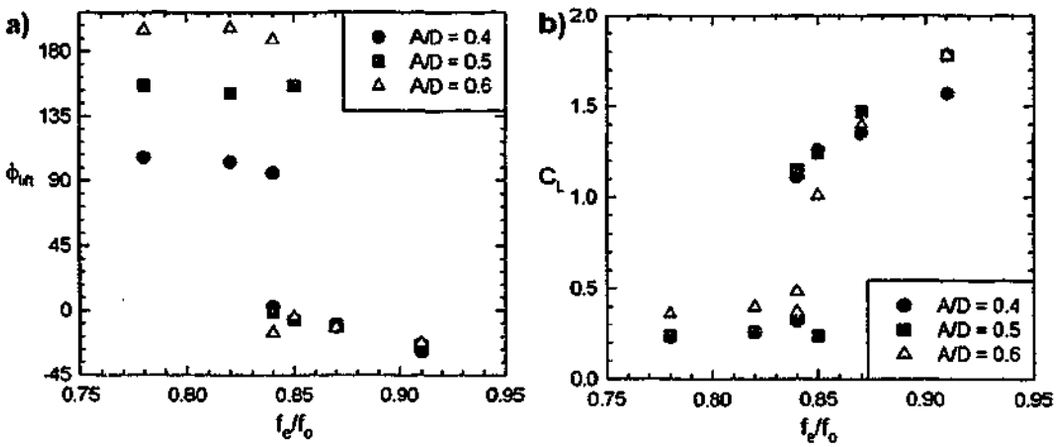

Figure 3-13 Frequency dependence of a) ϕ_{lift} and b) C_L for A/D = 0.4, 0.5 & 0.6 at Re = 2300.

At the higher Reynolds number of 4410, shown in Figure 3-14, similar trends in the behaviour of the total lift force are observed. In Figure 3-14(a) as A/D changes from 0.25 to 0.5 there is a large change in the value of ϕ_{lift} for the low-frequency state and a corresponding change in the direction of energy transfer, but for the high-frequency state ϕ_{lift} does not vary significantly with A/D. In Figure 3-14(b) the amplitude of the total lift force at Re = 4100 increases with A/D and, particularly for the high-frequency state, the increase in C_L is more obvious than at Re = 2300.

For the same values of f_e/f_o and A/D as in Figure 3-13 the vortex forces on the cylinder are plotted in Figure 3-15. To recap, the vortex force is the force due to the movement of vorticity, *i.e.* the force component that is directly related to the wake. The vortex force is calculated by subtracting the apparent mass force from the total force, where the apparent mass force, F_{am}, is in-line and in-phase with the oscillation of the cylinder. The drag force on the cylinder is generally not specifically designated as a vortex force but as the apparent mass component of the drag force is

zero the total drag force is by definition a vortex force. The energy transfer between the cylinder and the fluid can be expressed in terms of either the vortex or total lift force, see equation 1-10. The apparent mass component of the total force makes no net contribution to the energy transfer, therefore C_E can be associated with the vortex lift force.

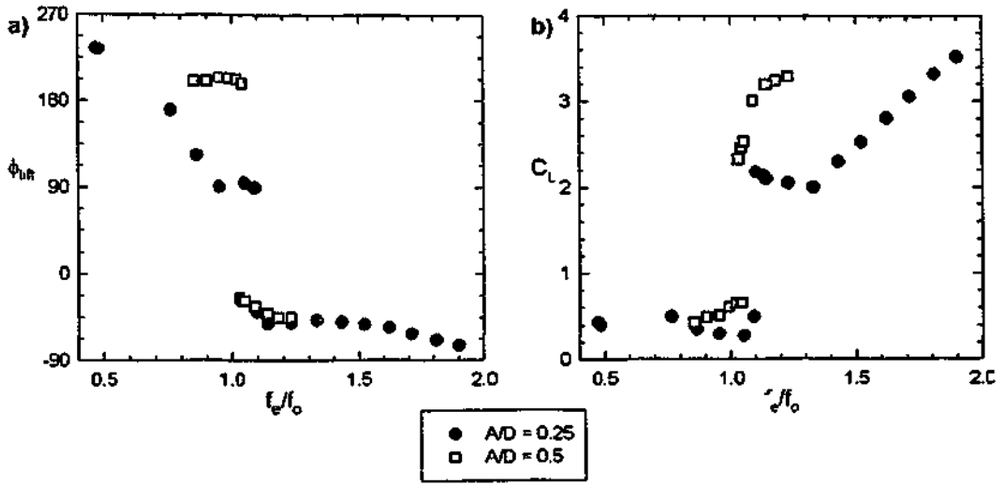

Figure 3-14 Frequency dependence of a) ϕ_{lift} and b) C_L for A/D = 0.25 & 0.5 at Re = 4410.

Figure 3-15(a) shows that for both the low- and high-frequency states as A/D increases from 0.4 to 0.6 there is very little variation in the phase of the vortex lift force. The collapse of $\phi_{lift\ vortex}$ in Figure 3-15(a) contrasts with the variation of ϕ_{lift} in Figure 3-13(a), where for the low-frequency state as A/D increases from 0.4 to 0.6 there is a shift in ϕ_{lift} of approximately 90° or ¼ of an oscillation cycle. The phase of the drag force, shown in Figure 3-15(b), also collapses for A/D = 0.4 to 0.6. The fact that the phase of both the vortex lift and drag forces collapse suggests that the phase of vortex shedding depends primarily on wake state and is approximately independent of the amplitude of oscillation. The relationship between the phase of the vortex forces and the phase of vortex shedding will be considered further in the remainder of section 3.5 as well as in section 3.6.

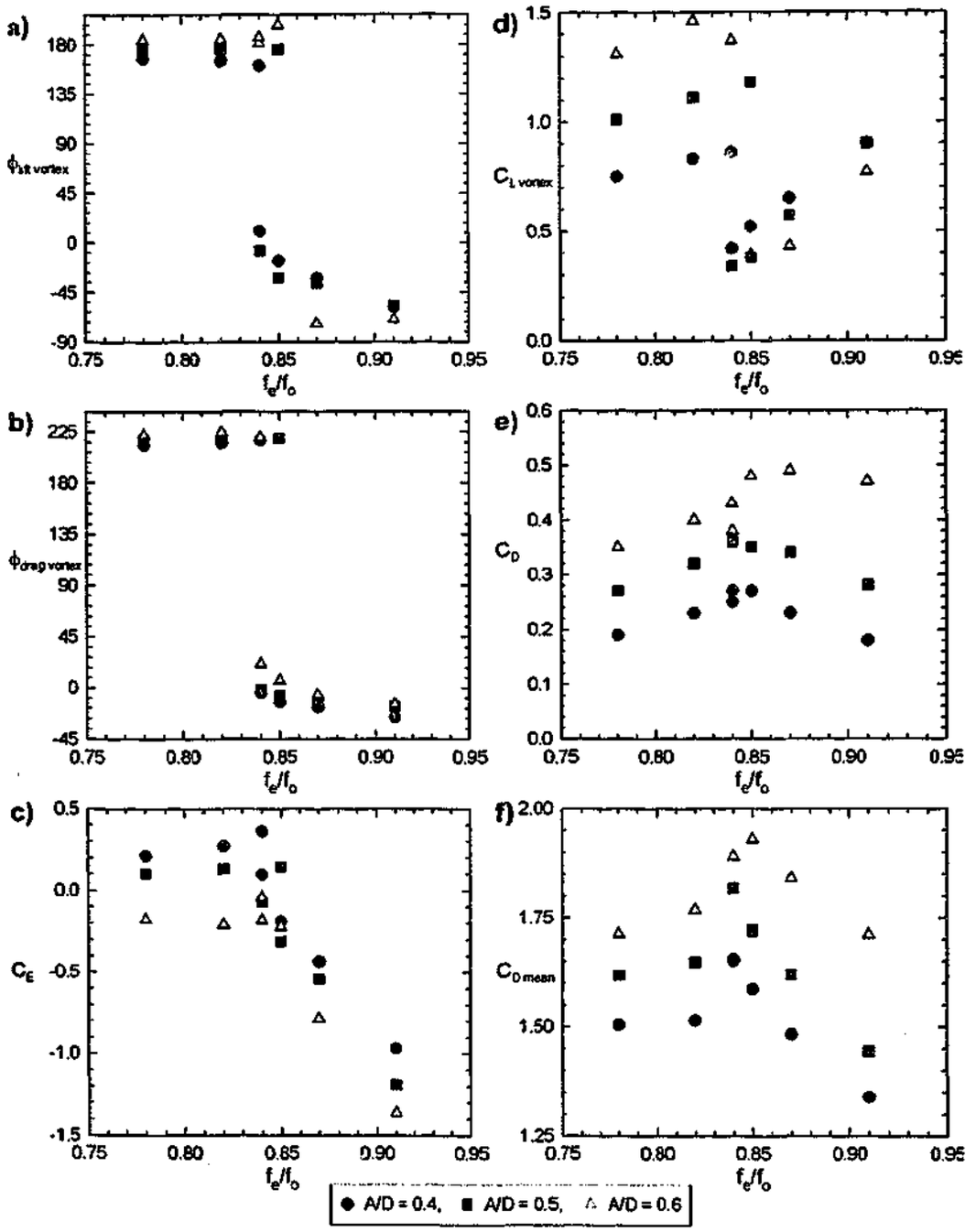

Figure 3-15 Frequency dependence of a) $\phi_{lift\ vortex}$, b) ϕ_{drag}, c) C_E, d) $C_{L\ vortex}$, e) C_D, f) $C_{D\ mean}$ for A/D = 0.4, 0.5 & 0.6 at Re = 2300.

Unlike the amplitude of the total lift force, the amplitude of the vortex lift force, shown in Figure 3-15(d), varies strongly with A/D. For the low-frequency state as A/D increases from 0.4 to 0.6 the value of $C_{L\ vortex}$ increases by more than 50%. However after the transition to the high-frequency state $C_{L\ vortex}$ does not vary strongly with A/D, and appears to decrease slightly with increasing A/D.

At the transition from the low- to high-frequency state C_L jumps upwards however at the same point in Figure 3-15(d) there a downward jump in $C_{L\,vortex}$, where the magnitude of this jump gets smaller as A/D decreases. If this trend continued then for even smaller oscillation amplitudes $C_{L\,vortex}$ would actually jump upwards at transition. Figure 3-15(d) shows that for both the low- and high-frequency states $C_{L\,vortex}$ increases with increasing f_e/f_o. The approximately linear increase of $C_{L\,vortex}$ with f_e/f_o is consistent with the discussion in section 3.2.4 relating the vortex forces to an idealised wake. As shown in Figure 3-15(e &f) both the amplitude of the fluctuating drag force and the mean drag force increase with increasing A/D. However, the general form of the variation of both C_D and $C_{D\,mean}$ with f_e/f_o does not change significantly as A/D increases from 0.4 to 0.6.

Unlike the phases of the vortex forces, which showed a relatively good collapse over the range of A/D studied, the amplitudes of the vortex forces do not collapse but vary systematically with A/D. For a given wake mode, it is expected that the displacement of vorticity will vary with A/D as for higher oscillation amplitudes the cylinder moves further during the oscillation cycle. Therefore, at a constant value of f_e/f_o, as A/D increases there is an increase in the rate at which vorticity is displaced. Thus, according to equation 3-2b both the mean and fluctuating components of the drag force would be expected to increase with A/D.

The energy transfer between the cylinder and the fluid is plotted in Figure 3-15(c), where, as described in equation 1-10, the magnitude of the energy transfer is directly related to A/D but the direction, or sign, of the energy transfer depends on the value of the lift phase. For the low-frequency state the energy transfer increases with decreasing A/D, passing through zero between A/D = 0.5 and 0.6. The corresponding lift phases, ϕ_{lift} and $\phi_{lift\,vortex}$ shown in Figure 3-13(a) and Figure 3-15(a) respectively, indicate that the negative energy transfer for the low-frequency state at A/D = 0.6 corresponds to a lift phase that is in the 3rd quadrant *i.e.* above 180°. At A/D = 0.4 and 0.5 the low-frequency state lift phases are in the 2nd quadrant and there is positive energy transfer from the fluid to the cylinder. The energy for the high-frequency state is negative for all cases except one point immediately following transition at A/D = 0.5. Outside the transition region the energy transfer for the high-frequency state becomes more negative as A/D increases.

Over the range of A/D studied, the frequency at which transition occurred did not change significantly. However, there were changes in the nature of the self-excited transition. At A/D = 0.4 and 0.5 there was a non-reversible self-excited transition from the low-frequency state to the high-frequency state that was consistent with the self-excited transition discussed previously. At A/D = 0.5 the self-excited transition from the low- to the high-frequency state occurred over a number of oscillation cycles. Moreover, after the self-excited transition the lift properties, particularly C_L and $\phi_{lift\,vortex}$, demonstrated significant unsteadiness. At A/D = 0.6 a self-excited transition was also initiated from the low-frequency state, but at f_e/f_o = 0.841 the combined properties of the total and vortex lift forces after the transition were not consistent with the high-

frequency wake state. Further investigations of these phenomena lead to the discovery of a third stable intermediate wake state, which will be discussed in detail in section 3.6.

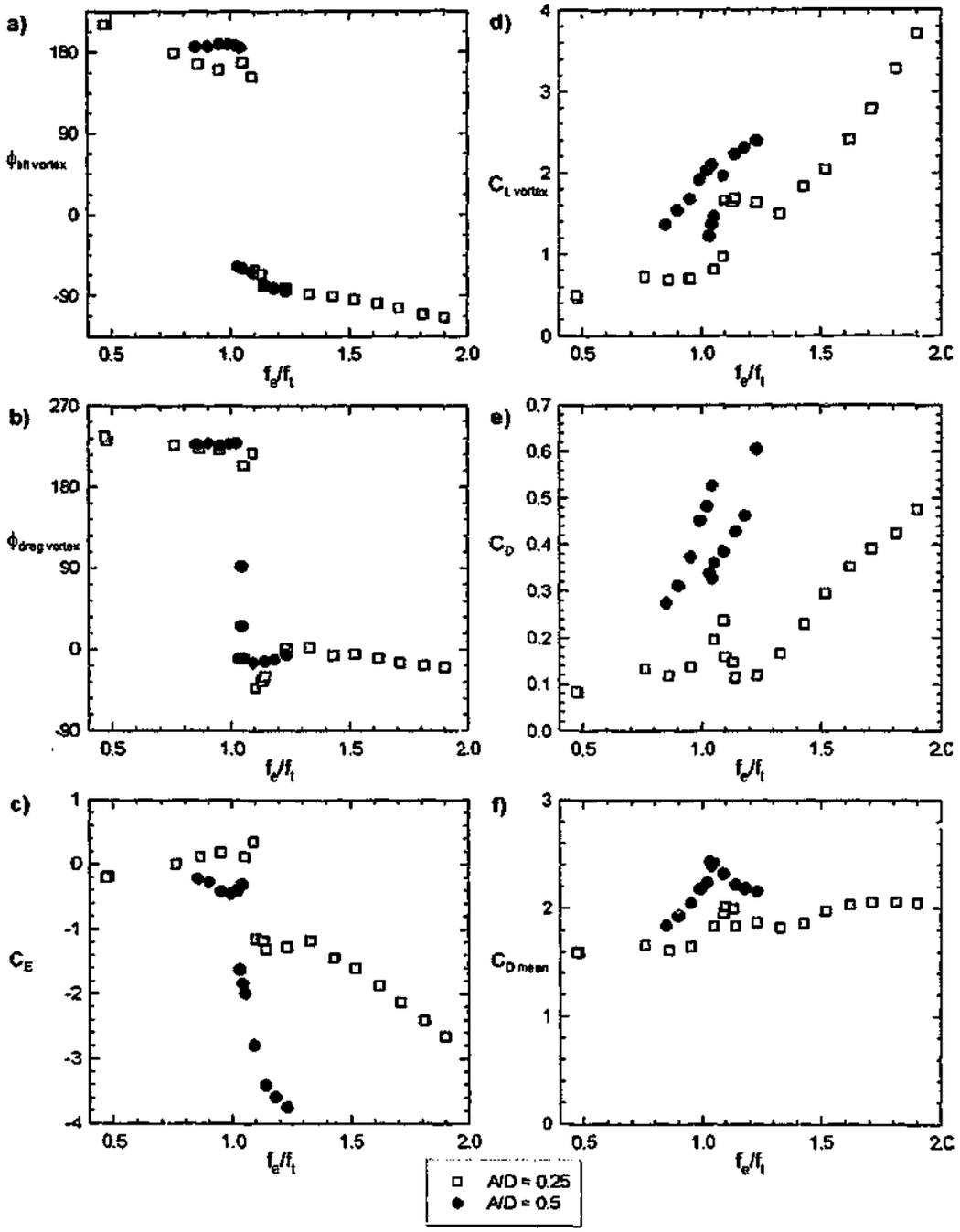

Figure 3-16 Frequency dependence of a) $\phi_{lift\ vortex}$ b) ϕ_{drag} c) C_E, d) $C_{L\ vortex}$ e) C_D, f) $C_{D\ mean}$ for A/D = 0.25 & 0.5 at Re = 4410.

In Figure 3-16 the same properties are plotted as in Figure 3-15, but for the higher Reynolds number of 4410 and oscillation amplitudes of A/D = 0.25 and 0.5. As A/D increases the trends

observed in Figure 3-16 are essentially the same as those at the lower Reynolds number and in both cases it appears that $\phi_{lift\ vortex}$ and ϕ_{drag} do not vary significantly with A/D, but depend primarily on wake state. These trends are also consistent with those observed at Re = 9100 as A/D was increased from, 0.25 to 0.5.

3.4.2 Variation of Total and Vortex Forces with Re

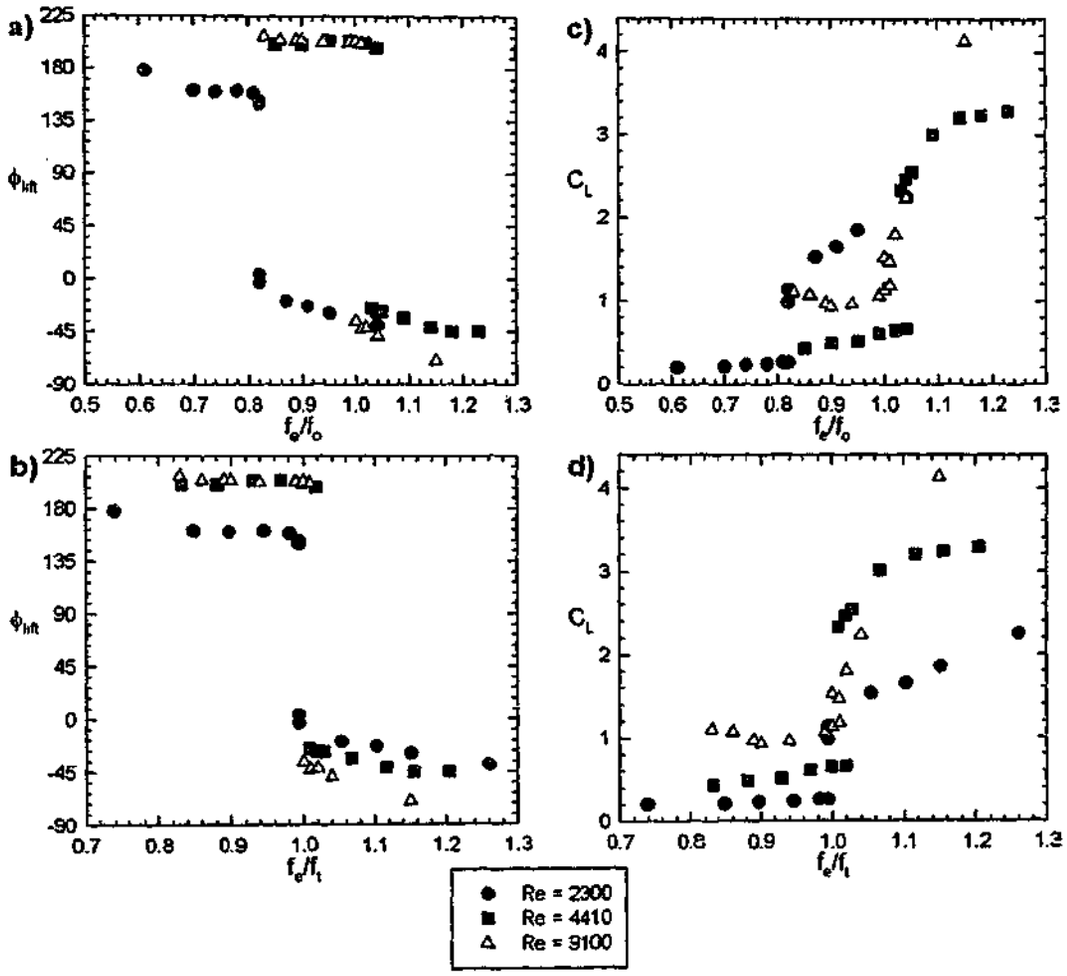

Figure 3-17 Variation of the total lift force at $A/D = 0.5$ for Reynolds numbers of 2300, 4410 and 9100. In a) and b) the phase and amplitude of the total lift force respectively are plotted against f_e/f_o, while in c) and d) ϕ_{lift} and C_L are plotted against f_e/f_t.

The frequency dependence of the total lift force shown in Figure 3-1 for Reynolds numbers ranging from 2300 to 60,000 indicates that the jump in ϕ_{lift} and C_L are universal features that occur over a wide range or Reynolds numbers. The effect of Reynolds number on an oscillating cylinder is however, complex. In Figure 3-1, and also in the work of Staubli (1983b), it is evident that the non-dimensional frequency, f/f_o, at which the transition from the low- to high-frequency state occurs, is generally not equal to unity. The transition frequency f/f_o varies in an apparently non-

systematic fashion with Reynolds number and the reasons for this variation are, at this stage, not well understood. It has already been observed that for $A/D = 0.5$ and $Re = 2300$ the self-excited transition occurs from the low- to the high-frequency state, while at $Re = 9100$ the direction of the transition is reversed. Although this observation does not explain why f/f_o varies with Re it does indicate that the relative stability of the low- and high-frequency states relative to the initial stationary cylinder state can vary with Reynolds number. It is therefore not unexpected that f/f_o also varies with Re. The variation of the forces with Reynolds number is often more clearly illustrated by plotting them against f_e/f_t rather than f_e/f_o. Although there may appear to be a stronger case for normalising the oscillation frequency with f_o, rather than f_t, it is important to remember that f_o describes the natural Kármán frequency of a stationary cylinder. When the cylinder is oscillating it is expected that changes in the generation and distribution of vorticity will alter the natural instability of the wake.

In the next section the variation of the forces on the cylinder with Reynolds number will be examined for two different oscillation amplitudes: $A/D = 0.25$ and 0.5. In Figure 3-17 the phase and amplitude of the total lift force at $A/D = 0.5$ is plotted against both f_e/f_o and f_e/f_t. The apparently non-systematic nature of the variation of the transition frequency, f_t, is evident in Figure 3-17(a & b); where the transition occurs well below $f_e/f_o = 1$ at $Re = 2300$, shifts to just above $f_e/f_o = 1$ at $Re = 4410$, while at the highest Reynolds number of 9100 the transition occurs almost exactly at $f_e/f_o = 1$. As Re increases from 2300 to 4410 there is a large increase in the value of ϕ_{lift} for the low-frequency wake state, however as Re increases further to 9100 ϕ_{lift} shows very small increase and remains essentially constant. For the high-frequency state when ϕ_{lift} is plotted against f_e/f_o, in Figure 3-17(a), the shift in the transition frequency makes it difficult to interpret the variation of ϕ_{lift} with Re. If the normalisation frequency, f_o, relates directly to the natural instability of the wake of the oscillating cylinder, then the results in Figure 3-17(a) suggest that for the high-frequency state ϕ_{lift} varies with f_e/f_o irregardless of the frequency at which transition occurs. However, it is not clear if the results can be interpreted in this way as f_o relates to the wake of a stationary cylinder. When the frequency of oscillation is normalised by the transition frequency in Figure 3-17(b), it appears that for the high-frequency state ϕ_{lift} becomes more negative as Re increases. When, as in Figure 3-17(a & b), the transition is plotted as a phase jump in the clockwise direction the magnitude of the jump in ϕ_{lift} appears to increase as Re increases. If however the transition were plotted as a phase jump in the anti-clockwise direction, *i.e.* the high-frequency state was plotted in the 4th quadrant, ϕ_{lift} would increase with increasing Re for both the low- and high-frequency states and the phase jump at transition would be relatively similar for all Re.

The large shift in the value of f_e/f_o at which the transition occurs also makes is difficult to determine the variation of C_L with Re in Figure 3-17(c). However, in Figure 3-17(d), where C_L is plotted

against f_e/f_o, it is appears that for the low-frequency state the amplitude of the total lift force increases as Re increases from 2300 to 9100. For both Re = 2300 and 4410 the transition between the low- and high-frequency states corresponds to a distinct jump in C_L. At Re = 9100 the transition corresponds to a relatively small jump in C_L, but following the transition to the high-frequency state C_L increases rapidly. Thus, for higher values of f_e/f_i it appears that that amplitude of the total lift force will increase with increasing Re, although closer to the transition region C_L is larger at Re = 4410 than at Re = 9100.

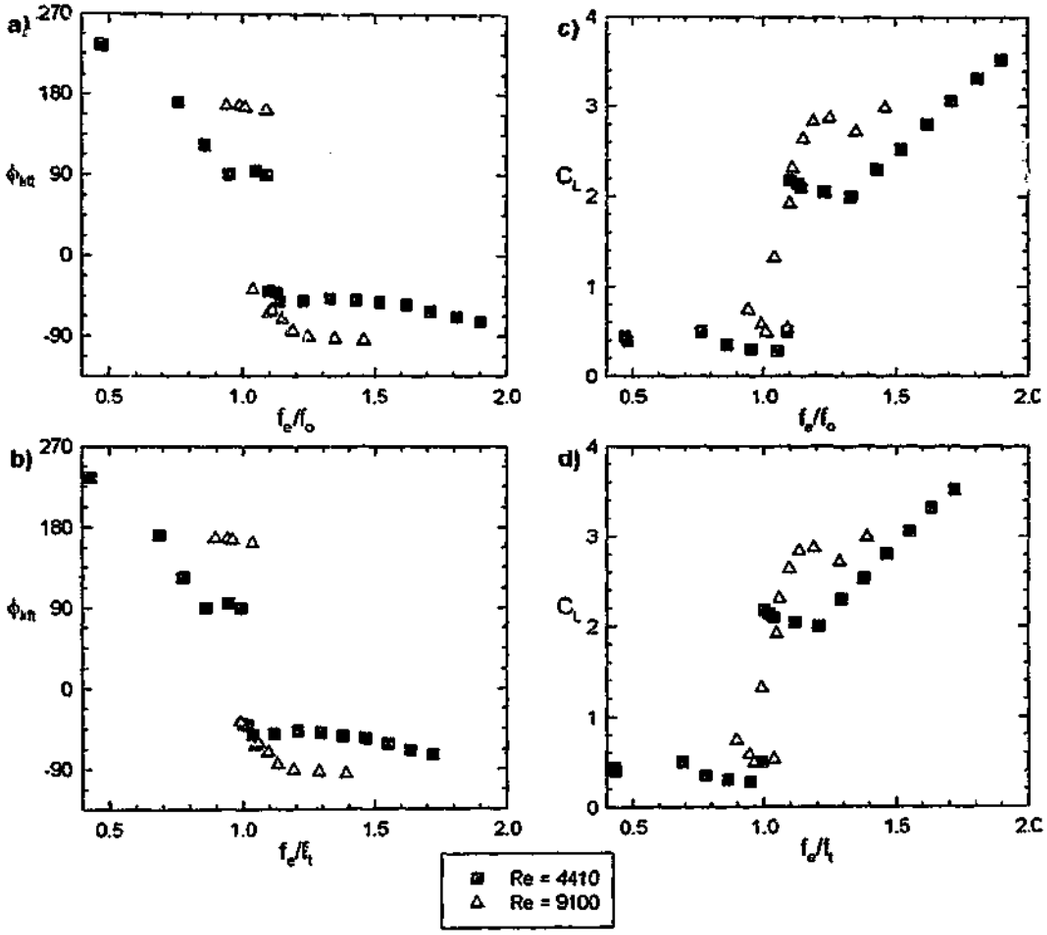

Figure 3-18 Variation of the total lift force at A/D = 0.25 for Reynolds numbers of 2300, 4410 and 9100. In a) and b) the phase and amplitude of the total lift force respectively are plotted against f_e/f_o, while in c) and d) ϕ_{lift} and C_L are plotted against f_e/f_i.

In Figure 3-18 the phase and amplitude of the total lift force at A/D = 0.25 are plotted for Reynolds numbers of 4410 and 9100. As for A/D = 0.5, the value of f_e/f_o at transition does not change by a large amount as Re increases from 4410 to 9100, however for completeness in Figure 3-18 the results have been plotted against both f_e/f_o and f_e/f_i. At the smaller amplitude of A/D = 0.25 Figure 3-18 shows similar trends to those observed at A/D = 0.5. At A/D = 0.25 as Re increases from 4410

to 9100 there is a relatively large increase in the value of ϕ_{lift} for the low-frequency state close to the transition region. At Re = 4410 the larger values of ϕ_{lift} for oscillation frequencies below $f/f_o \approx 0.85$ may be associated with the fact that the wake is approaching the lower bounds of lock-in. For the high-frequency state Figure 3-18(b) shows that ϕ_{lift} becomes more negative as Re increases from 4410 to 9100 and, in general, the changes in C_L as Re increases from 4410 to 9100 at A/D = 0.25 are quite similar to those observed at A/D = 0.5. In both cases the transition corresponds to an abrupt jump in C_L at Re = 4410 while at Re = 9100 the initial jump in C_L is much smaller.

The variation with Reynolds number of the vortex forces: $\phi_{lift\ vortex}$, $C_{L\ vortex}$, ϕ_{drag}, C_D and $C_{D\ mean}$, as well as the energy transfer are shown in Figure 3-19 and Figure 3-20 for A/D = 0.5 and 0.25 respectively. The phase of the drag force was not plotted for the lower amplitude of A/D = 0.25 as for many points the correlation coefficient of the drag force with a sinusoidal signal was less than 0.5. For both oscillation amplitudes $\phi_{lift\ vortex}$ and, where shown, ϕ_{drag} do not vary significantly over the range of Reynolds numbers examined, however the magnitude of the vortex forces: $C_{L\ vortex}$, C_D and $C_{D\ mean}$ and C_E all vary with Reynolds number.

For the low-frequency state the energy transfer tends to become more positive as Reynolds number decreases from 9100 to 2300. In Figure 3-15(c) we saw that decreasing the amplitude of oscillation can reverse the direction of energy transfer for the low-frequency state from negative to positive. A reversal in the direction of energy transfer is also shown in Figure 3-19(c) as Re decreases from 4410 to 2300. In Figure 3-20(b), at the smaller oscillation amplitude, the low-frequency state energy transfer is positive for both Re = 4410 and 9100, except for the very low oscillation frequencies at the edge of the lock-in region. For the high-frequency state at both oscillation amplitudes the energy transfer becomes more negative with increasing Re. At A/D = 0.5 there is a relatively small downwards jump in C_E as the wake transitions from the low- to the high-frequency state, while at A/D = 0.25 there is a relatively large jump in C_E.

At A/D = 0.25 and 0.5 both $C_{L\ vortex}$ and $C_{D\ mean}$ appear to increase with increasing Reynolds numbers. At A/D = 0.25 there is an interesting change in the direction of the jump in $C_{L\ vortex}$ at transition. In the previous section the size of the downward jump in $C_{L\ vortex}$ at transition, shown in Figure 3-15(d), decreased as A/D decreased from 0.6 to 0.4. When, as shown in Figure 3-20(c), A/D decreases further to 0.25 the direction of the jump is reversed and at the transition between the low- and high-frequency states $C_{L\ vortex}$ jumps upwards. An interesting feature of both Figure 3-19(e) and Figure 3-20(d) is that at Re = 4410 the transition from the low- to the high-frequency state corresponds to a distinct drop in C_D while at the other Reynolds numbers the changes in C_D at the transition are smaller.

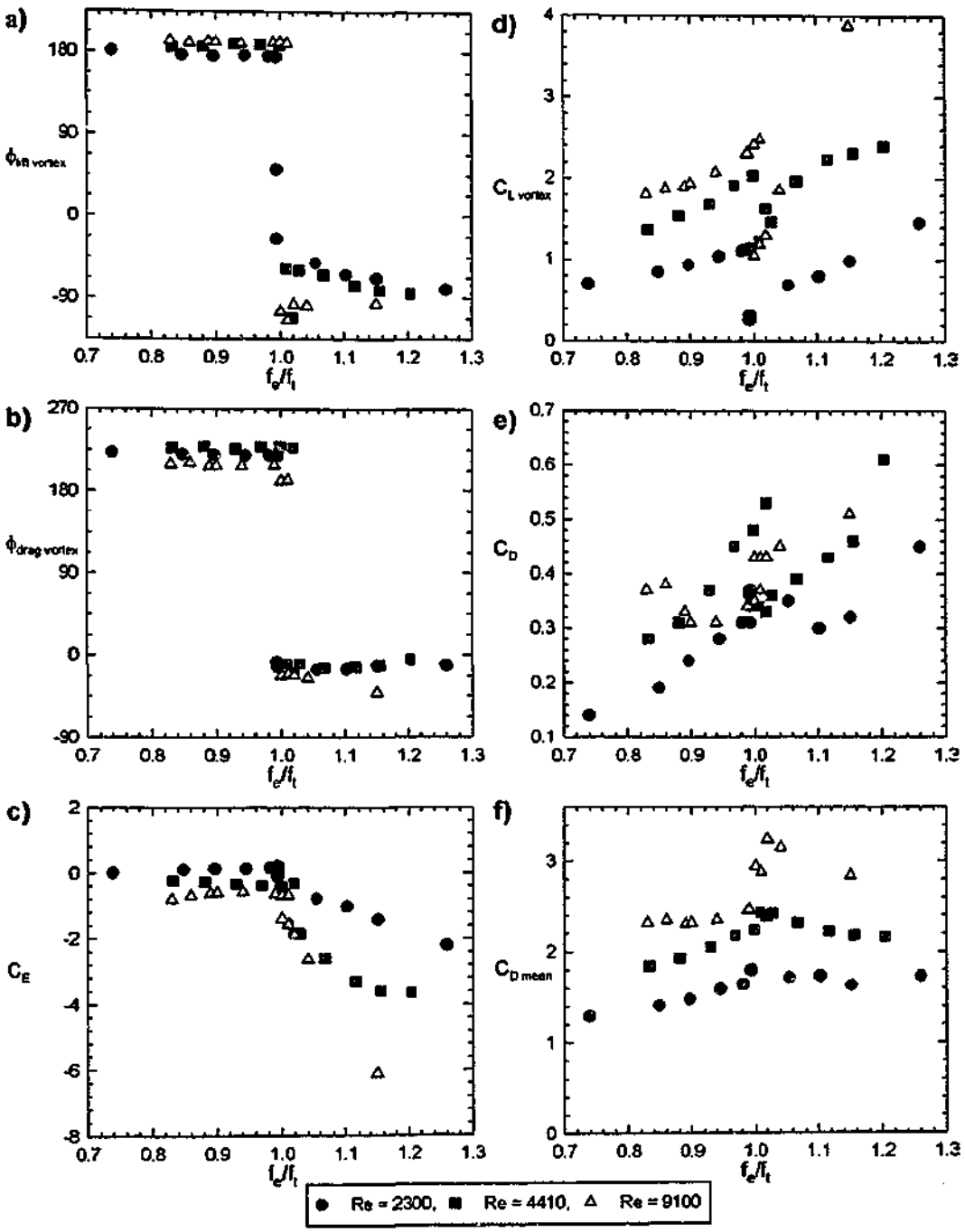

Figure 3-19 Frequency dependence of a) $\phi_{lift\ vortex}$ b) ϕ_{drag}, c) C_E, d) $C_{L\ vortex}$, e) C_D, f) $C_{D\ mean}$ at $A/D = 0.5$ for Re = 2300, 4410 and 9100. The frequency of oscillation f_e is normalised by f_t, the frequency at which the transition occurs.

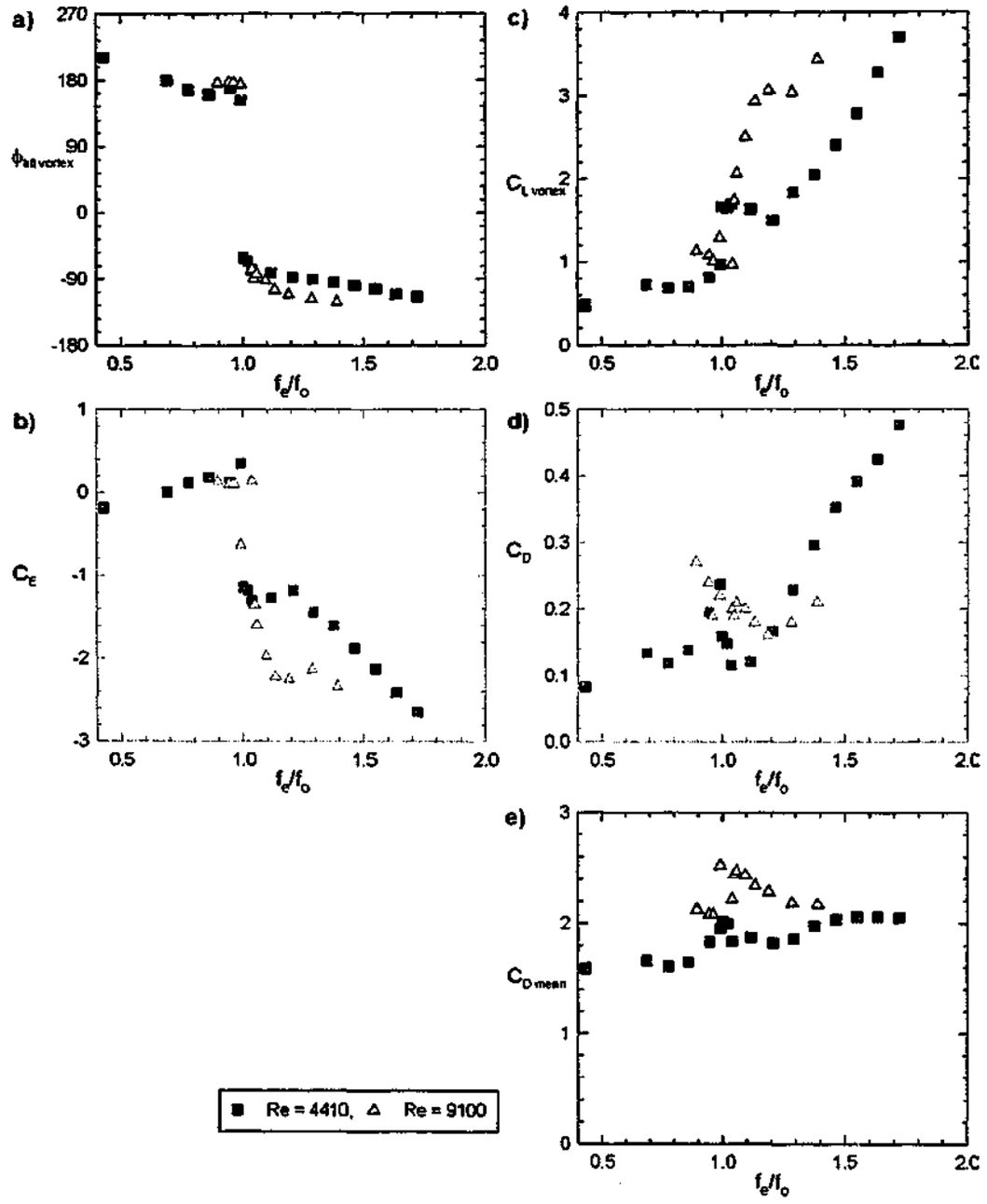

Figure 3-20 Frequency dependence of a) $\phi_{lift\ vortex}$ b) C_E, c) $C_{L\ vortex}$ d) C_D, e) $C_{D\ mean}$ at $A/D = 0.25$ for Re = 2300, 4410 and 9100. The frequency of oscillation f_e is normalised by f_n, the frequency at which the transition occurs.

The changes in the total and vortex lift forces as Reynolds number varies reveals that the apparently simple vectorial relationship between F_{vortex} and F_{total} in equation 1-7 is not always easy to interpret. For a given non-dimensionalised amplitude and frequency of oscillation the phase and amplitude of the apparent mass force does not vary with Reynolds number and the total lift force is equal to the vortex lift force plus a constant vectorial apparent mass force. However, as the vortex

lift force is generally not in-phase with the apparent mass force, the relationship between the phase and amplitude of the total and vortex lift forces remains complex. For example, in most cases the phase of the total lift force varies strongly with *Re*, however when the apparent mass force of constant phase and amplitude is subtracted from the various total lift forces the phase of the resulting vortex lift force is apparently independent of *Re*.

The most striking feature of this series of plots (Figure 3-13 to Figure 3-20) is that while the magnitude of the vortex forces: $C_{L\,vortex}$, C_D and $C_{D\,mean}$ as well as the energy transfer and the total lift forces all show significant variation with *Re* or *A/D*, the phase of the vortex forces $\phi_{lift\,vortex}$ and ϕ_{drag} do not vary significantly. It is expected that both Reynolds number and the amplitude of oscillation can change the relationship between the wake's natural instability and the large scale forced perturbation. However, without further extensive investigation it is not possible to quantify the nature and effect of these changes. In addition, it is likely that other factors such as end conditions, turbulence intensity and length scale also influence the forces on the cylinder and the direction of energy transfer. Given the complicated nature of this problem it is significant that the jump in the phase and amplitude of the lift force persist over a wide range of oscillation amplitudes and Reynolds numbers.

3.4.3 Vortex Force: Collapse of Vortex Phase

In Figure 3-15, Figure 3-19 and Figure 3-21 the phase of the vortex lift and drag forces are plotted for cases where either the amplitude of oscillation or the Reynolds number is varied. In all cases it was shown that $\phi_{lift\,vortex}$ and ϕ_{drag} did not change significantly as either *A/D* or *Re* was changed. In Figure 3-21 the values of $\phi_{lift\,vortex}$ and ϕ_{drag} resulting from all our experiments are plotted as a function of f_e/f_i on a single axis. The parameter set for these experiments is as follows {(*A/D*, *Re*) = (0.25, 4410), (0.25, 9100), (0.4, 2300), (0.5, 2300), (0.5, 4410), (0.5, 9100), (0.6, 2300)}. Over this parameter set Figure 3-21 demonstrates a striking collapse of both $\phi_{lift\,vortex}$ and ϕ_{drag} towards constant values for a given wake state. While there is a small degree of scatter, for the low-frequency state $\phi_{lift\,vortex}$ appears to collapse towards 180° for a wide range of oscillation frequencies. Immediately following the transition to the high-frequency state there is an increase in the scatter of $\phi_{lift\,vortex}$. The source of the scatter is that for *A/D* = 0.4 and 0.5 immediately following transition $\phi_{lift\,vortex}$ tends to be close to 0°, decreasing smoothly towards –90° as f_e/f_o increases further. At *A/D* = 0.25 and 0.6 $\phi_{lift\,vortex}$ tended to jump straight down to -90° at the transition to the high-frequency state. There is in fact only one recorded point at *A/D* = 0.5 and Re = 2300 where the value of $\phi_{lift\,vortex}$ for the high-frequency state was above 0°. The existence of this point is important as it is the only case where positive energy transfer is observed for the high-frequency state. Further away from the transition region the value of $\phi_{lift\,vortex}$ for all *A/D* and *Re* collapses

towards -90°. Thus, excluding the region just above $f_e/f_t = 1$, the transition corresponds to a clockwise (negative) vortex phase shift of approximately 270° as shown in Figure 3-21 or a counter-clockwise (positive) vortex phase shift of approximately 90°.

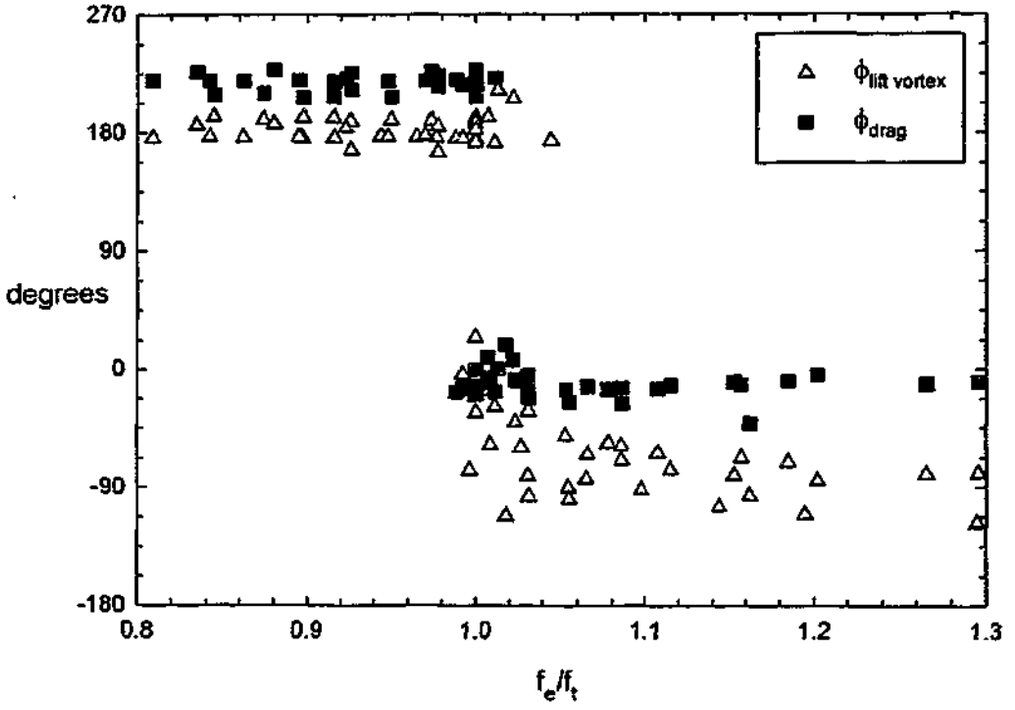

Figure 3-21 Phase of the vortex lift and drag forces, $\phi_{lift\ vortex}$ and ϕ_{drag} for all experiments with A/D ranging from 0.25 to 0.6 and Re ranging from 2300 to 9100.

The drag phase plotted in Figure 3-21 shows a very similar collapse to the vortex lift phase for the same range of A/D and Re. (Note: fewer points were plotted for the drag phase as at $A/D = 0.25$ and $Re = 4410$ the correlation of the drag force with a sinusoidal signal was less than 0.5 and could not used to calculate a value of ϕ_{drag}). As discussed in section 3.2.3 there are a number of valid ways to define and present the phase relationship between the drag force and the cylinder's displacement. In this section the drag phase has been defined using equation 3-1 and presented such that the jump in ϕ_{drag} at transition is of comparable magnitude, and in the same direction, as the jump in $C_{L\ vortex}$. For the low-frequency state the drag phase collapse towards $\phi_{drag} \approx 225°$ and the phase of both the vortex lift and drag forces are remarkably constant. There is a phase difference between $\phi_{lift\ vortex}$ and ϕ_{drag} of approximately 45°, which means that each local minimum in the vortex lift force coincides with a local minimum of the drag force. After the transition to the high-frequency state the drag phase is just under 0° and the scatter in ϕ_{drag} immediately following the transition is less that the scatter in $\phi_{lift\ vortex}$. Further away from the transition region the relative phase difference between the vortex lift and drag forces for the high-frequency state is approximately 75°, which is slightly larger than for the low-frequency state.

Together $\phi_{lift\ vortex}$ and ϕ_{drag} represent the timing of the movement of vorticity wake. However, as the frequency of the drag signal is twice that of the vortex lift it is difficult to assign a physical significance to the differences in $\phi_{lift\ vortex}$ and ϕ_{drag}. Closer consideration of equation 3-2 shows that the phase relationship between the vortex lift force and the drag force depends upon the relative phase of the movement of vorticity in the horizontal and vertical directions. Therefore, both the values of $\phi_{lift\ vortex}$ and ϕ_{drag} and relative phase between the vortex lift and drag forces ($\phi_{lift\ vortex}$ - ϕ_{drag}) depend on the way in which vorticity is distributed during the shedding cycle, and therefore on the mode of vortex shedding. As the wake state changes from the low- to high-frequency state there is a change in the distribution of vorticity but there are only relatively small changes in the relative phase between vortex lift and drag forces.

The collapse of the phases in Figure 3-21 indicates that the timing of the movement of vorticity within the oscillation cycle, and therefore the phase of vortex shedding, depends primarily on wake state and is relatively independent of *A/D* and *Re*. In the next section the phase-referenced vorticity fields are examined to determine if indeed the phase of vortex shedding is independent of *A/D* and *Re*. As shown in Figure 3-15, Figure 3-19 and Figure 3-20 C_D and $C_{L\ vortex}$ do not collapse towards a single value for a given wake state, indicating that, while the timing of vortex shedding is approximately constant, the level and distribution of vorticity depends on both *Re* and *A/D*. Unlike the phase of the vortex forces, which are in general approximately constant for a given wake state, the amplitude of the vortex lift forces also vary with the frequency of oscillation.

3.4.4 Vorticity Fields

Phase averaged vorticity fields at A/D = 0.25, 0.4, 0.5 and 0.6, are shown in Figure 3-22 and Figure 3-23, for the low- and high-frequency wake states respectively. The Reynolds number is 9100 for A/D = 0.25, while at the larger amplitudes (A/D = 0.4, 0.5 & 0.6) Re = 2300. The low-frequency wake modes, in Figure 3-22, are shown as the cylinder moves from the top of its oscillation, column *i*), through its downwards stroke, columns *ii*) to *iv*). Looking down the columns, at the same phase point in the oscillation, allows comparison of the wakes at different A/D, whereas looking along the rows shows the wake development as the cylinder moves through its downward stroke.

At the top of the cylinder's oscillation the low-frequency wake, shown in Figure 3-22 column *i*), has an attached negative shear layer which extends across the base of the cylinder into the lower half of the wake. The length of this shear layer increases with the amplitude of oscillation and is significantly longer in Figure 3-22(d)(*i*) at A/D = 0.6 than at A/D = 0.25in Figure 3-22(a)(*i*). In column (*ii*), ¼ of the way through the downward stroke, a portion of negative vorticity starts to separate from the end of the longer shear layers. The break in the shear layers is observed at A/D = 0.4, 0.5 and 0.6 and in column *ii*) the break is approximately adjacent to the bottom of the cylinder. At A/D = 0.25 the attached shear layer is much shorter, only just extending past the bottom of the cylinder, and a portion of vorticity does not separate from the end of the shear layer. As the cylinder approaches the mid-point of the downward stroke the lower positive shear layers swings upwards towards the negative shear layer. At A/D = 0.6 the upward angle of the lower shear layer is very pronounced and as expected this angle decreases with decreasing A/D. For all amplitudes of oscillation the interaction of the two shear layers causes the main section of the negative shear layer to separate from the cylinder. At the higher oscillation amplitudes the separation of the negative vorticity occurs closer to the cylinder, probably due to the increased angle of the lower shear layer. In column (*iv*) where the cylinder is ¾ through the downward stroke, for all amplitudes of oscillation the separation of the negative vorticity is essentially complete.

As A/D varies from 0.25 to 0.6 the general structure of the low-frequency wakes in Figure 3-22 is very similar. However, there are systematic changes in the location and size of the vortex structures in the near wake as the oscillation amplitude increases. Importantly, at each point in the cylinder's displacement cycle the low-frequency wakes in Figure 3-22 are essentially at the same point in their shedding cycle and the timing of vortex shedding is effectively independent of A/D and Re.

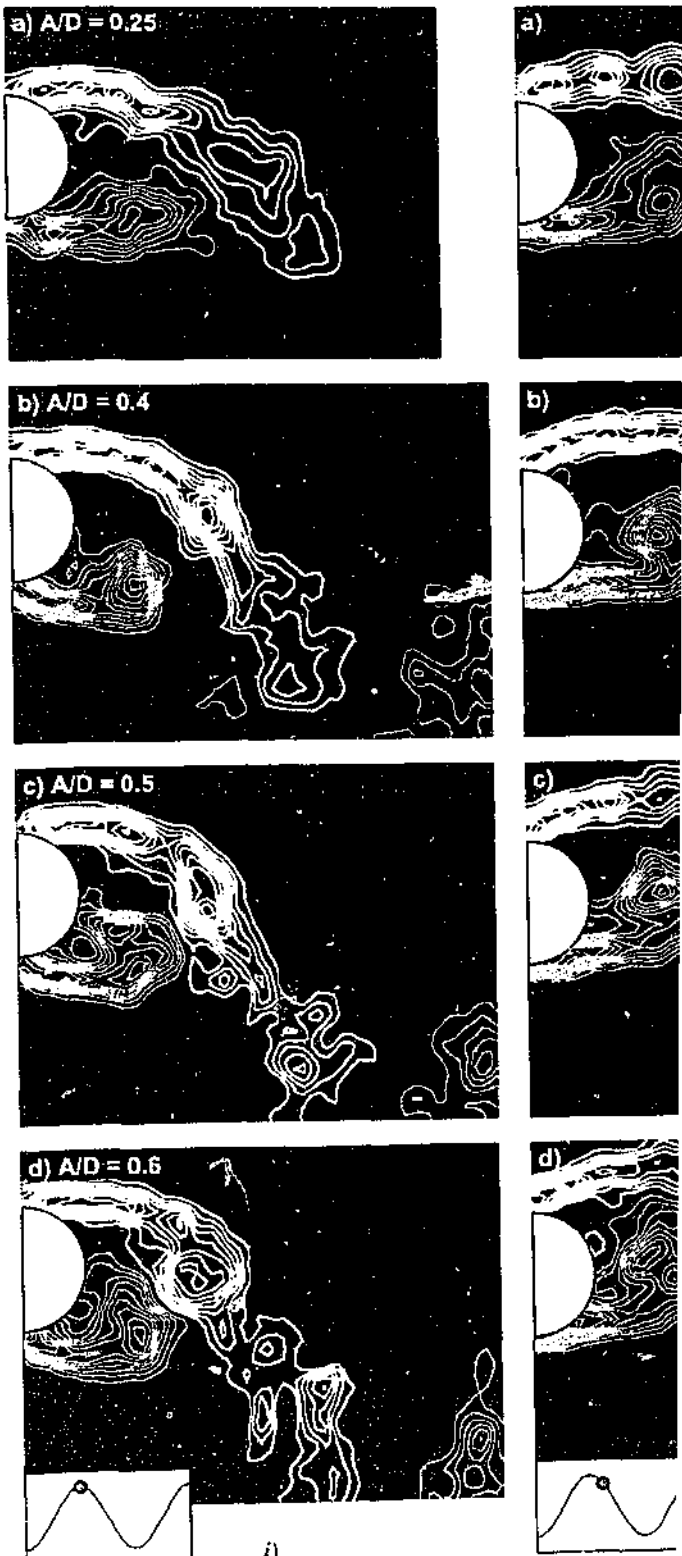

Figure 3-22 Phase averaged low-frequency state vorticity fields f
A/D = 0.4, c) A/D = 0.5 and d) A/D = 0.6 all at Re = 2300. The im
intervals such that *i*) is at the top of the cylinder's oscillation
downwards stroke.

Australasian Latch & Bone Bookbinders Melbourne

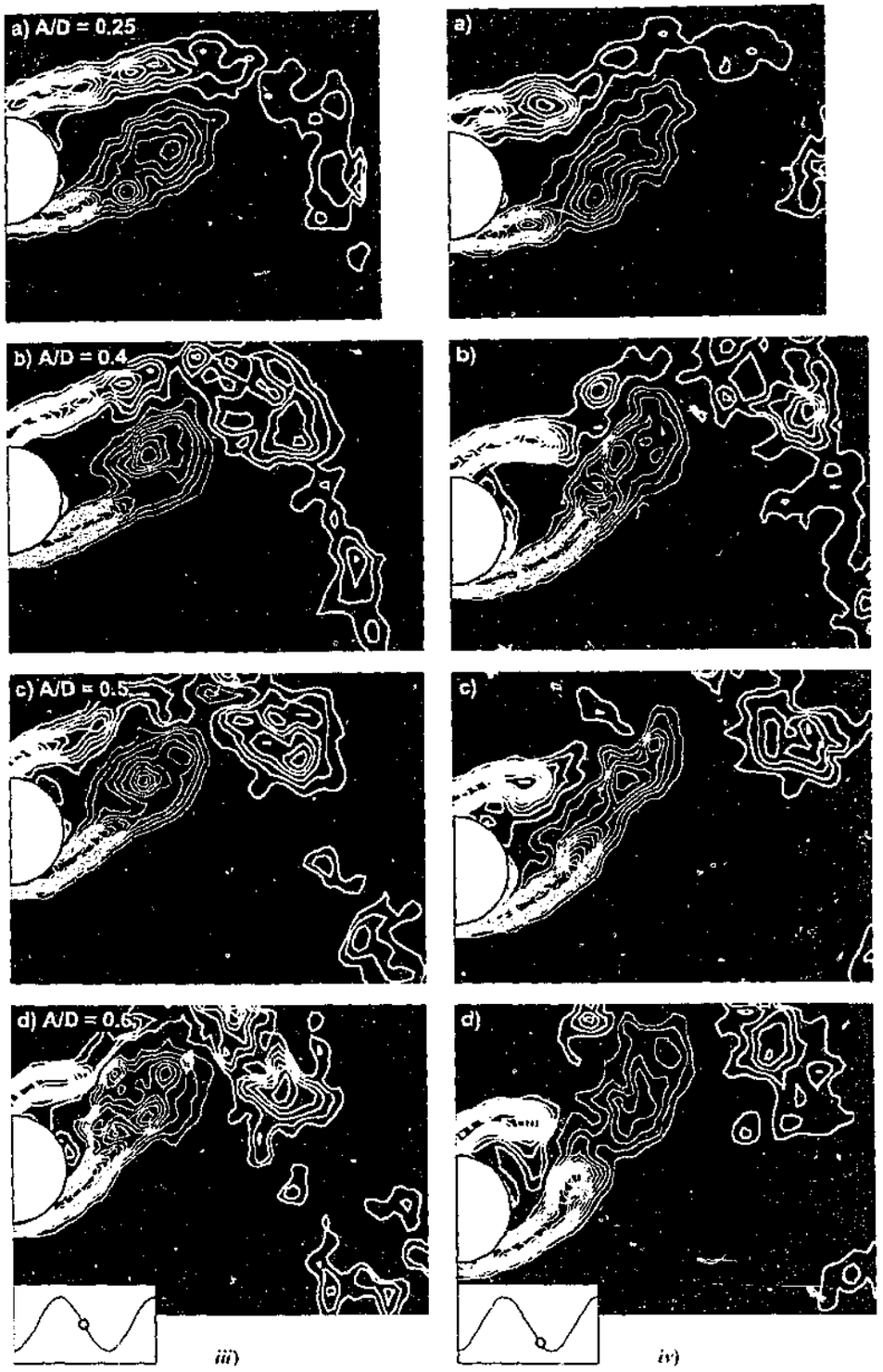

Figure 3-22 continued...

While the timing and general structure of vortex shedding appear to be independent of A/D and Re, Figure 3-22 shows that there are systematic variations in the distribution of vorticity in the near wake. At A/D = 0.5 and 0.6 the negative vorticity has been shed as two distinctly separate structures, while at A/D = 0.4 the negative vorticity is shed as a single vertical band which shows a propensity to break into two separate structures. At A/D = 0.25 a single negative vortex structure, elongated in the vertical direction, is shed into the near wake. The splitting of the shear layer into two separate structures is a key step in the formation of a 2P wake. At higher values of A/D (0.5 & 0.6, the splitting of the extended shear layer into two separate structures and the resulting 2P mode of shedding is quite pronounced. However, at the smaller values of A/D (0.25 & 0.4) the shear layer is shorter and the splitting of the shear layer either does not occur or is unclear. Therefore, while the other features of the low-frequency wake state persist at small amplitudes of oscillation, there appears to be a limiting amplitude, below which the shear layer is not long enough generate the 2P mode of shedding.

Figure 3-23 shows the high-frequency wake states at the top of the oscillation cycle. As for the low-frequency wake state, the timing of vortex shedding and the general structure of the wake is essentially unchanged as A/D increases from 0.25 to 0.6, at Re = 2300 and 9100. As A/D and Re change the differences in the distribution of the vorticity for the high-frequency wakes, shown in Figure 3-23, are quite subtle as the general structure of the wakes is quite condensed. Figure 3-15 shows that the phase and amplitude of the vortex lift force corresponding to the three images at A/D = 0.4, 0.5 and 0.6 are relatively constant and the only variation in the vortex forces for these three images as A/D increases is an increase in the mean and amplitude of the drag force. As A/D is increased the vorticity tends to break up more quickly as it moves downstream and additional images at higher Reynolds numbers indicate that as Re increases there is a similar increase in the break up of vorticity.

The robustness of the phase of vortex shedding for a particular wake state indicates that the vortex shedding is phase locked to the displacement of the cylinder. The relatively constant values of $\phi_{lift\ vortex}$ and ϕ_{drag} for each wake state, shown in Figure 3-21 for a range oscillation amplitudes and Reynolds numbers, are consistent with the constant phase and structure of vortex shedding illustrated in Figure 3-22 and Figure 3-23.

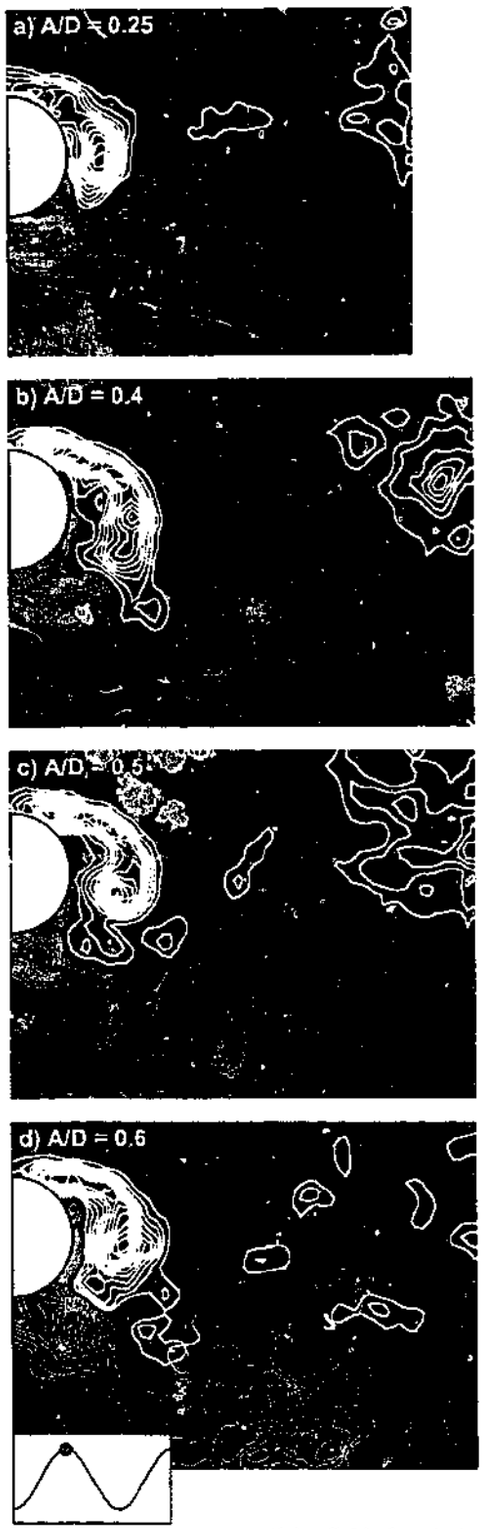

Figure 3-23 Phase averaged high-frequency state vorticity fields for a) $A/D = 0.25$ at $Re = 9100$ and b) $A/D = 0.4$, c) $A/D = 0.5$ and d) $A/D = 0.6$ all at $Re \approx 2300$.

3.5 SPECTRAL ENERGY AS A FUNCTION OF f_e/f_o

An elastically mounted cylinder vibrates at a frequency that depends on the reduced velocity, wake state and the properties of the cylinder and its supporting structure, including the structural spring constant, structural damping and mass. However, once a particular structure has been selected the natural frequency of the structure is constant during the experiment. When the oscillations are forced the situation is reversed: the forcing controls the frequency of oscillation but the frequency of the wake's natural instability varies with f_e and wake state.

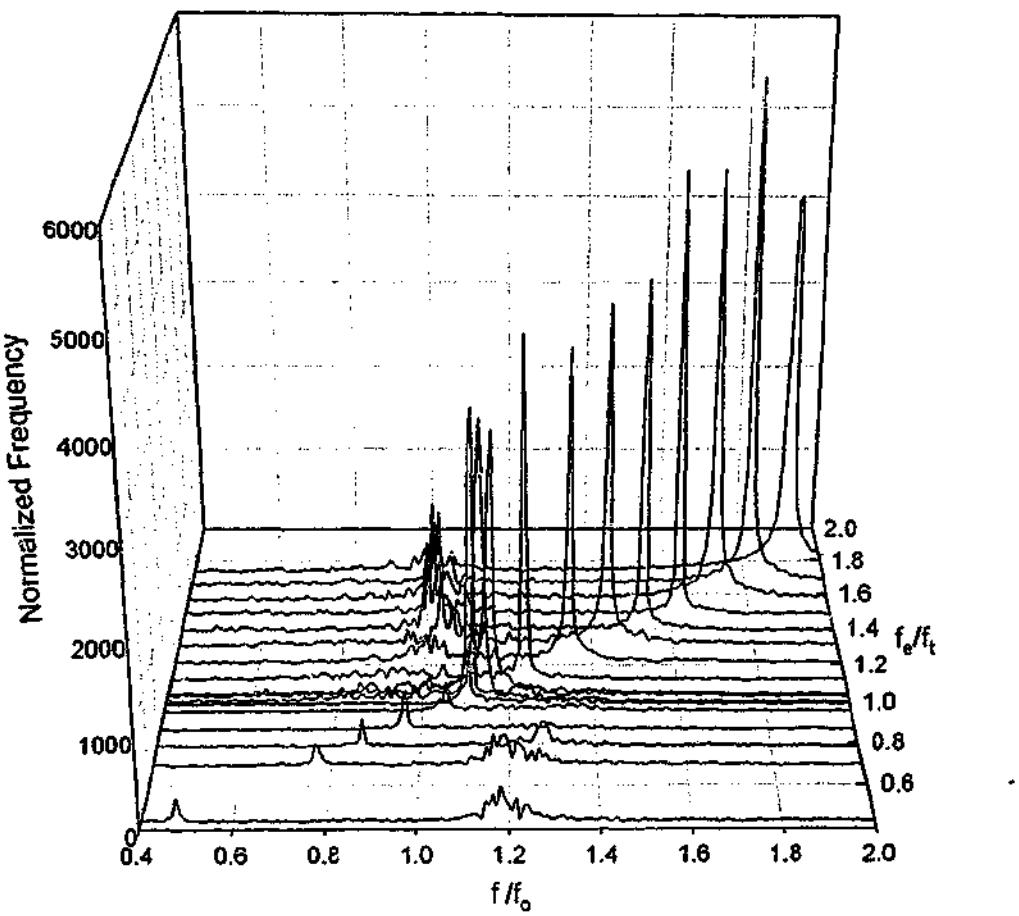

Figure 3-24 Variation of Lift spectra with oscillation frequency f_e/f_t at A/D = 0.25 and Re = 4410. The spectral frequencies f are normalised by f_o and the frequency of oscillation f_e is normalised by the transition frequency f_t, where f_t/f_o = 1.10.

In Figure 3-24 the lift spectra for a range of oscillation frequencies, at A/D = 0.25 and Re = 4410, are plotted on a single three-dimensional axis. Typically, the lift spectra have a strong peak at $f=f_e$, the frequency of oscillation, with a second smaller peak at a frequency f_{nos}, which as discussed in section 1.4.1, can be associated with the natural frequency of the oscillating cylinder wake. In general, f_{nos} is close to f_o, the natural frequency of the stationary cylinder wake. The

distribution of spectral energy between the peaks at f_e and f_{nos} depends on the response of the wake to the cylinder's oscillation. As discussed in section 1.3.1 the relative energy of the peak at f_e is often used to define when the cylinder's wake is locked-on to the imposed oscillation. As the wake moves beyond the lock-in region f_{nos} becomes the dominant, or most energetic frequency in the wake.

As shown in Figure 3-24 for $f_e/f_i > 0.8$ the wake is clearly locked-on to the cylinder and the most energetic frequency in the lift spectra corresponds to the oscillation frequency of the cylinder. For the lower frequencies of oscillation, however, the peaks at f_{nos} and f_e are small and of comparable energy levels. As f_e/f_i increases the energy at f_{nos} decreases and there is a gradual increase in the energy at f_e, until at transition, there is sharp jump in the energy at f_e. The jump in the energy at the oscillation frequency corresponds to the jump in the amplitude of the total lift force shown in Figure 3-18. At frequencies just above transition the second peak at f_{nos} could not be resolved. However, as f_e/f_o increases further the second peak at f_{nos} reappears.

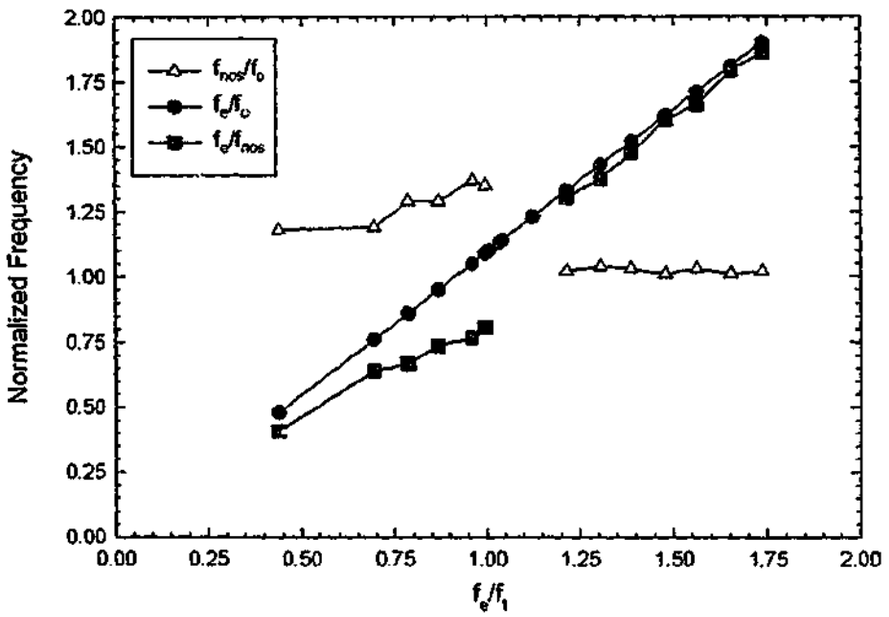

Figure 3-25 Variation of the most energetic frequencies with the frequency of oscillation for the lift spectra shown in Figure 3-24 at $A/D = 0.25$ and $Re = 4410$. In all cases the peak at f_e is more energetic than the peak at f_{nos}.

In Figure 3-25 the frequencies of the spectral peaks in Figure 3-24, f_{nos}/f_o, f_e/f_o and f_e/f_{nos} are plotted against the normalised oscillation frequency. For all frequencies of oscillation the natural frequency of the oscillating wake is greater than the natural frequency of the stationary wake, i.e. $f_{nos}/f_o > 1$ or equivalently $f_e/f_o > f_e/f_{nos}$. As the frequency of oscillation increases towards transition ($f_e/f_i \rightarrow 1$) both f_e and f_{nos} increase, however the relative rates of increase are such that the peaks move closer together. Prior to transition f_{nos} is greater than f_e and transition occurs before the peaks

intersect. Immediately following transition f_{nos} could not be resolved, however, for $f_e/f_t \geq 1.2$, f_{nos} is slightly greater than f_o and does not vary significantly with f_e/f_t. Therefore, after transition f_{nos} is less than f_e and the peaks move apart as the frequency of oscillation increases.

At transition there is a downward jump in f_{nos}, the natural frequency of the oscillating wake. As transition corresponds to a change in the mode and phase of vortex shedding, it is reasonable to expect that there could be a corresponding change in the natural frequency of the oscillating wake. Additionally, the transition between the two wake states corresponds to a change in the relationship between f_{nos} the natural frequency of the oscillating wake and the forcing frequency f_e, where for our locked-in wake f_e corresponds to the frequency of vortex shedding. At low frequencies, prior to transition, f_{nos} is greater than f_e, indicating that shedding controlled by the natural instability would occur faster than "allowed" by the forced oscillation. The resulting wake mode forms long extended shear layers. As f_e/f_o increases the peaks at f_{nos} and f_e move together and the wake contracts. After transition the natural frequency is less than the forcing frequency ($f_{nos} < f_e$) and as f_e/f_o increases the peaks move further apart. Thus, the forced vortex shedding occurs faster than it would if shedding were controlled by the wake's natural instability. In this case the wake is significantly shorter and the mode of vortex shedding is different.

3.6 INTERMEDIATE WAKE STATE

In the previous sections a cylinder undergoing forced oscillations has been shown to exhibit at least two distinctly different wake states: the low- and high-frequency states. However, at certain amplitudes of oscillation there is a third wake state, located between the low- and high-frequency states, which we will call the intermediate state. In the following section the properties of the intermediate state are described in terms of the forces on the cylinder and the phase referenced structure of the near wake. The properties of the intermediate wake state will be discussed using results from sets of experiments at two different oscillation amplitudes, A/D = 0.5 and 0.6, where for both cases Re = 2300. The intermediate state is a new, independent wake state whose properties are distinctly different from either the low- or high-frequency wake state.

3.6.1 Force properties

The low-frequency, intermediate and high-frequency wake states can be characterised in terms of the forces on the cylinder, as shown in Figure 3-26 and summarised in Table 3-1. In Figure 3-26 the phase and amplitude of the total lift, vortex lift and drag forces are plotted as a function of f_e/f_o for an oscillation amplitude of A/D = 0.6. At frequencies of oscillation where the wake undergoes a self-excited transition between wake states the data has been split into segments encompassing a single state only. The two intermediate state data points, at f_e/f_o = 0.84 and 0.85 in each graph of Figure 3-26, have been calculated from continuous time segments containing 57 and 13 cylinder oscillations respectively.

A distinguishing feature of the intermediate wake state is the large difference in the phases of the total and vortex lift forces. In section 3.4 we observed that the transition between the low- and high-frequency states corresponds to large changes in both ϕ_{lift} and $\phi_{lift\ vortex}$, where these changes are of a similar magnitude. However, as the wake moves to the intermediate state from either the low- or high-frequency states ϕ_{lift} and $\phi_{lift\ vortex}$ behave quite differently. When the wake moves from the low-frequency state to the intermediate there is a large downward jump in ϕ_{lift} while the value of $\phi_{lift\ vortex}$ remains relatively unchanged, as shown in Figure 3-26(a & c) respectively. Conversely, at the transition from the intermediate state to the high-frequency state there is a large downward jump in $\phi_{lift\ vortex}$ while ϕ_{lift} does not change significantly. Thus, for the intermediate wake state the values of ϕ_{lift} are essentially consistent with the values typically observed for the high-frequency state, while the values of $\phi_{lift\ vortex}$ are similar to those observed for the low-frequency state. The drag phase, shown in Figure 3-26e, has been plotted so that the variation in ϕ_{drag} over the three wake states is less than 180°, where, due to the way the drag phase is defined in equation (3-1), $\phi_{drag} = \phi_{drag} \pm 180°$. The drag phase for the high-frequency state has been plotted in the 2nd quadrant to emphasise the fact that the value of ϕ_{drag} for the intermediate state falls between

the values for the low- and high-frequency states. Thus, unlike the phases of the total and vortex lift forces, the values of ϕ_{drag} for the intermediate state are clearly different from those observed for both the low- or high-frequency states.

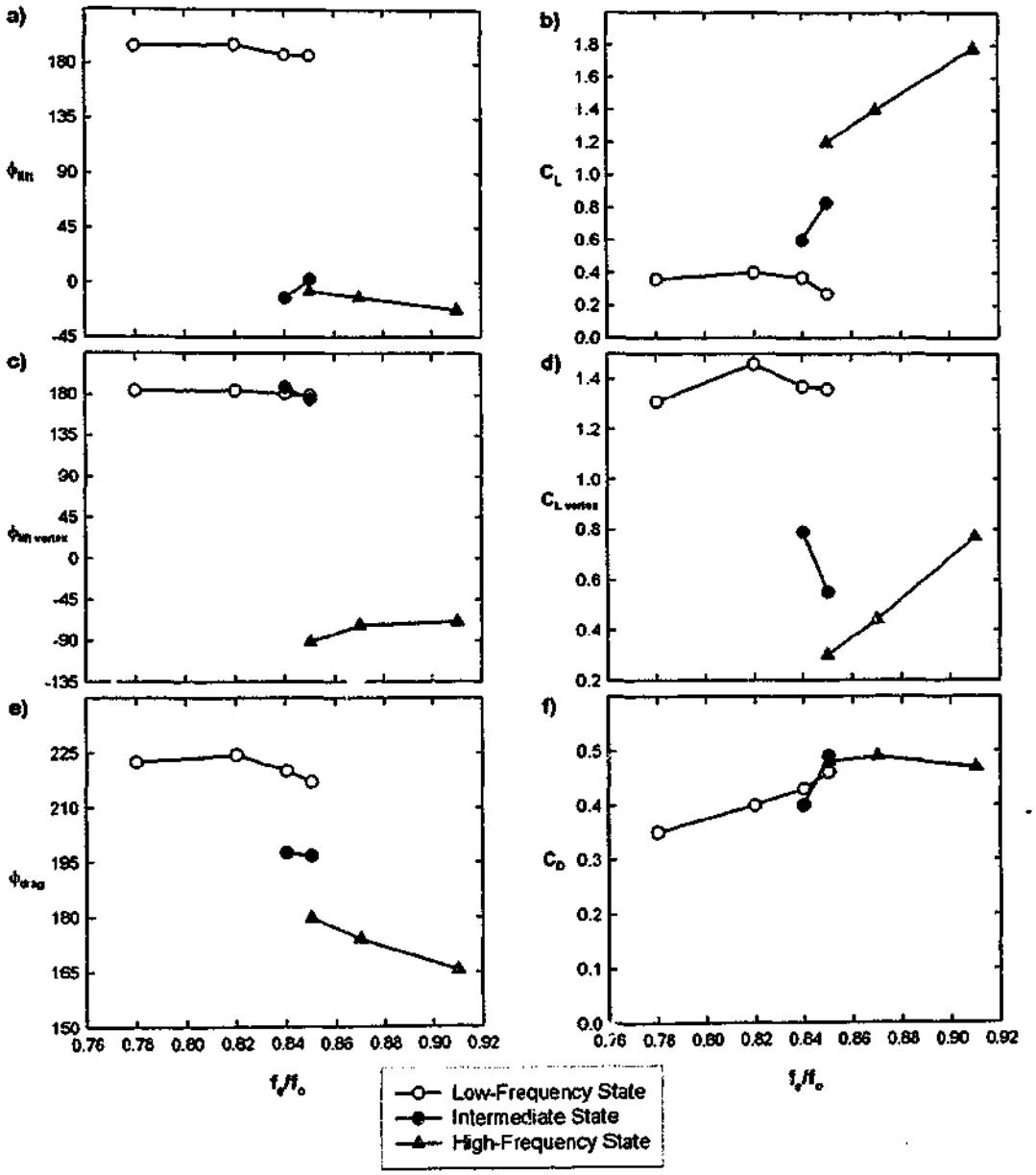

Figure 3-26 Phase and amplitude of the total lift force, the vortex lift force and the drag force on the cylinder as a function of fe/fo, A/D = 0.6 for the low-frequency, intermediate and high-frequency wake states.

As shown in Figure 3-26(b & d) the amplitudes of both the total and vortex lift forces for the intermediate state fall in between the corresponding amplitudes for the low- and high-frequency states. The transition from the intermediate to the high-frequency state corresponds to a drop in the

amplitude of the vortex lift force, and immediately after the transition $C_{L\,vortex}$ is very small. As f_e/f_o increases after the transition to the high-frequency state $C_{L\,vortex}$ grows quickly, and at higher oscillation frequencies $C_{L\,vortex}$ is greater than for the intermediate state. As discussed in section 3.4, the direction and magnitude of the jump in $C_{L\,vortex}$ at the transition between the low- and high-frequency states varies with both A/D and Re. The intermediate state was only observed at the two highest oscillation amplitudes considered in these experiments: $A/D = 0.5$ and 0.6. For the range of f_e/f_o considered, at both $A/D = 0.5$ and 0.6 the values of $C_{L\,vortex}$ for the high-frequency state are significantly smaller than for the low-frequency case. In contrast to the amplitudes of the total and vortex lift forces the amplitude of the drag force, shown in Figure 3-26(f), does not vary significantly as the wake moves between the low-frequency, intermediate and high-frequency states. In summary, the force properties shown in Figure 3-26 fall into three distinct categories representing the three wake states. The properties of the three wake states are catalogued in Table 3-1 and the changes that occur at the transitions between the wake states are listed in Table 3-2.

Table 3-1 Summary of the force and wake properties for the low-frequency, intermediate and high-frequency wake states.

STATE	LOW FREQUENCY	INTERMEDIATE	HIGH FREQUENCY
Wake Mode	2P (at mid to high A/D)	2S (at A/D = 0.5 & 0.6)	2S
ϕ_{lift}	High (2^{nd} or 3^{rd} quadrant)	Low (near zero)	Low (near zero)
C_L	Low (relatively constant)	Medium	High (increasing with f_e/f_o)
$\phi_{lift\ vortex}$	High (≈180°)	High (≈180°, less steady)	Low (moves towards -90° at higher f_e/f_o)
$C_{L\ vortex}$	High (relative value depends on A/D & Re)	Medium	Low (relative value depends on A/D & Re)
ϕ_{drag}	High (≈180°)	Medium	Low
C_D	Does not vary significantly with wake state		

Table 3-2 Summary of changes occurring at the transitions between the low-frequency, intermediate and high-frequency wake states.

Low Freq. → Intermediate	Intermediate → High Freq.
jump in ϕ_{lift}	constant ϕ_{lift}
constant $\phi_{lift\ vortex}$	jump in $\phi_{lift\ vortex}$
jump in $C_{L\ vortex}$	small jump in $C_{L\ vortex}$
small jump in ϕ_{drag}	small jump in ϕ_{drag}

For both $A/D = 0.5$ and 0.6, at oscillation frequencies were the intermediate state was observed the wake did not move to the intermediate state immediately after the cylinder started oscillating. Rather, the intermediate state was observed after a self-excited transition from either the low- or high-frequency wake states. In Figure 3-27 a self-excited transition from the low-frequency state to a stable intermediate state is shown at $A/D = 0.6$ and $f_e/f_o = 0.84$. Immediately after startup the wake is in the low-frequency state and both ϕ_{lift} and $\phi_{lift\ vortex}$ are close to 180°, while ϕ_{drag} is close to 225°. During the first 200 s of the experiment there are a number of transient self-excited transitions to the intermediate state. The transitions are characterised by a sharp, short-lived drop in ϕ_{lift} from approximately 180° to 0°, and much smaller variations in $\phi_{lift\ vortex}$ and ϕ_{drag}. However, the transitions in the first 200 s appear to be unstable, as the wake is in the intermediate state for only a small number of oscillations before returning to the low-frequency state. Interestingly, as the wake returns to the low-frequency state from the unsteady intermediate state the changes in ϕ_{lift} are more gradual, occurring over a number of oscillations.

At $t \approx 223$ s there is a stable self-excited transition from the low-frequency state to the intermediate state and, from this point until the end of the experiments at $t \approx 320$ s, the wake remains in the intermediate state. The most notable aspect of the transitions from the low-frequency state to the intermediate state is the large jump in ϕ_{lift} while $\phi_{lift\ vortex}$ remains relatively unchanged. Although the mean value of $\phi_{lift\ vortex}$ for the intermediate state is similar to the low-frequency state value there is a noticeable increase in the variance of $\phi_{lift\ vortex}$. Careful examination of Figure 3-27 shows that for $t < 233$ s $\phi_{lift\ vortex}$ is remarkably constant except for the periods corresponding to the transient transitions to the intermediate state. At the transition between the low-frequency state and the intermediate state there is a noticeable decrease in the ϕ_{drag}; this decrease occurs at both at the final transition and at the earlier transient transitions.

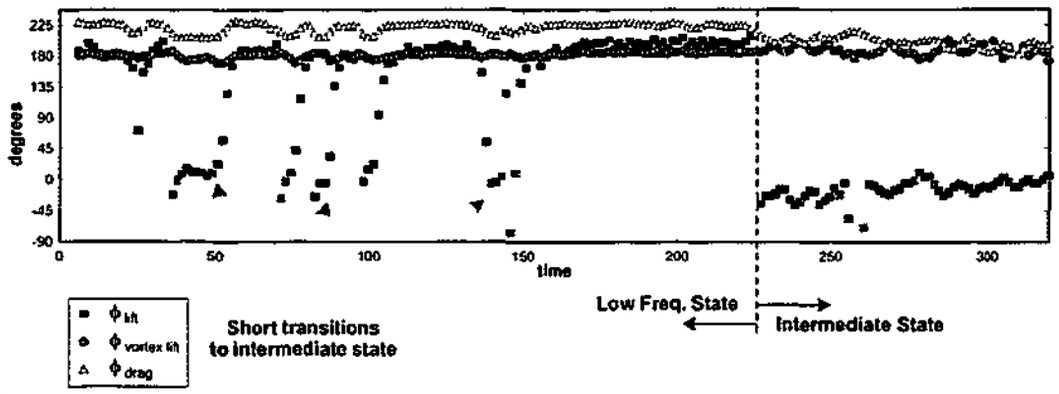

Figure 3-27 Variation of the instantaneous values of ϕ_{lift}, $\phi_{lift\ vortex}$ and ϕ_{drag} showing a self-excited transition from the low-frequency state to the intermediate state at A/D = 0.6, f_e/f_o = 0.84 and Re = 2300. The instantaneous phases were calculated using a correlation width of 3 oscillation cycles.

At the slightly higher oscillation frequency of f_e/f_o = 0.85, the properties of the total and vortex lift forces indicate that the wake exhibits all three wake states. However, the wake appears to be unstable and, as shown in Figure 3-28, the wake does not persist in any of these wake states for extended periods of time. After the cylinder starts oscillating at f_e/f_o = 0.85 the first wake state is the low-frequency state and both ϕ_{lift} and $\phi_{lift\ vortex}$ are close to 180°. After only a small number of oscillations at t ≈ 25 s ϕ_{lift} drops down to close to 0° while the value of $\phi_{lift\ vortex}$ remains high, thus the force properties are consistent with the intermediate state. The force properties remain consistent with the intermediate state for a relatively short period of time and at t ≈ 40 s $\phi_{lift\ vortex}$ drops towards values of between -45° and -90°, which are consistent with the high-frequency state. For the remainder of experiment $\phi_{lift\ vortex}$ alternates between high and low values, indicating that the wake is moving between the intermediate and high-frequency states.

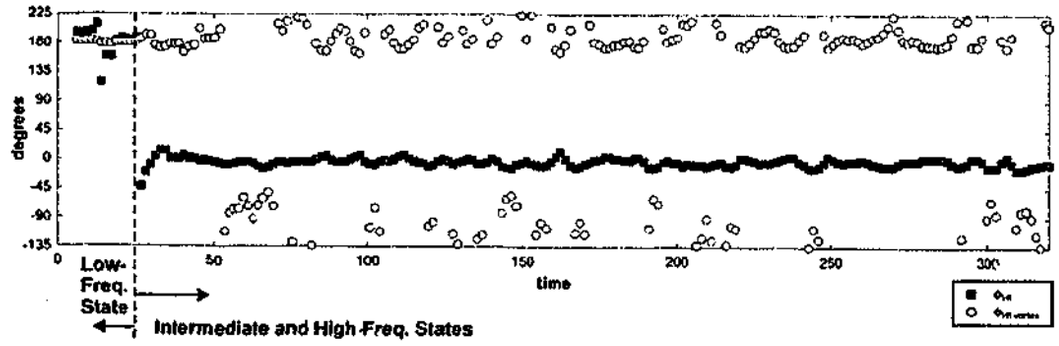

Figure 3-28 Variation of the instantaneous values of ϕ_{lift} and $\phi_{lift\ vortex}$ at A/D = 0.6, f_e/f_o = 0.85 and Re = 2300. The instantaneous phases were calculated using a correlation width of 3 oscillation cycles.

At A/D = 0.6 the intermediate state was observed both as a stable wake state, at f_e/f_o = 0.84, and as a relatively unstable state at f_e/f_o = 0.85. For all cases examined at A/D = 0.5 the intermediate state was observed either as a transitional state during a self-excited transition from the low- to the high-

frequency state, or for relatively short periods of time as a transient state after a transition from the high-frequency state. In Figure 3-29(a) the phase and amplitude of the total lift force are shown together as a function of time for A/D = 0.5 and f_s/f_o = 0.825. The corresponding phase and amplitude of the vortex lift force are plotted in Figure 3-29(b). Immediately after start-up the wake is in the low-frequency state. After approximately 46 s the wake begins to change state and after a number of oscillations, including a period of time when the properties of the wake are consistent with the intermediate state, the wake completes the transition to the high-frequency state. In this situation the intermediate state is observed as a transitional wake state, occurring as part of the transition between the low- and high-frequency states. Nevertheless, the properties of the transitional intermediate wake state, indicated by the left hand shaded region in Figure 3-29, are fully consistent with the stable intermediate wake state observed at $A/D = 0.6$.

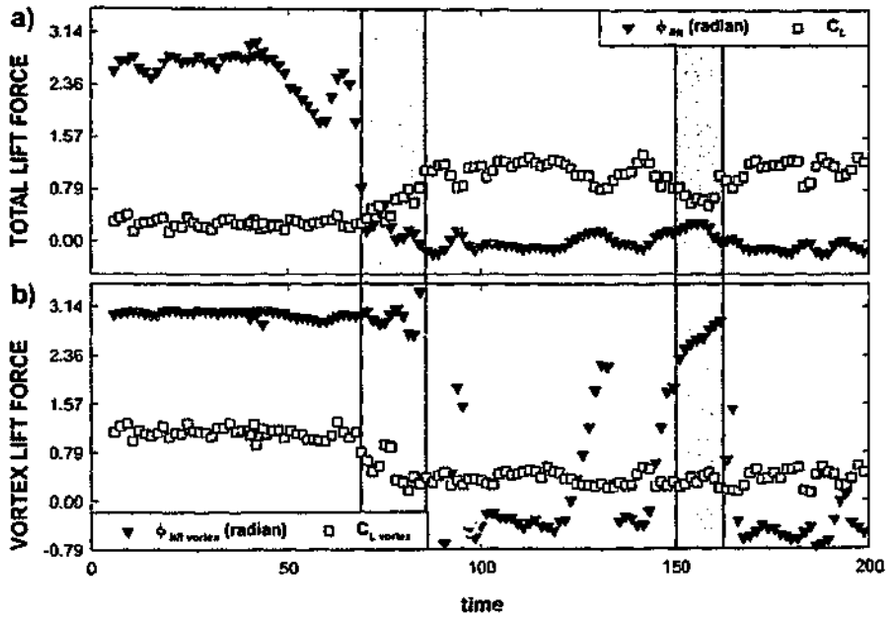

Figure 3-29 Variation of the phase and amplitude of a) the total lift force and b) the total lift force during self-excited transitions at A/D = 0.5, f_s/f_o = 0.825 and Re = 2300. The instantaneous phases and amplitudes were calculated using a correlation widths of 3.0 and 1.2 oscillation cycles respectively.

As the wake begins the transition from the low-frequency state the initial changes in ϕ_{lift}, shown in Figure 3-29(a), occur over approximately 16 oscillations, from $t \approx 46$ - 70 s. During this time there are only relatively small changes in $\phi_{lift\ vortex}$, C_L and $C_{L\ vortex}$, although as ϕ_{lift} drops sharply just before the end of this period there is a corresponding drop in $C_{L\ vortex}$. From $t \approx 70$ to 85 s the properties of the lift force are consistent with the intermediate state; $\phi_{lift\ vortex}$ remains close to 180° (3.14 radians), ϕ_{lift} is close to 0° and both C_L and $C_{L\ vortex}$ are in between the low- and high-frequency state values. After the first transition to the high-frequency state at $t \approx 85$ s there are a number of transient transitions to the intermediate state. In Figure 3-29 these transitions

correspond to an upward jump in $\phi_{lift\ vortex}$ towards 180°, a small dip in C_L and a small rise in ϕ_{lift}. The clearest of these transient transitions, at around t = 150 s, is highlighted by the right hand shaded region. The transient transitions from the high-frequency to the intermediate state are clearly discernable when we look at the phase of the vortex lift force. However, looking only at the total lift force it is not clear that the small changes in ϕ_{lift} and C_L within the second shaded region correspond to a transition to a different wake state. Figure 3-29 also demonstrates that during the transition between wake states the changes C_L and $C_{L\ vortex}$ are not necessarily of similar magnitude. From the force properties in Figure 3-26 and the instantaneous properties in Figure 3-29 it is clear that the transition between the low-frequency and intermediate states is most clearly identified by the large changes in ϕ_{lift} and $C_{L\ vortex}$. Conversely, at the intermediate to high-frequency state transition the most significant changes are in the values of $\phi_{lift\ vortex}$ and C_L.

The reasons for the apparently complicated relationships between ϕ_{lift}, $\phi_{lift\ vortex}$, C_L and $C_{L\ vortex}$ become apparent when we consider the vectorial relationship between the vortex and apparent mass lift forces. As discussed in section 1.3.3 $C_{L\ vortex}(t)$ and $C_{L\ am}(t)$ are the components which make up the total lift force $C_L(t)$. The schematic in Figure 3-30 shows phase plots for all three wake states using typical vectorial values of $C_{L\ vortex}(t)$, $C_{L\ am}(t)$ and $C_L(t)$. The apparent mass force is always in-phase with the displacement of the cylinder and, although its magnitude depends on the amplitude and frequency of oscillation, within the transition region $C_{L\ am}$ is approximately constant.

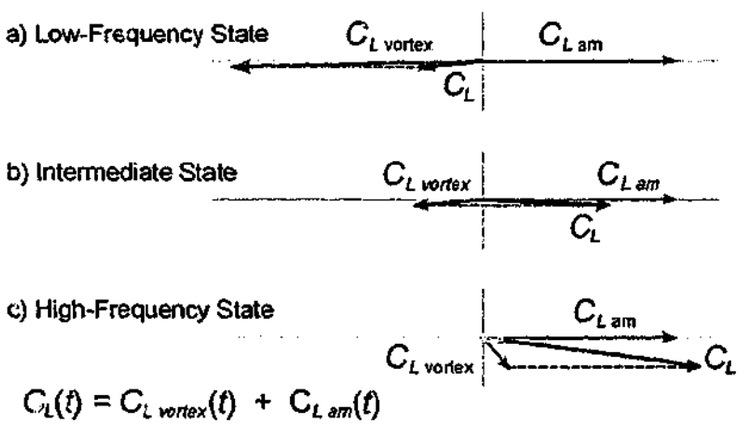

Figure 3-30 Phase plots showing typical vectorial relationships between $C_{L\ vortex}(t)$ and $C_{L\ am}$ and the resulting direction and magnitude of the total lift force for a) the low-frequency, b) intermediate and c) high-frequency wake states.

As the wake moves from the low-frequency state to the intermediate state the change in the phase of the vortex lift force, indicated by the direction of the $C_{L\ vortex}(t)$ vector, is relatively small. However, the magnitude of the vortex lift force decreases such that it is now smaller than the apparent mass force. This change in relative magnitude results in a large change in the phase of the

total lift force. Thus, as shown in Figure 3-27, the transition between the low-frequency and intermediate wake states corresponds to a large change in ϕ_{lift} but $\phi_{lift\ vortex}$ remains relatively unchanged. Furthermore, the change in the phase of the total lift force is clearly linked to the change in the magnitude of the vortex lift force. It is important to remember that the variation of the vortex lift force is directly related to changes in the vorticity field. Therefore, the changes in the total lift force effectively are linked to the vorticity field via the relationship between the vortex and apparent mass forces. At the transition between the intermediate and the high-frequency states Figure 3-29(b) and Figure 3-30 show that $C_{L\,vortex}$ is approximately constant, but there is a clockwise shift of around ¾ π (135°) (*i.e.* an anti-clockwise shift of 1¼ π (225°)) in $\phi_{lift\ vortex}$. The change in the phase of the vortex lift force causes only a small change in ϕ_{lift} but there is a significant change in C_L.

Another way to consider the relationship between the vortex and total lift forces is to consider the energy transfer. When the lift forces on the cylinder are accurately represented by a purely sinusoidal function the energy transfer can be approximated by equation 1-10, which is reproduced below for convenience:

$$C_E \approx \pi\, C_L\,(A/D)\sin(\phi_{lift}) = \pi\, C_{L\,vortex}\,(A/D)\sin(\phi_{lift\ vortex}) \qquad \text{(1-10 reproduced)}$$

Near the transition regions, and in particular for the intermediate wake states observed at $A/D = 0.5$ and 0.6, the lift forces are not always well represented by a purely sinusoidal function. In these cases the equation for energy transfer must be written in integral form. As in equation 1-10 the in-phase apparent mass force makes no contribution to the energy transfer and the integral can be expressed in terms of either the total or vortex lift force.

$$E = \int_{t=0}^{t=T} \vec{C}_L(t)\cdot\vec{V}(t)\,dt = \int_{t=0}^{t=T} \vec{C}_{L\,vortex}(t)\cdot\vec{V}(t)\,dt \qquad (3\text{-}3)$$

This equation also illustrates that the apparent mass component of the lift force makes no contribution to the energy transfer between the fluid and the cylinder. Thus, in terms of the relationship between the energy transfer and the forces on the cylinder, the only contribution to the energy transfer is from the out-of-phase component of the vortex lift force, where the out-of-phase components of $\phi_{lift\ vortex}(t)$ and $C_L(t)$ are equal.

3.6.2 Wake structure and corresponding lift forces

The force properties for the intermediate state, discussed in section 3.6.1, suggest that the structure of the intermediate wake is not consistent with the wakes structures for either the low- or high-frequency states. In this section the structure of the near wake, the mode of vortex shedding and the phase of vortex shedding for the three different wake states are considered. Finally, the nature of the total and vortex lift traces corresponding to the different wake structures are discussed.

The phase averaged vorticity fields in Figure 3-31 show the evolution of the near wake for each of the three wake states as the cylinder moves through its downward stroke at $A/D = 0.5$. The position of the cylinder in Figure 3-31 is indicated by the small insert and is the same for each vertical column, where the first column corresponds to the top of the cylinder's oscillation. Each image is the result of phase averaging 9 consecutive images representing 4½ cylinder oscillations. The images for the low- and high-frequency states, shown in Figure 3-31(a & c) respectively, were acquired at $f_e/f_o = 0.815$. The images in Figure 3-31(b), showing the intermediate state, were acquired at $f_e/f_o = 0.825$ and correspond to the 4½ cycles after $t = 150$ s in Figure 3-30.

The three wake states can be broadly described in terms of the mode of vortex shedding. However, it is also important to consider the timing of vortex shedding and other changes in the structure of the near wake. The low-frequency wake, shown in Figure 3-31(a), is characterised by the production of long attached shear layers and a relatively wide wake. At $A/D = 0.5$ the mode of vortex shedding for the low-frequency wake is weakly 2P and, as shown in Figure 3-31(a)(*iii*), the second vortex of each pairing is significantly weaker than the first. The high-frequency wake is shown at the same points in the oscillation cycle in Figure 3-31(c); the mode of vortex shedding is 2S and the wake is significantly narrower than the low-frequency wake. The evolution of the near wake for the intermediate state is shown in Figure 3-31(b). It is clear that the vortex shedding cycle for the intermediate wake is different from that of both the low- and high-frequency wakes. As the cylinder moves through the downward half of its oscillation cycle the intermediate wake sheds a single tightly formed positive vortex from the upper surface of the cylinder and the mode of vortex shedding can be described as 2S. At $A/D = 0.5$ the intermediate state has a 2S shedding mode, however the very small portion of separated positive vorticity at the end of the attached shear layer, shown in Figure 3-31(b)(*i*), indicates that at higher oscillation amplitudes the mode of vortex shedding for the intermediate wake may become weakly 2P.

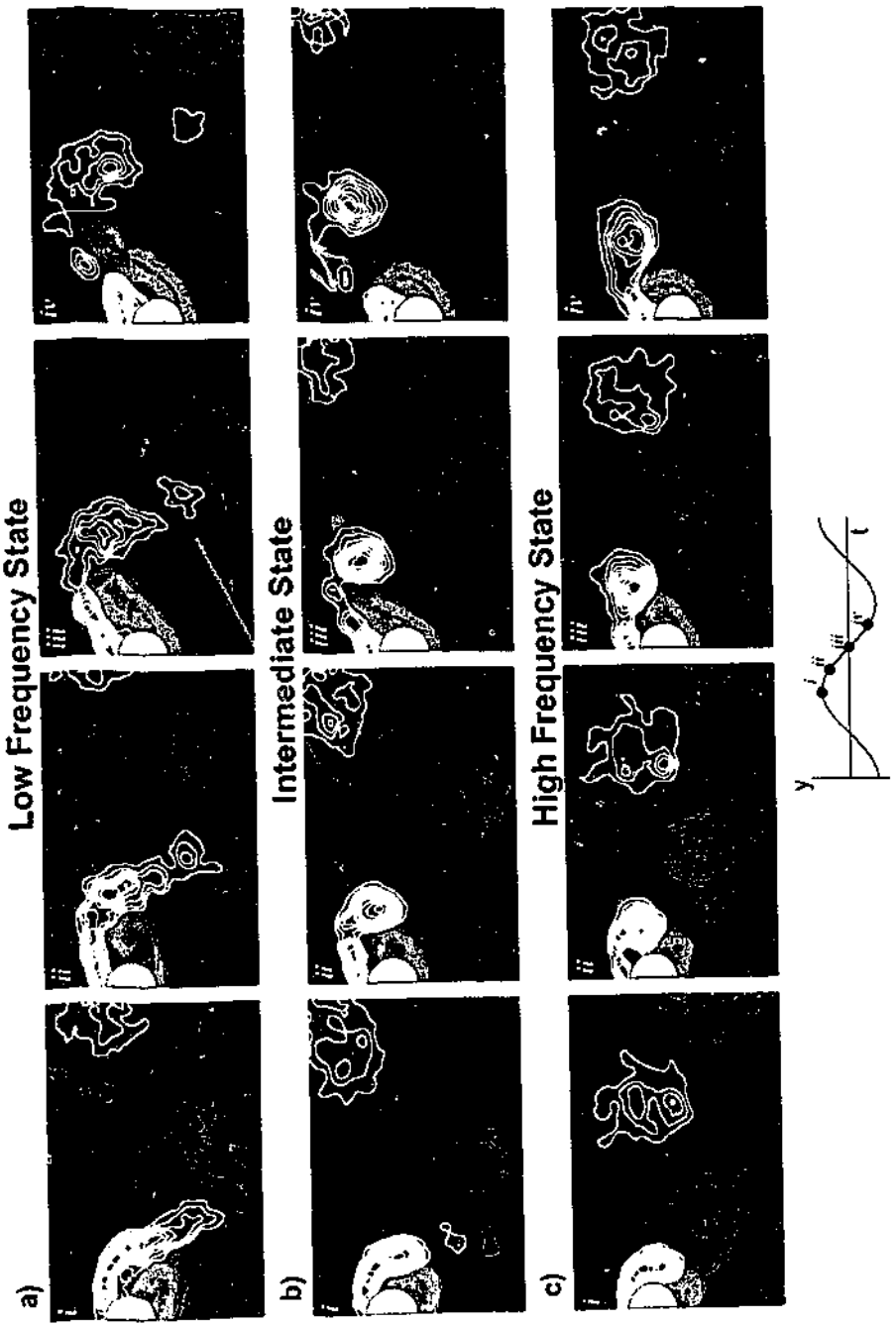

Figure 3-31 Wake patterns for the a) low-frequency, b) intermediate and c) high-frequency wake states at A/D = 0.5 f_s/f_o = 0.815 - 0.825 and Re = 2300. The position of the cylinder in each column (*i* to *iv*) is indicated by the insert.

The low-frequency and intermediate wakes, shown in Figure 3-31(a & b) respectively, share a number of common features; the major separation of negative vorticity from the shear layer occurs just after the mid-point of the downwards stroke, between columns (*iii*) and (*iv*), and the vertical

width of the wakes are similar. However, the mode of vortex shedding of the intermediate wake is clearly different from that of the low-frequency state. In fact, the intermediate wake has the same 2S mode of shedding as the high-frequency wake. Therefore, although the phase of vortex shedding appears to be the same for the intermediate and low-frequency wakes, the number and form of the vortex structure shed per oscillation are different. The different mode of vortex shedding for the low-frequency and intermediate wakes can be related back to differences in the structure of the attached shear layers prior to separation. Examination of the images in Figure 3-31(a & b) at the same phase point in the cylinder's oscillation shows that, compared to the low-frequency wake, both the attached and previously shed vortex structures in the intermediate wake are located further upstream. The low-frequency wake forms long elongated shear layers allowing a portion of the shear layer to separate independently and form the counter rotating pair. The corresponding vortex structures in the intermediate wake are tightly formed and are almost circular in shape, resulting in only a single vortex structure being shed from each shear layer per oscillation.

As the cylinder reaches its maximum downwards velocity in Figure 3-31(*iii*), the lower positive shear layer in the intermediate wake is closer to the base of the cylinder and the upper and lower shear layers have a greater upwards angle compared to the corresponding low-frequency wake. However, the interaction between the opposite shear layers in the two wakes still results in vortex shedding occurring at approximately the same phase point. The increased upward angle of the shorter shear layers of the intermediate wake results in a wake width which is very comparable to that of the low-frequency wake, despite the fact that the low-frequency wake formed much longer shear layers. As discussed in section 3.3.1, for increasing f_e/f_o the low-frequency wake contracts while the phase of vortex shedding remains essentially constant. However, in Figure 3-31(a & b) the contraction of the wake is associated with a transition between two different wake states. The difference in the length, angle and shape of the intermediate and low-frequency wakes results in different modes of vortex shedding, but the phase at which the major separation of vorticity occurs is approximately the same.

The phase of vortex shedding for the high-frequency wake, shown in Figure 3-31(c), is distinctly different from the shedding phase for both the low-frequency and intermediate wakes. As the cylinder moves through the downward stroke a positive vortex structure is shed from the high-frequency wake soon after the top of the oscillation, corresponding to column (*i*). However, during the same half cycle negative vortex structures are shed from the low-frequency and intermediate wakes soon after the mid-point of the downward stroke, corresponding to column (*iii*). The position, or phase, of the cylinder when vortex shedding occurs has a significant influence on the vertical width of the wake. The phase of vortex shedding from the high-frequency wake is such that the vorticity from the lower surface of the cylinder is shed just after the cylinder reaches its upper vertical displacement. Negative vorticity is shed from the upper surface of the cylinder half

a cycle later, when the cylinder is close to its lowest vertical position. The location of the cylinder when the vorticity is shed from it results in a wake that is much narrower than either the low-frequency or intermediate wakes. The difference in the widths of these wakes appears to be largely attributable to the phase, rather than the mode, of vortex shedding.

The total and vortex lift traces, corresponding to the 4½ cycles during which the images in Figure 3-31 were acquired, are shown in Figure 3-32 for each of the three wake states. The values of f_e/f_o for the three sets of force traces are very similar and therefore the amplitude of the apparent mass force is effectively constant. This means that the changes in the phase and amplitude of the total lift force are directly related to changes in the phase and amplitude of the vortex lift force. An important property of the lift forces, which will be considered qualitatively, is their sinusoidal nature. The total and vortex lift forces on a cylinder oscillating with a sinusoidal motion tend to be sinusoidal, and our definitions of the phase and amplitude of these forces in equations 2-4 and 2-9 utilise this property. The sinusoidal nature of the force traces is indicated by the relative amplitude of the spectral components within the traces, where a very sinusoidal trace is similar to a pure sinusoid and is dominated by energy at a single frequency.

For all parameters considered in this investigation the forces are locked-on to the motion of the cylinder and the dominant frequency within the lift traces is the forcing frequency, f_e. The apparent mass component of the total lift force is directly related to the motion of the cylinder and $F_{am}(t)$ is a purely sinusoidal signal with frequency f_e. Therefore, the vortex lift force is the only component of the total lift force containing frequencies other than f_e, and the magnitude of the non-f_e components must be exactly the same in the vortex and total lift forces. The out-of-phase components of the total and vortex lift forces are also equal. The lift traces for the three wake states shown in Figure 3-32 demonstrate that although the relationship between the total and vortex lift forces appears relatively simple, the total and vortex lift forces can differ significantly in their sinusoidal nature, phase and amplitude. The changes in the properties of the total and vortex lift forces shown in Figure 3-32 at $A/D = 0.5$ are consistent with the force properties shown in Figure 3-26 at the higher amplitude of $A/D = 0.6$.

For the low-frequency state both the total and vortex lift forces, shown in Figure 3-32(a), are approximately out-of-phase with the displacement of the cylinder. The total and vortex lift forces contain the same non-f_e components. However, because the magnitude of the f_e component is much larger in the vortex lift force, the vortex lift trace is relatively speaking more sinusoidal than the total lift trace.

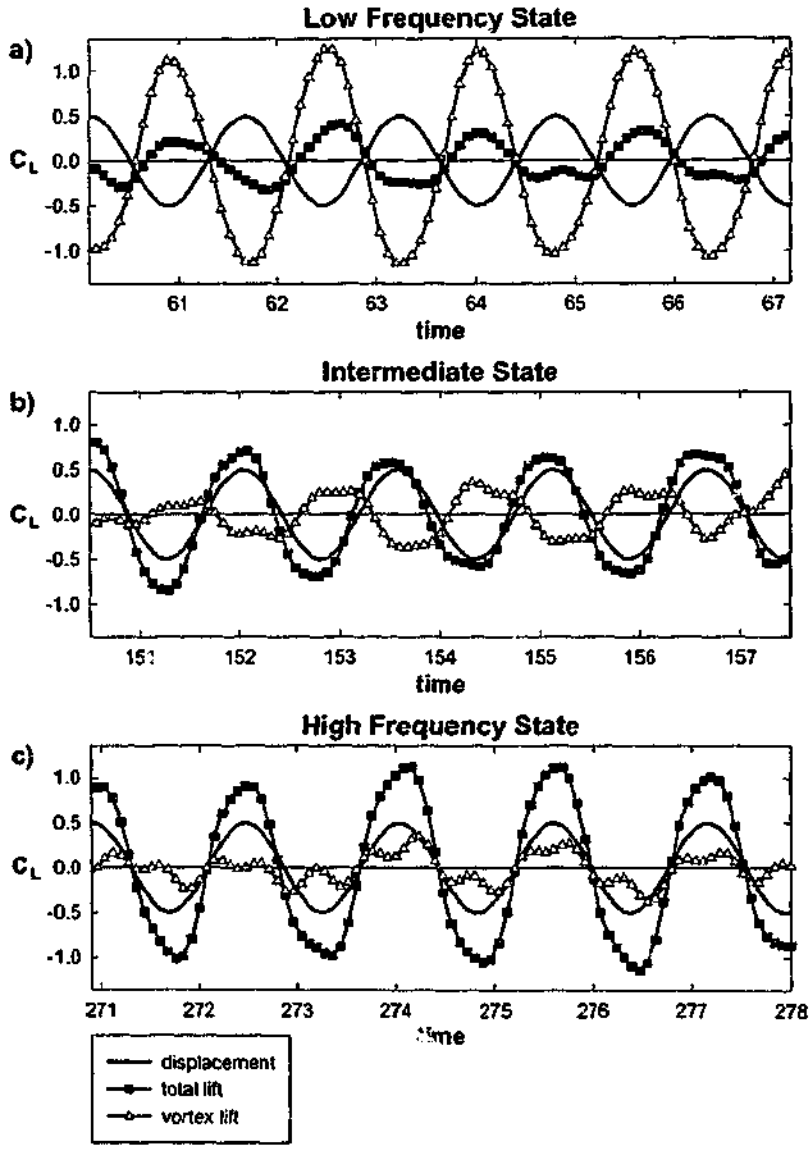

Figure 3-32 Total and vortex lift traces for a) low-frequency, b) intermediate and c) high-frequency wake states at A/D = 0.5 f_s/f_o = 0.815 - 0.825 and Re = 2300. The time segments correspond to the 4½ cycles over which the phase averaged images in Figure 3-31 were acquired.

As the wake moves from the low-frequency state to the intermediate state there is a large change in the relative phases of the total and vortex lift forces. The vortex lift force remains approximately out-of-phase with the displacement of the cylinder, while the total lift force and cylinder displacement are now almost in-phase. Equation 3.2(a) tells us that the phase of the vortex forces is related to the points in the oscillation cycle where the rate of change of the vortex moments are maximised. For similar distributions of vorticity, the phase of the vortex lift and drag forces is linked to the maximum rate of change of the vortex moment and generally, therefore, to the phase of vortex shedding. Changes in the distribution of vorticity within the shedding cycle can alter the

phase point at which the maximum change in the vortex moment occurs. However, unless these changes significantly alter the relationship between the phase of vortex shedding and the movement of vorticity within the shedding cycle, the phase of vortex shedding is the dominant factor that determines the phase of the vortex forces on the cylinder. The vorticity fields in Figure 3-31(a & b) show that the phase of vortex shedding is approximately the same for the low-frequency and intermediate wakes. As this transition occurs the changes in the vortex lift and drag phases are relatively small, of the order of 20°. The relatively small changes in the phases of the vortex lift traces, shown in Figure 3-32(a & b), are consistent with the fact that for the corresponding wakes in Figure 3-31(a & b) the phase of vortex shedding is very similar.

The vector diagram in Figure 3-30 demonstrates that the large change in ϕ_{lift} at the transition from the low-frequency to the intermediate state occurs as the magnitude of the vortex lift force becomes smaller than that of the apparent mass force. For the intermediate wake state the vortex lift force is both smaller in magnitude and considerably less sinusoidal that the total lift force. The decrease in the magnitude of the vortex lift is clearly shown in the force traces of Figure 3-32(a & b). The changes in $C_{L\,vortex}$ are consistent with the fact that there is a change in the structure of the corresponding wakes, shown in Figure 3-31(a & b).

At the transition between the intermediate and high-frequency states there is a large phase shift in the vortex lift force. For values of f_e/f_o close to the transition region, at A/D = 0.5 the high-frequency state total and vortex lift forces are approximately in-phase with the displacement of the cylinder ($\phi_{lift} \approx \phi_{lift\,vortex} \approx 0°$). The vortex lift force, shown in Figure 3-32(c), is very small in amplitude and the trace is quite irregular. The total lift force is much larger in amplitude than the vortex lift force, and the large difference in amplitude belies the fact that the non-f_e components are present in both the total and vortex lift signals. Despite the irregular nature of the vortex lift signal in Figure 3-32(c) the values of $\phi_{lift\,vortex}$, calculated using the segmented correlation method with a correlation period of three oscillation cycles, do not vary significantly with time unless the wake state is changing.

At A/D = 0.5 immediately following the transition to the high-frequency state both $\phi_{lift\,vortex}$ and $C_{L\,vortex}$ vary with f_e/f_o, as shown in Figure 3-15(a & d). As f_e/f_o increases $\phi_{lift\,vortex}$ moves rapidly from close to 0°, immediately after the transition to the high-frequency state at f_e/f_o = 0.815, towards -90° at $f_e/f_o \approx 0.9$ - 1.0. As discussed in 3.4.3, the variation of $\phi_{lift\,vortex}$ with f_e/f_o immediately following the transition to the high-frequency state does not occur for all flow and oscillation parameters. In many cases at the transition to the high-frequency state $\phi_{lift\,vortex}$ jumps straight down to values close to –90°. The amplitude of the vortex force varies systematically with increasing oscillation frequency, and at higher values of f_e/f_o the high-frequency state vortex lift trace is larger in amplitude and more sinusoidal.

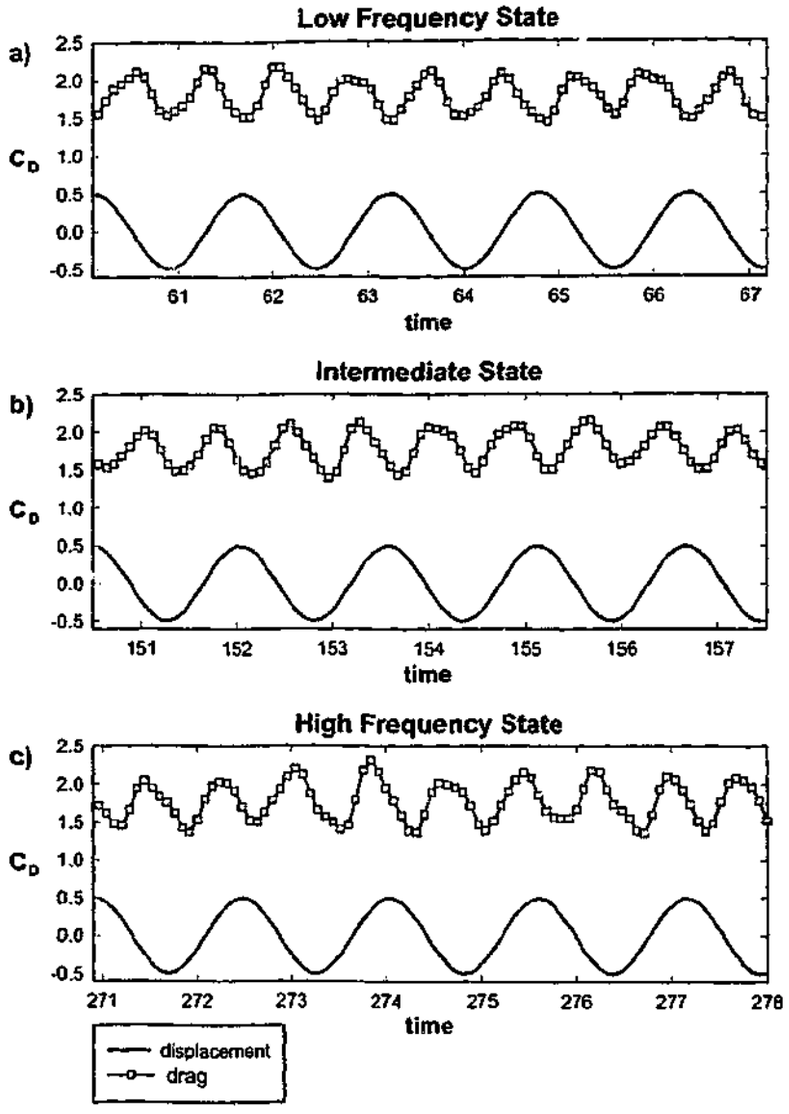

Figure 3-33 Drag traces for a) low-frequency, b) intermediate and c) high-frequency wake states at A/D = 0.5 f_v/f_e = 0.815 - 0.825 and Re = 2300. The time segments correspond to the 4½ cycles over which the phase averaged images in Figure 3-31 were acquired.

The vortex lift traces for both intermediate and the high-frequency states in Figure 3-32(a & b) appear to be slightly "double peaked" with a small dip in the middle of the peaks. Intuitively we associate these dips with an event that coincides with the peaks in the vortex lift force. However, as these dips correspond to a decrease in $C_{L\,vortex}(t)$ during the positive peak and an increase in $C_{L\,vortex}(t)$ during the negative peaks the "double peaked" nature of the vortex lift correspond mathematically to an increase in the energy of the third harmonic, $3f_e$.

The drag traces corresponding to the 4½ cycles during which the images in Figure 3-31 were acquired are shown for each of the three wake states in Figure 3-33. Despite the fact that the three wake states have different wake structures the drag traces are remarkably similar. This is consistent with the approximately constant value of C_D within the transition region, shown in Figure 3-26(f). Figure 3-33 also shows that $C_{D\,mean}$ and the general form of the drag traces do not change significantly at the transitions between the three wake states, although there is a small shift in phase. The constant amplitude and sinusoidal nature of the drag traces in Figure 3-33 is in contrast to the corresponding vortex lift traces, which vary significantly as the wake moves between the three states.

The previous paragraphs have considered the properties of the three wake states for an oscillation amplitude of $A/D = 0.5$, the same properties are now examined at the higher amplitude of $A/D = 0.6$. This 20 % increase in oscillation amplitude results in some changes in the structure of the near wake, the most obvious of these being an increase in the vertical width of the wake. However, the major features of these wake states are unchanged and the general properties of the low-frequency, intermediate and high-frequency wakes are consistent with the previous descriptions.

The phase averaged vorticity fields in Figure 3-34 show the evolution of the near wake for each of the three wake states at $A/D = 0.6$. Each phase averaged image has been calculated using 4 or 5 instantaneous fields corresponding to 2-2½ cylinder oscillations. The field of view for the vorticity fields in Figure 3-34 is smaller than the corresponding images at $A/D = 0.5$, however the different wake modes are clearly evident and the smaller wake structures, particularly in the shear layers, are well resolved. Compared to the vorticity fields at $A/D = 0.5$, the vortex structures for all three wake states in Figure 3-34 at $A/D = 0.6$ are more disorganised and are less clearly defined. Although the images in Figure 3-34 are averaged over a smaller number of fields than for the corresponding images at $A/D = 0.5$ this trend is also evident when the instantaneous images at the two oscillation amplitudes are compared. At $A/D = 0.6$ the low-frequency wake, shown in Figure 3-34(a), forms very long shear layers. The increase in A/D, and the corresponding increase in the length of the attached shear-layers, results in an increase in the relative strength of the second vortex shed into each counter rotating pair. Thus at $A/D = 0.6$ the mode of shedding for the low-frequency wake is clearly 2P. The vortex structures for the intermediate wake, shown in Figure 3-34(b), are less regular in shape than for the intermediate wake at $A/D = 0.5$, however in both cases the mode of shedding is 2S. The phase of vortex shedding for both the low-frequency and intermediate wakes at $A/D = 0.6$ is approximately the same as for the corresponding wakes at $A/D = 0.5$. This is consistent with the collapse of the vortex lift and drag phases over a range of A/D and Re shown in Figure 3-21.

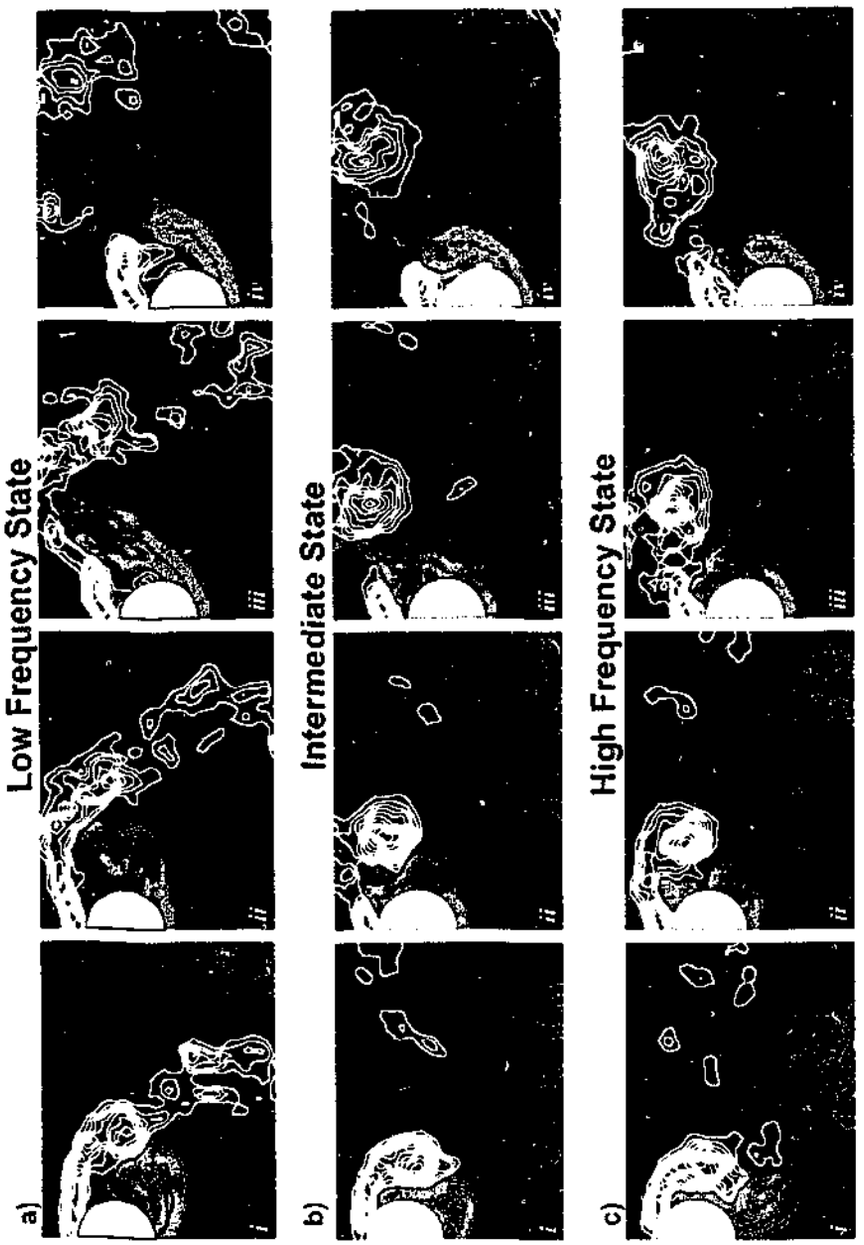

Figure 3-34 Wake patterns at A/D = 0.6 and Re = 2300 for a) the low-frequency state; $f_v/f_o = 0.82$, b) the intermediate state; $f_v/f_o = 0.85$ and c) the high-frequency state; $f_v/f_o = 0.87$. The position of the cylinder in each column (*i* to *iv*) is the same as in Figure 3-31.

The high-frequency wakes at both $A/D = 0.6$ and $A/D = 0.5$ are 2S and the distribution of vorticity within the wakes is very similar. However, at $A/D = 0.6$ the vortex shedding appears to happen earlier in the oscillation cycle. The difference in the phase of vortex shedding is most obvious at the points in the oscillation cycle where the positive and negative vortex structures separate from the attached shear layer. At the top of the oscillation in Figure 3-34(c)(*i*) at $A/D = 0.6$ the positive vorticity is already well separated from the cylinder, while at $A/D = 0.5$ in Figure 3-31(c)(*i*) the

positive vorticity has not yet completed the separation process. Similarly, just before the bottom of the oscillation in Figure 3-34(c)(*iv*) the negative vorticity has separated from the cylinder, while at the same phase point in Figure 3-31(c)(*iv*) the corresponding vortex structure is still attached to the cylinder. This difference in the phase of vortex shedding and the corresponding phase of the vortex lift force will be discussed further later in this section.

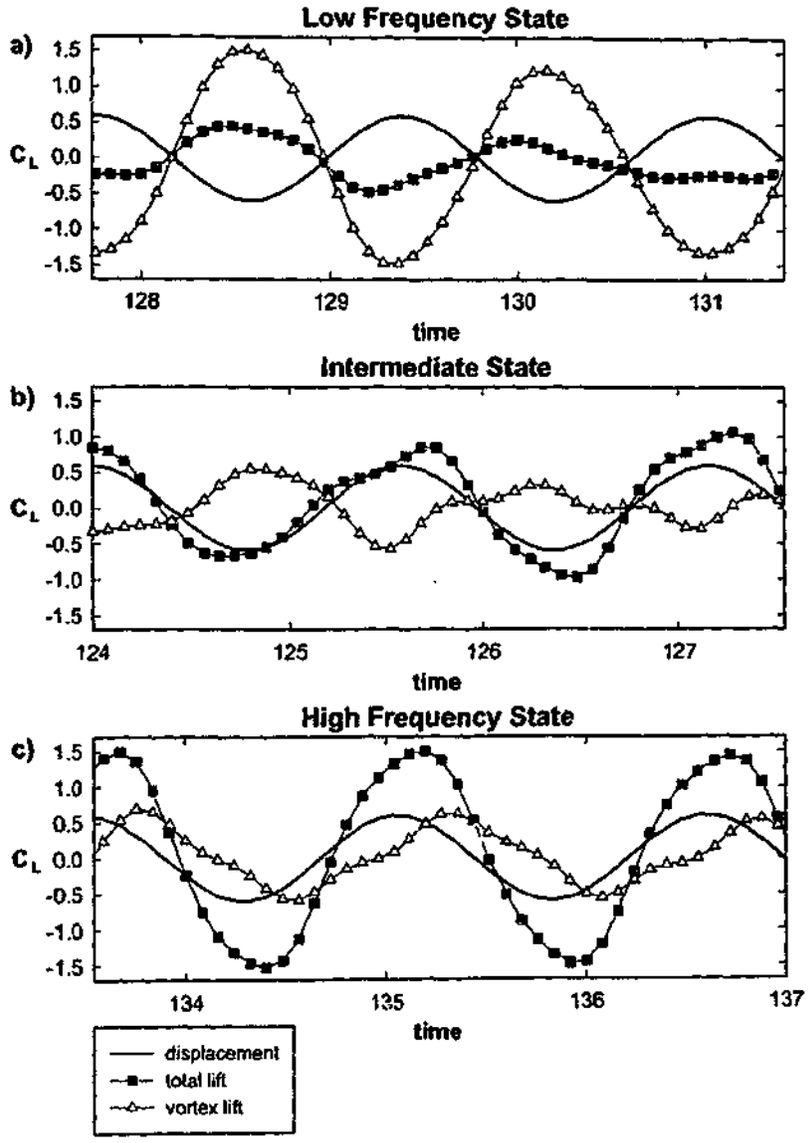

Figure 3-35 Total and vortex lift traces at A/D = 0.6 and Re = 2300 for a) the low-frequency state; f_v/f_o = 0.82, b) the intermediate state; f_v/f_o = 0.85 and c) the high-frequency state; f_v/f_o = 0.87. The time segments correspond to the 2½ cycles over which the phase averaged images in Figure 3-34 were acquired.

The force traces in Figure 3-35 show the total and vortex lift forces corresponding to the vorticity fields in Figure 3-34, where the traces correspond to the same time periods over which the flow

fields were phase averaged. As the force traces in Figure 3-35 were acquired over a narrow range of oscillation frequencies there is a small variation in the amplitude of the apparent mass force as f_c/f_o increases from 0.82 to 0.87, and the relationship between the total and vortex lift forces changes accordingly. The total and vortex force traces for the three wake states at $A/D = 0.6$ are generally consistent with the corresponding traces at $A/D = 0.5$. The two most notable differences are the phase of the total lift force for the low-frequency state and the phase of the vortex lift force for the high-frequency state. Without knowledge of the vortex lift force the shift in the phase of the total lift force as A/D increased from 0.5 to 0.6 may be incorrectly interpreted as a change in the phase of vortex shedding. However, careful consideration of the vector diagram in Figure 3-30 indicates that the shift in ϕ_{lift}, while $\phi_{lift\ vortex}$ remains approximately constant, is due to a change in the relative amplitudes of the vortex and apparent mass forces. The shift in the phase of the vortex lift force for the high-frequency state appears to be linked to a change in the phase of vortex shedding. As shown in Figure 3-15(a), at $A/D = 0.6$ the phase of the lift force drops to just above -90° immediately following the transition to the high-frequency state, whereas for $A/D = 0.5$ immediately following the transition $\phi_{lift\ vortex}$ is close 0°. The difference between the values of $\phi_{lift\ vortex}$ for $A/D = 0.5$ and 0.6, soon after the transition to the high-frequency state, is demonstrated by the vortex lift traces in Figure 3-32(c) and Figure 3-35(c). Examination of the vortex shedding cycle for the corresponding wakes, shown in Figure 3-31(c) and Figure 3-34(c), indicates that the difference in the phase of the vortex lift force is directly related to a shift in the phase of vortex shedding.

3.6.3 Variation of lift and drag phases

The temporal variations of the instantaneous values of ϕ_{lift}, $\phi_{lift\ vortex}$ and ϕ_{drag} at $A/D = 0.5$ are plotted in Figure 3-36 for a range of oscillation frequencies that incorporate all three wake states. At $f_e/f_o = 0.739$ and 0.781 the phases of the lift and drag forces indicate that the wake is in the low-frequency state, while at the two highest frequencies, $f_e/f_o = 0.869$ and 0.914, the wake is in the high-frequency state. At both $f_e/f_o = 0.815$ and 0.825 the first wake state after the oscillations begin at $t = 0$ is the low-frequency state; however, after a number of oscillation cycles the wake begins a self-excited transition, moving first to a transient intermediate state and then to the high-frequency state. In Figure 3-36 the intermediate state corresponds to the points when the values of ϕ_{lift} have jumped downwards, and are typically slightly above the values for the high-frequency state, but the values of $\phi_{lift\ vortex}$ remain high and are similar to low-frequency state values. In other words, the values of ϕ_{lift} and $\phi_{lift\ vortex}$ for the intermediate state are consistent with neither the low- or high-frequency states. Figure 3-36 also shows that, for both $f_e/f_o = 0.815$ and 0.825, after the initial self-excited transition there are further self-excited transitions between the high-frequency and intermediate states. However, in these cases the intermediate state does not appear to be very stable and after a number of oscillations the wake returns to the high-frequency state. Figure 3-36(a & b) shows that for values of f_e/f_o above the transition region both ϕ_{lift} and $\phi_{lift\ vortex}$ decrease with increasing f_e/f_o.

Perhaps the most interesting aspect of Figure 3-36 is the variation of the drag phase as the wake moves between the three wake states. The values of ϕ_{drag} for the low- and high-frequency states are clearly separated as shown in Figure 3-36(c). The self-excited transitions to the intermediate state are characterised by a large change in either ϕ_{lift} or $\phi_{lift\ vortex}$, while the other lift phase remains approximately constant, or changes by only a small amount. However, the values of the drag phase for the intermediate are between the values that characterise the low- and high-frequency states. Therefore, when the wake moves to the intermediate state from either the low- or high-frequency states there is a change in the value of ϕ_{drag}. The definition of the drag phase, and the subsequent fact that any value of ϕ_{drag} is equivalent to $\phi_{drag} \pm 180°$, means that the drag phase can be plotted in a number of ways. Consequently, care must be taken when interpreting the magnitude of the changes in ϕ_{drag}. The physical reason for the multi-valued and somewhat ambiguous nature of ϕ_{drag} is that the drag phase does not include the same information as the lift phase. As discussed in section 3.2.4, vortex shedding from a bluff body typically involves the net vertical displacement of positive vorticity downwards and negative vorticity upwards, as well as the net downstream movement of both signs of vorticity. Examination of equation 3-2 reveals that a local maximum in the drag force can be generated by either the net movement of positive vorticity downwards or negative vorticity upwards, and as long as the wake is symmetric, the drag force does not

Abbeydale Hotel & Spa Bookfinders Melbourne 95236025

differentiate between these two cases. However, the vortex lift force does differentiate between the streamwise movements of different signed vorticity; downstream movement of positive vorticity generates positive lift while the equivalent movement of negative vorticity generates negative lift. Therefore, the lift force has one local maximum per oscillation but the drag force has two.

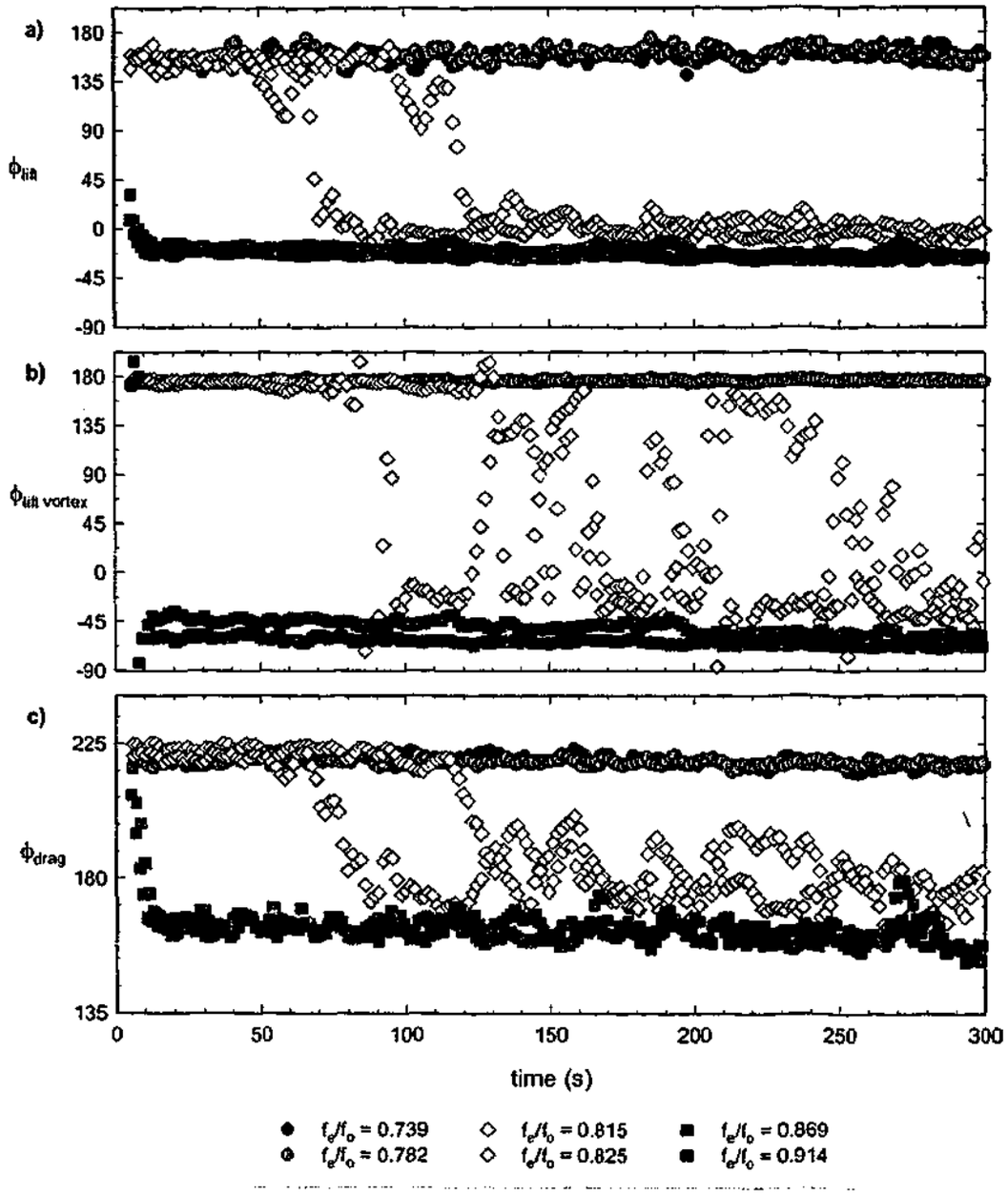

Figure 3-36 Variation of a) total lift phase, b) vortex lift phase and c) drag phase after the cylinder begins oscillating at t = 0 for a range of oscillation frequencies at A/D = 0.5 and Re = 2300. In all cases the instantaneous phases were calculated using a correlation width of 3 oscillation cycles.

The lift and drag phases are calculated by taking the peaks in the force traces and correlating them with the peaks in the cylinder's displacement. A local maximum in the lift force is generally

associated with the net movement of positive vorticity downstream. However, when the drag phase is calculated, one of the two peaks in the drag peaks per oscillation cycle is selected for the correlation. If the other peak were selected the drag phase would be shifted by 180°, assuming the drag force is periodic and synchronised. Thus, using this method any value of ϕ_{drag} is equivalent to $\phi_{drag} \pm 180°$. This is why the drag phase contains less information than the lift phase. Moreover, when there is a change in the phase of vortex shedding it is not possible to differentiate between the two peaks in the drag force either before or after the transition, and the change in the drag phase at the transition, $\Delta\phi_{drag}$ is also equal to $\Delta\phi_{drag} \pm 180°$.

Without detailed examination of the temporal movement of vorticity throughout the wake allowing the application of equation 3-2, it is not possible to associate a peak in the drag force with the movement of a particular vortex structure. The limited time resolution of the vorticity fields in the current investigation precluded the application of equation 3-2. Consequently the finer details of the relationships between the vorticity fields and the vortex forces for the three wake states remain a question for future investigation.

In both Figure 3-26 and Figure 3-36 the drag phase has been plotted in a way that minimises the magnitude of the jumps in ϕ_{drag}. The drag phases can also be plotted so that the variation in ϕ_{drag} is most similar to the corresponding changes in the vortex lift phases, as shown in Figure 3-37(b). In this case the transition between the low-frequency and intermediate states corresponds to a relatively small change in ϕ_{drag}, while the transition between the intermediate and high-frequency states corresponds to a large change in ϕ_{drag}. The vorticity fields indicate that this is perhaps the most physically meaningful way of plotting ϕ_{drag}, as the phase of vortex shedding is essentially constant at the transition between the low-frequency and intermediate states. In Figure 3-37(b) there is also a relatively large jump in ϕ_{drag} at the transition between the intermediate and high-frequency states, which corresponds to a large change in the phase of vortex shedding. For the transverse oscillations the drag force is a purely vortex force and, in that respect, is analogous to the vortex lift force. The fact that the phases of these forces show similar behaviour, particularly in the collapse of $\phi_{lift\ vortex}$ and ϕ_{drag}, strengthens our interpretation of the relationship between the vortex forces and the structure of the wake. Thus, despite the limitations in interpreting of the drag phase, discussed above, it has still has provided valuable insight.

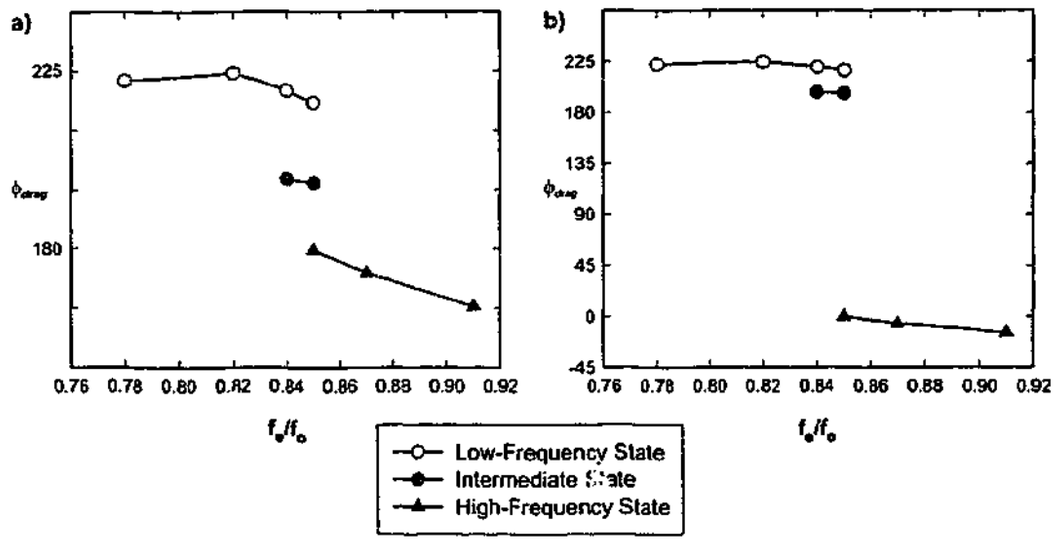

Figure 3-37 Two different methods of plotting the variation of ϕ_{drag} for the three different wake states: $A/D = 0.6$, $Re = 2300$.

The instantaneous values of ϕ_{lift}, $\phi_{lift\ vortex}$ and ϕ_{drag} at the higher amplitude of $A/D = 0.6$ are plotted in Figure 3-38 where, for the range of oscillation frequencies considered, the wake demonstrates all three wake states. The vortex lift phase is plotted twice to demonstrate the effect of plotting all the phase values between 0° and 360°, rather than using the traditional method of plotting most of the 3rd and 4th quadrant phases as negative values. For f_e/f_o = 0.78, 0.82 and 0.91in Figure 3-38 there are no self-excited transitions and the wake is in either the low- or high-frequency states. The variation of the forces for two values of f_e/f_o where self-excited transitions occur, f_e/f_o = 0.84 and 0.85, were discussed in detail in section 3.6.1. The force trace indicates that at f_e/f_o = 0.84 there is a self-excited transition from the low-frequency state to a stable intermediate state. At both f_e/f_o = 0.85 and 0.87, after an initial transition from the low-frequency state through to the high-frequency state, the wake alternates between the high-frequency and intermediate states. The force traces show that at f_e/f_o = 0.85 the wake is predominantly in the intermediate wake state, while at the higher frequency of f_e/f_o = 0.87 the wake spends most time in the high-frequency state. The wake exhibits all three sates within the transition region, f_e/f_o = 0.84 – 0.87, but as f_e/f_o increases the percentage of time that the wake spends in a given wake state changes and there is a clear shift in the relative stability of the different states. Within the transition region, at both A/D = 0.5 and 0.6 the low-frequency state appears to be a meta-stable state, which the wake tends to move to immediately after the cylinder starts oscillating. As f_e/f_o increases within the transition region there is a decrease in the time after start up at which the transition from the initial low-frequency state to a more stable state occurs, as discussed in section 3.3.2. This phenomenon is also illustrated in Figure 3-36 and Figure 3-38 and appears to occur irrespective of the final state or the nature of the transition.

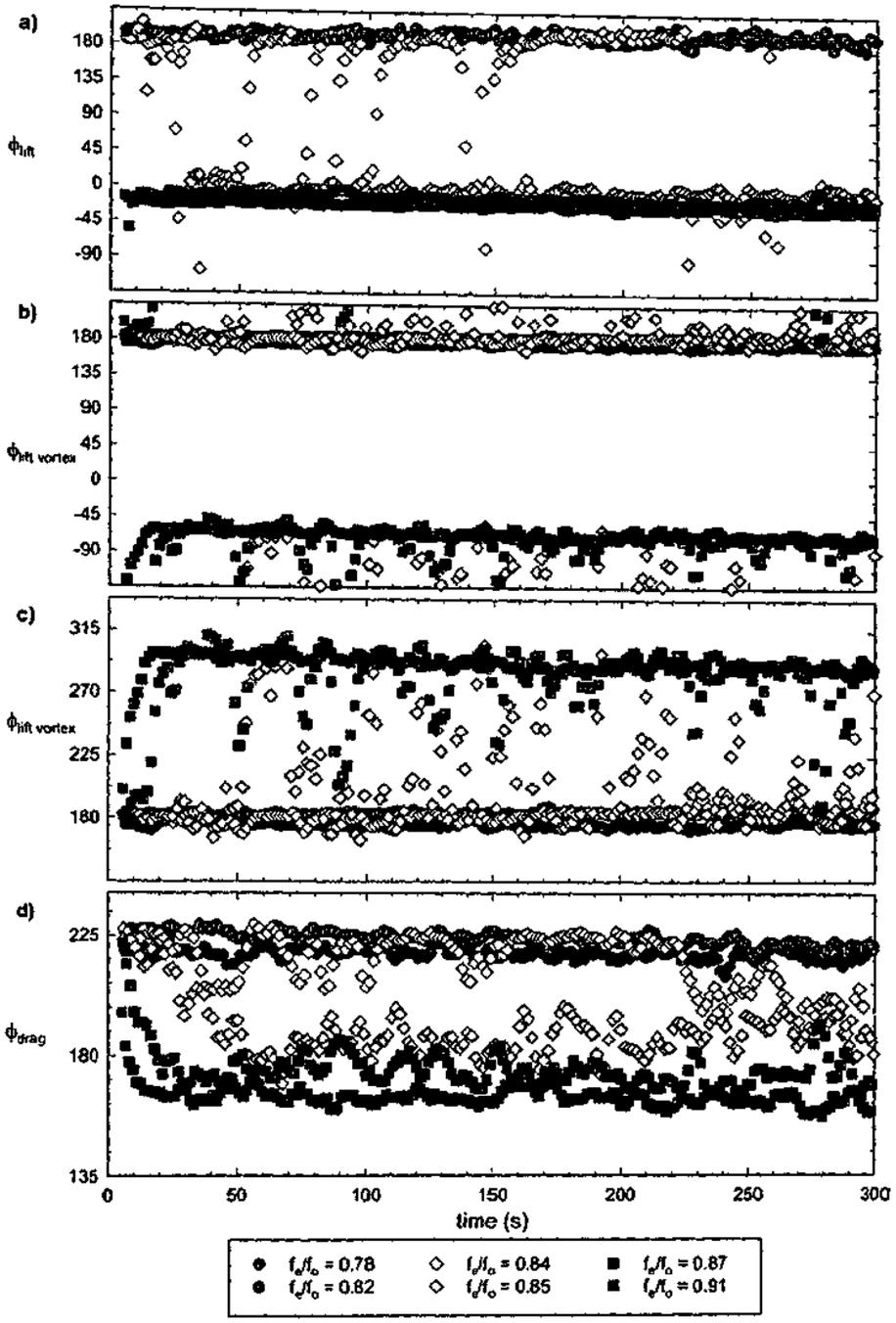

Figure 3-38 Variation of a) total lift phase, b) vortex lift phase and c) drag phase after the cylinder begins oscillating at t = 0 for a range of oscillation frequencies at A/D = 0.5 and Re = 2300. In all cases the instantaneous phases were calculated using a correlation width of 3 oscillation cycles.

The traditional method of plotting $\phi_{lift\ vortex}$ in Figure 3-38(b) shows the transition between the intermediate and high-frequency states as a large change in $\phi_{lift\ vortex}$ of the order of 240°. However, when $\phi_{lift\ vortex}$ is replotted in Figure 3-38(c) the change in $\phi_{lift\ vortex}$ is of the order of 120°. The two

different methods of plotting $\phi_{lift\ vortex}$ demonstrate a very interesting point about the transition between the intermediate and high-frequency states. The direction of the phase shift can be inferred from the phase values that occur as the wake state changes. Using this methodology, Figures 3-36 and 3.38 show that the low-frequency to intermediate state transition, at both A/D = 0.5 and 0.6, corresponds to a anti-clockwise shift in the total lift phase. The direction of this phase shift does not represent a shift in the phase of vortex shedding but instead a change in the relative amplitudes of the vortex and apparent mass forces. During the transition from the intermediate state to the high-frequency state at A/D = 0.5 the values of $\phi_{lift\ vortex}$ move through the 2nd and 1st quadrants, indicating that the transition corresponds to a clockwise shift in the phase of vortex shedding. However, at A/D = 0.6 Figure 3-38(c) clearly shows that during the transition between the same states the values of $\phi_{lift\ vortex}$ move in the opposite direction, through the 4th quadrant, thus the transition corresponds to an anti-clockwise shift in the phase of vortex shedding. As A/D increases from 0.5 to 0.6 we have also observed a change in the behaviour of ϕ_{lift} and $\phi_{lift\ vortex}$ as f_e/f_o increases immediately following the transition to the high-frequency state, as discussed in sections 3.4.1 and 3.6.2. However, it is not known if this difference is related to the apparent change in the direction of the phase shift. Gopalkrishnan (1993) also found a similar change in the direction of the phase shift at transition as the oscillation amplitude increased from A/D = 0.5 to 0.75. However, his observations were made for the total lift phase, and without evaluation of the vortex lift force it is difficult to compare the two cases, particularly as the oscillation amplitude for the current investigations do not extend past A/D = 0.6.

The behaviour of the drag phase at A/D = 0.6 in Figure 3-38 is similar to that observed at A/D = 0.5, and in both case the intermediate state corresponds to values of ϕ_{drag} that are between the values for the low- and high-frequency states. At A/D = 0.6 the intermediate state is observed over a wider range of f_e/f_o, and examination of Figure 3-38(d) shows that as f_e/f_o increases within the transition region the average value of ϕ_{drag} for the intermediate state decreases. In fact, as f_e/f_o increases the drag phase of the intermediate state appears to decrease gradually from values that are slightly below the low-frequency state values towards values that are observed for the high-frequency state. However, as discussed earlier, the nature of the variation of ϕ_{drag} depends on how this property is plotted.

3.7 RELATE FORCED AND FREELY OSCILLATING CYLINDERS

One of the important questions arising from the investigations of forced and freely oscillating cylinders is whether the results from the forced oscillations can be used to predict and interpret the oscillations of a freely vibrating system. As discussed in section 1.6.3 this question has been considered by a number of investigators, most notably Staubli (1983) who attempted to use the results of forced oscillations to predict the motion of an elastically mounted cylinder with limited success. The flow-induced motion of a cylinder is a complicated problem as the structure of the wake and the motion of the cylinder are a coupled, interdependent system. This problem can be simplified by replicating the flow-induced motion using a predefined controlled motion, which allows the investigation to focus on the response of the wake to the cylinder's motion.

In this section we consider the relationship between a cylinder forced to oscillate with a purely sinusoidal motion at frequencies close to the natural frequency of the wake and the free oscillations of an elastically mounted cylinder. Despite the fact that the relationship between these two cases has proved surprisingly complicated, our results show that many of the fundamental features of the free and forced cases are in fact strikingly similar.

3.7.1 Link Between Forced Wake States and Free Response Branches

As discussed in section 1.5 the vortex-induced motion of cylinder that is free to oscillate transverse to the free-stream has been shown to exhibit two or three response branches, depending on the mass and damping of the structure. The response of an elastically mounted, freely oscillating cylinder is generally considered as a function of the free-stream velocity and the response properties are plotted against U^* or $(U^*/f^*)St_o$, where both these parameters vary inversely with f_e/f_o. Both the wake states for the forced oscillations and the response branches of the freely oscillating cylinder are characterised in terms of the wake structure and the forces on the cylinder. The variations of C_L and $C_{L\,vortex}$ with f_e/f_o have distinctive shapes for both the forced and freely oscillating cases. However, it is difficult to compare these shapes as for the free motion the amplitude of oscillation varies with f_e/f_o, while for the forced case A/D is held constant. The parameters that best allow comparison between the forced and freely oscillating cases are ϕ_{lift} and $\phi_{lift\,vortex}$. In the previous sections the values of ϕ_{lift} and $\phi_{lift\,vortex}$ were used to identify the three different wake states for the forced oscillations. The same parameters were also used by Govardhan & Williamson (2000) to identify the different response branches of an elastically mounted cylinder. The values of ϕ_{lift} and $\phi_{lift\,vortex}$ also indicate the direction of the energy transfer, which in terms of the relationship between the forced and freely oscillating cylinder is a crucial parameter.

In the following discussion the properties of the force wake states and free response branches will be compared and it will be shown that the three wake states are analogous to the three response branches. At low values of f_e/f_o, corresponding to higher U* and $(U^*/f^*)St_o$ values, the low-frequency state is observed for the forced oscillations and the freely oscillating cylinder is in the lower response branch. At higher values of f_e/f_o, corresponding to lower U^* and $(U^*/f^*)St_o$, the forced and freely oscillating cases exhibit the high-frequency state and the initial response branch respectively. The intermediate state and the upper branch are only observed for certain conditions and are generally associated with larger oscillation amplitudes, which for the freely oscillating case occur at lower mass-damping values. In parameter space, the intermediate state and upper branch occur in between the other states or branches close to the resonance conditions, where for the forced case $f_e \approx f_o$ and for the free case $f_o \approx f_{stmc}$ and typically $U^* \approx 5$.

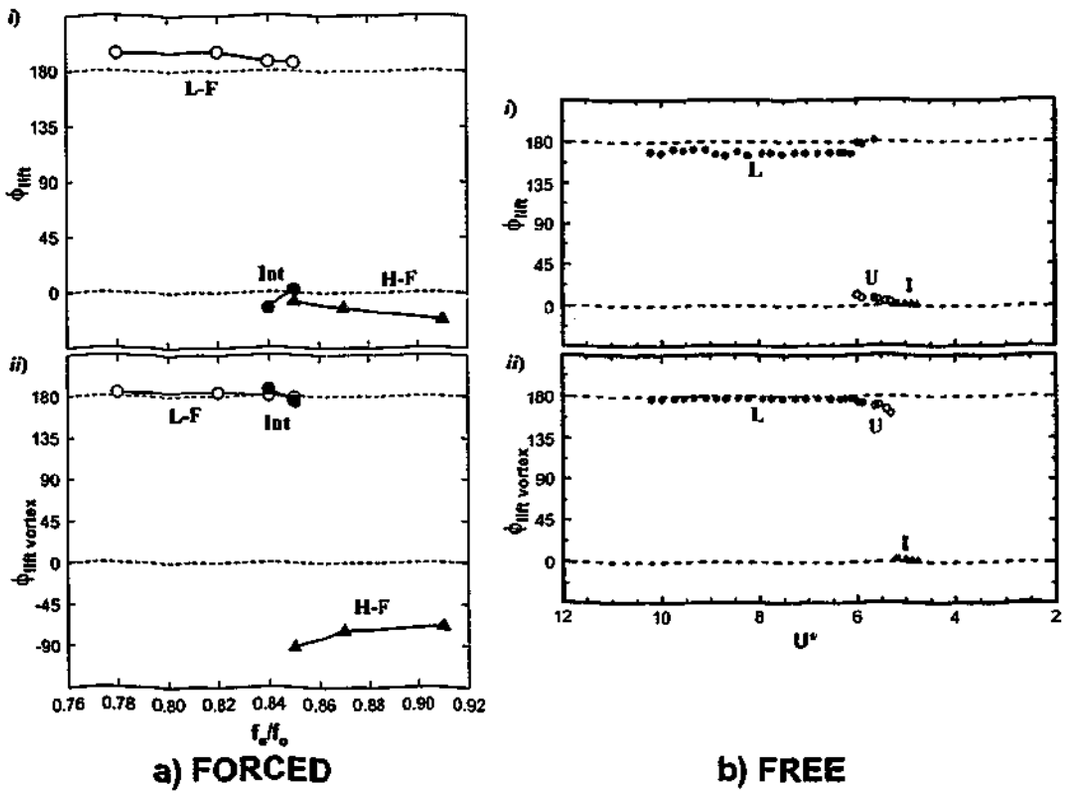

Figure 3-39 a) Variation of i) ϕl and ii) ϕlift vortex with fe/fo, showing the low-frequency (L-F), intermediate (Int) and high-frequency wake states for forced oscillations at A/D = 0.6 and Re = 2300. b) Variation of i) ϕlift and ii) ϕlift vortex with U*, showing the lower (L), upper (U) and initial (I) response branches for the freely oscillating cylinder with low m*ζ, [m* = 8.63 and ζ = 0.00151]. Note the decreasing U* axis. Reproduced from Govardhan & Williamson (2000).

In Figure 3-39 the phases of the total and vortex lift forces are shown for both the forced and freely oscillating cylinders. At A/D = 0.6 and Re = 2300, shown in Figure 3-39(a), the forced intermediate state is observed; correspondingly in Figure 3-39(b) the lift phases are shown for an elastically mounted cylinder with low mass-damping where the upper response branch is observed.

The values of the lift phases for the three wake states and three response branches are summarised in Table 3-3. The values of ϕ_{lift} and $\phi_{lift\ vortex}$ for the low-frequency state and lower response branch are similar, as are the values for the intermediate state and upper response branch. At both the low-frequency ↔ intermediate state transition and the lower ↔ upper branch transition the vortex lift phase shows very little change, but there is a large jump in the total lift phase. The values of $\phi_{lift\ vortex}$ for high-frequency state are significantly lower than for the corresponding initial response branch. However, the behaviour of the lift phases at the intermediate ↔ high-frequency state transition and the upper ↔ initial branch transition are essentially the same; ϕ_{lift} remains relatively unchanged while there is a large jump in $\phi_{lift\ vortex}$. Despite the fact that the behaviour of the lift phases shown in Figure 3-39(a) for the forced and free cases are very similar all but one data point for the forced oscillations fall outside the range $0°<(\phi_{lift}$ or $\phi_{lift\ vortex})<180°$. Therefore, the energy transfer for all but one of the forced cases is negative.

Table 3-3 Summary of the lift force phases for the forced wake states and the free response branches.

STATE	LOW-FREQUENCY	INTERMEDIATE	HIGH-FREQUENCY
ϕ_{lift} (varies with A/D & Re)	High (around 180° 2nd or 3rd quadrant)	Low (near 0°)	Low (near 0°)
$\phi_{lift\ vortex}$ (independent of A/D & Re)	High (≈180°)	High (≈180°)	Low (→ -90° at higher f_e/f_o)
BRANCH	**LOWER**	**UPPER**	**INITIAL**
ϕ_{lift} (varies with $m^*\zeta$)	High (2nd quadrant)	Low (just above 0°)	Low (above 0°)
$\phi_{lift\ vortex}$ (varies with $m^*\zeta$)	High (just below180°)	High (just below180°)	Low (just above 0°)

The total and vortex lift traces measured by Govardhan & Williamson (2000) for the initial, upper and lower free response branches are reproduced in Figure 3-40. The vortex force for the upper response branch is much smaller in amplitude than the corresponding potential force, where in this case the potential force is equivalent to the apparent mass force and is in-phase with the cylinder's displacement. Interestingly, the upper branch vortex lift trace has the same characteristic "double humps" as the intermediate state vortex lift traces shown in Figure 3-32(b) & Figure 3-35(b). The vortex lift trace for the initial response branch shown in Figure 3-40 is similar in magnitude to the

corresponding apparent mass trace. However, the amplitude of the vortex lift for the segment of the force trace in Figure 3-40 is actually significantly larger than the average value of $C_{L\,vortex}$ over the duration of the force trace. As discussed in the previous sections, our investigation of the forced case showed that immediately following the transition to the high-frequency state the vortex lift force was much smaller than the apparent mass force and, as shown in Figure 3-32(c), the small amplitude vortex lift force is not very sinusoidal. However, as f_e/f_o increases the relative amplitude of the vortex lift force for the high-frequency state increases and the vortex lift trace becomes more sinusoidal. The initial branch vortex lift trace in Figure 3-40 is similar to the high-frequency vortex lift trace shown in Figure 3-35(c) at higher values of f_e/f_o above the transition region.

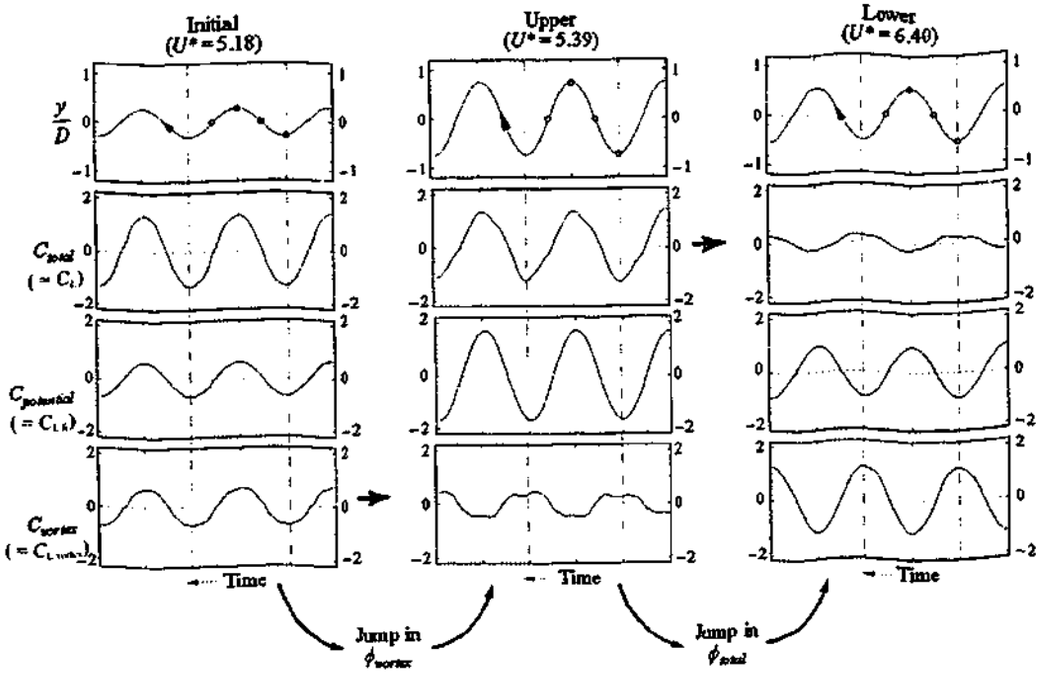

Figure 3-40 Relationship between the total lift force, potential or apparent mass force and the vortex lift force in the three response branches of an elastically mounted freely oscillating cylinder. Low $m^*\zeta$, [$m^* = 8.63$, $\zeta = 0.00151$]. Reproduced from Govardhan and Williamson (2000).

The results for the forced oscillation of a cylinder presented in section 3.4.3 show that the vortex lift and drag phases for a given wake state collapse reasonably well over a wide range of A/D and Re. However, the results of Govardhan & Williamson (2000) for a freely oscillating cylinder show that the value of $\phi_{lift\,vortex}$ varies with the mass and damping of the structure. As shown Figure 3-39(b), depending upon the response branch, at low values of mass-damping the vortex lift phase is close to either 0° or 180° and therefore close to the edges of the positive energy transfer region. At higher $m^*\zeta$ values only the initial and lower branches are observed and, as shown in Figure 3-41, the values of ϕ_{lift} and $\phi_{lift\,vortex}$ for both branches have moved away from the boundaries of positive energy transfer. Therefore, for a given free response branch $\phi_{lift\,vortex}$ does not collapse but

as $m^*\zeta$ increases the values of $\phi_{lift\ vortex}$ appear to move away from either 0° or 180° towards 90°. The variation of the lift phases with $m^*\zeta$ is consistent with the classical response of a mass on a spring described by numerous textbooks on the subject of vibrations.

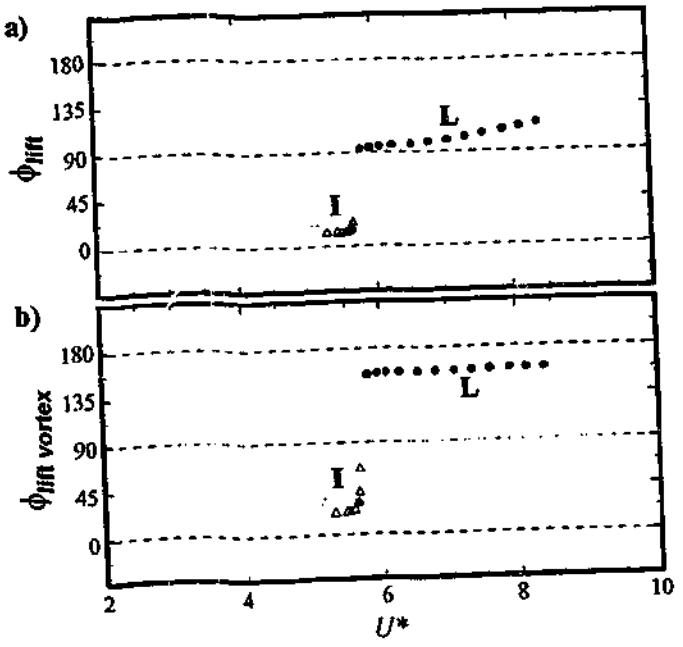

Figure 3-41 Variation of a) total lift phase and b) vortex lift phase for a freely oscillating cylinder with high $m^*\zeta$, [$m^* = 320$ and $\zeta = 0.00078$]. Reproduced from Govardhan & Williamson (2000)

As U^* varies for the freely oscillating cylinder both the cylinder's amplitude response and the Reynolds number vary. The largest variations in A/D occur at the transitions between the different response branches and also during the initial response branch. For a given free response branch the values of $\phi_{lift\ vortex}$ appear to be approximately constant, with the exception of the initial response branch at higher $m^*\zeta$ just before the transition to the lower branch. Therefore, for a given value of mass-damping the vortex lift phase for a particular response branch generally does not vary significantly with smaller changes in Re or A/D. The fact that $\phi_{lift\ vortex}$ does not vary significantly as A/D or Re changes is consistent with the collapse of $\phi_{lift\ vortex}$ over a wide range of A/D and Re for the forced oscillations. Many of the parameters for the forced and free cases are analogous. However, it is difficult to relate the mass and damping of the freely oscillating system to the forced case as the controlled motion is independent of these structural properties.

Figure 3-42 reveals an interesting feature that is evident in both the initial branch and the high-frequency state. For the low-frequency state and the lower response branch $\phi_{lift\ vortex}$ is approximately constant, however immediately following the transition to either the high-frequency state or the initial branch $\phi_{lift\ vortex}$ decreases sharply as f_e/f_o increases. This behaviour is not observed in the freely oscillating cylinder at lower $m^*\zeta$ values, and for the forced oscillations was

only observed at A/D = 0.4 and 0.5. The shape of the plots for the forced and freely oscillating cylinders in Figure 3-42 are almost identical, however the values of $\phi_{lift\ vortex}$ for the forced case clearly extend over a wider range than for the freely oscillating cylinder, which is constrained to regions of positive energy transfer.

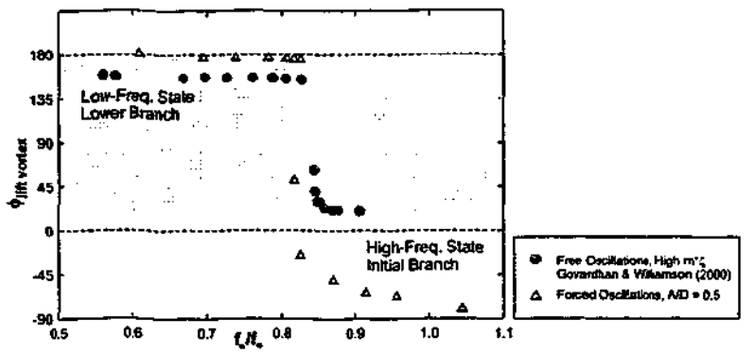

Figure 3-42 Variation of $\phi_{lift\ vortex}$ with f_e/f_o for both forced and free oscillations. The free oscillations at high $m^*\zeta$ have been replotted from the results of Govardhan & Williamson in Figure 3-41b. Forced oscillations: A/D = 0.5, Re = 2300. The shading indicates the region of positive energy transfer.

The variation of the forces, in particular ϕ_{lift} and $\phi_{lift\ vortex}$, for the forced and freely oscillating cases allows us to conclude that there is a strong link between the following forced wake states and free response branches:

low-frequency state ↔ lower branch

intermediate state ↔ upper branch

high-frequency state ↔ initial branch

3.7.2 Wake Structures

In this section the vorticity fields from the current investigation of forced cylinder oscillations are compared with the vorticity fields measured by Govardhan & Williamson (2000) for the freely oscillating case. Where possible the comparisons are made for similar values of A/D and Re. In general, we find that for the corresponding free response branches and forced wake states the phase of vortex shedding and the distribution of vorticity within the near wake are very similar.

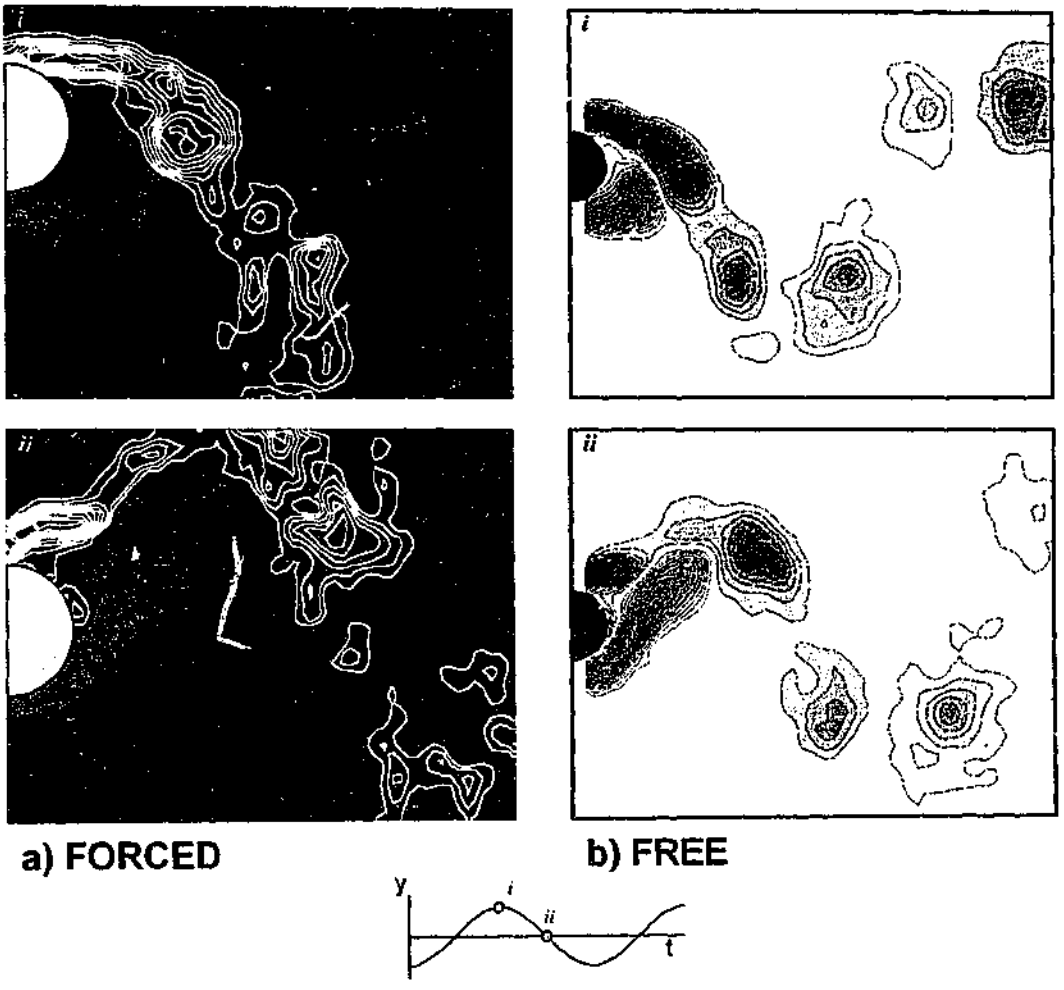

Figure 3-43 Phase averaged vorticity fields for a) forced low-frequency state, $A/D = 0.6$, $f_e/f_o = 0.82$, $Re = 2300$ and b) free lower response branch, $A/D = 0.6$, $U^* = 6.40$, $Re \approx 3700$, from Govardhan & Williamson (2000). The fields are shown (*i*) at the top and (*ii*) the mid-point of the downwards motion as shown in the displacement curve.

The phase averaged vorticity fields in Figure 3-43 show the wakes for the low-frequency state and the lower response branch, which occur at lower values of f_e/f_o or equivalently at higher U^* and $(U^*/f^*)St_o$ values. The forced and free cases are shown at similar Reynolds numbers of 2300 and 3700 respectively and at the same oscillation amplitude of $A/D = 0.6$. At the top of the oscillation the wakes of both the forced and freely oscillating cylinders in Figure 3-43(a & b)(*i*) show almost

identical formations of vorticity. In both cases the upper negative vorticity forms a long attached shear layer that extends well into the lower half of the wake. The portion of vorticity at the end of these shear layers is beginning to separate and in both cases will form a counter rotating pair with previously shed positive vorticity. At the mid-point in the cylinder's oscillation, shown in Figure 3-43(a & b)(*ii*), in both the forced and free cases the lower positive shear layer has a very similar upwards angle and the upper negative shear layer is about to separate from the cylinder. The general structure of the near wake, the timing of vortex shedding and the mode of vortex shedding for the low-frequency and the lower branch wakes in Figure 3-43 are remarkably similar.

The intermediate state and upper response branch are generally observed at values of f_s/f_o close to 1 or equivalently at reduced velocities close to 5. Characteristic phase averaged vorticity fields for these two cases are shown in Figure 3-44. The oscillation amplitude of $A/D = 0.5$ for the forced case is significantly smaller than for the free upper branch which is shown for $A/D = 0.81$, as our forced experiments did not extend to these large oscillation amplitudes. The "Griffin" plot reproduced from Govardhan & Williamson (2000) in Figure 1-29 shows that the upper response branch was observed at peak oscillation amplitudes of between $A/D \approx 0.75$ and 1.2. For the forced oscillations at $A/D = 0.5$ the intermediate state was observed for relatively short periods of time and was not observed at lower oscillation amplitudes. Thus, for the forced constant amplitude oscillations, the lower bounds of A/D at which the intermediate state exists appear to lie between $A/D = 0.4$ and 0.5. The values of A/D at which the intermediate state is observed is also expected to vary with other parameters such as Re and turbulence levels. The vorticity fields for the intermediate state in Figure 3-44(a) are shown at $A/D = 0.5$ rather than $A/D = 0.6$ because of the larger field of view allows improved comparison with the vorticity fields of the upper branch.

Despite the difference in the values of A/D for the forced and free cases in Figure 3-44 the structure of the wake and, in particular, the phase point at which large scale vortex shedding occurs are very similar. At the top of the oscillation the formations of attached vorticity for the intermediate wake and the upper branch wake are similar. However, for the free case at $A/D = 0.81$ in Figure 3-44b(*i*) a small portion of negative vorticity has separated from the end of the upper shear layer and the subsequent mode of vortex shedding is weakly 2P. The relative strength of the second vortex in each pairing is such that the first vortex dominates the pairing and, as shown by the evolution of the wake in Figure 3-44(b), the second vortex quickly dissipates. For the forced wake at the smaller oscillation amplitude, Figure 3-44(a)(*i*) shows that at the top of the oscillation a very small portion of negative vorticity has separated from the attached shear layer. However, this vortex structure is too small for the mode of vortex shedding to be described as 2P and the intermediate wake is 2S. At the mid-point of the downward stroke the near wakes for the intermediate wake and the upper branch wake are very similar and in both cases the large-scale negative vortex is about to be shed

high into the upper wake. The phase, with respect to the cylinder's displacement, of large-scale vortex shedding for the intermediate wake is the same as for the lower branch wake.

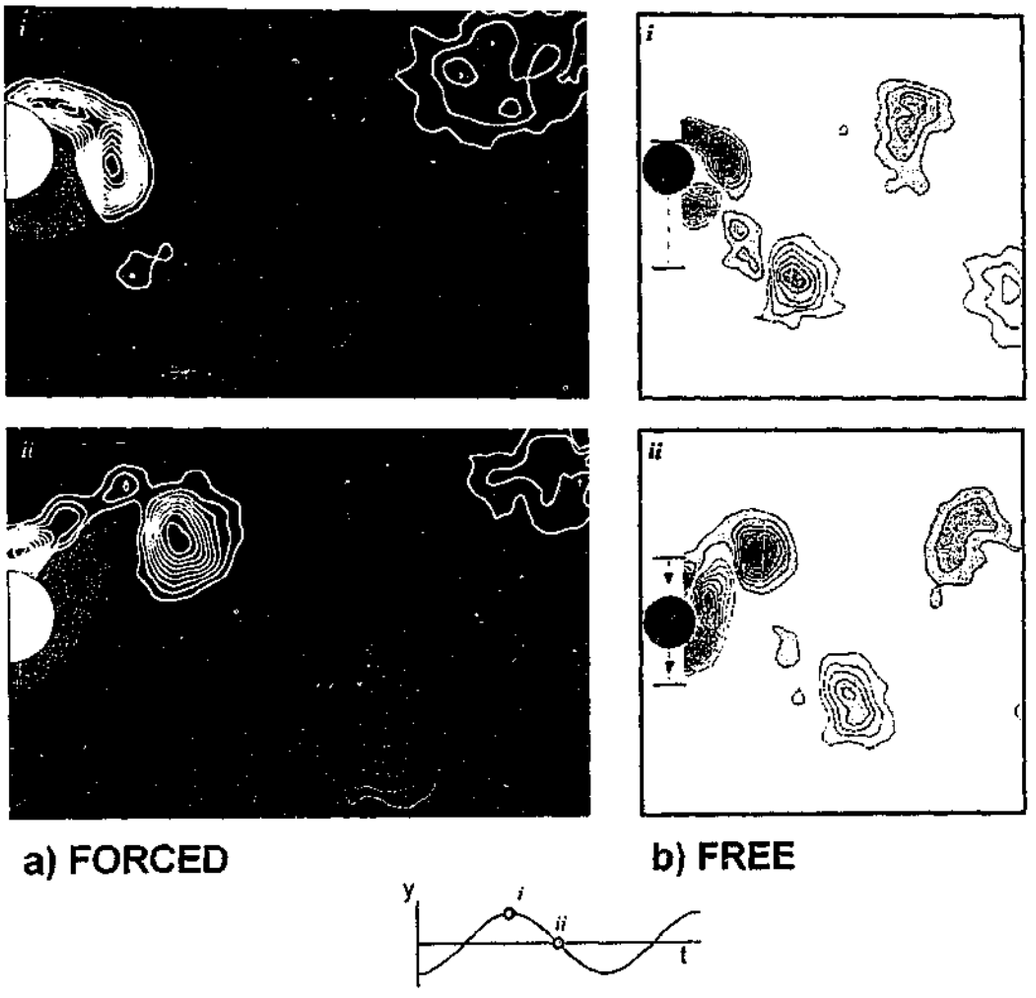

Figure 3-44 Phase averaged vorticity fields for a) forced intermediate state, $A/D = 0.5$, $f_e/f_o = 0.825$, $Re = 2300$ and b) free upper response branch, $A/D = 0.81$, $U^* = 5.39$, $Re \approx 3100$, from Govardhan & Williamson (2000). The fields are shown (*i*) at the top and (*ii*) the mid-point of the downwards motion as shown in the displacement curve.

Although the mode of vortex shedding for the intermediate state is classified as 2S and the upper branch wake is considered to be 2P, the general structure of the two wakes are very similar and they are both characterised by a very wide vertical distribution of shed vorticity. Our investigation of the 2P mode of vortex shedding for the low-frequency state, discussed in section 3.4, concluded that the formation of the second pairing in the 2P mode corresponds to the formation of long extended shear layers and is less likely to occur at lower oscillation amplitudes. Given that at $A/D = 0.81$ the wake in Figure 3-44(b) is only weakly 2P at lower values of A/D the wake may tend to the 2S mode of shedding. Thus, the observation of the 2S mode of shedding for the intermediate

wake at $A/D = 0.5$ and 0.6 is not inconsistent with weakly 2P mode of shedding observed for the upper branch at $A/D = 0.81$.

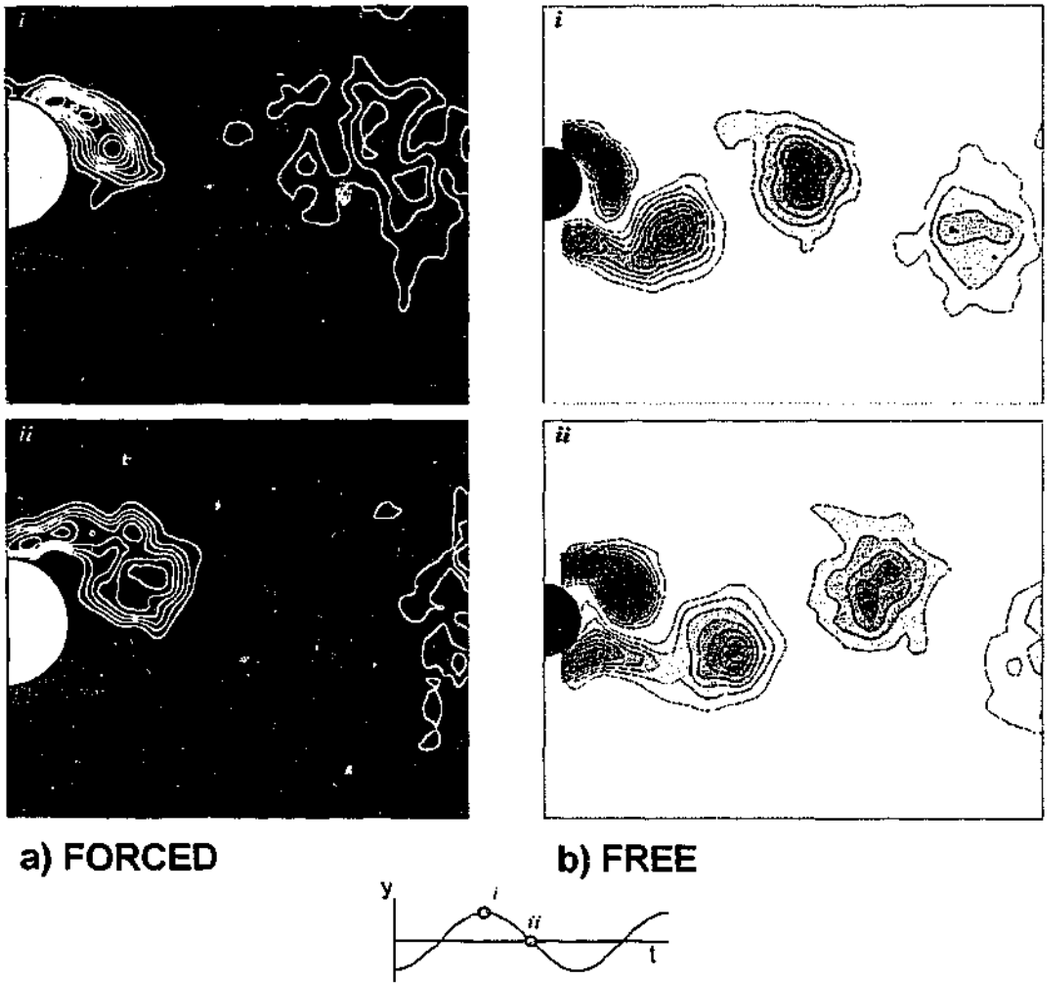

Figure 3-45 Phase averaged vorticity fields for a) forced high-frequency state, $A/D = 0.25$, $f_e/f_o = 1.145$, $Re \approx 4400$ and b) free upper response branch, $A/D = 0.33$, $U^* = 5.18$, $Re \approx 3000$, from Govardhan & Williamson (2000). The fields are shown (*i*) at the top and (*ii*) the mid-point of the downwards motion as shown in the displacement curve.

Examples of the vorticity fields for the forced and freely oscillating cylinders at higher values of f_e/f_o are shown in Figure 3-45 and Figure 3-46. These figures allow the comparison of the initial branch wake at $A/D = 0.33$ with high-frequency wakes at oscillation amplitudes of $A/D \approx 0.25$ and 0.4. In all cases the mode of vortex shedding is 2S and relative to the oscillation amplitude both the high-frequency and initial branch wakes are significantly narrower than the two sets of wakes at lower values of f_e/f_o (low-frequency, lower branch, intermediate and upper branch wakes). The phase point at which the positive vorticity is shed into the near wake appears to be similar for the high-frequency and initial branch wakes, although closer examination indicates that for the forced cases vortex shedding occurs slightly earlier in the oscillation cycle.

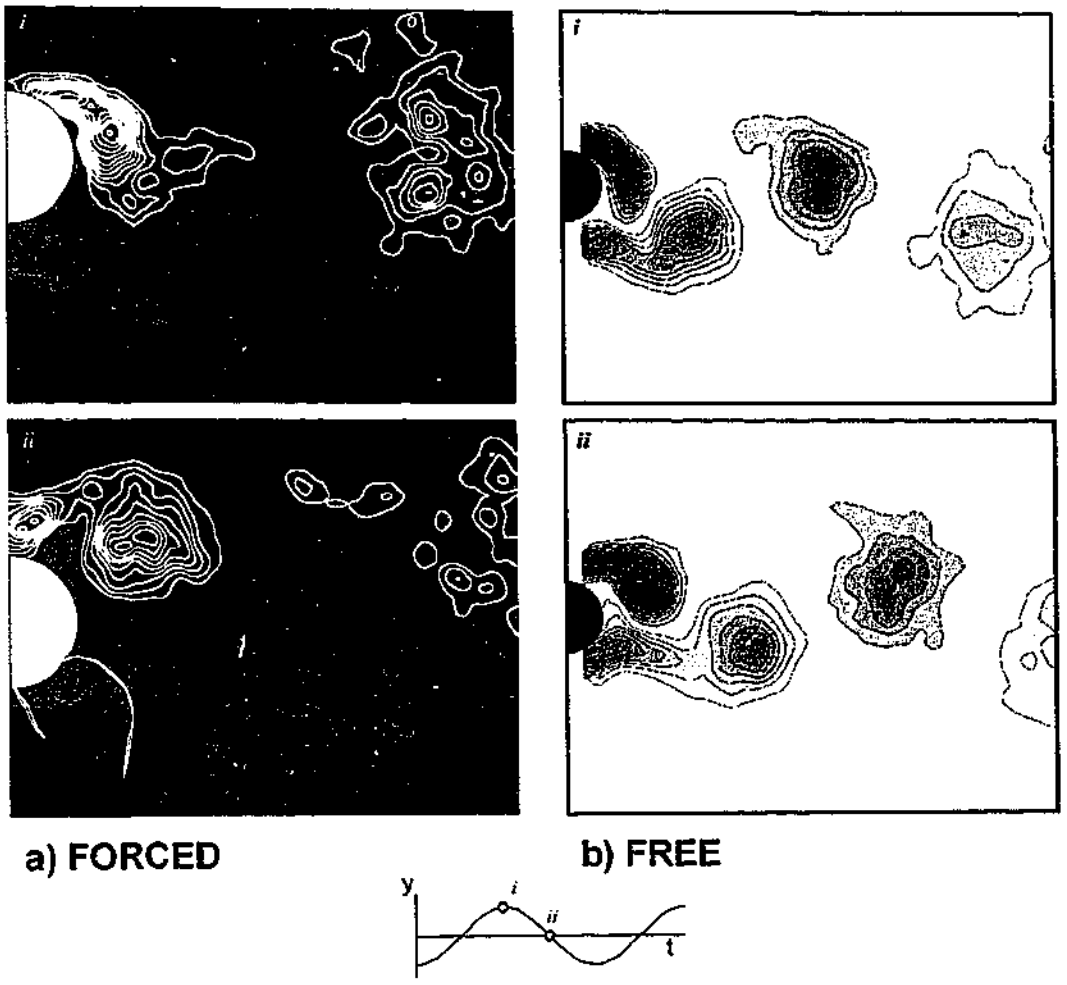

Figure 3-46 Phase averaged vorticity fields for a) forced high-frequency state, A/D = 0.4, f_e/f_o = 0.91, Re = 2300 and b) free upper response branch, A/D = 0.33, U^* = 5.18, $Re \approx 3000$, from Govardhan & Williamson (2000). The fields are shown (*i*) at the top and (*ii*) the mid-point of the downwards motion as shown in the displacement curve.

In general, the phase point at which separation of the large-scale vortex structures occurs is more difficult to determine for the high-frequency and initial branch wakes than for the wakes observed at lower values of f_e/f_o. The primary reason for this is that the vertical width of the high-frequency and initial branch wakes is quite small and, particularly at smaller oscillation amplitudes, the vortex shedding occurs over a longer portion of the oscillation cycle and is therefore not as clearly defined. The reduced wake width and less distinct vortex shedding for these wakes may be linked to the phase point at which vortex shedding occurs and the corresponding angle of the wake. For both the high-frequency and intermediate wakes, vortex shedding occurs as the acceleration of the cylinder causes the wake to angle away from the shear layer from which the vortex structure is about to be shed. For example, in Figure 3-46 the positive vorticity is being shed from the lower

shear layer, however the shedding occurs as the wake begins to tilt upwards due to the acceleration of the cylinder. In contrast, the vortex shedding from the low-frequency, lower branch, intermediate and upper branch wakes occurs as the acceleration of the cylinder causes the wake to angle towards the shear layer from which the vortex structure is about to be shed. The distinct upwards angle of these wakes as the negative vorticity is about to be shed from the upper shear layer is clearly evident in Figure 3-43 and Figure 3-44 and in these cases the phase of vortex shedding is more clearly defined.

In Figure 3-47 the average vorticity fields for the three forced regimes are compared with the corresponding averaged fields measured by Govardhan & Williamson for the freely oscillating cylinder. The average fields for each of the regimes are clearly different and there is a strong similarity between the average fields for the corresponding forced and free regimes. The regions of positive and negative vorticity in the average vorticity fields indicate that averaged over an oscillation cycle a region in the wake was dominated by vorticity of a particular sign. For a bluff body typically the lower half of the average vorticity field is dominated by positive vorticity shed originating from the lower shear layer, while the upper half of the field is dominated by negative vorticity. The average vorticity fields for the low-frequency and lower branch wakes correspond to the 2P mode of shedding. Near the base of the cylinder the 2P wakes have distinct regions of vorticity that originated from the opposite side of the wake. The regions of average vorticity which have crossed the centre-line of the wake are indicative of the strength of the vorticity in the long attached shear layers which, at certain points in the oscillation, extend across the base of the cylinder into the other half of the wake.

In Figure 3-47 two average wakes are shown for the low-frequency state at $A/D = 0.5$ and one corresponding lower branch wake is shown at $A/D = 0.6$. Of these three wakes the relative strength of the second vortex in the 2P pairing is strongest for the lower branch image in Figure 3-47(b)(*i*). Additionally, as discussed in 3.3.1, for the forced oscillations at $A/D = 0.5$ the relative strength of the second vortex decreases as f_e/f_o increases towards transition. In Figure 3-47(b)(*i*) where the second vortex in the 2P pairing is strongest the level of average vorticity more than 2 diameters downstream of the cylinder is very low, indicating that on average in this region there are roughly equal levels of positive and negative vorticity. As the relative strength of the vortices in the 2P pairing becomes less equal in Figure 3-47(a)(*i* & *ii*), there is an increase in the average vorticity further downstream of the cylinder.

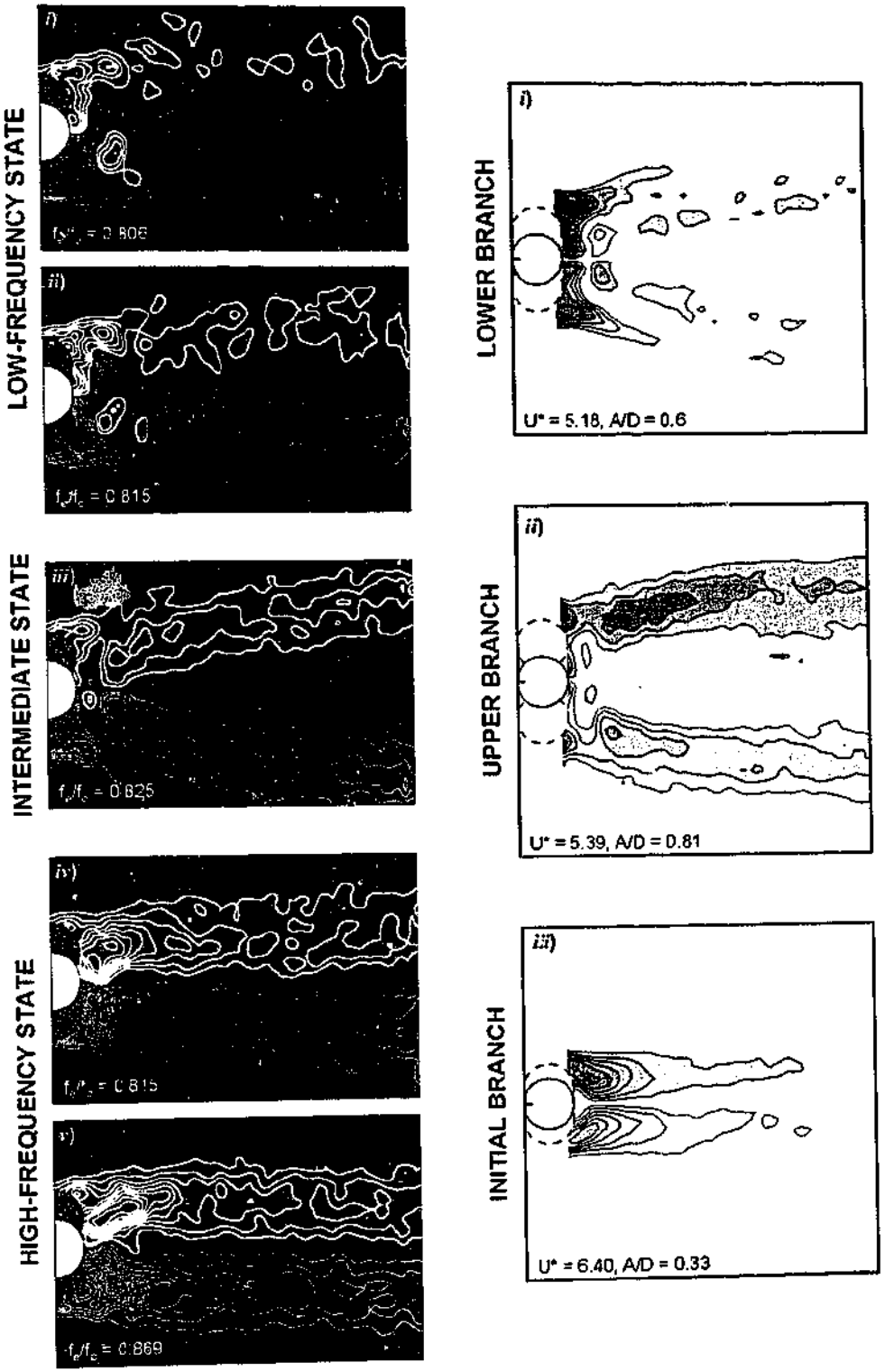

Figure 3-47 Average vorticity fields for the three wake regimes for a) forced oscillations at $A/D = 0.5$ and b) the freely oscillation cylinder, from Govardhan & Williamson (2000).

The average vorticity fields for the intermediate and upper branch wakes are characterised by wide bands of positive and negative vorticity that angle away from the centreline of the wake. The region immediately adjacent to the base of the cylinder has very low levels of average vorticity, with the exception of small portions of positive and negative vorticity that have crossed the wake's centreline. The average vorticity field adjacent to the base of the cylinder is consistent with the wake formation in Figure 3-44(a & b)(*ii*) where the attached shear layers from each side of the cylinder extend directly across the base of the cylinder. The angle of these shear layer is clearly greater than for the low-frequency and lower branch wakes in Figure 3-43. The increased angle of the intermediate and upper branch shear layers means that at different points in the oscillation cycle the attached positive and negative shear layers tend to occupy the same regions of space immediately adjacent to the base of the cylinder. Thus, the average levels of average vorticity adjacent to the base of the cylinder are very low. Further downstream of the cylinder, the shear layers occupy different regions of space, resulting in higher levels of average vorticity. The amplitude of oscillation for the averaged intermediate state wake in Figure 3-47(a)(*iii*) is much lower than for the corresponding upper branch wake in Figure 3-47(b)(*ii*), but despite the obvious difference in the width of the wakes the characteristics of the average fields are very similar.

The mode of vortex shedding for the high-frequency and initial branch wakes is 2S and the average vorticity fields in Figure 3-47 are very narrow. The averaged vorticity fields indicate that the positive and negative vorticity tends to be restricted to the lower and upper half of the wake respectively. Immediately after the transition to the high-frequency state at f_e/f_o = 0.815 the averaged high-frequency wake appears to be slightly wider than at the higher oscillation frequency of f_e/f_o = 0.869. This is consistent with our observations from the instantaneous and phase averaged vorticity fields.

3.7.3 Prediction of VIV Using Forced Oscillations

In the previous sections we have shown that forces on the cylinder and the structure of the wake for the different regimes of the forced and freely oscillating cylinders have many features in common. The cylinder is forced to oscillate with a purely sinusoidal motion and the key question is whether this motion adequately represents the motion of a freely oscillating cylinder? A second closely related question is whether the forced oscillations can predict the flow-induced motion?

For the cylinder to undergo sustained free motion there must be a net positive energy transfer per oscillation and thus $0° < \phi_{lift} < 180°$, or equivalently $0° < \phi_{lift\ vortex} < 180°$. The constraints of positive energy transfer for the free oscillations are clearly evident in the phase plots of Figure 3-39 and Figure 3-42. The results of both the current and previous experiments on the forced purely sinusoidal oscillation of the cylinder show that the energy transfer per oscillation can be either negative or positive. If the forced sinusoidal oscillations accurately simulate the vortex-induced

motion, then the regions where the forced oscillations generate negative energy transfer correspond to oscillation and flow parameters [$(U^*/f^*)St_o$, A/D, Re] at which vortex-induced vibrations do not occur. Similarly, if the above condition holds, the regions of positive energy transfer for the forced oscillations represent cases where vortex-induced vibrations may occur. If however, the purely sinusoidal controlled motion does not accurately simulate the vortex-induced motion then, for cases where free oscillations occur, the corresponding forced oscillations can result in either positive or negative energy transfer.

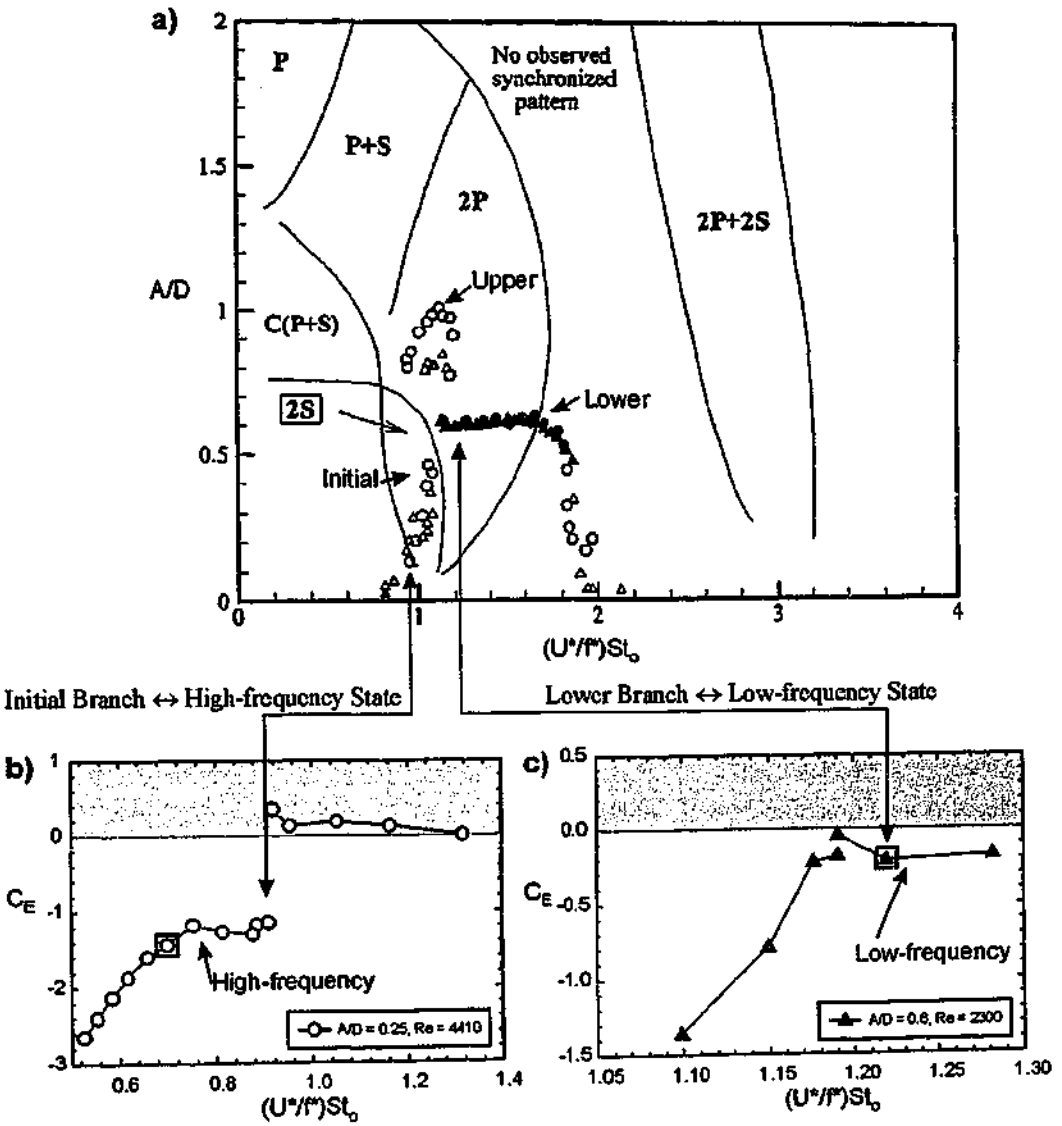

Figure 3-48 a) The parameters obtained by Khalak & Williamson (1999) for the initial and lower branches of a freely oscillating case are compared with the energy transfer for the forced oscillations for b) the high-frequency state at $A/D = 0.25$ and c) the low-frequency state at $A/D = 0.6$. The data points in b) and c) with the square around them correspond to the vorticity fields in Figure 3-45(a) and Figure 3-43(a) respectively.

Results from the current investigation are now compared with the results from Khalak & Williamson's (1999) investigation of the vortex-induced motion of an elastically mounted cylinder. For corresponding wake states and response branches and for parameters [$(U^*/f^*)St_o$, A/D, Re] where vortex vibration occurs it will be shown that the forced purely sinusoidal oscillations can generate negative energy transfer. In Figure 3-48(a) the amplitude response of the freely oscillation cylinder is plotted against $(U^*/f^*)St_o$, for $m^* = 1.19$ and $m^* = 8.63$. For these cases of relatively low $m^*\zeta$, the amplitude response shows a good collapse for the initial and lower branches. In Figure 3-48(b & c) the energy transfer for the forced oscillations are plotted as a function of $(U^*/f^*)St_o$ at $A/D = 0.25$ and 0.6 respectively, where the points corresponding to the vorticity fields in Figure 3-45(a) and Figure 3-43(a) are highlighted. For values of $(U^*/f^*)St_o$ between 1.19 and 1.29 the energy transfer for the low-frequency state at $A/D = 0.6$ and $Re = 2300$ is negative. However, Figure 3-48(a) shows that for values of $(U^*/f^*)St_o$ between 1.1 and 1.6 lower branch flow-induced vibrations occur at $A/D = 0.6$ and at similar Reynolds number of $Re \approx 3700$, where in this case the energy transfer must be positive. The images in Figure 3-43 show that despite the different directions of energy transfer the vorticity fields corresponding to these oscillation and flow parameters are very similar. Similarly, the free initial branch in Figure 3-48(a) shows that free oscillations occur at $A/D = 0.25$ for values of $(U^*/f^*)St_o$ of just under 1.0. However, the forced oscillations at $A/D \approx 0.25$ and similar values of $(U^*/f^*)St_o$ result in negative energy transfer.

The results in Figure 3-48 show that there are a number of cases where the forced purely sinusoidal oscillations result in negative energy transfer for flow and oscillation parameters where free oscillations are known to occur. In these cases, the forced sinusoidal motion does not predict the flow-induced motion and therefore, the sinusoidal motion does not simulate all the key components of the flow-induced motion. The failure of the forced motion to adequately model the vortex-induced motion for a single set of parameters indicates that the forced purely sinusoidal oscillations can not be used *a priori* to determine the flow-induced motion.

s from Khalak &
mounted cylinder.
$U^*/f^*)St_o$, A/D, Re]
dal oscillations can
nse of the freely
For these cases of
initial and lower
ns are plotted as a
rresponding to the
alues of $(U^*/f^*)St_o$
0.6 and $Re = 2300$
n 1.1 and 1.6 lower
nber of $Re \approx 3700$,
re 3-43 show that
sponding to these
h in Figure 3-48(a)
of just under 1.0.
, result in negative

d purely sinusoidal
meters where free
oes not predict the
he key components
model the vortex-
usoidal oscillations

4 STATIONARY CYLINDER NEAR A FREE-SURFACE

The close proximity of a boundary is known to affect the flow around a circular cylinder as discussed by Bearman & Zdravkovich (1978), Miyata *et al.* (1990), Sheridan *et al.* (1997), Hoyt & Sellin (2000) and Price *et al.* (2000). In this chapter, the modification of the Kármán wake as the cylinder approaches a free-surface is examined at relatively low Froude number. The different wake states as the cylinder approaches the free-surface are defined in terms of both wake and force properties. In particular, a link is established between changes in the structure of the near wake and the lift and drag forces on the cylinder.

As discussed in section 1.7 the boundary conditions generated by a free-surface differ from those of a solid boundary in at least two key areas: a free-surface is able to deform in response to pressure variations underneath the surface and along a clean free-surface (no surfactants) the shear stress is effectively zero. Therefore, in contrast to a solid surface, vorticity is not generated along a flat clean free-surface. The only circumstances where vorticity is generated at a free-surface are when free-surface deformation results in a curved boundary or when surface contamination results in non-zero surface shear. For the relatively low value of Fr used in this study (Fr = 0.166) disturbances of the free-surface tend to be damped out and large scale deformation of the free-surface is not observed. Thus, for all but the smallest cylinder depths the free-surface remained flat and the generation of vorticity due to the surface deformation was not observed.

4.1 FORCES ON A CYLINDER NEAR A FREE-SURFACE

Within the region where the cylinder's wake is affected by the free-surface, or the free-surface region, three distinctly different wake states were observed, described as modes I, II and III. Mode I occurs as the cylinder moves from the fully submerged state into the free-surface region, followed by modes II and III as the cylinder approaches, but does not pierce, the free-surface. In this section the different modes are described in terms of the lift and drag forces on the cylinder.

4.1.1 Variation of Lift and Drag with *h/D*

The variation of both the standard deviation and mean of the lift force are shown as the cylinder approaches the free-surface in Figure 4-1(a), while the corresponding values of the standard deviation and mean drag are shown in Figure 4-1(b). For cylinder depths of $h/D \geq 3.0$ the forces on the cylinder do not change significantly as the cylinder's depth is increased further, therefore for $h/D \geq 3.0$ the cylinder is effectively fully submerged. The net lift force on a fully submerged cylinder is zero and the mean distribution of vorticity about the centre-line of the wake is symmetric. The fact that the value of $C_{L\,mean}$ in Figure 4-1(a) is not exactly equal to zero at h/D = 3.0, is attributed mainly to experimental drift of the strain gauges. Within the free-surface region,

Australasian Book & Copy Bookbinders Melbourne 95236026

$h/D < 3.0$, there is a net negative lift force on the cylinder for all three modes, as shown in Figure 4-1(a). This result is consistent with the findings of Bearman & Zdravkovich (1978), Miyata *et al.* (1990) and Price *et al.* (2000) for a cylinder near either a solid-surface or free-surface. The net lift force on the cylinder indicates that the generation and distribution of vorticity is not symmetric about the centre-line of the cylinder; an analogous case is non-symmetric flow over an aerofoil. The value of $C_{L\,mean}$ becomes progressively more negative as the cylinder nears the free-surface, indicating that the wake becomes increasingly non-symmetric. The value of $C_{L\,mean}$ close to the free-surface is larger than the fluctuating component of the lift force, therefore at all times in the shedding cycle the forces generated by the flow field act to push the cylinder away from the free-surface.

In contrast to the relatively smooth variation of $C_{L\,mean}$ as the cylinder approaches the free-surface, there is a peak in the mean drag just before the transition from mode I to mode II. The peak value of $C_{D\,mean}$ is 14% higher than for a fully submerged cylinder. As h/D decreases further $C_{D\,mean}$ decreases and at $h/D = 0.079$, when the top of the cylinder is almost adjacent to the free-surface, the mean drag on the cylinder is slightly less than for a fully submerged cylinder.

The time varying lift and drag forces for mode I are sinusoidal, however for mode II and III the forces are neither sinusoidal nor periodic. Therefore, the standard deviation of the force signal, rather than the peak value, is used to describe the magnitude of the fluctuating component of the lift and drag forces. As h/D decreases below 3.0 initially there is a marked increase in $C_{L\sigma}$, the standard deviation of the lift, while the standard deviation of the drag $C_{D\sigma}$ shows only a slight increase. However, closer to the free-surface the values of both $C_{L\sigma}$ and $C_{D\sigma}$ for mode II and III drop below the values for a fully submerged cylinder. Examination of the lift traces and spectra show that as h/D decreases from 3.0 to 0.7 there is a significant increase in the energy at the Strouhal frequency, f_o, and the lift trace is strongly periodic. However, below $h/D = 0.5$ there are no distinct spectral peaks and the lift force is not periodic. At $h/D = 0.5$ the wake appears to be switching between mode I and mode II; at times the lift trace is strongly periodic and is consistent with mode I, while other times the lift force is consistent with mode II as it has only a small and irregular fluctuating component. The fluctuating component of the drag force for mode I is not as sinusoidal as the corresponding lift force and, while the transition from the submerged cylinder wake to mode I at $h/D \approx 3.0$ corresponds to a significant increase in $C_{L\sigma}$, $C_{D\sigma}$ is almost unchanged. At the transition from mode I to mode II there is a sharp decrease in the values of $C_{L\sigma}$ and $C_{D\sigma}$ as well a decrease in the spectral energy at f_o. Thus, as the cylinder approaches the free-surface it appears that periodic vortex shedding is suppressed.

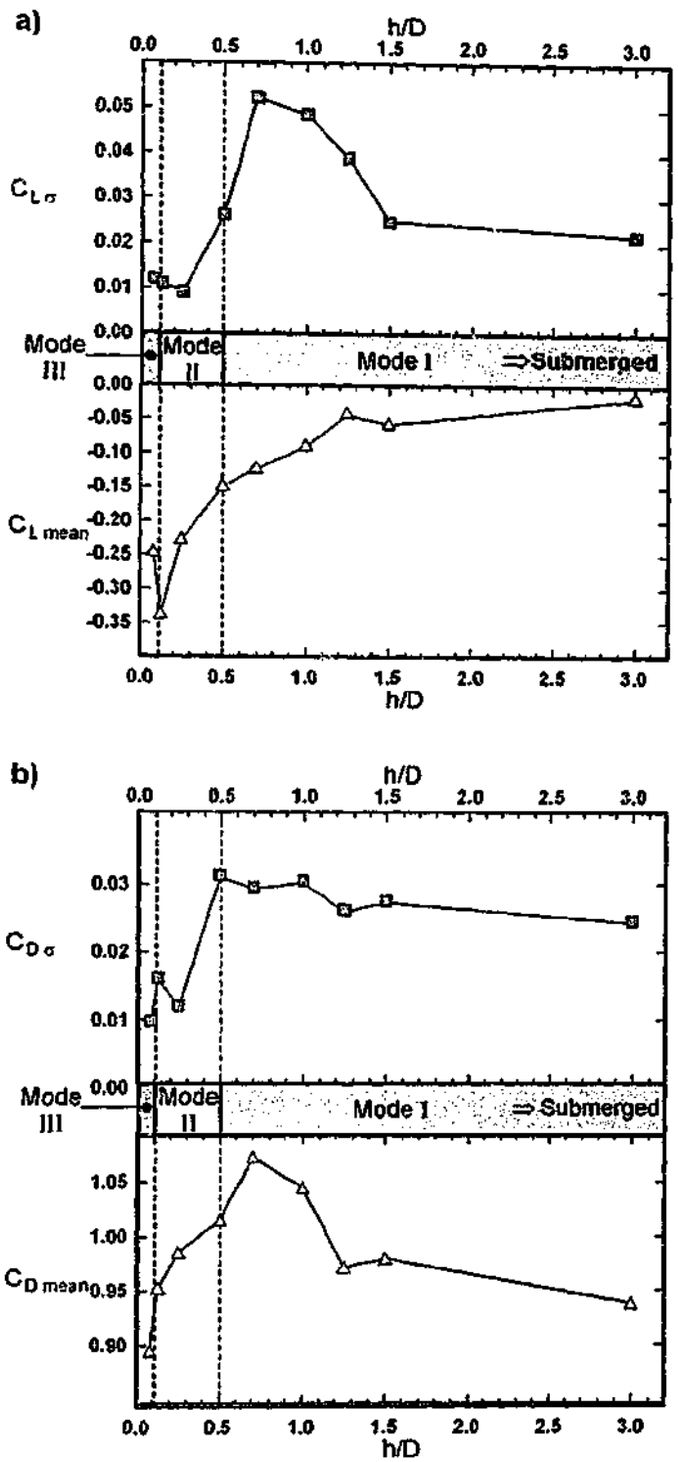

Figure 4-1 Variation of the mean and standard deviation of a) the lift force coefficient, and b) the drag coefficient with cylinder depth, h/D. The standard deviation of the lift and drag forces, CL σ and CD σ, respectively, are used to represent the amplitude of the forces, as for h/D < 0.5 the lift and drag traces are neither sinusoidal or periodic.

4.2 WAKE MODES NEAR A FREE-SURFACE

In section 4.1 the three different modes are described in terms of their characteristic force properties, however they can also be characterised by distinct changes in the structure of the near wake as the cylinder approaches the free-surface. In this section the instantaneous and mean vorticity fields for the three modes are presented and related to the forces on the cylinder.

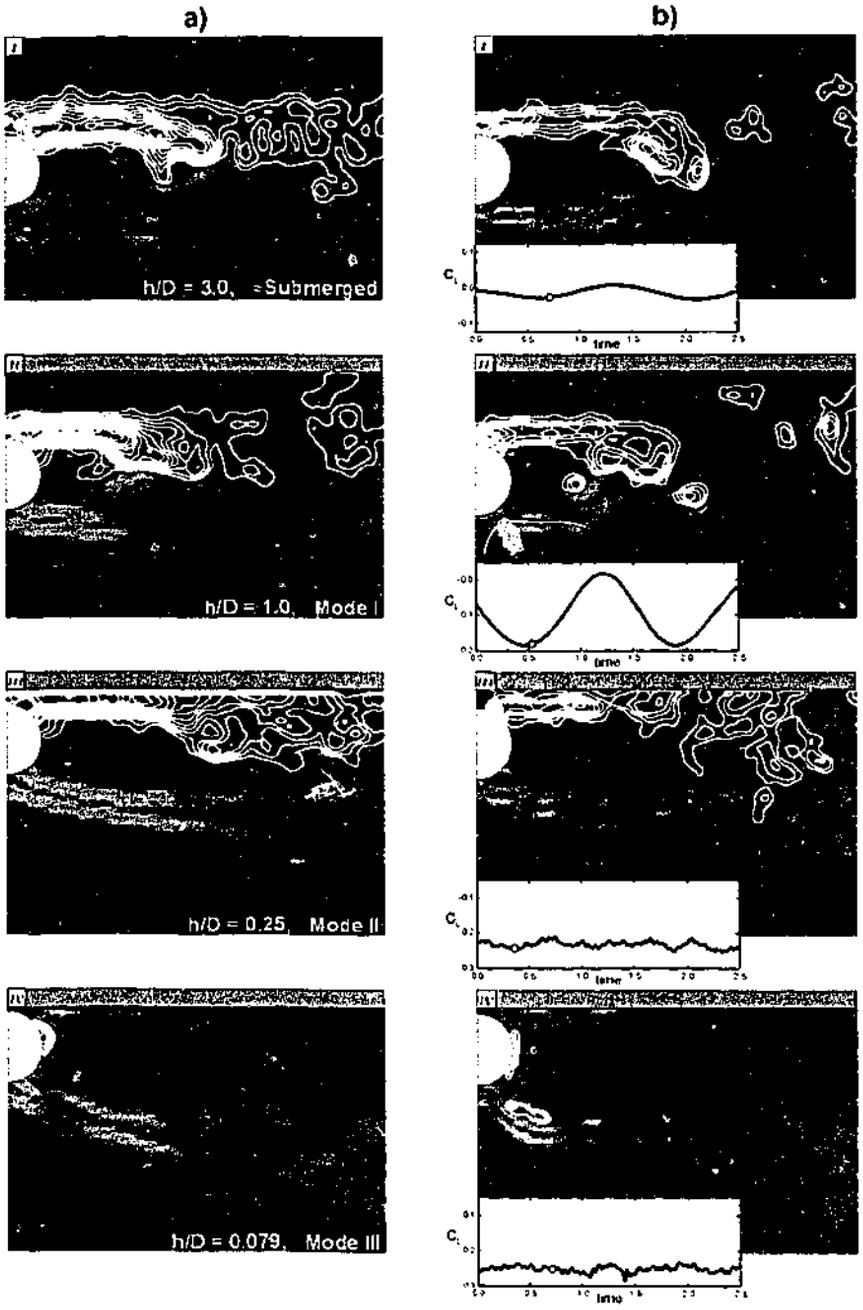

Figure 4-2 a) Mean vorticity fields, $\Delta\omega = 3.0$, and b) Instantaneous vorticity fields, $\Delta\omega = 1.0$, at h/D = *i*) 3.0, *ii*) 1.0, *iii*) 0.25 and *iv*) 0.079. The circle in the inserts represents the timing of each instantaneous image.

In Figure 4-2(a & b) the mean and instantaneous vorticity fields are shown for the three free-surface wake modes at h/D = 1.0, 0.25 and 0.079, as well as at h/D = 3.0 where the cylinder is effectively fully submerged. For the periodic mode I and fully submerged wakes at h/D = 1.0 and 3.0 the mean vorticity fields in Figure 4-2(i & ii) were calculated over 2 and 1 full Kármán cycles respectively.

4.2.1 Mode I Wake: Modified Kármán Wake

At the Reynolds number used for the current experiments, Re = 2100, the fully submerged cylinder wake has a very long formation length and, as shown by data reviewed in Zdravkovich (1997), the amplitude of the corresponding fluctuating lift is relatively small. The instantaneous wake of the fully submerged cylinder, shown in Figure 4-2(b)(*i*), is characterised by the development of long attached shear layers and the corresponding mean vorticity field in Figure 4-2(a)(*i*) shows that the recirculation region extends well downstream of the cylinder. For cylinder depths between $0.5<h/D<3.0$ vorticity of alternating sign is shed periodically into the near wake and the mode I wake is effectively a modified Kármán wake. However, comparing Figures 4-2(a)(*i*) and 4-2(a)(*ii*) it is clear that the formation length for the mode I wake is much smaller than for the fully submerged cylinder. Additionally, the force insert shows that there is a corresponding increase in the amplitude of the fluctuating lift force for the mode I wake.

For mode I Figure 4-1(a) shows that the standard deviation of the lift force increases as h/D decreases, where the values of $C_{L\sigma}$ are calculated over more than 300 Kármán cycles. In Figure 4-3 the instantaneous mode I vorticity fields and corresponding lift traces are shown at three different submergence depth: h/D = 1.5, 1.0 and 0.7. For comparison the effectively fully submerged case, at h/D = 3.0, is also shown. The instantaneous images were all acquired at times corresponding to local minima in the lift force. Thus, the wakes are at approximately the same point in their shedding cycles allowing direct comparison of the near wake structures as h/D decreases. As the cylinder moves from the fully submerged state to the mode I wake state there is a significant shortening in the wake length and a corresponding increase in the amplitude of the fluctuating lift force. Closer examination of the instantaneous wake lengths in Figure 4-3 reveals an inverse relationship between the instantaneous wake length and the instantaneous amplitude of the fluctuating lift force. This relationship is summarised in Figure 4-4(b) where, as shown in Figure 4-4(a), $L_{f\,inst}$ is a qualitative measure of the instantaneous wake length and $C_{L\,inst}$ is the instantaneous amplitude of the fluctuating lift force. $L_{f\,inst}$ is defined as the downstream distance from the centre of the cylinder to the topological centre of the attached positive vorticity, where to allow direct comparison $L_{f\,inst}$ is always measured at a local minimum of the lift force.

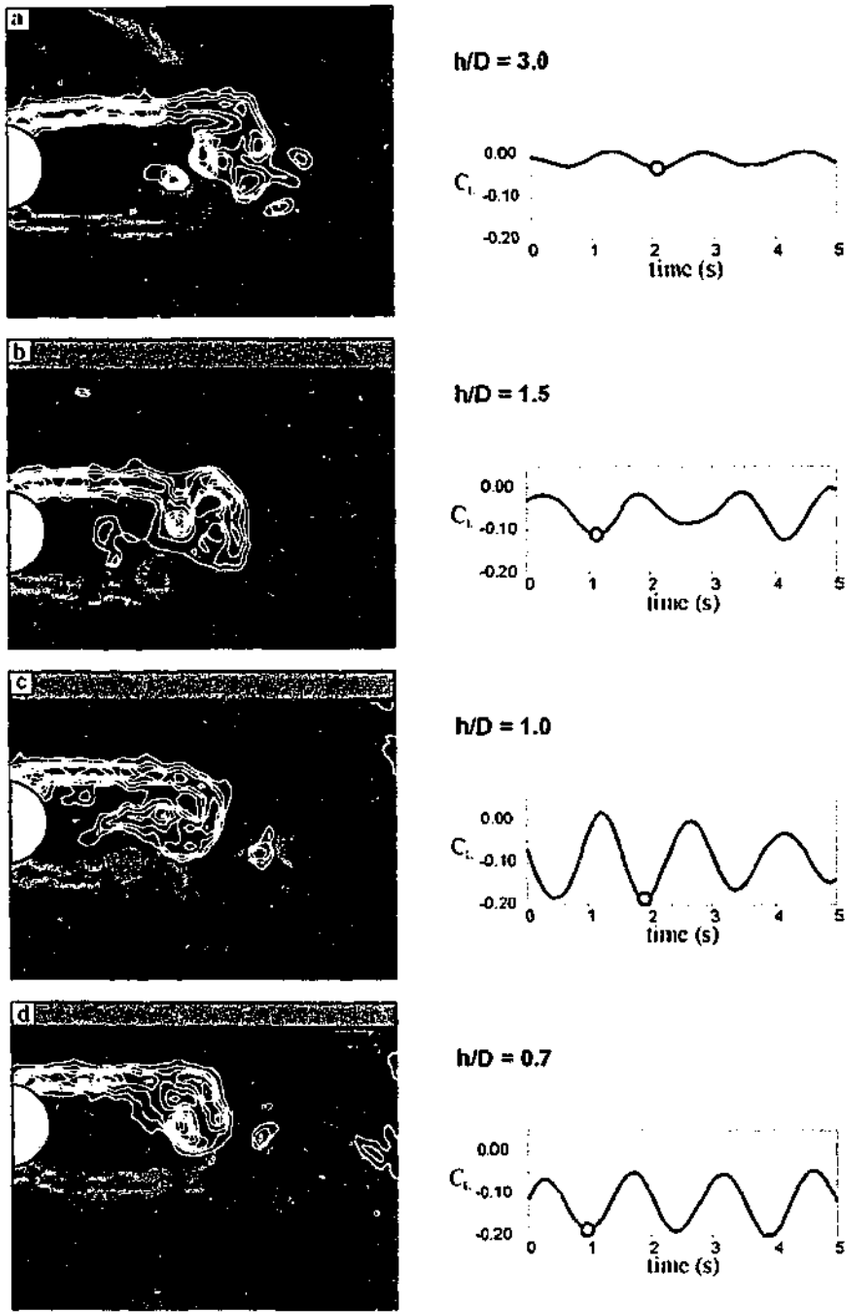

Figure 4-5 Instantaneous vorticity fields and lift traces for the mode I wake at a) $h/D = 3.0$, b) $h/D = 1.5$, c) $h/D = 1.0$ and d) $h/D = 0.7$. The timing of the images corresponds to local minima in the lift forces and is represented by the circles in the lift traces.

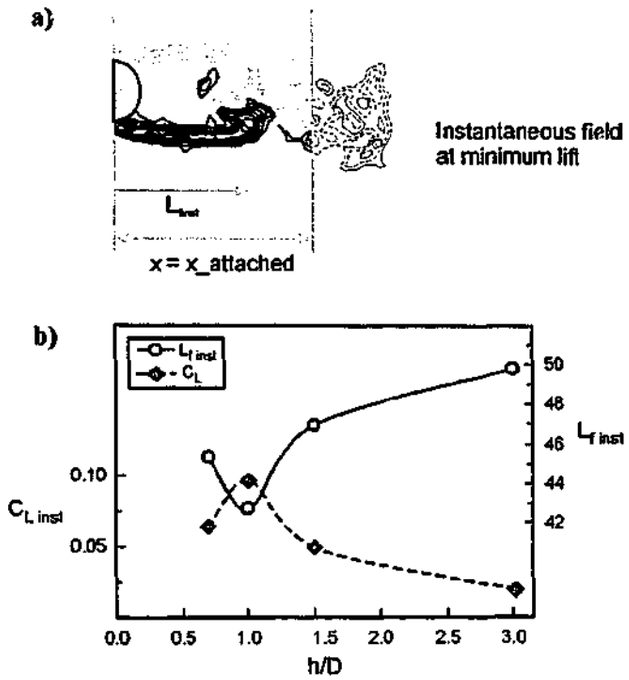

Figure 4-4 a) Instantaneous vorticity field showing the definition of instantaneous formation length, $L_{f\,inst}$ b) variation of $L_{f\,inst}$ and $C_{L\,inst}$ with h/D, where the data points correspond to the instantaneous images in Figure 4-3.

The wake of a stationary cylinder typically has a strong spectral peak at the Strouhal frequency and the large-scale features of the wake are essentially periodic. However, as evidenced by the changes in the amplitude of the fluctuating lift traces in Figure 4-3 there is some variation in the structure of the wake and the corresponding forces on the cylinder between cycles. The time averaged lift forces on the cylinder in Figure 4-1(a) show that for the mode I wake the amplitude of the fluctuating lift force increases with decreasing h/D. However, at a given instant this trend does not always hold and in Figures 4-3 and 4-4 the amplitude of the fluctuating lift force at $h/D = 0.7$ is less than at $h/D = 1.0$. The smaller lift amplitude at $h/D = 1.0$ corresponds to a slightly longer wake length, and the inverse relationship between $L_{f\,inst}$ and $C_{L\,inst}$ appears to hold at all times. This suggests that there might be a similar inverse relationship between the mean formation length and $C_{L\sigma}$. The wake length was not qualitatively measured over a large number of cycles and therefore it is not possible to definitively establish a link between $C_{L\sigma}$ and a mean formation length as the cylinder approaches the free-surface. However, it is clear that as the cylinder moves closer to the free-surface the initial increase in $C_{L\sigma}$ is associated with a decrease in the wake length.

The Kármán wake of a fully submerged cylinder has a symmetric mean distribution of vorticity about the centre-line of the cylinder and the corresponding mean lift force on the cylinder is zero. The values of $C_{L\,mean}$ for the mode I wake become increasingly negative as the cylinder approaches

the free-surface indicating that there is a net generation of positive vorticity and the mode I wake becomes increasingly non-symmetric about the cylinder's centre-line. However, due to the periodic nature of the mode I vortex shedding and the limited field of view, it is difficult to quantify the net circulation of the wake. Interestingly, for $h/D \geq 0.7$ the non-symmetry of the wake appears to amplify the response of the wake to the Kármán instability; the vortex shedding occurs closer to the cylinder and there is a corresponding increase in the amplitude of the fluctuating forces on the cylinder. Intuitively this suggests that a relatively small imbalance in the level of vorticity increases the interaction between the shear layers, resulting in vortex shedding occurring closer to the cylinder. Significant variations in the frequency of the Kármán shedding were not observed. Therefore, despite the fact that the interaction between the shear layers occurs closer to the cylinder, the duration or period of a shedding cycle is relatively unchanged. As h/D is decreased further there appears to be a point, $h/D \approx 0.5$, where the non-symmetry of the wake begins to inhibit, rather than enhance, the interaction between the shear layers. Beyond this point periodic Kármán shedding was not observed.

4.2.2 Mode II Wake: Flow Attached to Free-Surface

As h/D decreases below $h/D = 0.5$ there is a sharp drop in the amplitude of the fluctuating forces on the cylinder and, as shown in Figure 4-2(*iii*), a marked change in the structure of the near wake. The mode II wake is characterised by the formation of long shear layers and there and there is no periodic shedding of vorticity. As shown by the force insert in Figure 4-2b(*iii*) the lift trace is no longer periodic and there are no strong peaks in the corresponding lift spectra. Additionally, examination of the lift traces indicates that the major contributions to the standard deviation of the lift force, $C_{L\,\sigma}$, are associated with fluctuations in $C_{L\,mean}$. For the mode II wake the attached shear layers of both the instantaneous vorticity field, shown in Figure 4-2b(*ii*) and the mean vorticity field in Figure 4-2a(ii) are longer than for either the mode I or fully submerged wakes. The upper negative shear layer is parallel to the free-surface while the positive shear layer has a distinct downward angle. The flow over the top of the cylinder forms a jet of high-speed fluid that separates from the cylinder but remains attached to the free-surface, where the width of this jet appears to depends primarily on h/D. The angle at which the upper shear layer separates from the cylinder is similar to the corresponding angle for the fully submerged and mode Kármán type wakes. The fluid underneath the cylinder separates earlier than for a Kármán wake and the lower shear layer has a distinct downward angle away from the free-surface. The flow visualisation of the mode II wake at $h/D = 0.25$ in Figure 4-5, clearly shows the jet of high speed fluid flowing over the cylinder and the extended region of low speed flow behind the cylinder. The movement of the lower separation point and the resultant angle of the positive shear layer is consistent with the rotation of the front stagnation point towards the free-surface observed by Miyata *et al.* (1990).

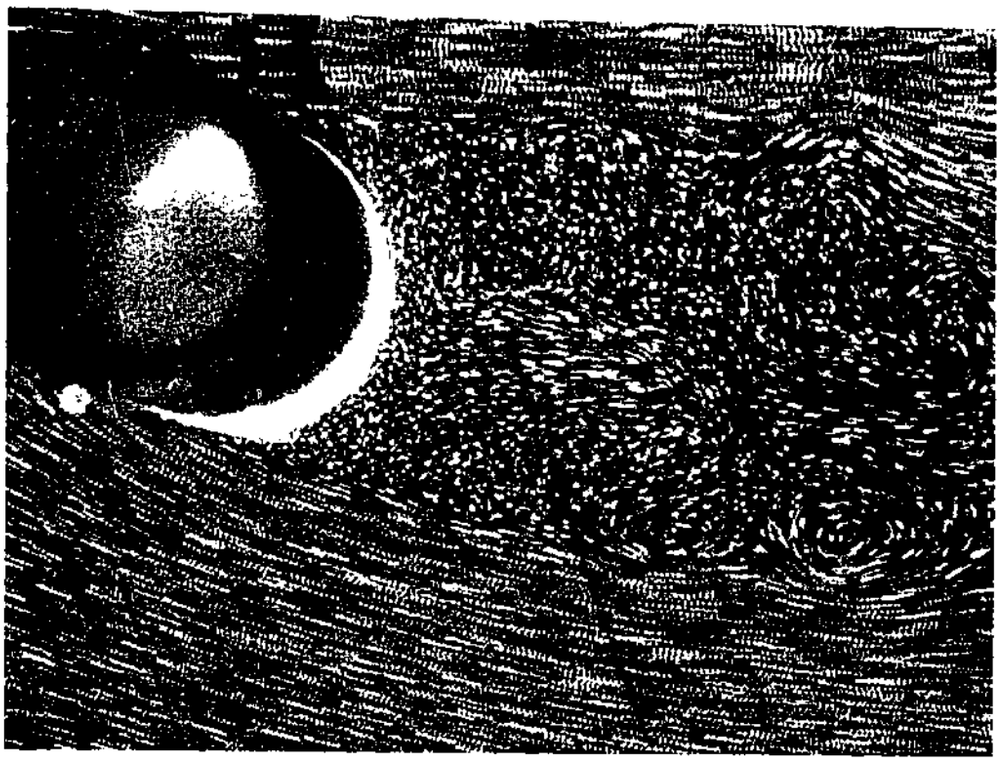

Figure 4-5 Flow visualisation of the mode II wake at h/D = 0.25 using multiply exposed particles with no bias velocity.

The general structure of the mode II mean vorticity field in Figure 4-2(a)(*iii*) is not significantly different from that of the corresponding instantaneous wake in Figure 4-2(b)(*iii*). Thus, the dominant structures in the near wake are non-periodic. Vorticity is shed from the mode II wake but the final separation of the vorticity from the long shear lays occurs well downstream from the cylinder and the shear layers interact in a relatively disorganised fashion. The sharp drop in $C_{L\sigma}$ and $C_{D\sigma}$ as *h/D* decreases below 0.5 is consistent with the non-periodic nature of the mode II wake and the cessation of coherent vortex shedding. The marked non-symmetry of the wake is also consistent with the large net negative lift force on the cylinder.

The mode II wake does not appear to cause deformation of the free-surface and the corresponding generation of free-surface vorticity, and is essentially the same as the wake state observed by Sheridan *et al.* (1997) at *Fr* = 0.22. Sheridan *et al.* (1997) found that when they increased the Froude number to 0.35 and 0.60 the wake state still displayed characteristic features of the mode II wake, including the characteristic jet of high speed fluid over the cylinder and the angled lower wake. However, as discussed in section 1.7.4 at higher *Fr* there was also significant free-surface deformation and the generation of free-surface vorticity.

4.2.3 Mode III Wake: Separated Jet

The mode III wake was observed at the smallest submergence depths of $h/D < 0.125$. At these depths the separation of the upper shear layer from the cylinder is delayed and the thin jet of fluid above the cylinder separates from the free-surface. At $h/D = 0.079$ the jet was unsteady and alternated between remaining attached to the back of the cylinder and separating from the cylinder to form a thin free jet. For the majority of the time the thin jet of fluid remained attached to the cylinder and there was a systematic upstream movement of the low speed fluid directly behind the cylinder. The migration of fluid upstream appeared to result in the attached jet becoming unstable causing it to separate from the cylinder as a free jet. The free jet persisted for short periods of time and tended to "flap" at angles of between 45 and 60 degrees to the free-surface. The short periods of time during which the jet separated from the cylinder coincided with a general downstream movement of the low speed fluid behind the cylinder.

In Figure 4-2(b)(*iv*) the high speed fluid between the free-surface and the cylinder separates from the free-surface but remains attached to the back of the cylinder, forming an attached jet of flow running downwards into the lower shear layer. The separation of the jet of fluid from the free-surface indicates that positive free-surface vorticity is generated at the point of separation. The jet on the back surface of the cylinder clearly contains both positive and negative vorticity and there is also significant positive vorticity underneath the free-surface, thus the separation of the jet of high speed fluid coincides with the generation of positive free-surface vorticity. Despite the generation of free-surface vorticity, a clear deformation of the free-surface above the cylinder was not detected during the experiments. The fact that free-surface deformation was not observed indicates that either that the deformation of the free-surface was small, or that the free-surface vorticity was generated by another mechanism. For the case of a perfectly clean free-surface the effectively zero shear stress along the free-surface precludes the generation of free-surface vorticity by any mechanism other than free-surface deformation. However, if the free-surface is contaminated the shear stress generated by surfactants on the free-surface may result in the generation of free-surface vorticity.

For the mode III wake the jet of fluid generated by flow over the top of the cylinder is very thin and the finer structures of the jet were not resolved by the PIV data. When the jet remained attached to the cylinder it tended to be better resolved than the separated free jet, indicating that the attached jet may be slightly wider. The mean vorticity field in Figure 4-2a(*iv*) was calculated over a time period where the jet remained attached to the cylinder and therefore does not fully represent the unsteady wake. However, the percentage of time during which the jet was separated from the cylinder was relatively small, consequently it is expected that a mean vorticity field calculated over much longer time periods would not differ significantly from the field in Figure 4-2(a)(*iv*). With the exception of the relatively short lived formation of the free jet the general structure of the mode

III wake is relatively steady and the instantaneous wake in Figure 4-2(b)(*iv*) does not differ significantly from the mean vorticity field in Figure 4-2(a)(*iv*).

The flow visualisation in Figure 4-6 shows the formation of the free jet where the fluid moving over the top of the cylinder separates from both the cylinder and the free-surface. The free jet angles across the back of the cylinder and in Figure 4-6 the formation of a recirculation region between the jet and the cylinder as well as the interaction of the jet with the lower shear layer are clearly visible.

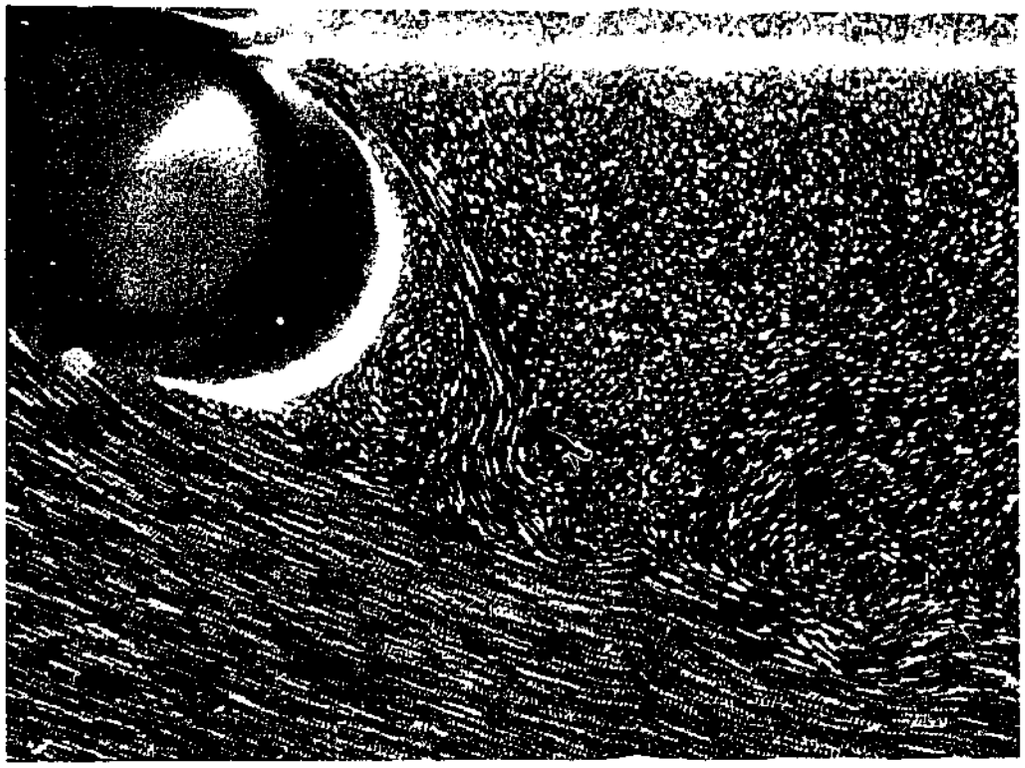

Figure 4-6 Flow visualisation of the mode III wake at h/D = 0.079 using multiply exposed particles with no bias velocity.

The generation of net positive vorticity is particularly obvious for the mode III wake in Figure 4-2(a)(*iv*), and the corresponding value of $C_{L\,mean}$ is large and negative. The reason for the small increase in $C_{L\,mean}$ at $h/D = 0.079$ is not known, although it may be due to the relatively small sample time for this data point or it may be directly related to changes in the structure of the wake. As for the mode II wake, the lack of organised vortex shedding from the mode III wake results in small non-periodic fluctuations of the lift force, and the lower shear layer has a characteristic downwards angle.

At $Fr = 0.16$ the mode III wake was only observed at $h/D = 0.079$, however the work of Sheridan *et al.* (1997) indicates that at higher Froude number the mode III wake state persists through to deeper cylinder depths. Sheridan *et al.* (1997) found that for the smallest values of h/D considered in their

experiments the jet of fluid over the top of the cylinder remained attached to the cylinder and the wake appeared very similar to mode III wake in Figure 4-2(*iv*). When the cylinder was moved further away from the free-surface the high speed fluid formed a strong, apparently stable free-jet and there was a clear depression of the free-surface behind the cylinder. The deformation of the surface did not result in the formation of large scale free-surface waves and the majority of the free-surface vorticity separated from the free-surface. Sheridan *et al.* (1997) also found that by increasing Froude number there was an increase in the cylinder depths at which the free-jet wake mode was observed. This trend is consistent with the results of our experiments at much lower *Fr*, as in our experiments mode III wake was only observed for very small values of *h/D*. The experiments at higher Froude number indicate that the jet separating from the free-surface can exhibit two stable wake states; the formation of a jet which remains attached to the cylinder and the formation of a free-jet, where the wake state depends on both *h/D* and *Fr*. It is therefore possible that the mode III wake observed in these experiments at much lower *Fr* is actually alternating between two different wake states.

4.2.4 Angle of Lower Shear-Layer

The lower shear layer for both the mode II and III wakes has a characteristic downward angle. As shown schematically in Figure 4-7, the angle of the lower shear layer, $\theta_{shear\ Layer}$ was quantified by finding the locus of maximum positive vorticity and calculating the average angle over one cylinder diameter downstream of the cylinder. The four instantaneous vorticity fields in Figure 4-8(a - d) and the corresponding values of $\theta_{shear\ layer}$ plotted in Figure 4-8(e) clearly show that there is an increase in the downward angle of the lower shear layer as the cylinder approaches the free-surface.

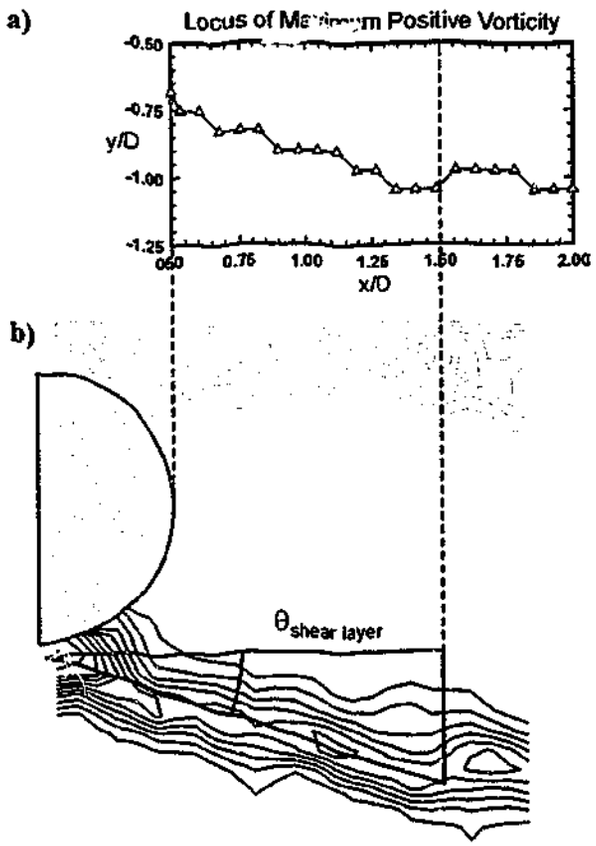

Figure 4-7 The instantaneous angle of the lower shear layer as defined by the average angle of the locus of maximum positive vorticity in the first cylinder diameter downstream of the back of the cylinder. The maximum positive vorticity in a) corresponds to the instantaneous mode II wake in b).

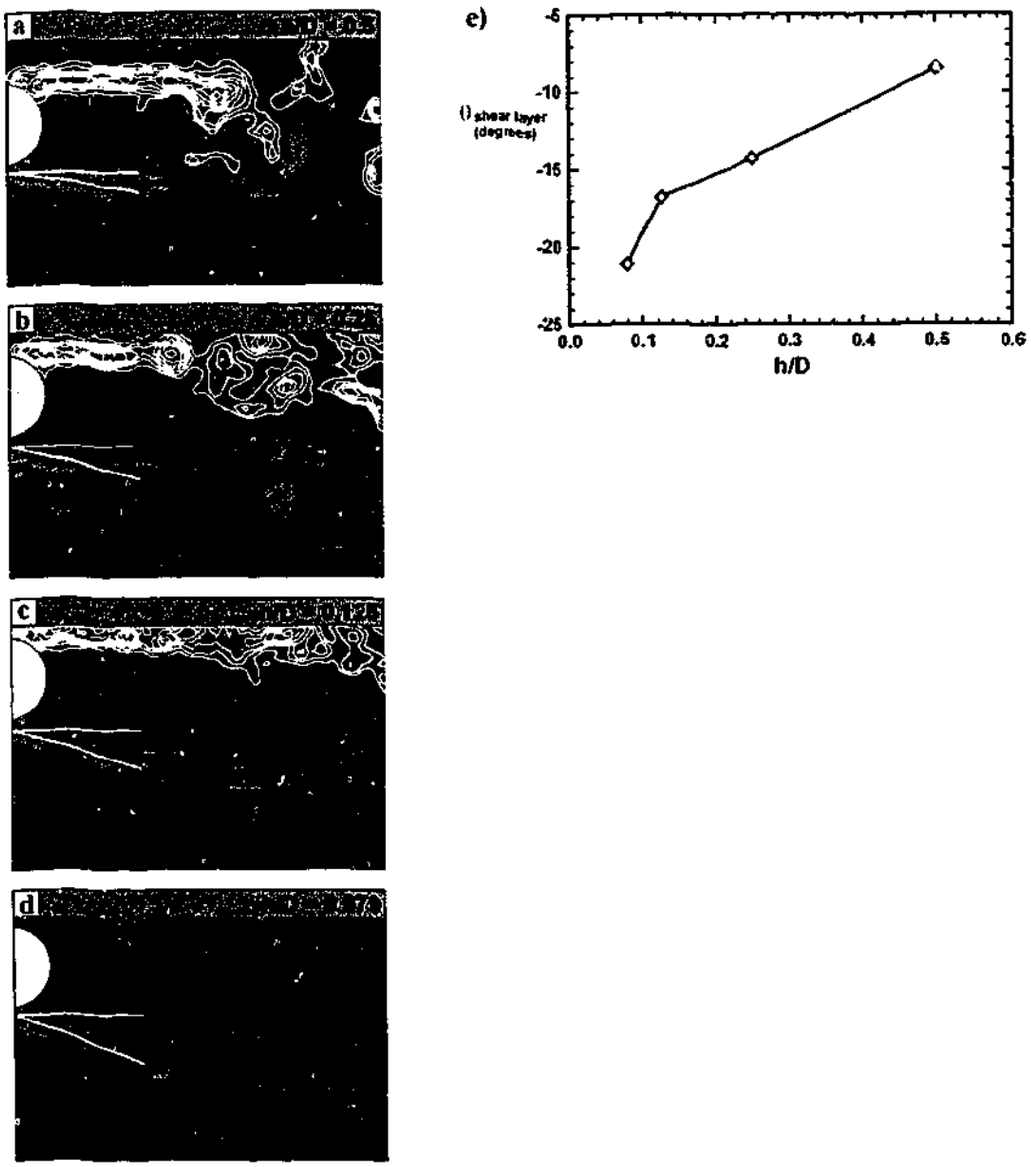

Figure 4-8 Instantaneous vorticity fields for mode I$_s$ and mode III wakes at a) h/D = 0.5, h/D = 0.025, c) h/D = 0.125 and d) h/D = 0.079.

4.2.5 Contamination of Free-Surface

As discussed in section 1.7.5, in a free-stream flow a surfactant on the free-surface is pushed downstream and the point at which the free-surface becomes contaminated tends to be clearly defined, typically by a small ridge known as the Reynolds ridge. Downstream of the ridge the contamination forms a boundary layer and vorticity can be generated at the surface without free-surface deformation. The boundary layer underneath a contaminated free-surface is typically thin and often difficult to detect. The illumination of the free-surface by the laser allows the detection

of free-surface contamination and in negative PIV and flow visualisation images the contamination corresponds to a solid white line.

At the deeper cylinder depths, $h/D \geq 0.25$, free-surface contamination was not observed in the vicinity of the cylinder. However, as the cylinder approached the free-surface the restriction of flow over the cylinder appeared to reduce the velocity of the free-surface flow behind the cylinder, allowing the accumulation of surfactant. It is not known if the blockage caused by the close proximity of the cylinder to the free-surface allowed a pre-existing region of free-surface contamination to move upstream, or if the blockage caused the formation of a separate region of free-surface contamination. The free-surface contamination appeared to contain a significant number of PIV particles, indicating that it might be difficult to obtain a perfectly clean free-surface and still use PIV to measure the velocity field.

For the mode II wake at $h/D = 0.125$ the free-surface contamination began approximately three cylinder diameters downstream of the cylinder and at this point the high speed fluid separated from the free-surface. The boundary layer underneath the contaminated free-surface grew rapidly and there was significant positive surface vorticity downstream of the Reynolds ridge. At the very smallest cylinder depth of $h/D = 0.079$, the free-surface contamination, clearly obvious in Figure 4-6, started directly above the cylinder. This was only the cylinder depth where the high speed fluid over the top of the cylinder separated from the free-surface before separating from the cylinder. The separation of the jet from the free-surface is not possible without the formation of positive vorticity at the free-surface and, as discussed above, the only mechanisms that would cause this are free-surface deformation and surface contamination. Therefore the presence of the surface contamination may have promoted the separation of the jet from the free-surface. The experiments of Sheridan *et al.* (1997) were conducted in a similar experimental facility and the flow was seeded with identical PIV particles but it is not known to what extent those experiments were affected by free-surface contamination. However, at the higher Froude numbers used by Sheridan *et al.* (1997) it is expected that the accumulation of surfactant behind the cylinder is less likely.

4.3 SUMMARY

For low Froude numbers, three different wake states were observed within the free-surface region as the depth of the stationary cylinder below a free-surface is decreased. At the deeper submergence depths the mode I wake is a modified Kármán wake, where the presence of the free-surface results in a shorter formation length and a corresponding increase in the amplitude of the fluctuating lift force. Thus, it appears that for the mode I wake the effect of the Kármán instability is amplified by the close proximity of the free-surface. However, as the cylinder is moved closer to the free-surface periodic vortex shedding is suppressed and for the mode II and III wakes the fluctuating lift force is very small. The mode II wake, which has high velocity fluid moving

underneath the free-surface, and the mode III wake where a thin jet of fluid separates from the free-surface are similar to the wakes observed by Sheridan *et al.* (1997) at higher *Fr*. However, at lower *Fr* the free-surface appears flat and significant levels of free-surface vorticity, possibly corresponding to free-surface contamination, were detected only at $h/D = 0.125$ and 0.075.

The presence of the free-surface appear to either magnify or suppress periodic vortex shedding and the corresponding fluctuating forces experienced by the cylinder. It is expected that the range of submergence depths over which the free-surface region and associated wake modes extend is a function of *Fr*. Additionally, the nature of the wake modes will also vary with Froude number as demonstrated by the extensive free-surface deformation and free-surface vorticity observed by Sheridan *et al.* (1997) at higher *Fr*.

underneath the free-surface, and the mode III wake where a thin jet of fluid separates from the free-surface are similar to the wakes observed by Sheridan *et al.* (1997) at higher *Fr*. However, at lower *Fr* the free-surface appears flat and significant levels of free-surface vorticity, possibly corresponding to free-surface contamination, were detected only at $h/D = 0.125$ and 0.079.

The presence of the free-surface appear to either magnify or suppress periodic vortex shedding and the corresponding fluctuating forces experienced by the cylinder. It is expected that the range of submergence depths over which the free-surface region and associated wake modes extend is a function of *Fr*. Additionally, the nature of the wake modes will also vary with Froude number as demonstrated by the extensive free-surface deformation and free-surface vorticity observed by Sheridan *et al.* (1997) at higher *Fr*.

5 CONCLUSIONS

In this work, we describe in detail the wake states of a cylinder forced to oscillate transverse to a free-stream. The nature of the interaction between the wake's natural instability and the cylinder oscillations was studied using simultaneous measurements of the vortex structures in the near wake and the forces on the cylinder. The modification of the wake of a stationary cylinder due to the close proximity of a free-surface was also studied using simultaneous flow and force field measurements.

The wake's dependence on the oscillation frequency was examined for a range of oscillation amplitudes and Reynolds numbers. For the cases examined, the wake spends the majority of its time in one of either of two stable wake states, however at higher oscillation amplitudes a third wake state was observed. Primarily, these wake states depend on the normalised frequency of oscillation, f_e/f_o, and thus we characterise the two most commonly observed states as the low- and high-frequency wake states. The third wake state was observed at intermediate values of f_e/f_o, between the low- and high-frequency states, and is consequently termed the intermediate wake state. The structure of the near wake and, in particular, the timing of vortex shedding is distinctly different for the low- and high-frequency wake states. These differences can be characterised in terms of a number of universal features, which were observed over the full range of A/D and Re studied. The phase of vortex shedding relative to the cylinder's motion varies only slightly with A/D and Re and appears to depend primarily on the wake state. The phases of the vortex lift and drag forces are directly related to the timing of large scale changes in the vorticity field and, as shown in Figure 3-21, the low- and high-frequency wake states have characteristic values of $\phi_{lift\ vortex}$ and ϕ_{drag} which are observed over a wide range of A/D and Re. The wake states can also be characterised by the structure of the near wake and typically the mode of vortex shedding. The low-frequency wake state generates long attached shear layers, which, except for very low values of A/D, result in the 2P mode of vortex shedding. The high-frequency wake state has a much shorter wake length and vortices are shed in the 2S or Kármán mode. At the oscillation amplitudes considered in this investigation the intermediate wake is also 2S, however the phase of vortex shedding and the vertical width of the wake are similar to that of the low-frequency wake.

At the transition between the low-frequency and intermediate states there is a large change in ϕ_{lift}, corresponding to a change in the relative amplitudes of the apparent mass and vortex components of the total lift force. However, $\phi_{lift\ vortex}$ is relatively unchanged and examination of the flow fields shows that the phase of large-scale vortex shedding is also unchanged. At the intermediate to high-frequency transition the value of ϕ_{lift} is relatively constant, but there is a jump in the value of $\phi_{lift\ vortex}$ and a corresponding change in the phase of vortex shedding. At the transitions between the low-frequency, intermediate and high-frequency states there are jumps in the values of C_L and

$C_{L\,vortex}$; however, surprisingly, there are only relatively small changes in the values of C_D and $C_{D\,mean}$. For flow and oscillation parameters where the intermediate state was not observed the transition between the low- and high-frequency states corresponds to simultaneous jumps in the phase and amplitude of both the total and vortex lift forces. However, as there are significant changes in both the structure of the near wake and the phase of vortex shedding, it is difficult to directly compare the change in timing of vortex shedding with the change in the value of $\phi_{lift\,vortex}$.

For a given wake state the magnitude of the vortex forces: $C_{L\,vortex}$, C_D and $C_{D\,mean}$ as well as the energy transfer and the total lift forces all show significant variations as the oscillation amplitude and Reynolds number vary. For the low- and high-frequency states the phase of the vortex forces $\phi_{lift\,vortex}$ and ϕ_{drag} do not vary significantly with *Re* or *A/D*, and with the exception of the region immediately following the transition to the high-frequency state, Figure 3-21shows a remarkable collapse of $\phi_{lift\,vortex}$ and ϕ_{drag}. A similar collapse may occur for the intermediate state but additional data is required to show this. While the jump in the phase of the vortex lift and drag at the transition between the low- and high-frequency states is relatively independent of *A/D* and *Re*, the jump in the magnitude of both the vortex and total forces depends on both variables.

For certain flow and oscillation parameters there is a self-excited transition between wake states at a constant frequency of oscillation. Thus, for a small region of parameter space, two or even three states can exist at different times. Usually, one of these states appears to be metastable; its existence depending on the start up conditions. During the self-excited transition between the different states the mode of vortex shedding and the forces on the cylinder vary smoothly in the time domain. This contrasts with the abrupt jump between the states in the frequency domain.

The relative stability of the wake states, and their susceptibility to transition, varies with f_e/f_o. As f_e/f_o changes a number of variables, including the natural frequency of the oscillating wake, respond in a non-linear fashion and it is not possible to quantify the relationship between the stability of the wake states and f_e/f_o. However, there are a number of systematic changes that occur as f_e/f_o increases towards transition region. For the low-frequency wake state, the length of the wake contracts as f_e/f_o increases and there is a greater disparity in the relative strength of the vortices in the 2P pairing. As the wake approaches transition region from either higher or lower f_e/f_o the oscillation frequency f_e and the natural frequency of the oscillating wake f_{nos} converge and at the transition from the low- to the high-frequency state f_e/f_{nos} jumps through unity. Despite these systematic changes, for a given wake state the general characteristics of the wake state, in particular the phase of vortex shedding, remain relatively constant.

An important feature of the study is the extraction of the vortex force from the total force. Use of this approach allows a direct link between the forces on the cylinder and the cylinder's wake to be established. When the total lift force, $C_L(t)$, and the vortex lift force, $C_{L\,vortex}(t)$, are compared with

the phase of vortex shedding for a range of flow parameters, it becomes evident that the relationship between the force on the cylinder and the structure of the near wake should be interpreted using F_{vortex} rather than F_{total}. This is best illustrated by the cases where the intermediate state is observed; the transitions between the intermediate and either the low- or high-frequency states demonstrate the qualitative link between $\phi_{lift\ vortex}$ and the phase of vortex shedding, as well as the link between $C_{L\ vortex}$ and the distribution of vorticity. However, if these transitions are considered in terms of the total force on the cylinder the change in the phase of vortex shedding does not correspond to the jump in ϕ_{lift}.

One of the primary motivations for investigating the forced cylinder oscillations is the potential to understand and predict flow-induced motion. This investigation shows, for the first time, a link between the wake states of a cylinder forced to oscillate and the response branches of a freely oscillating cylinder. This link is shown in terms of both the forces on the cylinder and the phase-reference structure of the near wake. In summary, we find a strong correlation between the wake states and response branches as listed below:

Low-frequency state	$\leftrightarrow$	Lower branch
Intermediate state	$\leftrightarrow$	Upper branch
High-frequency state	$\leftrightarrow$	Initial branch

The upper response branch for the free-oscillations is only observed for low mass-damping values and exhibits high oscillation amplitudes. Interestingly, the corresponding forced intermediate state was only observed at the two highest oscillation amplitudes considered in our investigation.

One of the major unsolved problems for this class of flows is whether the results of forced oscillation experiments can be used to predict the vortex-induced vibration of a structure that is free to oscillate. Whilst this investigation did not seek to answer this question a number of interesting issues have arisen. The forced purely sinusoidal oscillations appear to reproduce the different wake structures and lift phases observed for a freely oscillating cylinder. This indicates that the forced oscillations are simulating many of the important features of the flow-induced motion. The variation of ϕ_{lift} and $\phi_{lift\ vortex}$ are remarkably similar, however many of the values of ϕ_{lift} and $\phi_{lift\ vortex}$ for the forced oscillations are outside the region of positive energy transfer, $0° < (\phi_{lift}$ or $\phi_{lift\ vortex}) < 180°$, and therefore predict that flow induced motion will in fact not occur. Thus although the forced oscillations replicate many features of the flow-induced motion there are still some important aspects that are not resolved.

For the case of a stationary cylinder beneath a free-surface three different wake states, described as modes I, II and III, are observed as the depth of the cylinder is decreased. The modification of the Kármán wake by the free-surface in the mode I wake results in a shorter formation length and an

increase in $C_{L\sigma}$. The mode II wake, with high velocity fluid moving underneath the free-surface, and the mode III wake with a thin jet of fluid separating from the free-surface are similar to the wakes observed by Sheridan *et al.* (1997) at higher *Fr*. However, at lower *Fr* the free-surface appears flat and, for all but the very smallest submergence depths, significant levels of positive free-surface vorticity were not detected. Periodic vortex shedding does not occur for the mode II and mode III wakes and $C_{L\sigma}$ is very small. The presence of the free-surface causes a non-symmetry of the wake; the lower shear layer has a characteristic downward angle and $C_{L\,mean}$ is negative. Thus it appears that the presence of the free-surface can act to either amplify or suppress the periodic vortex shedding associated with the Kármán instability.

5.1 FUTURE WORK / RECOMMENDATIONS

Spanwise Wake Structure

When a cylinder oscillates there is an increase in the spanwise coherence of vortex shedding. However, the wake is not 2-dimensional and the levels of vorticity across the span of the cylinder have been shown to be as high as 1/3 of the vorticity in the streamwise plane, Cetiner (1998). Similarly, for $Re > 180$ the wake of a stationary cylinder is also 3-dimensional. In this work a number of different wake states have been observed for both an oscillating cylinder and a cylinder beneath a free-surface. These wake states have been characterised in terms of the wake structure in the x-y plane perpendicular the cylinder's axis. However, the spanwise wake structures, in particular their dependence on wake state and their contribution to the forces experienced by the cylinder, remain unknown. Additionally, it is not known if the spanwise nature of the wake affects the transition between wake states and if self-excited transitions occur simultaneously along the span of the cylinder.

Intermediate State

A strong correlation was shown between the forced oscillation intermediate state and the free upper response branch. The intermediate state was observed over a small band of oscillation frequencies at the two highest amplitudes considered in this investigation, $A/D = 0.5$ and 0.6, where these amplitudes are slightly below the smallest upper branch amplitudes observed by Govardhan & Williamson (2000). At $A/D = 0.6$ the intermediate state was observed as a stable wake state following a self-excited transition but at $A/D = 0.5$ the intermediate state was only observed for short periods of time. In combination with the correlation between the upper branch and intermediate state these results suggest that the intermediate state will occur as a stable wake state at higher oscillation amplitudes. Moreover, it is likely that, in-line with the results of the freely oscillating cylinder, the intermediate state will be observed over a wider range of f_e/f_o at higher oscillation amplitudes.

Relationship Between Force and Vorticity

It has been known for some time that the forces on a body due to the vorticity field can be expressed in terms of the time rate of change of the vortex moment, as described by equation 3.2. However, in practical terms the link between the forces experienced by a body, moving or stationary, and the time varying vorticity distribution is not well understood. For example, looking at the time varying vorticity fields for the low-frequency, intermediate and high-frequency wakes it is not immediately apparent why the vortex lift forces on the cylinder are of different amplitude. Additionally, for the same fields it is also not clear why the amplitude of the (vortex) drag forces

do not vary significantly as the wake state changes. Clearly more work is required to understand this important relationship.

Prediction of Flow-Induced Motion

Our results have shown that the controlled purely sinusoidal motion of a cylinder can replicate many of the flow structures and force properties of a freely oscillating cylinder. However, in a number of cases there are fundamental differences between the forced and freely oscillations, as relatively small changes in the phase of the lift force causes the direction of energy transfer to be different. These results have serious implications for the predication of flow-induced motion using forced oscillation results as it indicates that the flow-induced motion can not be accurately predicted using forced purely sinusoidal oscillations. In order to determine if the flow-induced motion can be predicted using controlled oscillation results we need first to understand how, and preferably why, the two cases are different. The most obvious difference between the two cases is the cylinder motion; as if the motions were identical the wakes and therefore the forces on the cylinder and the energy transfer would also be identical. The flow-induced motion is directly related to the structure of the wake. Therefore, an understanding of the differences in the wake structure, including the spanwise component, may be important in determining the differences between the forced and freely oscillating cases.

Wake States Below a Free-Surface

A number of different mechanisms can be used to perturb or alter the Kármán instability. In this investigation two such mechanisms were considered; the presence of a free-surface and large-scale cylinder oscillations. In both cases a number of different wake states were observed, where these wake states display characteristic features that depended primarily on either the depth of the cylinder below the free-surface or the frequency of oscillation. An obvious extension of this investigation is to consider the case of a cylinder oscillating beneath a free-surface, where these two mechanisms are combined. In particular, it would be interesting to determine if, when the two mechanisms are combined, do the characteristic features observed for the two individual cases persist. In particular; are the features which characterised the effect of the free-surface on the flow over a stationary cylinder, i.e. the downwards angle of the wake and the net negative lift force on the cylinder, present for the oscillating case; and is there a transition between different wake states as f_e/f_o passes through unity?

5.2 SUPPORTING PAPERS

Refereed Journal Articles

SHERIDAN, J., CARBERRY, J., LIN, J.-C. & ROCKWELL, D. 1998, "On the near wake topology of an oscillating cylinder", *Journal of Fluids and Structures*, 12, 215-220.

CARBERRY, J., SHERIDAN, J. & ROCKWELL, D. 2001, "Forces and wake modes of an oscillating cylinder", *Journal of Fluids and Structures*, **15**, 523-532

CARBERRY, J., SHERIDAN, J. & ROCKWELL, D., 2002, "Controlled oscillations of a cylinder: a new wake state", *Journal of Fluids and Structures, to appear.*

CARBERRY, J., SHERIDAN, J. & ROCKWELL, D., 2002, "Controlled oscillations of a cylinder: forces and wake modes", submitted to *J. Fluid Mech.*

International or Refereed Conference Publications

CARBERRY, J., LIN, J.-C., SHERIDAN, J. AND ROCKWELL, D. 1997, Formation of shear layer vortices from an oscillating cylinder at low Reynolds numbers, *Bulletin of American Physical Society*, p2177, San Francisco, 1997.

CARBERRY, J., SHERIDAN, J., LIN, J.-C. AND ROCKWELL, D. 1998, Cross-stream oscillations of a cylinder adjacent to a free-surface; Flow patterns and loading, *Proc. 13th Australasian Fluid Mechanics Conference*, Melbourne, Dec., 1998.

CARBERRY, J., SHERIDAN, J. & ROCKWELL, D. 2000, "Forces and wake modes of an oscillating cylinder", (Proceedings of) *Bluff Bodies Wakes and Vortex-Induced Vibrations (BBVIV2)* 13-16 June 2000, Marseille, France.

CARBERRY, J., SHERIDAN, J. & ROCKWELL, D., 2001, "A comparison of forced and freely oscillating cylinders", *Proceedings 14th Australasian Fluid Mechanics Conference, Adelaide*, 701-704.

CARBERRY, J., SHERIDAN, J. & ROCKWELL, D., 2001, Stationary and oscillating cylinders in the presence of a free-surface, *Proceedings 14th Australasian Fluid Mechanics Conference, Adelaide*, 285-788

CARBERRY, J., SHERIDAN, J. & ROCKWELL, D., 2002, "Cylinder oscillations beneath a free-surface", *IUTAM Symposium Unsteady separated flows, Toulouse, France.*

CARBERRY, J., SHERIDAN, J. & ROCKWELL, D., 2002, "Vortex forces on an oscillating cylinder", *ASME International Mechanical Engineering Congress and Exposition November 17-22 2002, New Orleans*

CARBERRY, J., GOVARDHAN, R., SHERIDAN, J., WILLIAMSON, C. H. K. & ROCKWELL, D., 2002, "Wake States and Response Branches of Forced and Freely Oscillating Cylinders", *submitted Bluff Body Vortex Induced Vibration Conference, Port Douglas*

REFERENCES

ANGRILLI, F., BERGAMASCHI, S. & COSSALTER, V., 1982, "Investigation of wall induced modifications to vortex shedding from a circular cylinder", *J. Fluids Eng.* **104**, 518-522

ANAGNOSTOPOULOS, P 2000, "Numerical study of the flow past a cylinder excited transversely to the incident stream. Part 1: Lock-in zone, hydrodynamic forces and wake geometry", *Journal of Fluids and Structures* (2000) **14**, 819-851

ADRIAN, R. J., 1986, "Image shifting technique to resolve directional ambiguity in double-pulsed laser velocimetry", *Applied Optics*, **25**, 3855-3858

ADRIAN, R. J., 1991, "Particle-imaging techniques for experimental fluid mechanics", *Annu. Rev. Fluid. Mech.* **23**, 261-304

ARMSTRONG, B. J. & BARNES, F. H., 1986, "The effect of a perturbation on the flow over a bluff cylinder", *Phys. Fluids*, **29** (7), 2095-2102

BATCHELOR, G. K., "An introduction to fluid dynamics", *Cambridge University Press*, 1967

BEARMAN, P. W. & ZDRAVKOVICH, M. M., 1978, "Flow around a circular cylinder near a plane boundary", *J. Fluid Mech.*, **89**, 33-47.

BLACKBURN, H. M., GOVARDHAN, R. N. & WILLIAMSON, C. H. K., (2001) "A complementary numerical and physical investigation of vortex-induced vibration", *Journal of Fluids and Structures*, **15** (3/4). in press

BLACKBURN, H. M. & HENDERSON, R. D., 1999, "A study of two-dimensional flow past an oscillating cylinder", *J. Fluid Mech.*, **385**, 255-286.

BLACKBURN, H. M. & MELBOURNE, W. H., 1997, "Sectional lift forces for an oscillating circular cylinder in smooth and turbulent flows", *Journal of Fluids and Structures*, **11**, 413-431.

BARBI, C., FAVIER, D. P., MARESCA, C. A. & TELIONIS, D. P. 1986, "Vortex shedding and lock-on of a circular cylinder in oscillatory flow", *J. Fluid Mech.* **170**, 527-544

BEARMAN, P. W., DOWNIE, M., J., GRAHAM, J. M. R. & OBASAJU, F. D., 1985 "Forces on cylinders in viscous oscillatory flow at low Keulegan-Carpenter numbers", *J. Fluid Mech.* **154**, 481-508

BISHOP, R. E. D. & HASSAN, A. Y., 1963, "The Lift and Drag Forces on a Circular Cylinder in a Flowing Fluid", *Proceedings of Royal Society, London, Series A*, vol. **277**, 32 – 50.

BLEVINS, R. D., 1985, "The effect of sound on vortex shedding from cylinder", *J. Fluid Mech.* **161**, 217-237

BRIKA, D. & LANEVILLE, A, 1993, "Vortex-induced vibrations of a long flexible circular cylinder", *J. Fluid Mech.* **250**, 481-508

CETINER, O. N. L, 1998, "Flow structure and loading due to an oscillating cylinder in steady current", Thesis(PhD), Lehigh University

DALHEIM, J., 1997, "A numerical procedure for predicting transverse forces on a body submitted to Lock-in motion", *International Journal of Offshore and Polar Engineering*, 7 (4), 271-276

DENIZ, S. & STAUBLI, T., 1998, "Oscillating rectangular and octagonal profiles: modelling of fluid forces", *Journal of Fluids and Structures*, **12**, 859-882

DENIZ, S. & STAUBLI, T., 1997, "Oscillating rectangular and octagonal profiles: interaction of leading- and trailing-edge vortex formation", *Journal of Fluids and Structures*, **11**, 3-31

FENG, C. C., 1968, "The measurements of vortex-induced effects in flow past a stationary and oscillating circular and D-section cylinders", *Master's thesis, University of British Columbia, Vancouver, B.C., Canada.*

GHARIB, M. R. 1999, "Vortex-induced vibration, absence of lock-in and fluid force deduction", *Ph.D. thesis CALTEC, Pasadena, California, USA.*

GHARIB, M. & WEIGAND, A., 1996, "Experimental studies of vortex disconnection and connection at a free-surface", *J. Fluid Mech.*, **321**, 59-86.

GOPALKRISHNAN, 1993, Vortex Induced Forces on Oscillating Bluff Cylinders, *MIT Doctoral Dissertation.*

GOVARDHAN, R & WILLIAMSON, C. H. K. 2000, "Modes of vortex formation and frequency response of a freely vibrating cylinder", *J. Fluid Mech.*, **420**, 85-130.

GOVARDHAN, R. & WILLIAMSON, C. H. K. 2001, "Mean and Fluctuating Velocity Fields in the Wake of a Freely-Vibrating Cylinder", *Journal of Fluids and Structures*, 15, 489-502

GRIFFIN, O. M. & HALL, M. S., 1991, "Review-Vortex shedding lock-on and flow control in bluff body wakes", *Journal of Fluids Engineering*, Vol. **113**, 526-537

GREEN, S. I., 1995, "Fluid Vortices, Chapter 1, Introduction to vorticity", *S. I Green (ed.), Fluid Vorticies, Kluwer Academic Publishers,* 1-34

GU, W., CHYU, C. & ROCKWELL, D., 1994, "Timing of vortex formation from an oscillating cylinder", *Physics of Fluids*, **6** (11), 3677-3682

HALL, M. S. & GRIFFIN, O. M., 1993, "Vortex shedding and lock-on in a perturbed flow", *Journal of Fluids Engineering*, Vol. **115**, 283-291

HOVER, F. S., TECHET, A. H. & TRIANTAFYLLOU, M. S. 1998, "Forces on oscillating uniform and tapered cylinders in crossflow", *J. Fluid Mech.* **363**, 97-114

HOYT, J. W. & SELLIN, H. H. J., 2000, "A comparison of tracer and PIV results in visualizing water flow around a cylinder close to the free surface", *Experiments in Fluids* **28**, 261-265

HUERRE, P. & MONKEWITZ, F. A., 1990, "Local and global instabilities in spatially developing flows", *Annu. Rev. Fluid Mech.* **22**, 473-537

JEON, D. & GHARIB, M., 2000, "On circular cylinders undergoing two-degree-of-freedom forced motions", Abstracts IUTAM *Symposium on Bluff Body Wakes and Vortex-Induced Vibrations*, Marseille

KHALAK, A & WILLIAMSON, C. H. K. 1996, "Dynamics of a hydroelastic cylinder with very low mass and damping." *Journal of Fluids and Structures*, **10**, 455-472

KHALAK, A & WILLIAMSON, C. H. K. 1997, "Fluid forces and dynamics of a hydroelastic structure with very low mass and damping" *Journal of Fluids and Structures*, **11**, 973-982

KHALAK, A & WILLIAMSON, C. H. K. 1999, "Motions, forces and mode transitions in vortex induced vibrations at low mass-damping" *Journal of Fluids and Structures*, **13**, 813-851

KARNIADAKIS, G. E. M. & TRIANTAFYLLOU, G. S., 1989, "Frequency selection and asymptotic states in laminar wakes", *J. Fluid Mech.* **199**, 441-469

LIGHTHILL, M. J., 1986, "Fundamentals concerning wave loading on offshore structures", *J. Fluid Mech.*, **173**, 667-681

LIGHTHILL, M. J., 1954, "The response of laminar skin friction and heat transfer to fluctuations in the stream velocity", *Proceedings of the Royal Society of London, Series A Mathematical and Physical Sciences*, **224**, no. 1156, pp 1-23

LOTFY, A. & ROCKWELL, D., 1993, "The near-wake of an oscillating trailing edge: mechanisms of periodic and aperiodic response", *J. Fluid Mech.* **251**, 173-201

MAGNESS, C., 1990, "Streaming function generator, SFG", software, Fluid Mechanics Lab., Lehigh University.

MAGNESS, C. & TROIANO, J., 1990, " Automated laboratory technician, ALT", software, Fluid Mechanics Lab., Lehigh University.

MERCIER, J. A., 1973, "Large amplitude oscillations of a circular cylinder in a low-speed stream", *Stevens Institute of Technology, Ph.D., 1973. Engineering, Mechanical.*

MIYATA, H., SHIKAZONO, N. & KANAI, M., 1990, "Forces on a circular cylinder advancing steadily beneath the free-surface", *Ocean Engng.* **17** (1/2), 81-104.

MOE, G. & WU, Z.-J., 1990, "The lift force on a cylinder vibrating in a current", *Journal of Offshore Mechanics and Arctic Engineering*, **112**, 297-303.

MONKEWITZ, P. A., 1988, "The absolute and convective nature of instability in two-dimensional wakes at low Reynolds numbers", *Phys. Fluids*, **31** (5) 999-1006

MORTON, B. R., 1983, "The generation and decay of vorticity", *Geophys. Astrophys. Fluid Dynamics, 1984.* **28.** 277-308

NOCA, F., 1997, "On the evaluation of time-dependent fluid-dynamic forces on bluff bodies", PhD Thesis, California Institute of Technology.

NOCA, F., SHIELDS, D. & JEON, D., 1997, "Measuring instantaneous fluid dynamic forces on bodies , using only velocity fields and their derivatives", *Journal of Fluids and Structures*, **11**, 345-350

NOCA, F., SHIELDS, D. & JEON, D., 1999, "A Comparison of methods for evaluating time-dependent fluid dynamic forces on bodies, using only velocity fields and their derivatives", *Journal of Fluids and Structures*, **13**, 551-578

NORBERG, C., 1994, "An experimental investigation of the flow around a circular cylinder: influence of aspect ratio", *J. Fluid Mech. (1994)*, **258**, 287-316

NORBERG, C., 1998, "LDV-measurements in the near wake of a circular cylinder", ASME Fluids Engineering Division, Washington D.C., *Bluff Body Wakes and Vortex-Induced Vibration*, Ed. Bearman & Williamson, Paper 42.

ONGOREN, A. & ROCKWELL, D, 1988a, "Flow structure from an oscillating cylinder Part 1. Mechanisms of phase shift and recovery in the near wake", *J. Fluid Mech.* **191**, 197-223

ONGOREN, A. & ROCKWELL, D, 1988b, "Flow structure from an oscillating cylinder Part 2. Mode competition in the near wake", *J. Fluid Mech.* **191**, 197-223

PANTAZOPOULOS, M. S., 1994, "Vortex-Induced Vibration Parameters: Critical Review", OMAE, Offshore Technology ASME, vol. **1**, 199-255.

PRASAD, A. & WILLIAMSON, C. H. K., 1997, "The instability of the shear layer separating from a bluff body", *J. Fluid Mech.* **333**, 375-402

PRICE, S. J., SMITH, J. G., LEONG, K. & PAIDOUSSIS, M. P., 2000, "Flow visualization around a circular cylinder near to a plane wall", *Proceedings of the 7th International Conference on Flow Induced Vibration, Lucerne, Switzerland 2000,* Ed. Ziada & Staubli, Balkema, Rotterdam, 105-112.

RAFFEL, M. & KOMPENHANS, J., 1995, "Theoretical and experimental aspects of image shifting by means of a rotating mirror system for Particle Image Velocimetry", *Measurement Science Technology*, **6**, 795-808

REYNOLDS, W. C. & CARR, L. W., 1985, "Review of unsteady, driven, separated flows", *AIAA Pap.* 85-0527

ROCKWELL, D., 1990, "Active control of globally-unstable separated flows", Invited lecture at Symposium on Unsteady flows, ASME, Toronto

Robinson, O., 1992, "V3 Post-Processing Software", Fluid Mechanics Lab., Lehigh University.

ROCKWELL, D. & LIN, J.-C., 1993, "Quantitative interpolation of complex, unsteady flows vis High-Image-Density Particle Image Velocimetry", SPIE *International Symposium on Optics, Imaging and Instrumentation*, San Diego, CA

ROCKWELL, D., MAGNESS, C., ROBINSON, O., TOWFIGHI, J., AKIN, O., GU, W. & CORCORAN, T., 1992, "Instantaneous structure of unsteady separated flows via Particle Image Velocimetry using scanning techniques", *Report PI-I*, Fluid Mechanics Lab., Lehigh University.

ROCKWELL, D., MAGNESS, C., TOWFIGHI, J., AKIN, O. & CORCORAN, T., 1993, "High-Image Density Particle Image Velocimetry using scanning techniques" *Experiments in Fluids* **14**, 181-192.

SARPKAYA, T., 1978, "Fluid forces on oscillating cylinders", *Journal of the waterway port coastal and ocean division*, **106** (WW4), 275 - 290

SCOTT, J. C., "Flow beneath a stagnant film on water – the Reynolds ridge", *J. Fluid Mech.* **116**, 283-296

SEKE, E., 1993, "PIV3", Interrogation software, Fluid Mechanics Lab., Lehigh University.

SHERIDAN, J., LIN, J.-C. & ROCKWELL, D., 1995, "Metastable states of a cylinder wake adjacent to a free-surface", *Phys. Fluids* 7 2099-2101

SHERIDAN, J., LIN, J.-C. & ROCKWELL, D., 1997, "Flow past a cylinder close to a free surface", *J. Fluid Mech.*, **330**, 1-30.

SHERMAN, F. S., 1990, "Viscous flow", *McGraw-Hill*

SKOP, R. A. & BALASUBRAMANIAN, S., 1997, "A new twist on an old model for vortex-excited vibrations", *Journal of Fluids and Structures*, **11**, 395-412

STANSBY, P. K., 1975, "The locking-on of vortex shedding due to the cross-stream vibration of circular cylinders in uniform and shear flows", *J. Fluid Mech.* 74 641-665

STAUBLI, T. 1983a, "Untersuchung der oszillierenden Krafte am querangestromten, schwingenden Kreiszylinder", PhD. Dissertation ETH 7322.

STAUBLI, T., 1983b, "Calculation of the vibration of an elastically mounted cylinder using experimental data from forced oscillation", *Journal of Fluids Engineering*, Vol. **105**, 225-229

STAUBLI, T. & ROCKWELL, D., 1989, "Pressure fluctuations on an oscillating trailing edge", *J. Fluid Mech.* **203**, 307-346

SZECHENYI, E & LOISEAU, H., 1975, "Portances instantionnaires surun cylinder vibrant dans un ecoulement supercritique" (Fluctuating lift on a cylinder vibrating in supercritical flow), *La Recherche Aerospatiale*, **1**, 45-57.

TECHET, A. H., 1998, "Vortical patterns behind a tapered cylinder", *MIT Masters Thesis.*

TECHET, A. H., HOVER, F. S. & TRIANTAFYLLOU, M. S., 1998, "Vortical patterns behind a tapered cylinder oscillating transversely to a uniform flow", *J. Fluid Mech.* **363**, 79-96

TOEBES, G. H., 1969, "The unsteady flow and wake near an oscillating cylinder", *Journal of Basic Engineering* **91**, 493-502

TOMLINSON, E. A., 1996, "Strain gauge stings", ATLSS Instrumentation. Lehigh University.

UNAL, M. F. & ROCKWELL, D., 1987, "On vortex formation from a cylinder, Part 2. Control by splitter-plate interference", *J. Fluid Mech.* **190**, 513-529

VISINTIN, A., 1991, "Differential models of hysteresis", Springer-Verlag, Chap 1

WARNCKE, A., GHARIB, M. & ROESGEN, T., 1996, " Flow measurements near a Reynolds ridge", *J. Fluids Eng.* **118**, 621-624

WARNCKE-LANG, A. & GHARIB. M., 1998, ""On the effects of surface contamination in the wake of a surface-piercing cylinder", ASME Fluids Engineering Division, Washington D.C., *Bluff Body Wakes and Vortex-Induced Vibration*, Ed. Bearman & Williamson, Paper 28.

WILLERT, C. & GHARIB, M., 1997, "The interaction of spatially modulated vortex pairs with free-surfaces", *J. Fluid Mech.* **345**, 227-250

WILLERT, C. & GHARIB, M., 1994, "The interaction of modulated vortex pairs with free surfaces", ASME Fluids Engineering Division, Lake Tahoe, Nevada, *Free-surface Turbulence*, Ed. Rood & Katz

WILLIAMSON, C. H. K., 1996a, "Vortex dynamics in the cylinder wake", *Annu. Rev. Fluid. Mech.* **328**, 345-407

WILLIAMSON, C. H. K., 1996b, "Three-dimensional wake transition", *J. Fluid Mech.* **190**, 513-529

WILLIAMSON, C. H. K., 1988, "Defining a universal and continuous Strouhal-Reynolds number relationship for the laminar vortex shedding of a circular cylinder", *Phys. Fluids*, **31**, 2742-2744

WILLIAMSON, C. H. K. & ROSHKO, A. 1988, "Vortex Formation in the Wake of an Oscillating Cylinder", *Journal of Fluids and Structures*, **2**, 355-381.

WU, J.C., 1981, "Theory for Aerodynamic Force and Moment in Viscous Flows", *AIAA Journal*, **19**, 432-441

WU, J. Z & WU, J. M., 1996, "Vorticity Dynamics on Boundaries", *Advances in applied Mechanics.* **32**

ZDRAVKOVICH, M. M., 1997, "Flow around circular cylinders, Vol 1: Fundamentals", *Oxford University Press.*

ZDERO, R., TURAN, O. F. & HAVARD, D. G., 1995, "Toward understanding galloping: near wake study of oscillating smooth and stranded circular cylinders in forced motion", *Experimental Thermal and Fluid Science*, **10** 28-43